



*Ray Dredbury*

# **Self-healing cementitious materials**

**Ben Isaacs**

**Cardiff School of Engineering,  
Cardiff University,  
Wales, UK**

**PhD. 2011**

UMI Number: U567179

All rights reserved

INFORMATION TO ALL USERS

The quality of this reproduction is dependent upon the quality of the copy submitted.

In the unlikely event that the author did not send a complete manuscript and there are missing pages, these will be noted. Also, if material had to be removed, a note will indicate the deletion.



UMI U567179

Published by ProQuest LLC 2013. Copyright in the Dissertation held by the Author.  
Microform Edition © ProQuest LLC.

All rights reserved. This work is protected against  
unauthorized copying under Title 17, United States Code.



ProQuest LLC  
789 East Eisenhower Parkway  
P.O. Box 1346  
Ann Arbor, MI 48106-1346

***Life is “trying things to see if they work”***

*Ray Bradbury*

## **Acknowledgements**

The list of people I would like to thank, who have helped, influenced, taught and laughed with me during the completion of this PhD thesis is a long one.

I would like to thank my family for which this thesis is dedicated to. This would not have been made possible without your constant love and support.

I would like to acknowledge Tony Jefferson and Bob Lark for believing in my abilities and providing the opportunity for me to undertake this study. In addition, I would like to sincerely thank Chris Joseph for his guidance in the field of research. I am indebted to all three for their active encouragement and supervision.

I would like to acknowledge the facilities provided by the Civil Engineering Department at the Cardiff School of Engineering. In particular, I would like to thank the laboratory technical staff, Carl, Harry, Len, Des, Mark, Ian, Paul, Alan and Brian.

I would like to thank my research group and office friends for their enthusiasm and support, Simon C, Iulia, Andrea, Diane and Barry. In particular I would like to thank Simon Dunn with whom it has been a pleasure to work alongside.

Finally, I would like to thank all my friends. I feel very fortunate to have such a great group and your support has helped immensely.

## Declaration

This work has not previously been accepted in substance for any degree and is not concurrently submitted in candidature for any degree.

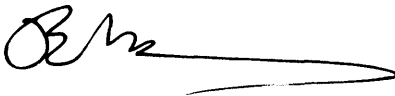
Signed: *Ben Isaacs* (candidate)      Date: 9<sup>th</sup> March 2011



### STATEMENT 1

This thesis is being submitted in partial fulfilment of the requirements for the degree of PhD.

Signed: *Ben Isaacs* (candidate)      Date: 9<sup>th</sup> March 2011



### STATEMENT 2

This thesis is the result of my own independent work/investigation, except where otherwise stated. Other sources are acknowledged by explicit references.

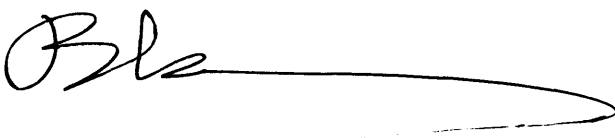
Signed: *Ben Isaacs* (candidate)      Date: 9<sup>th</sup> March 2011



### STATEMENT 3

I hereby give consent for my thesis, if accepted, to be available for photocopying and for inter-library loan, and for the title and summary to be made available to outside organisations.

Signed: *Ben Isaacs* (candidate)      Date: 9<sup>th</sup> March 2011



## Summary

The thesis presents a study of autonomic and autogenous self-healing mechanisms in cementitious materials.

Two distinct self-healing systems are investigated. The first of these is a system to investigate the autonomic healing of small scale reinforced mortar beams with embedded glass capillary tubes filled with a low viscosity cyanoacrylate adhesive. These tubes break and release glue into a crack when it crosses a tube, thereby healing the crack. The study investigated the effects of loading rate, level of reinforcement and specimen age on the autonomic healing ability of the specimens. The study showed that the specimens exhibit a primary and secondary healing response during the first and second loading stages respectively, with the latter response providing an increase in peak load and a full recovery of stiffness.

The second system employs embedded shrinkable PET tendons as a crack closure system for small scale mortar beams. The tendons are activated by the application of heat, once cracking has occurred, and apply a prestress to the cementitious matrix. A parametric study showed that autogenous healing can be greatly enhanced by the correct choice of Activation-Healing (AH) regime. In addition, a numerical procedure was developed in order to predict the capacity and response of these beams. Non-linear damage mechanics and a beam idealisation were used in the development of a numerical tool for simulating the material system. The results obtained from the numerical model showed good consistency with the experimental data.

A general conclusion from the work is that both systems require considerable development before being ready for industrial application. However, of the two systems investigated, it is the latter which shows the greatest potential to not only greatly enhance the durability of cementitious composites, but also to improve their strength and ductility.

## Publications

The author's contributions to publications are:

Isaacs, B., Lark, R.J., Jefferson, A.D., Dunn, S.C. & Joseph, C. 2010. Crack healing using a shrinkable polymer cementitious material system. Cement and Concrete Composites. Submitted September 2010.

Jefferson, A.D., Joseph, C., Lark, R.J., Isaacs, B., Dunn, S.C. & Weager, B. 2010. A new system for crack closure of cementitious materials using shrinkable polymers. Cement and Concrete Research, 40(5), pp.795-801.

Dunn, S.C., Jefferson, A.D., Lark, R.J. & Isaacs, B. 2010. Investigation into the shrinkage behaviour of Polyethylene Terephthalate (PET) for a new cementitious-shrinkable polymer material system. Journal of Applied Polymer Science, 120(5), pp.2516-2526.

Joseph, C., Jefferson, A.D., Isaacs, B., Lark, R.J. & Gardner, D. 2010. Experimental investigation of adhesive-based self-healing of cementitious materials. Magazine of Concrete Research, 62(11), pp.831-843.

Joseph, C., Gardner, D., Jefferson, A.D., Isaacs, B. & Lark, R.J. 2010. Self-Healing Cementitious Materials: A review of recent work. Proceedings of the ICE: Construction Materials, 164(CM1), pp.29-41.

Isaacs, B., Joseph, C., Jefferson, A.D., Lark, R.J. & Dunn, S.C. 2009. Enhancement of Self-Healing in Cementitious Materials, Post-Tensioned with Shrinkable Polymers. Proceedings of the Second International Conference on Self-Healing Materials, Chicago, IL USA. ICSHM2009.

Joseph, C., Jefferson, A.D., Isaacs, B., Lark, R.J. & Gardner, D.R. 2009. Adhesive Based Self-Healing of Cementitious Materials. Proceedings of the Second International Conference on Self-Healing Materials, Chicago, IL USA. ICSHM2009.

Dunn, S.C., Jefferson, A.D., Lark, R.J., Isaacs, B. & Joseph, C. 2009. A Numerical Model for the Shrinkage of Polymer Elements in Active Self-Healing. Proceedings of the Second International Conference on Self-Healing Materials, Chicago, IL USA. ICSHM2009.

Lark, R.J., Jefferson, A.D., Joseph, C., Dunn, S.C. & Isaacs, B. 2009. Active Confinement of Cementitious Composites with Shape Memory Plastics. Proceedings of the Second International Conference on Self-Healing Materials, Chicago, IL USA. ICSHM2009.

The author is a member of the RILEM Technical Committee 221-SHC: Self-Healing phenomena in Cement-based materials and has contributed to the production of a State of the Art Report (STAR) into self-healing cementitious materials (Due for publication 2011).

## Table of contents

Acknowledgements .....	ii
Declaration .....	iii
Summary.....	iv
Publications .....	v
Table of contents .....	vi
List of tables.....	xi
List of Figures.....	xi
Symbols and abbreviations.....	xv
<b>Chapter 1 Introduction .....</b>	<b>1</b>
1.1 Inspiration from nature .....	1
1.2 Cementitious materials .....	2
1.3 The issues of durability.....	2
1.4 The financial and environmental impact.....	3
1.5 Scope and objectives .....	4
1.6 Outline of the thesis .....	6
<b>Chapter 2 Literature Review .....</b>	<b>8</b>
2.1 Introduction.....	8
2.2 Classification of materials and structures .....	8
2.2.1 Intelligent materials.....	8
2.2.2 Smart materials .....	9
2.2.3 Smart Structures.....	9
2.2.4 Sensory structures.....	10
2.2.5 Self-healing materials .....	10
2.2.6 Active and Passive self-healing.....	11
2.3 Autogenous Healing .....	12
2.3.1 Mechanisms of autogenous healing.....	13
2.3.2 Mechanical response of autogenous healing.....	16
2.3.3 Enhancement of autogenous healing.....	22
2.4 Autonomic Healing .....	23
2.4.1 Autonomic healing in polymer composites.....	24



2.4.2 Autonomic healing in cementitious materials .....	26
2.4.3 Mechanical response of autonomic healing .....	26
2.4.4 Healing agents .....	30
2.4.5 Encapsulation techniques.....	32
2.4.6 Further studies.....	33
2.5 Shape Memory Polymers .....	35
2.5.1 Shape memory materials .....	35
2.5.2 Shape memory effect in polymers .....	37
2.5.3 Transformation temperature .....	39
2.5.4 Thermomechanical characterisation.....	40
2.5.5 SMP classification .....	41
2.5.6 Activation methods .....	44
2.5.6.1 Thermal activation: direct and indirect.....	44
2.5.6.2 Light activation .....	46
2.5.7 SMP applications .....	46
2.6 Conclusion .....	49
2.6.1 Self-healing cementitious materials.....	49
2.6.2 Shape memory polymers.....	50
<b>Chapter 3 Autonomic healing .....</b>	<b>52</b>
3.1 Introduction.....	52
3.2 Preliminary Investigations .....	53
3.2.1 Encapsulation methods .....	53
3.2.2 Healing agents .....	54
3.2.3 Reinforcement.....	55
3.2.4 Cementitious mix design .....	56
3.2.5 Observation of the sensing and actuation mechanism.....	57
3.3 Experimental procedure.....	58
3.3.1 Parametric study.....	58
3.3.2 Specimen preparation .....	61
3.3.3 Test set up .....	62
3.4 Results and discussion .....	63

3.4.1 Mechanical response to autonomic healing .....	64
3.4.2 Effect of loading rate .....	66
3.4.3 Effect of reinforcement .....	67
3.4.4 Effect of specimen age .....	69
3.4.5 Qualitative results.....	69
3.4.5.1 New crack formation .....	69
3.4.5.2 Glue flow.....	71
3.5 Conclusions.....	72
<b>Chapter 4 Autogenous healing (proof of concept).....</b>	<b>74</b>
4.1 Introduction.....	74
4.2 The concept .....	75
4.3 Polymer criteria .....	76
4.3.1 Activation temperature .....	76
4.3.2 Minimum shrinkage stress .....	76
4.3.3 Young Modulus.....	77
4.3.4 Resistant to an alkaline environment.....	77
4.3.5 Relaxation .....	77
4.4 Polymer investigation.....	77
4.4.1 Screening tests.....	77
4.4.2 Preliminary tests – first phase .....	79
4.4.3 Preliminary tests – second phase .....	80
4.4.3.1 Constant displacement tests .....	81
4.4.3.2 Constant load tests.....	85
4.4.4 Conclusion of preliminary tests.....	87
4.5 PET Shrink-tite experimental investigation .....	88
4.5.1 PET Shrink-tite specimen preparation.....	88
4.5.2 PET Shrink-tite experimental set up.....	90
4.5.3 PET Shrink-tite parametric investigation.....	91
4.5.4. Results and discussion .....	93
4.6 Cementitious material investigation .....	96
4.6.1 Specimen preparation .....	96

4.6.2 Specimen configuration.....	98
4.6.3 Cementitious mix design .....	99
4.6.4 Experimental procedure.....	100
4.6.5 Results and discussion.....	102
4.7 Conclusion .....	107
<b>Chapter 5 Autogenous healing (parametric investigation).....</b>	<b>109</b>
5.1 Introduction.....	109
5.2 Testing programme .....	110
5.3 Digital Image Correlation.....	112
5.4 Results.....	114
5.4.1 Recovery of mechanical properties.....	114
5.4.2 Qualitative results.....	118
5.4.3 Autogenous healing measured using DIC.....	119
5.5 Discussion .....	121
5.5.1 Mechanical response of PETr specimens .....	122
5.5.2 Mechanical response of PET specimens.....	123
5.6 Conclusions.....	124
<b>Chapter 6 Theoretical analysis.....</b>	<b>126</b>
6.1 Introduction.....	126
6.2 Analysis .....	126
6.3 Analytical solution .....	130
6.4 Numerical solution .....	132
6.5 Concrete behaviour.....	133
6.5.1 Concrete shrinkage.....	134
6.5.1.1 Types of shrinkage.....	134
6.5.1.2 Actions of shrinkage .....	135
6.5.2 Concrete creep .....	136
6.6 Results and discussion.....	137
6.7 Conclusions.....	139
<b>Chapter 7 Conclusions and recommendations for further work.....</b>	<b>141</b>
7.1 Conclusions.....	141

7.2 Recommendations for further work.....	144
7.2.1 Autonomic healing.....	145
7.2.2 Autogenous healing.....	147
<b>References</b> .....	<b>149</b>
<b>Appendix A Rite-Lok data sheet</b> .....	<b>159</b>
<b>Appendix B Autonomic healing results</b> .....	<b>161</b>
Set 1. Lightly reinforced, notched beams.....	162
Set 2. Lightly reinforced, notched beams.....	163
Set 3. Moderately reinforced, notched beams .....	164
Set 4. Heavily reinforced, notched beams .....	165
Set 5. Lightly reinforced, un-notched beams .....	166
Set 6. Lightly reinforced, notched beams with varied loading rate .....	167
<b>Appendix C Autogenous healing results</b> .....	<b>170</b>
Proof of concept results .....	170
AH 1 test results.....	172
AH 2 test results.....	174
AH 3 test results.....	176
<b>Appendix D Shrink-tite data sheet</b> .....	<b>178</b>
<b>Appendix E Digital image correlation strain profiles</b> .....	<b>181</b>

## List of tables

Table 2.1	Comparison of the typical properties of shape memory polymers and shape memory alloys
Table 2.2	Summary of shape memory polymer classification properties
Table 3.1	Properties of capillary tubes used in preliminary investigation
Table 3.2	Mechanical properties for bar diameters 3.15 mm and 6.7 mm
Table 3.3	Specimen configurations for sets one to six of the experimental programme
Table 4.1	Polymer investigation
Table 4.2	Material system classes
Table 4.3	Candidate materials studied in collaboration with NetComposites
Table 4.4	Stages of experimental procedure
Table 4.5	Summary of specimen details
Table 4.6	Mean load, coefficient of variance and load recovery percentages
Table 4.7	Measured material properties
Table 5.1	Heat activation methods and healing regimes
Table 5.2	Results of test specimens
Table 5.3	Mean gradient recovery for loading curves of typical specimen's pre-peak at stage 3 testing
Table 5.4	Measured material properties
Table 5.5	Compressive strength of small scale mortar cubes
Table 6.1	Specimen dimensions
Table 6.2	Numerical solution data

## List of Figures

Figure 1.1	Billions of pounds spent on repair and maintenance and new construction work
Figure 1.2	Timeline of the research
Figure 2.1	Scales in materials and structures
Figure 2.2	Material classification

- Figure 2.3 Active method of repairing cracks by melting wax coated fibres to release methylmethacrylate
- Figure 2.4 Passive release initiated by the physical cracking of the test sample
- Figure 2.5 (a) Normalised flow rate for specimens at various crack widths at a constant temperature (b) Normalised flow rate for specimens with a constant crack width at various temperatures
- Figure 2.6 (a) Three-point bending test setup (b) Compression device for initially cracked specimens
- Figure 2.7 Stress-displacement curve of healed specimen with and without compressive stress, compared with unhealed cracked specimen
- Figure 2.8 Tensile strain-hardening behaviour of ECC in comparison with FRC
- Figure 2.9 (a) Cracks in ECC material (b) New crack formed over previously healed crack
- Figure 2.10 The three stages (a, b and c) of the autonomic healing concept in polymers
- Figure 2.11 Repeated healing in a microvascular network
- Figure 2.12 Specimen configuration and test set up
- Figure 2.13 Load vs. CMOD for specimens
- Figure 2.14 (a) Alkali-silica repairing agent B (b) Alkali-silica repairing agent B' (c) epoxy resin repairing agent C, and (d) CMOD vs. self recovery ratio
- Figure 2.15 (a) ESEM specimen loading configuration (specimen dimensions are 10 x 10 x 1.5 mm) (b) formation of cracks in ESEM specimens
- Figure 2.16 Schematic illustration of the two glass fibre arrangements
- Figure 2.17 Schematic illustration of the selective heating concept
- Figure 2.18 Schematic representations of polymer structures
- Figure 2.19 Schematic representation of the shape memory effect
- Figure 2.20 Temperature dependency of elasticity modulus of SMP
- Figure 2.21 Schematic representation of a 3D result for thermomechanical cycle tests
- Figure 2.22 Schematic representation of the shape memory effect of class 2 SMPs
- Figure 2.23 Magnetically induced shape memory effect of the SMP TFX
- Figure 2.24 Light induced shape memory effect in a polymer

- Figure 2.25 Six stages of self-tightening knot from the temporary shape (1) to its parent shape (6) in 20 seconds when heated to 41°C
- Figure 2.26 Shape memory activating wires
- Figure 2.27 The triple shape effect in TSPs: (a) application as a stent, and (b) as a fastener consisting of a plate with anchors
- Figure 3.1 Schematic illustration of autonomic healing concept
- Figure 3.2 Schematic illustration of the specimen configuration for the two preliminary test sets using 3 mm diameter, 100 mm glass capillary tubes with (a) a single layer (SL-5), and (b) a double layer (DL-5)
- Figure 3.3 Schematic illustration of capillary forces within the glass capillary tubes
- Figure 3.4 Capillary glass tubes and reinforcement preparation for specimens
- Figure 3.5 Specimen configuration for sets 2, 3, 4, 5 and 6
- Figure 3.6 Test set up of a typical specimen subject to three-point bending
- Figure 3.7 SH beam 3 and control 1 from set 4 (a) Load-CMOD and (b) Load-central deflection
- Figure 3.8 Load-CMOD response for loading rates (a) 0.00075 mm/s, SH beam 1 from set 6 (b) 0.003 mm/s, SH beam 4 from set 6, and (c) 0.012 mm/s, SH beam 7 from set 6
- Figure 3.9 Load-CMOD response of (a) Single 3.15 mm reinforcement, SH beam 1 from set 2 (b) Double 3.15 mm reinforcement, SH beam 3 from set 1, and (c) Single 6.7 mm reinforcement, SH beam 4 from set 4
- Figure 3.10 New crack formation as a result of autonomic healing of the original crack for SH beam 1 from set 6
- Figure 3.11 Typical examples of glue stringing and bonding exhibited in specimens
- Figure 3.12 (a) control specimen exhibiting ink migration during testing (b) SH beam exhibiting glue flow after the first loading cycle
- Figure 3.13 Capillary rise of glue in crack zone (a) SH beam 1 (b) SH beam 4, for set 1 specimens
- Figure 4.1 Schematic illustration of concept for the material system LatConX
- Figure 4.2 Results from candidate material tests
- Figure 4.3 Restrained heating tests for GFRPP strips for: (a) 140 °C for 2 hours, and (b) 145 °C for 1 hour

- Figure 4.4      Restrained heating tests for WPP strips for: (a) 140 °C for 1.5 hours, and (b) 145 °C for 1 hour
- Figure 4.5      Restrained heating tests for PET tape with heating rates: (a) Instant heating, (b) Incremental heating, and (c) Soaking
- Figure 4.6      Young's modulus-temperature for GFRPP
- Figure 4.7      Restrained heating tests for PET tape with applied constant load of: (a) 20 N, and (b) 30 N
- Figure 4.8      Specimen preparations: (a) Specially designed jig for specimen manufacture, and (b) Bonding of strips
- Figure 4.9      Tendon specimen set up
- Figure 4.10     Experimental set up: (a) Schematic illustration of test arrangement, (b) Specimen inside thermal chamber, and (c) Tensile machine grips
- Figure 4.11     (a) Restrained heating tests for PET tendons of various strips, and (b) Thermal analysis of PET
- Figure 4.12     Stress development with temperature
- Figure 4.13     Stress development with soak time
- Figure 4.14     (a) PP chords cast in-situ with mortar specimens, and (b) Hollow void in mortar specimens
- Figure 4.15     Load displacement responses in initial tests
- Figure 4.16     Specimen configuration
- Figure 4.17     Three-point bend test set up
- Figure 4.18     Load-CMOD results for specimens loaded in stage 1
- Figure 4.19     Load-CMOD results for stages 1 and 3 for: (a) PET specimens and, (b) PETr specimens
- Figure 4.20     Control specimens
- Figure 4.21     PET specimen: (a) cracked after stage 1 loading and, (b) with crack closed as a result of tendon activation (stage 3)
- Figure 5.1      Test set up of a typical specimen subject to three-point bending with DIC measurement
- Figure 5.2      Speckled image pattern for correlation
- Figure 5.3      Comparisons between DIC and clip gauge CMOD values for Ctrl2b specimen in AH regime 2



- Figure 5.4 Results for typical specimens in AH1: (a) PETr, and (b) PET
- Figure 5.5 Results for typical specimens in AH2: (a) PETr, and (b) PET
- Figure 5.6 Results for typical specimens in AH3: (a) PETr, and (b) PET
- Figure 5.7 Results for control specimens for all AH regimes (a) stage 1, and (b) stage 3
- Figure 5.8 Specimen with (a) induced crack at stage 1, and (b) after tendon activation and healing at stages 2a and 2b
- Figure 5.9 Strain profile analysis 1- 4 using DIC
- Figure 5.10 Strain profile CMOD points
- Figure 5.11 Strain profiles for a healed specimen using DIC: (a) CMOD I, (b) CMOD II, and (c) CMOD III
- Figure 6.1 Crack softening relationship
- Figure 6.2 Beam model
- Figure 6.3 Specimen dimensions
- Figure 6.4 Numerical response
- Figure 6.5 Stress development of PET
- Figure 6.6 Stress development of PET at 90 °C
- Figure 7.1 Autonomic healing system with continuous supply network and a dual-layer supply tube set up that prevents blockages
- Figure 7.2 Triaxial confinement for the shrinkable polymer cementitious material system

## Symbols and abbreviations

$b$	width of specimen
$b_w$	width of hollow
$d_n$	depth of notch
$E$	Young's modulus
$F$	peak load
$f_{cu}$	cube strength of specimen
$f_{healed}$	healed cracking stress
$f_{split}$	splitting tensile strength of specimen

---

$f_{ti}$	cracking stress
$G_f$	specific fracture energy
$h$	height of specimen
$h_w$	height of hollow
$T_g$	glass transition temperature
$T_m$	melting temperature
$T_{trans}$	transformation temperature
$w_c$	crack band width
$y$	strain at a given level
$\epsilon$	strain
$\sigma$	beam fibre stress
$\sigma_p$	polymer prestress
$\psi$	curvature
AH	activation-healing
BFSC	blast furnace slag cement
CMOD	crack mouth opening displacement
CMOD <sub>cg</sub>	crack mouth opening displacement from clip gauge
CMOD <sub>dic</sub>	crack mouth opening displacement from digital image correlation
CSMP	castable shape memory polymer
Ctrl	control specimen
Darpa	Defence advanced project research agency
DIC	digital image correlation
DL-5	double layer of 5 capillary tubes
DMA	dynamic mechanical analyser
ECC	engineered cementitious composite
ESEM	environmental scanning electron microscope
FRC	fibre reinforced concrete
FRCC	fibre reinforced cementitious composite
FRP	fibre reinforced polymer
GFRPP	glass fibre reinforced polypropylene
LVDT	linear variable differential transducer
NiTi	nickel titanium alloy

---

OPC	ordinary Portland cement
PE	polyethylene
PET	polyethylene terephthalate
PP	polypropylene
RC	reinforced concrete
RILEM	Réunion Internationale des Laboratoires d'Essais et de Recherches sur les Matériaux et les Constructions
SH	self-healing
SL-5	single layer of 5 capillary tubes
SMA	shape memory alloy
SMM	shape memory material
SMP	shape memory polymer
SWNT	single-wall carbon nanotube
TFX	magnetically induced shape memory polymer
TSP	triple shape polymer
UPV	ultrasonic pulse velocity
W/C	water/ cement
WPP	woven polypropylene

# Chapter 1

## Introduction

### 1.1 Inspiration from nature

The ability of natural materials to continuously adapt and evolve to environmental changes has been recognised by material scientists and engineers in attempts to emulate these processes. This transfer of technology from nature into man-made materials is termed biomimetics, coined by Otto Schmitt in 1957 (Vincent et al., 2006).

This inspiration from nature is shown in various aspects of daily life. Examples include the design of aircraft and the development of wing technology influenced by birds, the replication of shark skin to reduce drag in bodies and the development of functional materials such as Velcro. The latter was invented by George de Mastral who was inspired by the hooked seeds of the Burdock plant that became caught in the fur coat of his dog (Bhushan, 2009).

An area that has attracted particular interest in recent times is that of natural materials that have the ability to self-heal. The self-healing properties of lime cement used by the Romans and the oxide layers that prevent corrosion in certain metals have encouraged self-healing studies (van der Zwaag, 2007). As discussed by van der Zwaag (2007), the strategies to improve the strength and reliability of man-made materials have been largely based on the concept of “damage prevention”. In this case, materials are designed with the function of delaying damage. More recently, material scientists and engineers have addressed the strategy of “damage management”. In this case, materials are developed to be more efficient and have built in functions such as the ability to self-repair and are often termed smart materials.

Li et al. (1998a) suggested several factors that smart materials require in order to be practical in civil engineering. These include low cost, a smartness that has a passive

capability requiring no external monitoring and which is distributed throughout the material. The development of smart materials is becoming a much more attractive option as highlighted in dedicated conferences of self-healing materials (Delft 2007, Chicago 2009, and Bath 2011). The motivation is therefore to provide more durable materials that will enhance the service life and provide efficient, functioning and sustainable solutions.

## **1.2 Cementitious materials**

Providing more sustainable solutions for cementitious materials is necessary because concrete is the most used man-made building material on the planet (van Oss, 2005). Since the development of hydraulic cements and the patent of Portland cement (PC) in 1824, the use of concrete structures has been considerable (Neville, 1999). The reaction of PC in the presence of water forms hydration products that result in a bonding agent. In time, this forms a hardened cement paste. The combination of PC, water and sand results in the material called mortar and the addition of aggregate to the mix results in the material called concrete.

The compressive strength of concrete is typically between 20 and 60 MPa and can be deemed its most valued asset. Concrete strength is governed by the mix proportions and to an extent the degree of its compaction. Although strong in compression, concrete is weak in tension and in general the tensile strength of concrete is approximately one tenth of the compressive strength. The production of high strength concrete can provide compressive strengths between 150 and 200 MPa that are obtained by a low water/cement ratio and often the addition of superplasticiser.

## **1.3 The issues of durability**

Cracking is one of the major causes of concrete degradation and is typically initiated by thermal effects, early age shrinkage, mechanical loading or a combination of these actions. These cracks can in turn lead to the ingress of water, acid rain and carbon dioxide. The design of reinforced concrete (RC) structures has addressed this aspect of durability for many years by requiring crack widths to be limited. However, significant

proportions of RC structures still have problems with durability (Richardson, 2002). By comparison, pre- and post-tensioned structures are generally designed to be uncracked and provide a more durable solution. However, the application of pre- and post-tensioning is relatively costly and requires the use of jacking and anchorage operations.

Several investigations have explored the use of shape memory alloys (SMAs) (Czaderski et al., 2006; El-Tawil & Ortega-Rosales, 2004) and the use of fibre reinforced polymers (FRP) (Lees, 2001) to replace traditional pre- and post-tensioning tendons. In both cases the provision of pre- and post-tensioning has proven to be effective. SMAs provide the advantages of simplifying the tendon installation with the absence of jacking equipment as SMAs can be triggered by an external stimulus to induce post-tensioning. As a result, relaxation and friction losses through the anchorage system can also be minimised. FRPs provide a lightweight and non-corrosive option in comparison to its steel counterpart. However, in both SMAs and FRPs the associated high costs of the raw materials, new technology, individual cases and low production volume have limited their use to generally specialised applications.

## **1.4 The financial and environmental impact**

In the UK, the costs of repair and maintenance account for almost half of the total spend in construction per year as highlighted in Figure 1.1. These high costs provide the motivation to develop more sustainable solutions with the aim of minimising the costs associated with maintenance.

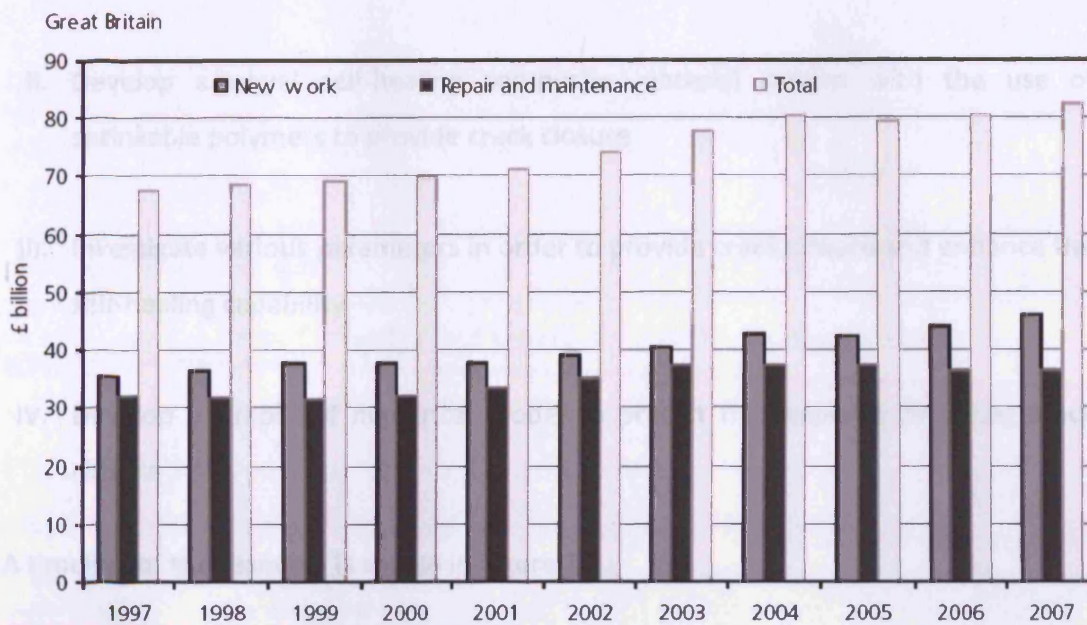


Figure 1.1 Billions of pounds spent on repair and maintenance and new construction work (ONS, 2008)

Concrete also has a substantial environmental impact due to the associated high levels of CO<sub>2</sub> output. The production of one tonne of concrete produces approximately one tonne of CO<sub>2</sub> and it is estimated that more than 10 billion tonnes of concrete are produced each year. On a worldwide scale, concrete is responsible for about 7 % of all CO<sub>2</sub> generated (Meyer, 2009). The concrete industry is now focused on providing more sustainable solutions toward reducing the CO<sub>2</sub> output. The methods of reducing CO<sub>2</sub> include the replacement of PC with materials such as fly ash, silica fume, ground granulated blast furnace slag and the use of recycled materials. The motivation to reduce both the financial and environmental impacts fundamentally comes down to developing more durable materials with greater mechanical performance that will enable a longer service life and minimise the amount of material required in structures.

## 1.5 Scope and objectives

The scope and objectives of this research are to:

- I. Investigate the self-healing mechanisms associated with cementitious materials addressing both autonomic and autogenous healing

- II. Develop a novel self-healing composite material system with the use of shrinkable polymers to provide crack closure
  
- III. Investigate various parameters in order to provide crack closure and enhance the self-healing capability
  
- IV. Develop a simplified numerical model to predict the response following crack closure

A timeline of the research is shown in Figure 1.2.



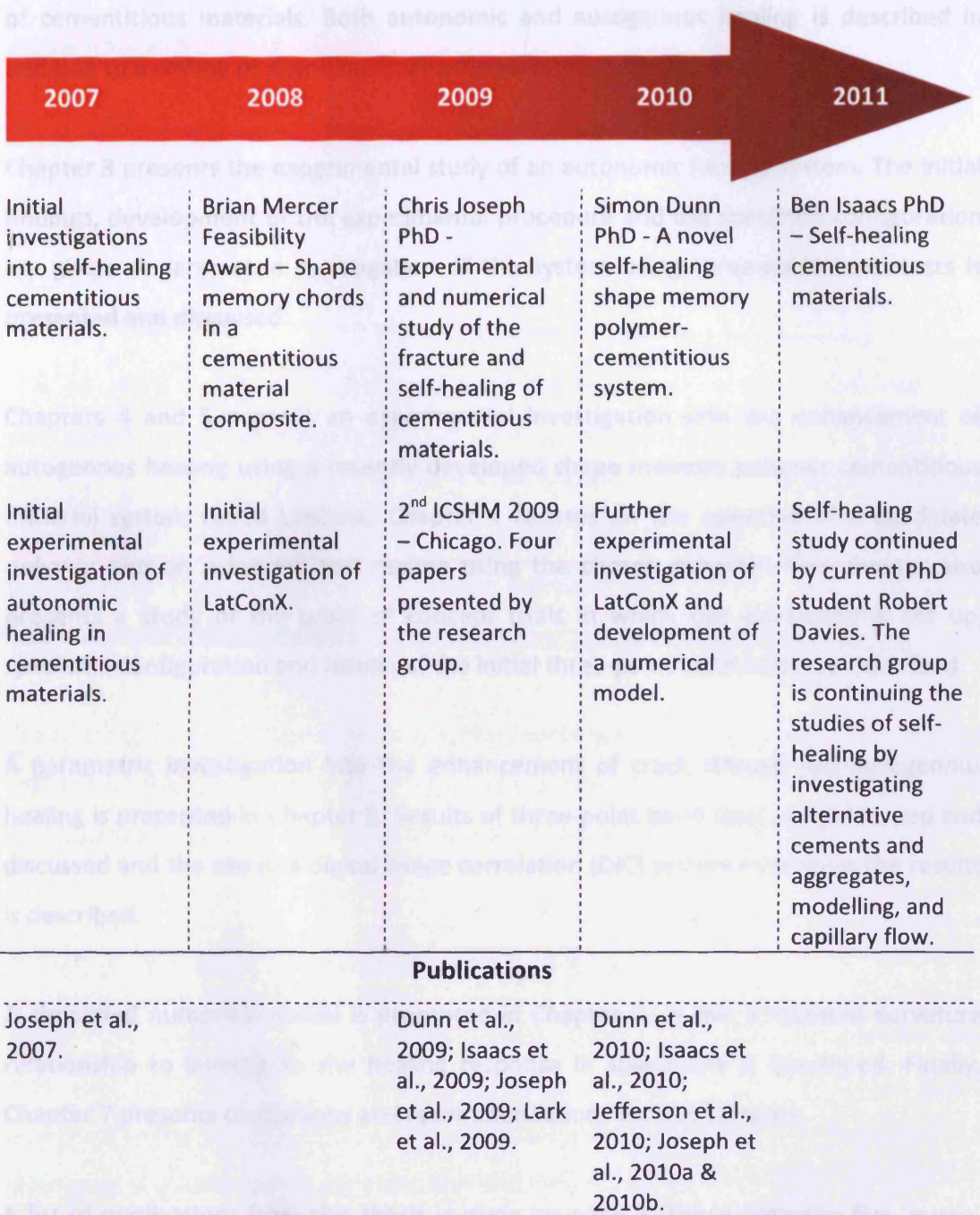


Figure 1.2 Timeline of the research

## 1.6 Outline of the thesis

This thesis is divided into 7 Chapters and 5 appendices. Chapter 2 reviews the current state of the art in self-healing materials with particular focus given to the self-healing

of cementitious materials. Both autonomic and autogenous healing is described in addition to a review of shape memory polymers.

Chapter 3 presents the experimental study of an autonomic healing system. The initial findings, development of the experimental procedure and the specimen configuration are given. A parametric investigation of the system using three-point bend tests is presented and discussed.

Chapters 4 and 5 present an experimental investigation into the enhancement of autogenous healing using a recently developed shape memory polymer cementitious material system called LatConX. Chapter 4 focuses on the selection of a candidate polymer and an extended test regime using the chosen polymer. This chapter also presents a study of the proof of concept trials in which the experimental set up, specimen configuration and results of the initial three-point bend tests are described.

A parametric investigation into the enhancement of crack closure and autogenous healing is presented in Chapter 5. Results of three-point bend tests are presented and discussed and the use of a digital image correlation (DIC) system to process the results is described.

A simplified numerical model is presented in Chapter 6. In this a moment curvature relationship to investigate the healing response in specimens is developed. Finally, Chapter 7 presents conclusions and recommendations for further work.

A list of publications from this thesis is given on page v. These comprise five journal papers, four of which are in print and one of which is presently under consideration, as well as four conference publications. In addition, two further publications are to be presented at the forthcoming International Conference on Self-Healing Materials (ICSHM 2011).

## **Chapter 2**

### **Literature review**

#### **2.1 Introduction**

This literature review investigates the current development of self-healing materials with specific attention given to the self-healing of cementitious materials. Details of the healing mechanisms associated with both autogenous and autonomic healing are described. In addition, the current research into shape memory polymers is investigated. The classification of shape memory polymer structures, activation methods and current applications is described.

The purpose of this review is to identify the conditions that enhance both autogenous and autonomic healing and review the application of shape memory polymers to facilitate crack closure and hence, autogenous healing of cementitious materials.

#### **2.2 Classification of materials and structures**

Within the engineering and material science community, the development and characterisation of new and existing materials and structures has led to some ambiguity between terms. Within the literature, increasing attention has been made of intelligent and smart materials; and smart and sensory structures due to their scientific significance. Several authors have identified a classification of these terms (Joseph, 2009; RILEM, 2011; Mihashi et al., 2000; Wei et al., 1998) which will be described.

##### **2.2.1 Intelligent materials**

Intelligent materials, as described by Takagi (1996), possess sensing, processing and actuating functions. The sensing function can detect an environmental change or inner

anomaly; the processing function will make a decision and the actuating function then provides the material's response. Mihashi et al. (2000) lends a further insight, defining intelligent materials as having a "higher level function" that incorporates the notion of information as well as a physical index such as strength and durability. This self control capability of intelligent materials is perhaps best observed in natural materials such as skin, bone and tendons. Schmets (2003) attributes the mechanisms of self control in natural materials to the result of a highly organised hierarchical structure that is present at all levels (length scales) in the material.

The mechanisms inherent in natural materials are difficult to reproduce in man-made materials due to the unique microstructures of the former. However, the challenge to develop intelligent materials is being actively pursued in the fields of medicine, bioengineering, polymers, metallurgy and aerospace.

### **2.2.2 Smart materials**

In comparison to intelligent materials, smart materials are engineered in order to produce a unique beneficial response to an environmental change (Sharp and Clemena, 2004). As described by Wei et al. (1998), a smart material should be able to respond to an environmental stimulus in a predetermined manner within an appropriate time, and revert back to an original state when the stimulus is removed. Examples of smart materials include shape memory materials, piezoelectric composites, which convert electric current to mechanical forces, electro-rheological and magneto-rheological fluids, which can change from liquid to solid (or vice versa) in electric and magnetic fields (Chong and Garboczi, 2002). As defined by Joseph (2009), the difference between smart and intelligent materials is the degree to which the material can gather and process information and react in an appropriate manner.

### **2.2.3 Smart Structures**

Smart structures are similar to smart materials in the fact that both exhibit sense, actuation and response properties. Smart structures are engineered composite materials with the individual component properties ultimately providing the sense,

actuation and response functions. The classification of smart materials and smart structures by Chong and Garboczi (2002) is defined according to the size of the components as shown in Figure 2.1. A smart material can be designed at the nanoscale, molecule by molecule whereas a smart structure is more likely to be designed at a meso or macro scale that is typical of its components. Examples of smart structures can therefore include the self-healing materials which will be discussed in greater detail in Section 2.2.5.

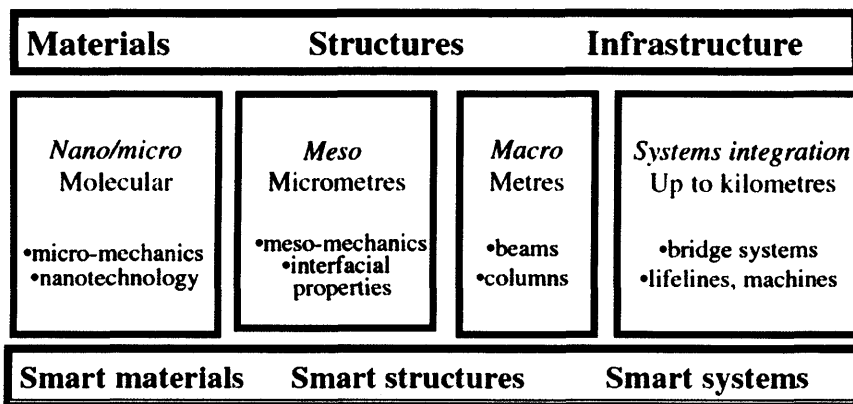


Figure 2.1 Scales in materials and structures (Chong and Garboczi, 2002)

### 2.2.4 Sensory structures

Sensory structures have the ability to sense an environmental change but do not possess the properties to trigger a response. Examples of sensory structures include: smart fibres that incorporate tiny strain sensors in which real-time strains can be monitored to act as a structural health check for detection of damage; smart paints that contain silicon microspheres that act as a coating degradation sensor; and smart bricks which are able to monitor movement, vibration and temperature (Sharp and Clemena, 2004).

### 2.2.5 Self- healing materials

Within the context of the classifications described, many self-healing materials fall into the category of smart structures (Joseph, 2009) as highlighted in Figure 2.2.

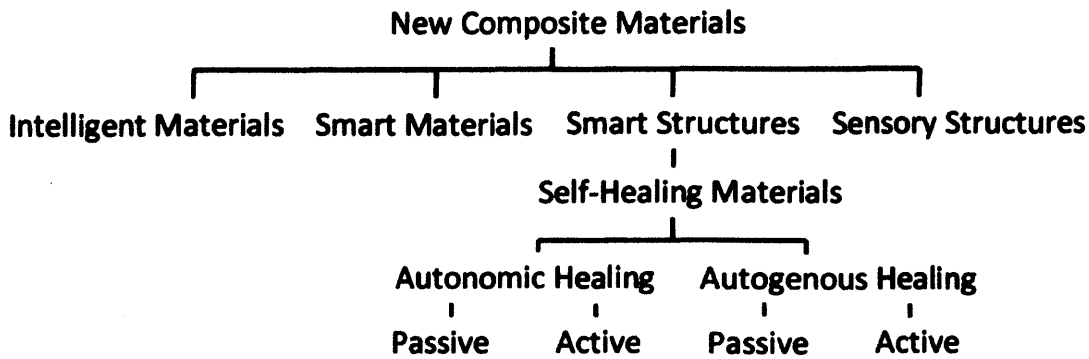


Figure 2.2 Material classification

Self-healing materials can be classed as smart structures because they are often composite structures that exhibit sensing, actuation and response characteristics. The healing response is a product of the materials ability to sense an environmental change, process this information and act upon it. van der Zwaag (2007) presented research in the self-healing fields of polymers, composites, ceramics, metals, coatings and adhesives. Within the field of new composite materials, the self-healing of cementitious materials can be classed as smart structures (Kuosa, 2000). These smart, self-healing structures rely on the previous knowledge of failure/damage mechanisms to which they are at risk and are consequently classed as smart rather than intelligent (Joseph, 2009).

The self-healing capability of cementitious materials can be classed as either autogenous or autonomic. Autogenous healing is where the healing properties of the material are generic to that material; and autonomic healing is where the self-healing capabilities are due to the release of encapsulated healing agents. Autogenous and autonomic healing methods will be discussed in greater detail in Sections 2.3 and 2.4 respectively.

### **2.2.6 Active and Passive self-healing**

Active and passive are the terms given to the actuation mode of smart self-healing materials and structures. Materials that require activation by intervention are known

as active, whereas passive materials do not require intervention in order to react to an external stimulus. Dry (1994) studied the self-healing response of cementitious materials using both active and passive modes as illustrated in Figures 2.3 and 2.4. The active mode investigated the use of wax fibres that required melting in order to release the healing agent into cracks. The benefit of this is the confidence gained from human intervention, but this in turn increases the cost.

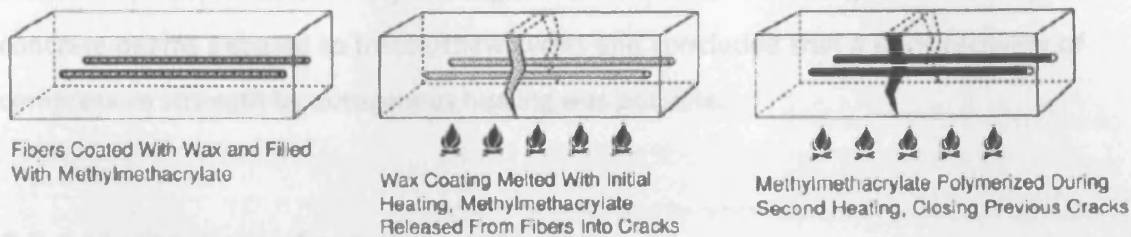


Figure 2.3 Active method of repairing cracks by melting wax coated fibres to release methylmethacrylate (Dry, 1994)

The passive mode investigated the release of healing agents from hollow glass fibres into concrete to fill cracks. The ability to react with freedom from external control has the potential to reduce costs due to the self-healing capability that could limit the need for maintenance. The passive mode also addresses the issues of limited access to damage.

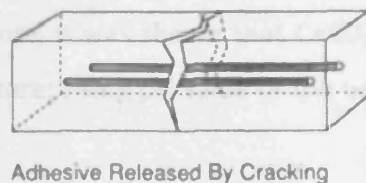


Figure 2.4 Passive release initiated by the physical cracking of the test sample (adapted from Dry, 1994)

## 2.3 Autogenous Healing

Autogenous healing in cementitious materials is a natural healing process that has been recognised for many years and was first reported by the French Academy of

Science in 1836 (Hearn, 1998). This natural phenomenon to heal cracks in fractured cementitious material has been observed in old structures that come into contact with water. Studies have since investigated the self-healing of cracks that are exposed to moisture. Clear (1985) investigated the effects of autogenous healing upon the leakage of water through various crack widths in concrete and observed a self-sealing effect that was faster in smaller crack widths. Jacobsen et al. (1996) have considered the effect of cracking and healing on chloride transport in OPC concrete. Jacobsen and Sellevold (1996) examined the strength recovery due to autogenous healing of concrete beams exposed to freeze/thaw cycles and concluded that a 4-5% recovery of compressive strength by autogenous healing was possible.

### ***2.3.1 Mechanisms of autogenous healing***

Self-healing in concrete was studied by Edvardsen (1999) who conducted both experimental and theoretical research into the effects of crack healing. Water permeability tests on small scale concrete specimens with varying crack widths and crack lengths were conducted in order to determine the autogenous healing response. The results confirmed that cracked specimens subjected to water pressure were able to heal themselves and the greatest autogenous healing effect was shown to be in early age specimens exposed to water between 3 and 5 days. The precipitation of calcium carbonate ( $\text{CaCO}_3$ ) was reported as the sole cause of autogenous healing within the cracks. Furthermore, it was shown that  $\text{CaCO}_3$  precipitation was improved with a rising water temperature; rising pH value of the water; and a falling  $\text{CO}_2$  partial pressure in water.

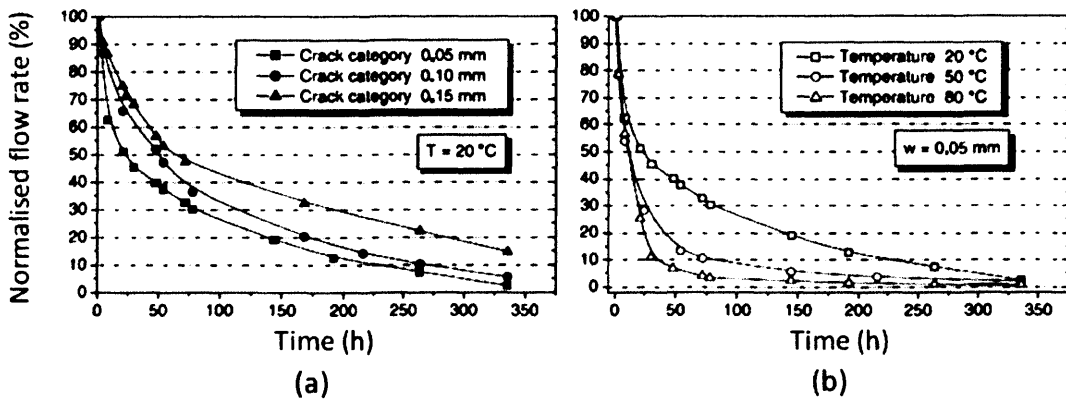
However, in addition to the formation of  $\text{CaCO}_3$  described by Edvardsen (1999) as the sole cause of autogenous healing, further mechanisms of autogenous healing, also referred to as self-closing mechanisms have been reported (RILEM, 2011; Schlangen and Joseph, 2009; ter Heide et al., 2005). The primary causes of autogenous healing can be summarised by (i) swelling and hydration of cement pastes, (ii) precipitation of calcium carbonate crystals, and (iii) blockage of flow paths due to deposition (Schlangen and Joseph, 2009). Consequently, for autogenous healing to occur in



cementitious materials, the presence of water and cement is needed in order to promote the chemical reactions at the crack surfaces. As a result of the reaction between water, unhydrated cement and  $\text{CO}_2$ , the crystallisation product ( $\text{CaCO}_3$ ) can be deposited on opposite faces of a crack that can eventually re-establish the continuity of the material. At present, very little information is presented with regard to the tensile capacity of these self-healing mechanisms.

The blockage of flow paths by a build up of  $\text{CaCO}_3$  is not necessarily the only healing process that reduces the permeability through a crack. The blockage can also be attributed to water impurities and concrete particles broken from the crack surfaces due to cracking. ter Heide et al. (2005) classified this blockage of a crack by small particles as “self-tightening”. However, these effects are believed to be of minor importance when compared to the mechanisms of self-closing.

Reinhardt and Jooss (2003) investigated the self-healing of cracked concrete as a function of crack width and temperature. Permeability tests were conducted on small scale high-performance concrete specimens. The specimens were tested at crack widths of 0.05, 0.10 and 0.15 mm and subject to temperatures of 20, 50 and 80 °C. Figure 2.5(a) shows the normalised flow rates through specimens with varying crack widths subject to the same healing temperature. Figure 2.5(b) does likewise for specimens with the same crack width but subject to varying healing temperatures.



Note: the curves are derived from the mean values of tested specimens and the flow rate is normalised with respect to the flow rate at the beginning of the tests.

Figure 2.5 (a) Normalised flow rate for specimens with various crack widths at a constant temperature (b) Normalised flow rate for specimens with a constant crack width ( $w = 0.05\text{mm}$ ) at various temperatures (Reinhardt and Jooss, 2003)

The results concluded that a decrease in flow rate was dependant on crack width and temperature. Self-healing was found to be quicker in smaller cracks and a higher temperature favoured a faster self-healing process. However, what is unclear from the author’s findings is the mechanism of self-healing. Permeability tests that measure the flow rate through cracks do not identify the properties of the crack surfaces and therefore in this case, it is not clear whether autogenous healing and/or self-tightening was the mechanism by which the flow rates were controlled.

The influence of the degree of damage on the self-healing of small scale normal and high strength concrete specimens at different ages has been reported by Zhong and Yao (2008). In an alternative to permeability testing, ultrasonic pulse velocity (UPV) levels were measured in order to quantify the degree of self-healing. In this method, concrete cubes ( $100 \times 100 \times 100 \text{ mm}$ ) were damaged by compression testing and the effects of specimen age were studied. Normal strength cubes damaged on days 7, 14 and 28 were subsequently cured at  $20 \text{ }^\circ\text{C}$  for 30 days. High strength cubes damaged on days 3, 14, 28 and 60 were subsequently cured at  $20 \text{ }^\circ\text{C}$  for 60 days.

The results concluded that there exists a damage threshold for both normal and high strength concrete. When the damage degree is lower than the threshold, there is an increase in self-healing ratio with increasing degree of damage, whilst if the damage degree is higher than the threshold, the self-healing ratio decreases with increasing degree of damage. The results also found that the strength recovery was greatest in early age specimens. The authors claim that this was the result of less unhydrated cement grains in older specimens. As with the observations made by Reinhardt and Jooss (2003), the results only serve to measure the durability as a result of autogenous healing and do not provide quantitative answers with respect to mechanical recovery.

### ***2.3.2 Mechanical response of autogenous healing***

As previously reported, Edvardsen (1999) observed that autogenous healing had the greatest effect in early age specimens. In more recent work by ter Heide et al. (2005), crack healing was investigated by measuring both the mechanical strength and permeability of early age concrete specimens. Although permeability tests provide evidence of self-healing the use of mechanical testing is required to measure its effectiveness in terms of the recovery of the materials strength.

In order to measure the recovery of the mechanical properties of concrete, ter Heide et al. (2005) set up a three-point bend test using 40 x 40 x 160 mm prismatic specimens as shown in Figure 2.6(a). The specimens were initially loaded to a predetermined crack width and then unloaded. They were then stored in water for 2 weeks while subject to a compressive force (Figure 2.6(b)) in order to create contact points between the crack surfaces. After a 2 week healing period, the specimens were tested to failure. The variables included: the amount of compressive force applied during healing, which ranged between 0.0 and 2.0 N/mm<sup>2</sup>; the specimen age at initial cracking, which ranged between 20 and 72 hours; and the crack mouth opening of the initial crack, which ranged between 0.02 and 0.15 mm.

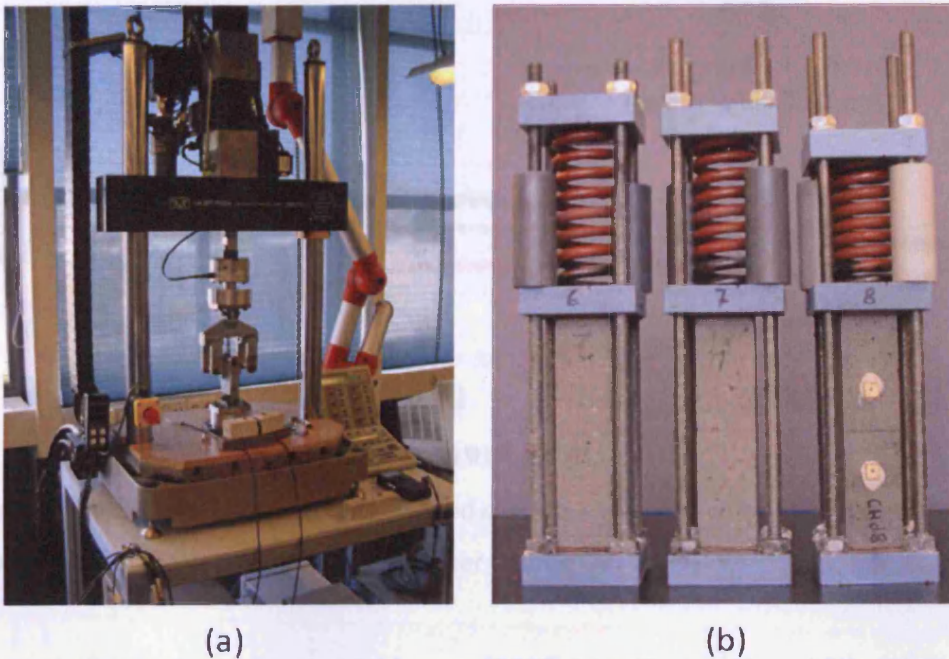


Figure 2.6 (a) Three-point bending test set up (b) Compression device for initially cracked specimens (ter Heide et al., 2005)

The experimental investigation concluded that crack healing was observed in early age specimens that were cured in water and thereafter subject to a compressive stress as shown in Figure 2.7. The width of cracks did not influence the strength recovery and it was observed that a minimal compressive stress of  $0.5 \text{ N/mm}^2$  was required in order to provide crack closure. Specimens damaged at the earliest age developed the greatest strength recovery and this decreased with specimen age. The authors commented that they believed the main process responsible for the healing behaviour was the ongoing hydration due to crack closure.

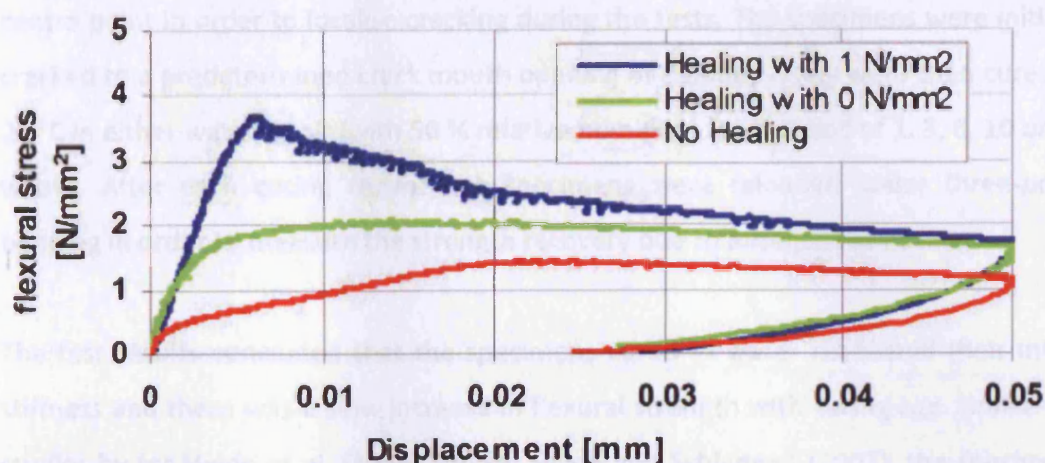


Figure 2.7 Stress-displacement curve of healed specimen with and without compressive stress, compared with unhealed cracked specimen (ter Heide et al., 2005)

Further studies by ter Heide and Schlangen (2007) investigated the additional variables of cement type and relative humidity during curing using the same experimental procedure described in ter Heide et al. (2005). It was observed that crack healing was achieved in both cement types studied, Ordinary Portland Cement (OPC) and Blast Furnace Slag Cement (BFSC). The potential for crack healing was found to be higher in OPC concrete due to the higher levels of unhydrated cement. This contradicts the results of permeability tests conducted by van Tittelboom and De Belie (2009a) who observed that BFSC resulted in a higher degree of healing.

ter Heide and Schlangen (2007) also concluded that only the specimens cured in water during healing exhibited a strength recovery. ESEM (environmental scanning electron microscope) observations were made which confirmed that the cracks were filled with a reaction product and that the disappearance of surface cracks was an indication of self-healing.

The mechanical behaviour of self-healed concrete under three-point bending has also been studied by Granger et al. (2007). The study investigated the effects of curing specimens in water and air for varying lengths of time. The ultra high performance cementitious material was considered a model material because it had a W/C ratio close to 0.2. Specimens (50 x 100 x 500 mm) were notched to a depth of 20 mm at the

centre point in order to localise cracking during the tests. The specimens were initially cracked to a predetermined crack mouth opening of 0.01mm. They were then cured at 20 °C in either water or air (with 50 % relative humidity) for a period of 1, 3, 6, 10 or 20 weeks. After each curing regime the specimens were reloaded under three-point bending in order to measure the strength recovery due to autogenous healing.

The test results concluded that the specimens cured in water recovered their initial stiffness and there was a slow increase in flexural strength with curing age. Unlike the studies by ter Heide et al. (2005) and ter Heide and Schlangen (2007), the specimens were not subject to compressive force in order to provide crack closure. In this instance, Granger et al. (2007) report that a build up of crystallised material between the crack surfaces generated the self-healing effect.

A comprehensive study of autogenous healing has been made on the engineered cementitious composites material known as ECC, developed at the University of Michigan (Yang et al., 2009). The composite material is often referred to as “bendable concrete” due to its highly ductile characteristics as a result of incorporating high-modulus polyethylene fibres into the cementitious matrix. Consequently, ECC has a tensile strain capacity that generally exceeds 1 % but has been known to measure up to 8 %. In Fibre Reinforced Concrete (FRC), after first cracking a typical post-peak tension softening curve is exhibited, but in ECC, first cracking is followed by a rising stress and increasing strain as shown in Figure 2.8. It is only after several percent of straining that the strain-hardening effect in ECC gives way to the common FRC response (Li and Kanda, 1998).

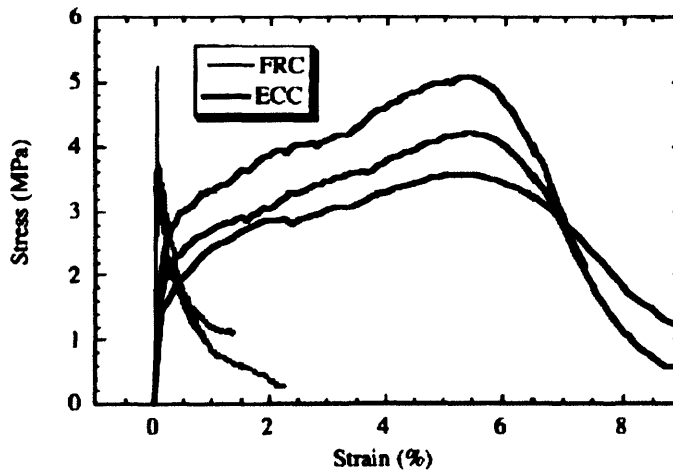


Figure 2.8 Tensile strain-hardening behaviour of ECC in comparison with FRC (Li et al., 1998a)

The autogenous healing of ECC has been examined by several methods: resonant frequency tests that analyse material degradation; tensile tests that measure the mechanical response; and permeability tests. Small scale specimens were prepared and left to air cure under laboratory conditions for 6 months, after which time they were subjected to predetermined uniaxial tensile strain levels of between 0.3 % and 3 %. After unloading, the specimens underwent one of two wetting and drying regimes, which consisted of either: submersion in water at 20 °C for 24 hours and drying in the laboratory at  $21 \pm 1$  °C for 24 hours (no temperature effects were considered); or submersion in water at 20 °C for 24 hours, oven drying at 55 °C for 22 hours, and cooling in the laboratory at  $21 \pm 1$  °C for 2 hours. Specimens that were subject to the tensile loading tests were notched to ensure that they exhibited a strain-softening response typical to FRC. Specimens were then loaded to predetermined crack widths of between 0 and 0.3 mm in order to measure the autogenous healing effect.

The results concluded that autogenous healing was observed in all the methods examined. In Figure 2.9, the autogenous healing of cracks (a) and the subsequent formation of new cracks (b) is shown. The authors attribute the mechanism of autogenous healing to the growth of calcites inside the tight cracks and noted that the majority of the self-healing products consisted of calcium carbonate crystals. In specimens subject to tensile straining, the extent of autogenous healing was greater in specimens subject to a lower strain. The authors concluded that for noticeable

autogenous healing to be achieved the crack width of specimens should be controlled to below 0.15 mm and preferably below 0.05 mm. The effects of curing regime showed that an increase in temperature led to an increase in ultimate strength but a decrease in strain capacity. Based on resonant frequency tests, the quality of self-healing was less in specimens subject to a higher temperature, which the authors claim was due to less uniform re-healing products being formed inside the crack.

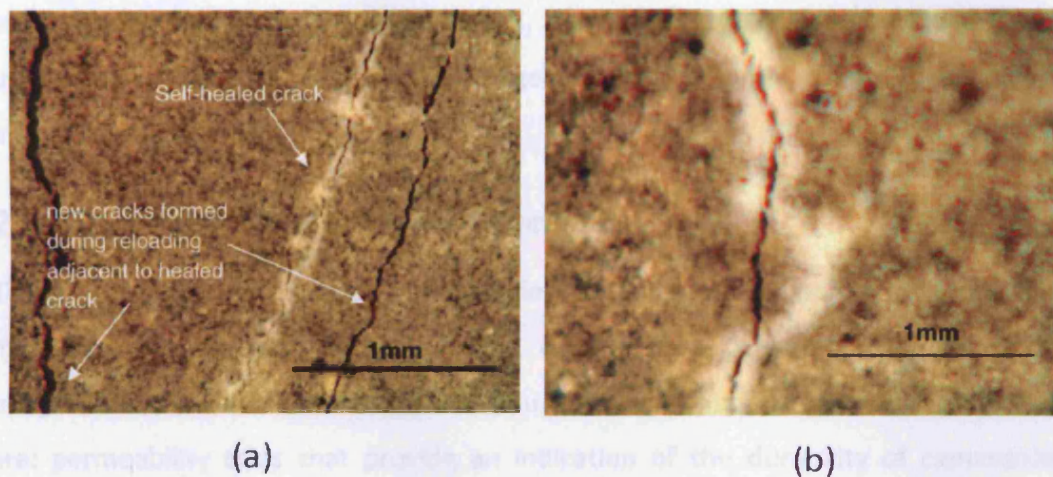


Figure 2.9 (a) Cracks in ECC material (b) New crack formed over previously healed crack (Yang et al., 2009)

In further studies exploring the potential of ECC, Qian et al. (2009a, 2009b) developed an ECC mixture incorporating local waste materials of blast furnace slag and limestone powder. The calcite build up attributed to autogenous healing was confirmed by ESEM observations and it was reported that the majority of the healing products within micro-cracks was calcium carbonate.

This has also been confirmed in other studies investigating autogenous healing in fibre reinforce cementitious composites (FRCC). Homma et al. (2009) investigated the self-healing capability of three types of FRCC. The inclusion of polyethylene fibres, steel cords and a hybrid fibre composite (both polyethylene and steel cord) were tested. Specimens were subject to cracking under tensile tests and subsequently cured in water for 28 days. Self-healing observations were made by permeability tests, microscope observation, tension tests and backscattered electron image analysis. The



results confirmed that a self-healing capability was present in all the FRCC specimens tested. The self-healing product was confirmed as calcium carbonate crystals, which reduced water permeability and increased recovery of tensile strength in specimens.

Other notable studies have investigated the autogenous healing of expansive agents in cementitious materials. Ahn and Kishi (2009) identified from microscopy observations that the incorporation of geo-materials and expansive agents in cementitious materials self-healed a 0.15 mm crack after 3 days. Kishi et al. (2007) also concluded that by using appropriate dosages of expansive agents and carbonates, the self-healing ability of cracks is increased.

### ***2.3.3 Enhancement of autogenous healing***

To date, the studies undertaken in the field of autogenous healing in cementitious materials have served to optimise the degree of self-healing. Various testing procedures have been observed that measure the effects of autogenous healing. These are: permeability tests that provide an indication of the durability of cementitious materials by measuring water flow through specimens; mechanical tests that provide an indication of the strength recovery in specimens due to autogenous healing; resonant frequency and UPV tests which can measure the degree of damage and the subsequent autogenous healing; and ESEM, that is utilised to assess the healing products that are deposited in the cracks.

These studies have shown that the self-healing effect that is exclusive to cementitious materials can be the result of autogenous healing and/or self-tightening. Further to this, a comprehensive set of parameters can be established that aims to enhance the autogenous healing effect. These include:

- Water - in order for autogenous healing to occur in cementitious materials the presence of water is required.
- Age – the degree of autogenous healing is greater in specimens at an early age.

- Crack width – the degree of autogenous healing is greater in specimens with smaller crack widths. Specimens with varying CMOD values have been reported in the literature that range between 0.01 mm to 0.30 mm (Granger et al., 2007; Reinhardt and Jooss, 2003; ter Heide et al., 2005; and Yang et al., 2009). Yang et al. (2009) report that for noticeable autogenous healing to occur, the crack width of specimens should be controlled to below 0.15 mm. However, at present a maximum allowable crack width is unknown.
- Temperature – an increase in water curing temperature provides an increase in the degree of autogenous healing. Furthermore, Yang et al. (2009) observed that high temperature curing in a dry environment served to decrease the degree of autogenous healing and stated that more research in this area was required.
- Compression – the degree of autogenous healing can be improved by crack closure due to a compressive force.

Studies have shown that specimens which exhibit autogenous healing have the ability to recover their initial strength. In studies by ter Heide et al. (2005), autogenously healed specimens exhibited a peak load recovery when compared to the peak loads of pre-damaged specimens. However, at present there is no published experimental data reporting either a significant increase or repeatability in strength recovery. Furthermore, ter Heide et al. (2005) describe that the strength of the healed crack as a result of autogenous healing is greater than the equivalent natural strength gain of the bulk material. ter Heide et al. (2005) attribute these findings to the access of water, whereby full hydration is possible around the crack region in comparison to limited water access in the bulk material.

## **2.4 Autonomic Healing**

The field of autonomic healing in cementitious materials is still very much in a conceptual design phase and in comparison to autogenous healing, has received far

less attention. In contrast, the self-healing in polymer composites has received great attention over the last decade as a result of the autonomic healing concept, inspired by biological systems and developed by researchers at the University of Illinois, Urbana-Champaign (Sottos, 2009; Kessler et al., 2003; White et al., 2001).

### 2.4.1 Autonomic healing in polymer composites

The concept of autonomic healing in polymer composites incorporates a micro-encapsulated healing agent and a catalyst into a polymer matrix. As a crack propagates, the microcapsule is ruptured, releasing the healing agent into the crack plane through capillary action. Once the healing agent comes into contact with the embedded catalyst, the process of polymerisation takes place, bonding the crack faces closed, as illustrated in Figure 2.10.

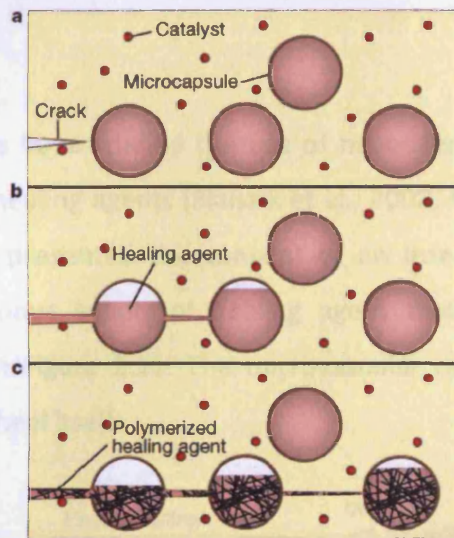


Figure 2.10 The three stages (a, b and c) of the autonomic healing concept in polymers (White et al., 2001)

The use of microcapsules allows for multiple cracks to be healed. However, in order for the concept to be successful, analysis of the geometry and toughness of the embedded microcapsules needs to be made. It was concluded that if the microcapsule walls were too thick, the crack may not rupture the microcapsule. Alternatively, if the capsule walls were too thin, they may rupture during processing. The study accounted for the toughness and relative stiffness of the microcapsules, as well as the strength of the

interface between the microcapsule and the matrix. Stinson (2001) highlighted that if the microcapsules were too stiff, the stress distribution would cause the crack to grow away from them. Helmer (2001) also suggested the healing agent within the microcapsules needed to remain stable, yet be fluid enough to fill the cracks once it had been released.

The results by White et al. (2001) showed that specimens exhibited a peak recovery of 75 % in toughness with an average healing efficiency of 60 %. The study also concluded that the addition of microcapsules and catalyst into the polymer matrix increased the inherent toughness. One of the notable limitations was that the encapsulation technique provided only a limited supply of healing agent in microcapsules. The random distribution of embedded microcapsules also provided a limited sensing capability by the fact there was no assurance of a crack propagating through a microcapsule.

More recent approaches have studied the use of nanocapsules and hollow fibres to enhance the release of healing agents (Blaiszik et al., 2008; Mookhoek et al., 2009). In addition, Sottos (2009) presented the concept of an interconnected microvascular network with a continuous supply of healing agent that enables repeated crack healing, as illustrated in Figure 2.11. The microvascular network is inspired by the ability of human skin to heal itself.

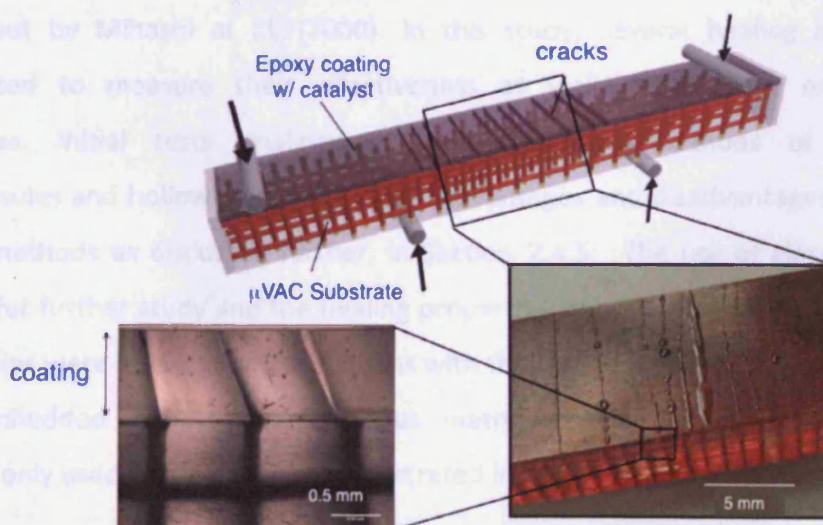


Figure 2.11 Repeated healing in a microvascular network (Sottos, 2009)

### **2.4.2 Autonomic healing in cementitious materials**

The first study of autonomic healing in cementitious materials by Dry (1994) adopted the same concept developed in polymers by White et al. (2001), as illustrated in Figure 2.10. The study by Dry (1994) investigated the internal release of chemicals from hollow fibres in both active and passive modes as previously discussed in Section 2.2.6.

The active mode investigated the release of methylmethacrylate from inside hollow wax coated polypropylene fibres into the cementitious matrix. Low heat was applied to the fibres in order to melt the wax coating and release the methylmethacrylate. The passive mode investigated the use of brittle hollow glass tubes, which when subject to a flexural stress, crack and release adhesive into the cementitious matrix. The release of the adhesive into the damaged zone was shown develop a strength recovery of the specimens. The results from both methods were largely qualitative but the concept of delivering a chemical from an internal release system into the outside matrix was proven. Further studies (Dry, 1996; Dry and Unzicker, 1998; Dry, 2000; Dry and Corsaw, 2003) have been undertaken in this area, but there is still a lack of quantitative measures of their success.

### **2.4.3 Mechanical response of autonomic healing**

One of the pioneering studies into autonomic healing of cementitious materials was carried out by Mihashi et al. (2000). In this study, several healing agents were investigated to measure their effectiveness as well as different encapsulation techniques. Initial tests analysed the encapsulation methods of embedded microcapsules and hollow glass tubes, with advantages and disadvantages recognised in both methods as discussed further, in Section 2.4.5. The use of glass tubes was selected for further study and the healing properties of both alkali-silica solutions and epoxy resins were investigated. Specimens with the two part epoxy resin had two glass tubes embedded into the cementitious matrix and specimens with alkali-silica solutions only used one glass tube, as illustrated in Figure 2.12.

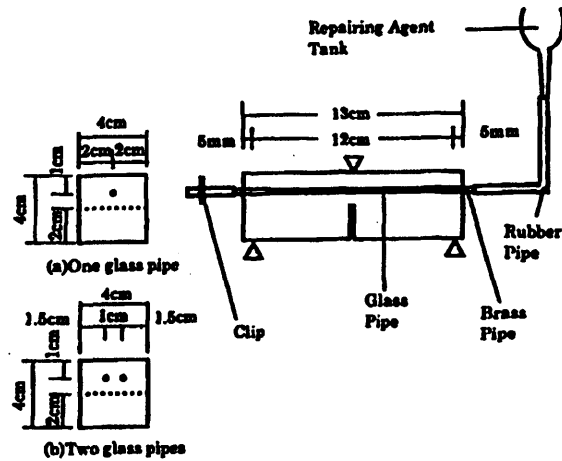


Figure 2.12 Specimen configuration and test set up (Mihashi et al., 2000)

Small scale (40 x 40 x 130 mm) specimens with a central notched region were subject to three-point bend tests. As illustrated in Figure 2.13, specimens were loaded beyond their peak flexural load and unloaded at a value  $P_1$ . After a curing period (healing time) the specimens were reloaded to measure the self-healing effect and the peak load,  $P_r$ , was used to measure the strength recovery ratio,  $P_r/P_1$ .

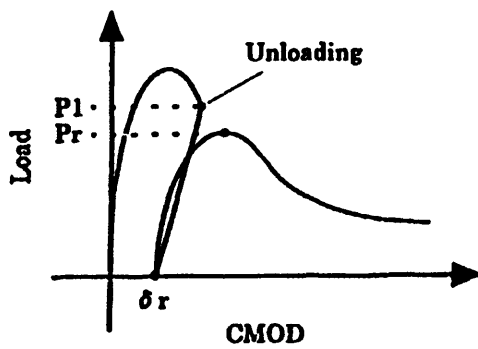
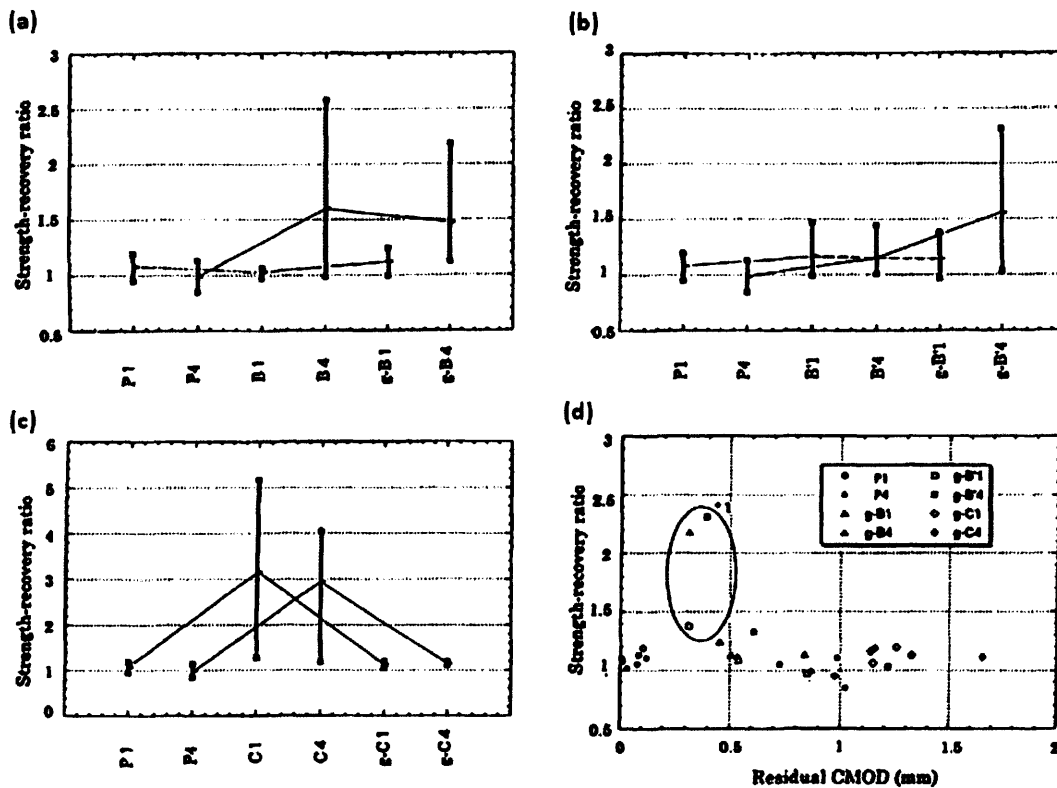


Figure 2.13 Load vs. CMOD for specimens (Mihashi et al., 2000)

A comparison was made between specimens containing both healing agents, control specimens containing no healing agent and specimens with manually injected healing agent. Figure 2.14 shows the results of all self-healing experiments carried out. The results showed that the specimens with alkali-silica solutions developed an increase in strength recovery ratio, with the diluted alkali-silica solution showing higher recovery due to its lower viscosity. The specimens containing epoxy resin showed no significant increase in strength recovery ratio when using glass tubes to supply the adhesive due

to insufficient mixing of the two part epoxy resin. However, by manual injection the strength recovery ratio showed a significant increase. Further to this, the results showed that the strength recovery was greater for specimens with a crack mouth opening displacement (CMOD) of less than 0.50 mm, as illustrated in Figure 2.14(d).



NOTE: P = control specimens (no healing agent); B = alkali-silica solution (27 % dilution); B' = alkali-silica solution; C = two part epoxy resin (low viscosity type); 1 = 7 days second curing duration; 4 = 28 days second curing duration.

Figure 2.14 (a) Alkali-silica repairing agent B (b) Alkali-silica repairing agent B' (c) epoxy resin repairing agent C, and (d) CMOD vs. self recovery ratio (Mihashi et al., 2000)

However, several issues relating to the validity of these results should be noted. As shown in Figure 2.14(d), although the strength recovery was shown to be greatest at a CMOD value of approximately 0.50 mm, at values below this the strength recovery is much lower. It is also noticeable in Figure 2.14, that a large range of values for specific parameters is shown, for example, in Figure 2.14(c), specimen C1, has a strength-recovery ratio of between approximately 1 and 5 %.

Li et al. (1998a) studied the feasibility of an autonomic healing system in ECC by embedding hollow glass fibres carrying an air curing superglue (ethyl cyanoacrylate). Two levels of testing were considered: Firstly, specimens with hollow glass fibres containing no superglue were subject to environmental scanning electron microscope (ESEM) loading as illustrated in Figure 2.15(a), in order to test the sensing and actuation mechanism of the hollow glass fibres; and, secondly, specimens with hollow glass fibres containing superglue were subject to flexural tests in order to measure the re-healing effectiveness of the superglue after crack damage.

Upon loading ECC to a crack damage state, ESEM tests observed that the hollow glass fibres also cracked, confirming an effective sensing and actuation mechanism. The study showed that the actuation mechanism of releasing superglue into the cracked zone was dependant on capillarity. Li et al. (1998a) claimed that the crack width of the matrix should be less than the inner diameter of the hollow glass fibres for effective actuation, as illustrated in Figure 2.15(b).

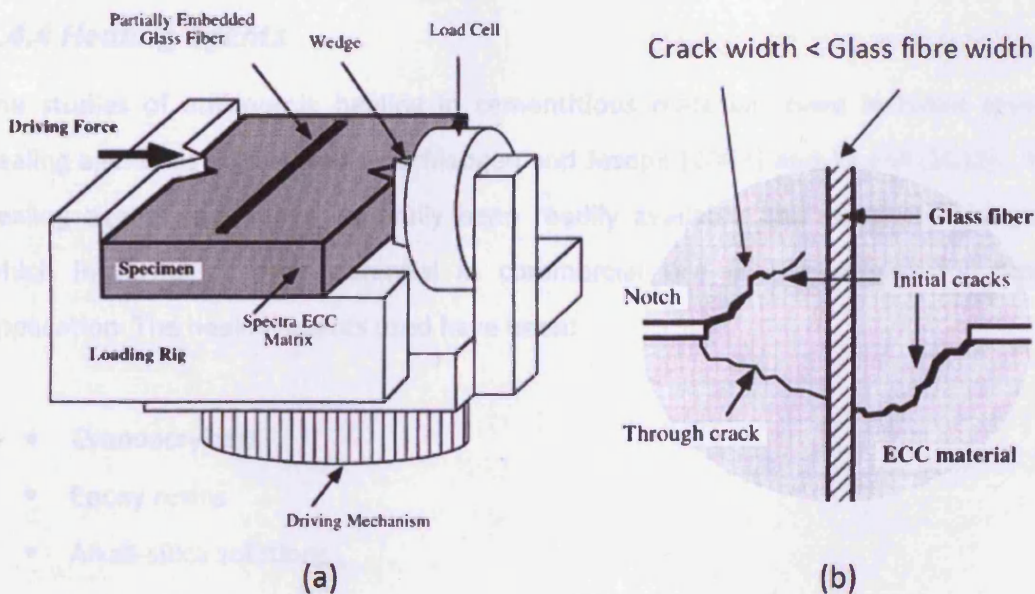


Figure 2.15 (a) ESEM specimen loading configuration (specimen dimensions are 10 x 10 x 1.5 mm) (b) formation of cracks in ESEM specimens (Li et al., 1998a)

Specimens with glass fibres containing superglue regained their stiffness under flexural tests. The glass fibres embedded in the specimens were sealed at both ends in order to



provide a pressurised environment and upon cracking the release of superglue was exhibited. For specimens that did not exhibit a regain in stiffness, post-mortem investigations indicated hardened sealing agent within the hollow glass fibres as a result of poor sealing. The study also investigated the location and the number of hollow glass fibres as illustrated in Figure 2.16. The results confirmed that a significant change in stiffness was found in specimens with a larger number of hollow glass fibres as a result of a larger quantity of superglue.

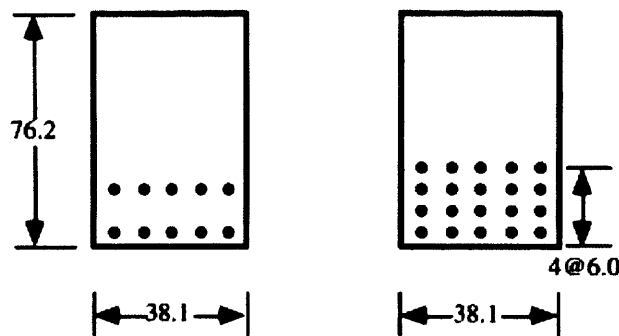


Figure 2.16 Schematic illustration of the two glass fibre arrangements (Li et al., 1998a)

#### 2.4.4 Healing agents

The studies of autonomic healing in cementitious materials have included several healing agents as highlighted by Schlangen and Joseph (2009) and RILEM (2011). The healing agents used have generally been readily available and relatively low cost, which in terms of their potential in commercial use is encouraging for future application. The healing agents used have been:

- Cyanoacrylates
- Epoxy resins
- Alkali-silica solutions
- Polyurethane

These studies have concluded that the properties of the healing agent need to adhere to specific criteria in order to carry out the self-healing function. As discussed by Joseph (2009), the healing effect is not only dependant on the capillary forces dictated

by the crack width for effective uptake, but also the viscosity of the healing agent. A lower viscosity provides a larger healing potential. Other factors include the setting time of the healing agent, which in cyanoacrylates can be a matter of seconds, but epoxy resins can take several hours or even days to set. The healing agent must also be able to adapt to the surrounding environment and form a sufficiently strong bond between the surfaces of cracks in order to carry out a self-healing function.

Cyanoacrylates, commonly known as superglues, are one part systems that have almost instant adhesive properties in the presence of moisture. In order to lengthen the pot life it is common for them to be stored in an air tight environment so that the solvent will not set. Cyanoacrylates have very low viscosities, making them desirable for seeping into micro-cracks that can be less than 100 microns wide and also provide a bond strength that often exceeds the strength of the original material (Joseph, 2009). This was confirmed in studies by Li et al. (1998a) that reported a stiffness recovery using ethyl cyanoacrylate as the healing agent. Dry (1994) also reported that specimens exhibited new crack formation as a result of initial cracks being sealed by cyanoacrylates.

An advantage of their application in concrete is that cyanoacrylates are acidic in solution and when in contact with an alkaline concrete environment, will provide neutralisation of the glue. This quick setting environment provides a fast self-healing response from the onset of damage; however, if the setting is too quick, the glue dispersion may be limited.

The studies investigating the use of epoxy resins as a healing agent have all shown insufficient mixing of the two part components. Mihashi et al. (2000) and van Tittelboom and De Belie (2009b) both reported that strength recovery was limited as a result of unequal mixing of the principal agent and the hardener and the latter reported that this could be due to the varying viscosities of the two parts. It was also noted that the rupturing of both encapsulation vessels would be required to release both parts of the epoxy resin for mixing. Dry (1994) also found that in comparison with

cyanoacrylates, the epoxy resins had a slower setting time and lower strength recovery.

As previously mentioned, Mihashi et al. (2000) also investigated the use of alkali-silica solutions as a healing agent. In comparison with epoxy resins, the strength recovery was reportedly smaller, but this can be considered irrelevant so long as the bond strength provided by the healing agent provides an increase in tensile strength to damaged specimens. Joseph (2009) reports that the use of alkali-silica based healing material is also likely to cause less compatibility problems in comparison to its polymer based counterparts.

More recently, the use of polyurethane foam has been studied by van Tittelboom and De Belie (2009b). In comparison with epoxy resins that were also used as a healing agent in this study, polyurethane showed a much larger regain in stiffness. This suggests potential for the future use of polyurethane as a healing agent.

#### ***2.4.5 Encapsulation techniques***

As highlighted by Schlangen and Joseph (2009) various encapsulation techniques have been reported in the literature. These have included:

- Microcapsules
- Continuous glass tube supply
- Glass capillary tubes

The use of microcapsules as studied by Mihashi et al. (2000) allow for multiple crack locations. However, only a limited supply of healing agent can be delivered as a result. Alternatively, the use of hollow glass tubes allows for a continuous supply of healing agent by use of an external delivery system. This allows for the quantity of healing agent to be controlled, which in larger fractures is advantageous. It also allows for the type of healing agent to be changed if required. Dry (1994) investigated the use of a continuous supply with an external vacuum pump acting as a delivery system. One of

the issues with this method is however, replicating the system on a construction site and is currently confined to testing in a laboratory environment.

As previously discussed, Li et al. (1998a) adopted the use of glass capillary tubes as a method of encapsulation. The glass tubes were sealed at both ends and embedded into the cementitious matrix. It was found that failure of the tubes was caused by tensile failure or flexural failure (shattering) as the angle between the crack plane and the longitudinal direction of the glass became more acute. Like microcapsules, the glass capillary tubes have a limited supply, but upon rupture provide more healing agent to a crack zone. As previously discussed in the context of polymers (Section 2.4.1), the encapsulation techniques need to account for geometry and toughness in order to provide a successful sensing and actuation mechanism.

#### **2.4.6 Further studies**

Other notable autonomic healing studies include the use of bacteria incorporated into a cementitious matrix that serve to increase calcium carbonate production as a result of micro-cracking in order to enhance the self-healing effect (Jonkers et al., 2010; Jonkers and Schlangen, 2009). These studies aim to identify bacteria that can survive concrete incorporation and which will be required to withstand a high alkaline environment and resist mechanical stresses due to mixing.

In these studies, the use of a two component healing agent represented by the bacteria (related to the genus *Bacillus*) plus calcium lactate were able to produce calcium carbonate based minerals upon activation by water ingress due to cracking. The studies have shown that the bacteria production was limited to only early age specimens. Jonkers et al. (2010) describe that the reduction of pore diameter in the cementitious matrix with specimen age decreased the viability of bacteria as bacteria spores became crushed. Furthermore, the mineral precipitation to provide crack-plugging was found to only repair cracks of less than 1 mm. In the latter, the authors attribute these findings to a maximum allowable amount of mineral precursor that

should not exceed a level that will influence the setting time and final strength of the cementitious material.

The studies of bacteria in cementitious materials as with all the autonomic healing studies in cementitious materials are still in their infancy. The use of bacteria is currently limited to healing in micro-cracks and the shelf life of bacteria spores in the matrix is restricted to only early age specimens. However, with continuing research in this area, it is certainly feasible to develop more durable cementitious materials with bacteria incorporation that can provide autonomic healing.

Selective heating devices as a method of self-repair have also been investigated that aim to provide a self-healing capability at a specified crack zone (Nishiwaki et al., 2009; and, Nishiwaki et al., 2007). The concept of a proposed selective heating system is illustrated in Figure 2.17. The cementitious matrix is embedded with a heating device and an organic film pipe containing a repair agent. As a crack is formed, electrical resistance is generated by the strain responsive heating device, which in turn develops the heat required to melt the film and enable the release of a repair agent into a crack.

The results by Nishiwaki et al. (2007) show that the developed material system is capable of selective crack healing as a result of cracking in specimens. The advantages of such as system include the potential to localise crack healing to a specific crack and provide a multiple crack healing ability. However, at present the authors describe that the concept is only aimed at repairing narrow width cracks and that its self-healing function is intended to recover water tightness rather than material strength. Furthermore, the material strength of specimens may be affected by the embedment of both a heating device and a pipe containing a repair agent.

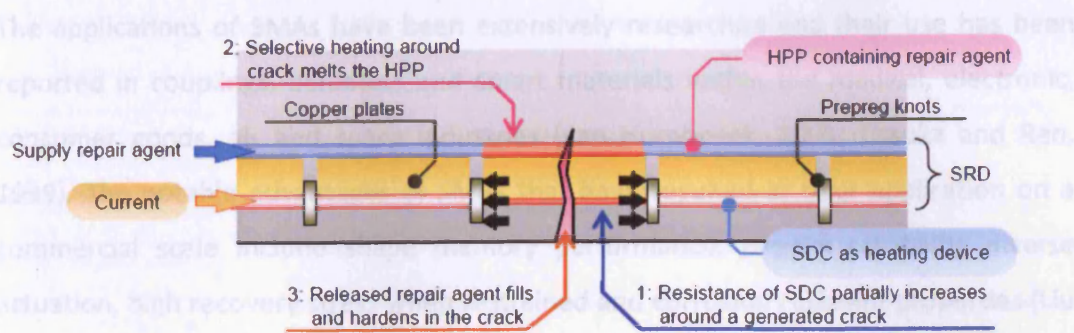


Figure 2.17 Schematic illustration of the selective heating concept (Nishiwaki et al., 2007)

## 2.5 Shape Memory Polymers

### 2.5.1 Shape memory materials

Shape memory materials (SMMs) have attracted increasing attention in recent years due to their ability to store a deformed (temporary) shape and recover to an original (parent) shape (Liu et al., 2006). SMMs include alloys, ceramics, hydrogels and polymers with all types providing applications in a vast number of fields (Wang et al., 2006).

The most recognised and widely used SMMs to date are shape memory alloys (SMAs). The shape memory effect in alloys was first reported in 1951 by Chang and Read who observed a memory effect in an AuCd alloy. In 1963 Buehler et al. discovered the shape memory effect in a nickel titanium alloy (NiTi, Nitinol®) which has since become recognised as the most common alloy in SMA applications. The shape memory effect in SMAs is a transformation between two stable crystal structures referred to as a solid-solid phase transformation. The solid phase obtained at a low temperature is known as the martensite phase whereby the alloy exhibits low yield strength allowing deformation into its new (cold) shape. The solid phase at high temperature, known as the austenite (parent) phase exhibits a cubic crystal structure in its permanent (hot) shape. The deformation to and from the martensite phase can be achieved by heating and cooling which is the basis of the shape memory effect (Wayman, 1964; Wayman and Duerig, 1990; Otsuka and Ren, 1992).

The applications of SMAs have been extensively researched and their use has been reported in couplings, actuators and smart materials within the medical, electronic, consumer goods, air and space industries (van Humbeeck, 2001; Otsuka and Ren, 1999). The notable advantages of SMAs that have resulted in their application on a commercial scale include shape memory performance, proven reliability, diverse actuation, high recovery stress when restrained and corrosion resistant properties (Liu et al., 2007; Wei et al., 1998). However, within civil engineering, the use of SMAs has been limited due to the associated high cost (Czaderski et al., 2006). In addition, SMAs have a very low young's modulus, a limited recoverable strain of less than 8% and a limited transition temperature range (Liu et al., 2007). It is perhaps these limitations that have provided the need for diversity and the motivation toward the development of alternative shape memory materials such as shape memory polymers (SMPs).

Shape memory polymers (SMPs) can be classed as a new type of “intelligent” polymer (Zheng et al. 2006). In comparison with SMAs, SMPs have gained great research interest due to their high elastic deformation (strain recovery of up to 200%), low cost and wide range of mechanical and physical properties (Liu et al 2007; Wang et al., 2006). In addition, SMPs are low density in comparison with SMAs and have a controllable activation temperature range (Li et al., 1999; Jeong et al., 2000; Tobushi et al., 1996). A comparison of the properties between SMPs and SMAs is shown in Table 2.1. As stated by Behl and Lendlein (2007) the inherent attributes in SMPs have led to their use in various areas of everyday life. Examples of applications include biomedical devices and deployable structures in the aerospace industry.

Table 2.1 Comparison of the typical properties of shape memory polymers and shape memory alloys (Liu et al., 2007)

	<b>SMPs</b>	<b>SMA</b> s
Density/g cm <sup>-3</sup>	0.9-1.1	6-8
Extent of deformation (%)	Up to 800%	<8%
Young's Mod at T < T <sub>trans</sub> /GPA	0.01-3	83 (NiTi)
Young's Mod at T > T <sub>trans</sub> /GPA	(0.1-10)x 10 <sup>-3</sup>	28-41
Stress required for deformation/MPa	1-3	50-200
Stress generated during recovery/MPa	1-3	150-300
Critical temperatures/°C	-10-100	-10-100
Transition breadth/°C	10-50	5-30
Recovery speeds	<1 s-several min.	<1s
Thermal conductivity/W m <sup>-1</sup> K <sup>-1</sup>	0.15-0.30	18 (NiTi)
Biocompatibility and biodegradability	Can be biocompatible and/or biodegradable	Some are biocompatible (i.e. Nitinol), not biodegradable
Processing conditions	<200°C, low pressure	High temperature (>1000°C) and high pressure required
Corrosion performance	Excellent	Excellent
Cost	<\$10 per lb	~£250 per lb

### 2.5.2 Shape memory effect in polymers

The purpose of this review is not to detail the complex chemistry of the shape memory effect in polymers, but the fundamental science of polymers needs to be addressed. Polymers consist of a chain of monomers. The majority of these are linear in nature consisting of a polymer molecule whereby the atoms are arranged in a long chain known as the backbone. Pendant chains consist of fewer atoms that are sometimes attached to atoms in the backbone chain that have hundreds of thousands of atoms. Sometimes the pendant chains can be as large as the backbone and these pendant chains can attach themselves to other pendant chains which results in non-linear polymers and larger specimens. The arrangement of chains determines the classification of the molecular structure. As illustrated in Figure 2.18, polymer structures can be linear, branched or cross-linked. (Rosen, 1993; van Krevelan, 1997).



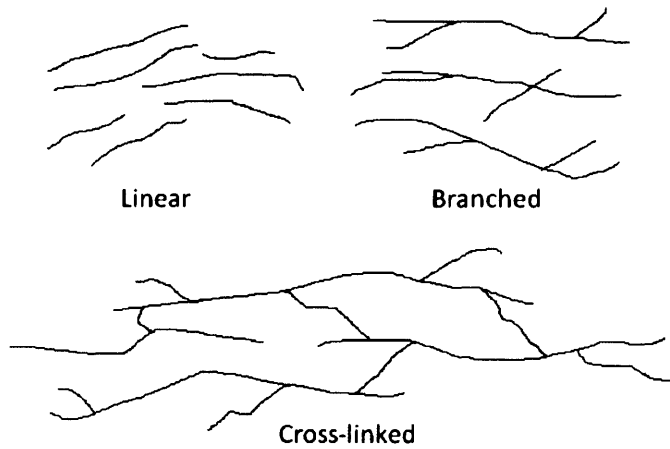


Figure 2.18 Schematic representations of polymer structures

The shape memory effect in SMPs is illustrated in Figure 2.19. The permanent shape is initially processed by for example, casting or injection moulding (Ni et al., 2007). The polymer then undergoes deformation and is subsequently fixed in its temporary shape in a process known as programming. In a thermally induced programming process the polymer will be heated above a transformation temperature ( $T_{trans}$ ) causing deformation. The polymer is then cooled, becoming fixed in its temporary shape. The permanent shape is stored and can be recovered once again by heating above the  $T_{trans}$ .

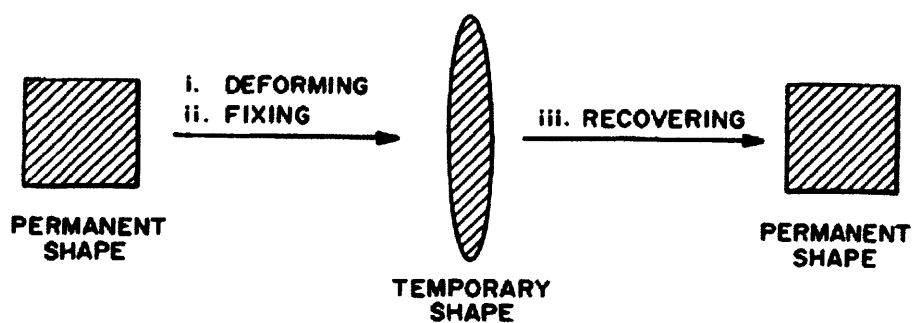


Figure 2.19 Schematic representation of the shape memory effect. Transformation from permanent shape to temporary shape and recovery (Liu et al., 2006)

The majority of SMPs reported in the literature are taken from the polyurethane (PU) chain. Zhang and Ni (2007) highlighted that polyurethane is one of the most studied shape memory polymers because its  $T_{\text{trans}}$  can be set up at any temperature within  $\pm 50\text{K}$  around room temperature. However, the shape memory effect is not exclusive to this polymer chain and the effect can be observed in other polymers by adaption of the polymer structure and morphology as well as the processing and programming techniques used (Lendlein and Kelch, 2002). As SMPs are an emerging technology it is worth noting that there are only a few data sets concerning the shape memory properties of SMPs that are comparable with each other (Ohki et al., 2004).

### **2.5.3 Transformation temperature**

The transformation temperature,  $T_{\text{trans}}$ , also referred to as the transition temperature (Lendlein and Kelch, 2002) is the temperature at which the material is activated and changes from its original permanent shape to the temporary stored shape. The transformation temperature can be either a glass transition temperature,  $T_g$ , or a melting temperature,  $T_m$  (Zheng et al., 2006). The  $T_{\text{trans}}$  of polymer materials generally depends on the strength of the intermolecular force (hydrogen bond and polarization), the stiffness and symmetry of the backbone chain and the geometry of the side chains and function groups (Hayashi et al, 2004). These properties can be tailored by the physical and chemical make up of the polymeric material that can subsequently influence the  $T_{\text{trans}}$ . This variation in  $T_{\text{trans}}$  gives potential for a wide range of applications due to the activation mode that is either above or below  $T_g$ .

Figure 2.20 illustrates the elastic modulus of a typical polymer below  $T_g$  and above  $T_g$ . In general, polymers can be described as viscoelastic materials because they can behave at intermediate positions between viscous liquids and elastic solids (Ward, 1979; Ward and Sweeney, 2004). At temperatures lower than  $T_g$  a polymer is in a glassy state and behaves as an elastic solid at small strains, polystyrene is a typical example (Liu et al., 2006). At temperatures above  $T_g$  a polymer exhibits low stiffness and is classed as rubbery as seen in materials such as elastomers which are flexible and

soft. As shown in Figure 2.20,  $T_g$  does not occur at a specific temperature but over a range and in general, the mid-point is classed as the  $T_g$ .

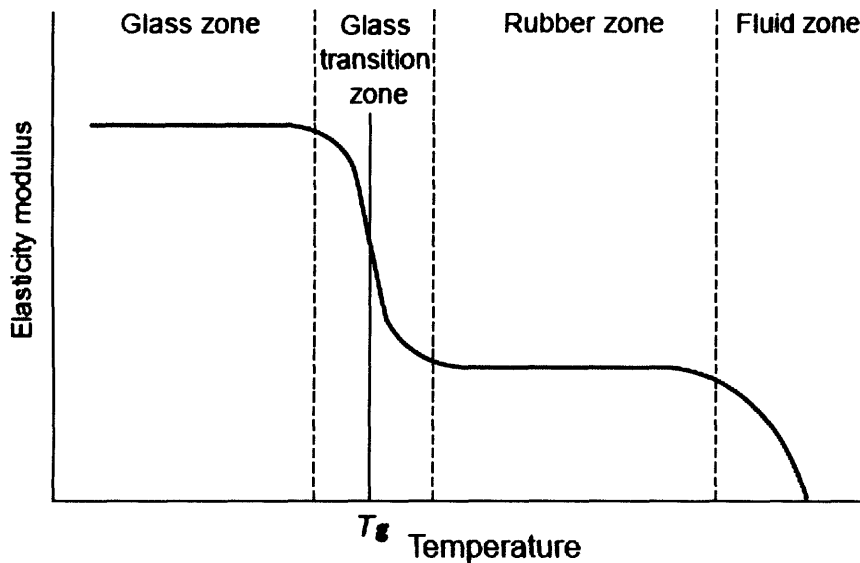


Figure 2.20 Temperature dependency of elasticity modulus of SMP (Hayashi et al., 2004)

### 2.5.4 Thermomechanical characterisation

The shape memory effect in polymers can be characterised by thermomechanical cycling. The cycling is performed in a thermo-chamber by means of a tensile tester or a dynamic mechanical analyser (DMA). A sample undergoes deformation and fixing to a temporary shape and recovery to a permanent shape. The cycling can be performed in either stress or strain controlled modes and although the control method between the two modes may generate slightly different results they will provide complimentary information (Rousseau, 2008). A typical 3D representation of thermomechanical cycling is shown in Figure 2.21. During a cycle a sample will exhibit deformation, cooling, fixing and recovery (Tobushi et al., 2001). A sample is heated up to a temperature above its transformation temperature ( $T > T_{trans}$ ) to a predetermined stress or strain ( $\sigma_m$  or  $\epsilon_m$ ). The sample is then cooled down below its  $T_{trans}$  under a constant  $\sigma_m$  or  $\epsilon_m$ . The sample becomes fixed in its temporary shape and the constraint

is released until a stress-free state is reached. The sample is then heated above its  $T_{trans}$  and the stored strain energy is used to recover the sample to its permanent shape.

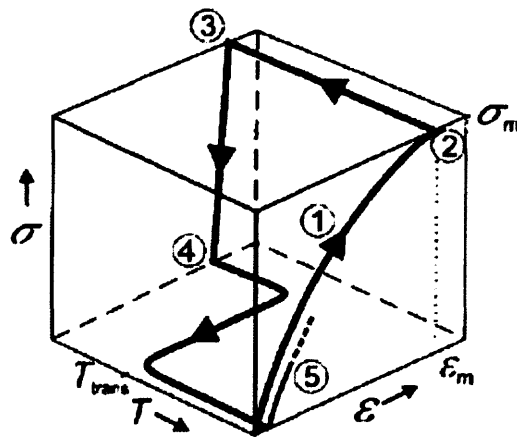


Figure 2.21 Schematic representation of a 3D result for thermomechanical cycle tests. 1: At  $T > T_{trans}$ , sample is stretched to  $\epsilon_m$ ; 2: Cooling down while  $\epsilon_m$  is kept constant; 3: constraint released to reach stress-free state; 4: Heating up to  $T > T_{trans}$ ; 5: Cycle repeated. (Lendlein and Kelch, 2002).

### 2.5.5 SMP classification

SMPs can be classified depending on their structures and  $T_{trans}$ . The structure of an SMP can be thermoset or thermoplastic with a cross-linked network that is physically or chemically cross-linked. The SMP structure can be divided into soft and hard segments. The soft segments control the deformation phase into a temporary shape by crystallisation. The hard segments form physical cross-links by for instance, hydrogen bonding, crystallisation or polar interaction, with the cross-links being able to withstand moderately high temperatures without being destroyed. It is through these segments that the shape memory behaviour can be tailored. The coexistence between the physical or chemical cross-linked structure (hard segment) and the amorphous or crystalline region (soft segment) determines the shape memory behaviour (Rousseau 2008; Wang et al., 2006).

Several authors have identified a classification for SMPs based on shape fixing and recovering mechanisms (Lendlein and Kelch, 2002; Liu et al., 2007; Ratna and Karger-

Kocsis, 2008). These classifications will be described in the context of thermal activation.

*Class 1: Chemically cross-linked glassy thermoset networks*

This class of polymers has excellent shape fixity and recovery due to the nature of cross-linking and the absence of slip between chains. The shape memory effect is initialised by deformation at a temperature above  $T_g$  and then fixed by cooling below  $T_g$ . Recovery to the permanent shape is then activated by heating above  $T_g$ . In general, this class of polymers exhibit a fast and almost complete fixing and recovery between 95 – 100% (Gall et al., 2004; Liu et al., 2006; Liu et al., 2004). Typical examples include epoxy based SMPs and thermosetting polyurethanes that exhibit a wide range of shape recovery temperature (typically between 30-70°C), high recoverable strain and biocompatibility (Yang et al., 2006).

*Class 2: Chemically cross-linked semi-crystalline networks as SMPs*

As with class 1 polymers, the permanent shape is established by chemical (covalent) cross-linking that can not be reshaped after processing. The shape memory effect is initiated by heating above  $T_m$  and fixed by cooling below the crystallisation temperature. Figure 2.22 shows a schematic representation of the shape memory effect. In comparison to class 1, the shape fixity and recovery can occur over a wider temperature range. These polymers are commonly used as heat shrink materials, such as Polyethylene terephthalate (PET) that exhibit recovery between 95 and 100% (Li et al., 1998b).

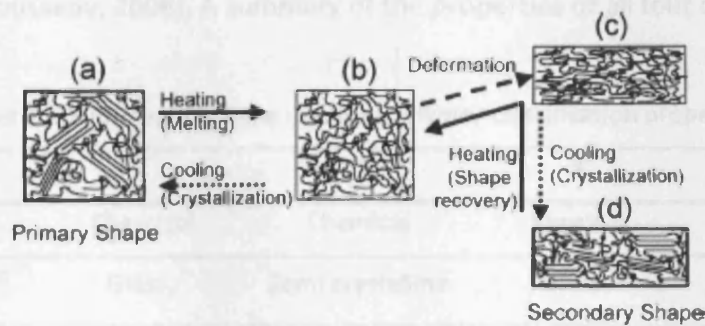


Figure 2.22 Schematic representation of the shape memory effect of class 2 SMPs. (a) Semi-crystalline stage showing cross-linked shape (low temperature); (b) Melted sample (high temperature); (c) deformed shape at melted stage (high temperature); (d) deformed crystal frozen shape (low temperature). (Liu et al., 2007)

### Class 3: Physically cross-linked glassy copolymers as SMPs

The shape memory behaviour of physically cross-linked polymers is attributed to the soft segment region whereas the permanent shape is provided by physical cross-linking of the hard segment. In this class, deformation is obtained by heating above  $T_g$  and fixed by cooling below  $T_g$ . An example of this class of polymer is glass fibre reinforced polyurethane that has been developed to improve the mechanical weakness in SMPs. In general, SMPs have been found to be much weaker than SMAs and studies by Ohki et al. (2004) concluded that the addition of glass fibre improved the material strength. The findings concluded that the weight percentage of glass fibres in the polymer matrix affected the specimens stress and strain characteristics. A percentage between 10 – 20 wt% provided an optimum tensile strength and resistance against the mechanical and thermal mechanical cyclic loading. Above 20 % by weight the polymer exhibited debonding between the glass fibres and the matrix resin.

### Class 4: Physically cross-linked semi-crystalline block copolymers as SMPs

As with class 3, these polymers are physically cross-linked structures. The shape memory effect is exhibited by heating above  $T_m$ . Deformation occurs in the soft segment and recovery to the permanent shape is achieved by cooling below  $T_m$  by physical cross-linking between hard segments through molecular interaction in the crystalline regions. The shape fixity and recovery has been reported to range between 56 and 100% depending on the composition of length and/or molecular weight

distribution (Rousseau, 2008). A summary of the properties of all four classes is shown in Table 2.2.

Table 2.2 Summary of shape memory polymer classification properties

Class	1	2	3	4
<b>Cross-linking</b>	Chemical	Chemical	Physical	Physical
<b>Transformation characteristic</b>	Glassy	Semi-crystalline	Glassy	Semi-crystalline
<b>T<sub>trans</sub> (deformation)</b>	$T > T_g$	$T > T_m$	$T > T_g$	$T > T_m$
<b>T<sub>trans</sub> (recovery)</b>	$T < T_g$	$T < T_m$	$T < T_g$	$T < T_m$
<b>Recovery range (%)</b>	95 – 100	95 – 100	75 – 100	56 - 100
<b>Example materials</b>	Epoxy resin based SMPs	Heat shrinkable materials, for example PET	Glass fibre reinforced polyurethane	Styrene-trans-butadiene-styrene (STBS)

### 2.5.6 Activation methods

The shape memory effect in SMPs is the response of the polymers structure to an external action. This external action that causes the polymer to change from its original permanent shape to a temporary stored shape is often termed the activation method. Such methods can include changes in temperature, moisture, pH, light, solvent compositions and electromagnetism. For instance, a shape change caused by a temperature change would be classed as a thermally activated SMP.

#### 2.5.6.1 Thermal activation: direct and indirect

The shape memory effect by thermal activation can be a direct or indirect actuation. By increasing the environmental temperature of an SMP above its  $T_{trans}$  the activation is classed as a direct actuation. This shape memory effect has previously been described in Section 2.5.2 and shown in Figure 2.19.

There are many studies investigating various methods of activation, most notably reviewed by Behl and Lendlein (2007) who highlight a diverse range of indirect thermal actuation methods. Such methods include indirect heating through electromagnetism, infrared light and moisture.

SMPs exhibiting a shape memory effect in response to magnetic actuation have been developed that incorporate magnetic nanoparticles consisting of Fe (III) oxide into polyurethane known as TFX (Evans, 2006; Mohr et al., 2006). In this instance, the specimen temperature is increased by inductive heating of the nanoparticles by an alternating magnetic field. As shown in Figure 2.23, specimens exhibit a shape memory effect when exposed to a magnetic field.

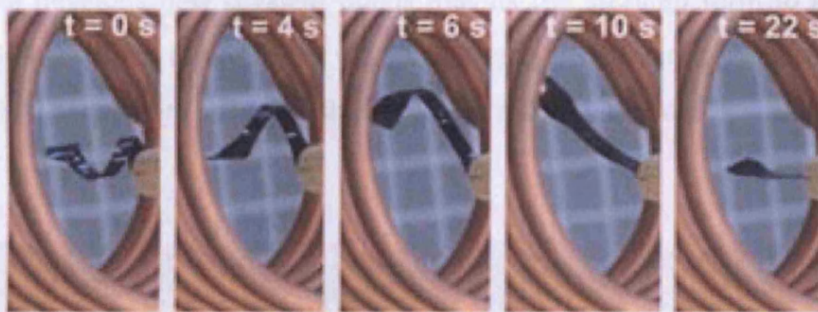


Figure 2.23 Magnetically induced shape memory effect of the SMP TFX (Mohr et al., 2006).

The use of activating polyurethane by infrared light has been studied. Instead of increasing the environmental temperature, this indirect thermal actuation uses heat transfer through conductive fillers that are incorporated into the polymer matrix. Biercuk et al. (2002) made use of single-wall carbon nanotubes (SWNTs) as conductive fillers to enhance the thermal transport properties in an epoxy. The incorporation of nanocomposites also influences the mechanical properties and studies have shown that the inclusion of nanocomposites produces higher elastic modulus (increased stiffness) and the potential to generate higher recovery forces (Liu et al., 2004; Gall et al., 2002).

A method of indirect thermal actuation by lowering  $T_{trans}$  in SMPs has been developed by Huang et al. (2006). When immersed in water, moisture diffuses into the polymer sample and acts as a plasticiser, resulting in shape recovery. It has been shown that the lowering of  $T_{trans}$  depends on the moisture uptake, which in turn depends on the immersion time (Huang et al., 2006). Studies have concluded that  $T_{trans}$  decreases when exposed to moisture due to the absorbed water causing a weakening of the C=O



and N-H bonds. However, upon heating,  $T > 180\text{ }^{\circ}\text{C}$ , the water is removed between the bonds and the activation of  $T_{\text{trans}}$  returns to a dry condition (Yang et al., 2006).

### 2.5.6.2 Light activation

A light induced shape memory effect is independent of any temperature effects. In light induced SMPs, photoreactive molecular switches are incorporated into the polymer matrix. The original shape is pre-programmed, resulting in strained, coiled polymer segments. Upon exposure to ultraviolet (UV) light with a wavelength  $> 260\text{nm}$  the sample develops new covalent bonds that fix the strained form to a temporary shape. When exposed to a UV light with a wavelength  $< 260\text{nm}$  the specimen returns to its original permanent shape, as shown in Figure 2.24 (Lendlein et al., 2005).

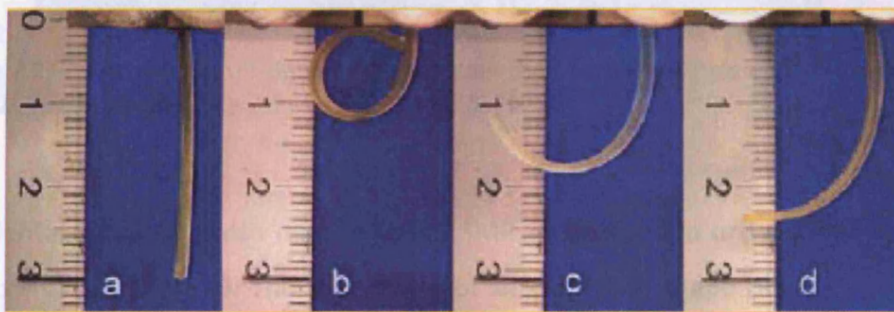


Figure 2.24 Light induced shape memory effect in a polymer: (a) original shape, (b) temporarily fixed form, and (c) and (d) recovered shape with increasing UV exposure time (Lendlein et al., 2005)

### 2.5.7 SMP applications

SMP application in cementitious materials is still very much an emerging technology but there is a potential for technology transfer between the uses of SMPs in established disciplines. In the medical profession the development of SMPs is at the forefront of SMP technology. SMP medical applications include scaffolding devices within the body such as stents in blood vessels for blood clot removal, assisting support for bones and the development of biodegradable properties. (Maitland et al., 2002; Lendlein and Langer, 2002; Wache et al., 2003). Lendlein (2002) demonstrated the application of a self-tightening knot, which could be used in stitching areas with limited access as shown in Figure 2.25.

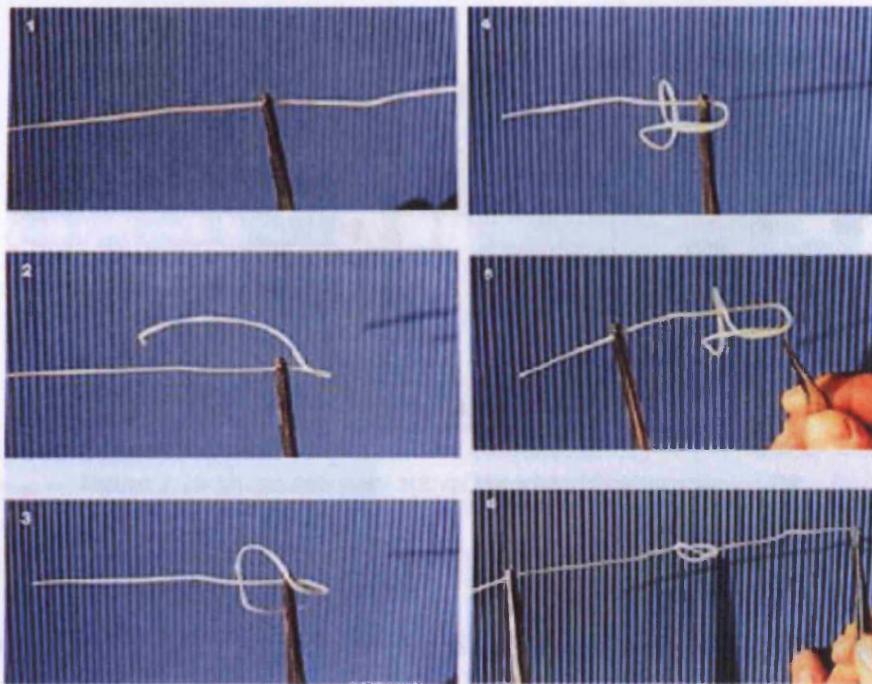


Figure 2.25 Six stages of self-tightening knot from the temporary shape (1) to its parent shape (6) in 20 seconds when heated to 41°C (Lendlein, 2002)

The dental industry is also making use of SMP technology in orthodontic applications as shown in Figure 2.26. The advantages of shape fixing, shape recovery and variable stiffness have led to the development of castable shape memory polymers (CSMP) and a shape memory rubber. Issues of water absorption, stain resistance and stress stability have been studied and comparisons made between existing orthodontic applications have revealed significant advantages of SMPs (Small IV., et al 2010; Liu et al., 2007).

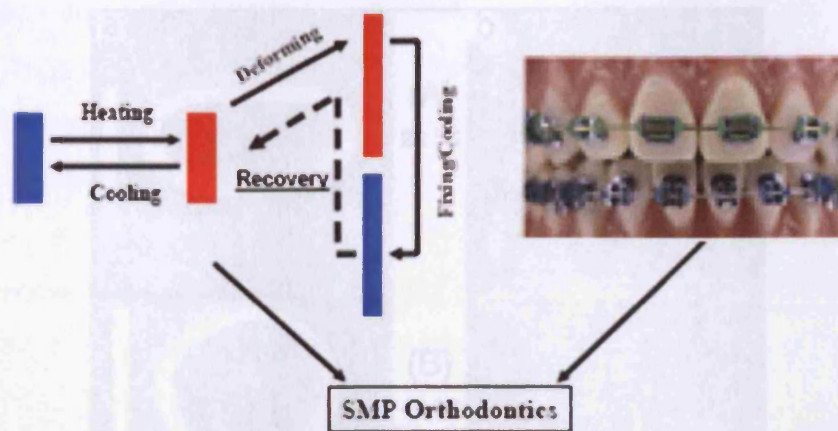


Figure 2.26 Shape memory activating wires (Polymer age, 2006)

One of the more ambitious applications of SMP technology is within the aerospace industry. The use of SMPs is favoured over SMAs due to their light weight. Studies by the Defence Advanced Research Project Agency (Darpa) have addressed the need to improve aircraft performance and efficiency. The ability to alter aircraft shape during flight could reduce drag forces that could in turn improve fuel consumption. Initial designs are investigating the action of morphing wings that change shape during flight by up to 150% (Toensmeier, 2005).

More recent studies have explored triple shape polymers (TSPs). These multiphase polymer networks have the ability to change from a first shape (A) to a second shape (B) to a third shape (C) due to the polymer having two distinct  $T_{trans}$  (Behl and Lendlein, 2010). In Figure 2.27, the thermally induced triple shape effect shows TSP application as a stent (a) and as a fastener consisting of a plate with anchors (b). The shape evolves as temperature increases with two clear transition temperatures at 40°C (in B) and 60°C (in C) (Bellin et al., 2006).

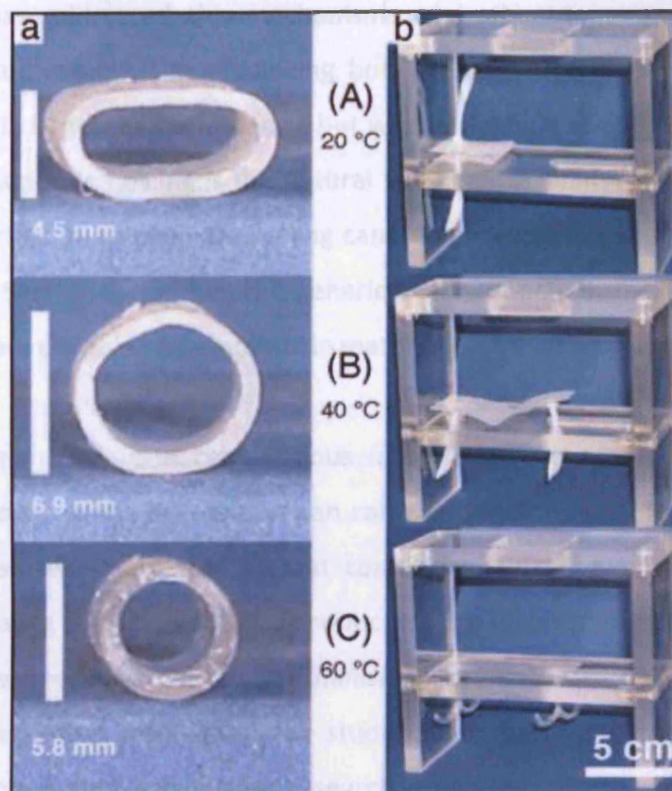


Figure 2.27 The triple shape effect in TSPs: (a) application as a stent, and (b) as a fastener consisting of a plate with anchors. (Bellin et al., 2007)

## 2.6 Conclusions

### 2.6.1 Self-healing cementitious materials

As the most used construction material in the world, concrete has enormous impacts both financially and environmentally. The cost of repair and maintenance that are associated with the issues of durability and the levels of CO<sub>2</sub> resulting from the use of concrete are testaments for the need to develop more sustainable and durable concrete structures. The concept of developing cementitious materials with a self-healing ability is therefore very attractive. The ability to heal cracks at the onset of damage can reduce the costs of maintenance and increase the service life, which in turn has the potential to reduce the demand and the production levels of concrete.

This chapter has addressed the mechanisms of both autogenous and autonomic healing. The studies aimed at enhancing both healing mechanisms in cementitious materials are still largely in their infancy, but what is notable about autogenous healing rather than autonomic healing is the natural self-healing ability that is generic to the material properties. If autogenous healing can be enhanced in cementitious materials, as described in Section 2.3.3, then this generic healing mechanism should be exploited to provide a more durable and sustainable material.

Unlike autonomic healing in cementitious materials, autogenous healing does not require additional healing agents that can carry additional costs. However, it is clear from the literature review that certain conditions must be present in order for autogenous healing to take place. Autonomic healing also requires certain conditions that include the need of a delivery mechanism in order to distribute a healing agent into a crack that forms. In addition, the studies described for autonomic healing are largely laboratory based and further research is required in order to develop more suitable healing systems for use on construction sites.

With the continued interest and research in both autogenous and autonomic healing, the function of self-healing in cementitious materials can only serve to enhance the durability of concrete structures.

### ***2.6.2 Shape memory polymers***

The literature review has given an overview of the state of the art and future outlook of SMPs. Particular focus has been given to the classification, thermally induced shape memory effect, activation and application of SMPs.

One of the fundamental questions that arise from this review is whether the use of SMPs has potential within the construction industry. It is perhaps not surprising that because of the low recovery stresses inherent in SMPs there is very little work investigating their use in cementitious materials. In comparison, the use of SMAs has been investigated as a result of their higher stiffness properties and yet studies of

SMA within civil engineering are also still in their infancy (Song et al., 2006; Janke et al., 2005). However, the advantage of incorporating shape memory materials into civil engineering structures is that they could facilitate active structures that could react to external conditions (Czaderski et al., 2006).

It has been noted that the associated costs of SMPs are significantly lower than those of SMAs due to the differences in processing/fabrication and the raw materials used. Coupled with the growth in SMP research, the potential use of SMPs for adaptation in civil engineering application is certainly feasible. The classification of SMPs shown in Table 2.2 provides an insight into their suitability, which will have to satisfy certain criteria in order to be used in concrete structures. A typical example of their use could be to generate shrinkage stresses in order to provide post-tensioning to concrete structures. In this case, Table 2.2 suggests SMPs in class I and class II would be suitable due to their high recovery percentage range. SMPs such as PET that have a temperature activation range above that of which concrete structures are exposed to in environment conditions, but below temperatures which will damage the cementitious material are therefore attractive. Other criteria for which SMPs would have to satisfy include suitable activation methods, high alkaline resistivity and a suitable relaxation percentage.

The future design of SMPs will depend strongly on an understanding of the rules between programming and recovery as well as the various actuation methods. Furthermore, research into alternative activation methods in SMPs can only increase the diversity of potential future applications. In time dependant applications the use of electrical, light or magnetic actuation may be more applicable than temperature actuation. In applications where access may be limited, for instance in medical implants, access for direct heating may be restricted and an alternative actuation would be required. Accessibility can also be considered a major factor for the potential use of SMPs in civil engineering by providing a passive capability.

## Chapter 3

### Autonomic healing

#### 3.1 Introduction

In order to develop an understanding of self-healing mechanisms in cementitious materials, it was considered necessary to first undertake an experimental investigation of the mechanisms of autonomic healing. As mentioned in Chapter 2, the studies on autonomic healing are currently limited and it was envisaged the results of the study would provide additional experimental data to an emerging area of research. As illustrated in Figure 3.1, the autonomic healing system provides a sensing and actuation mechanism by the embedment of adhesive filled brittle vessels into a cementitious matrix. When a crack in the cementitious matrix is formed, it causes fracture of the brittle vessels (sensing) and the release (actuation) of healing agent into a crack zone. In cementitious materials, this concept was originated by Dry (1994) as previously discussed in Sections 2.2.6 and 2.4.2.

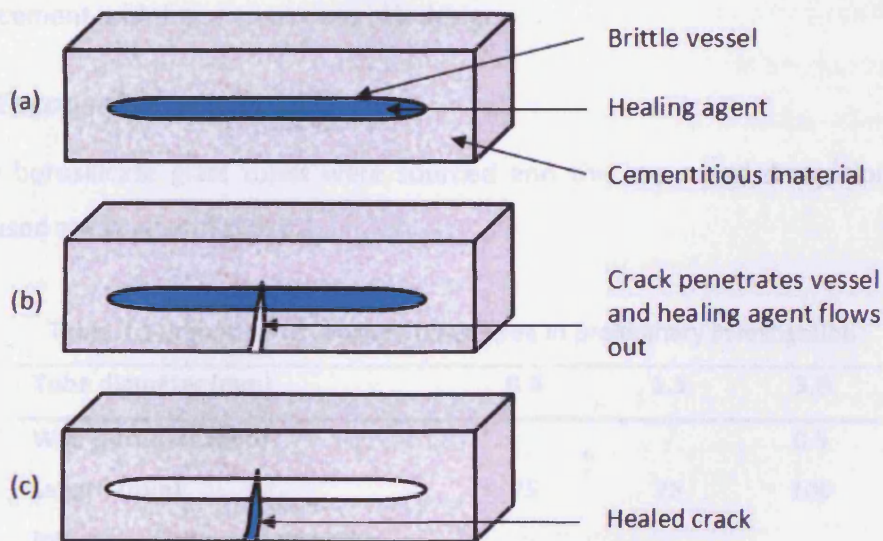


Figure 3.1 Schematic illustration of autonomic healing concept

An autonomic healing system has been developed by the research group at Cardiff University. The work comprised six sets of experimental tests, with the aims of investigating the effects of specimen age, level of reinforcement, loading rate and pre-notching of specimens. From the parametric study, it was envisaged that the results would provide new information with regard to the autonomic self-healing concept.

Test sets one, two, three and five were conducted by a colleague Christopher Joseph and test sets four and six were conducted by the author. Subsequently the studies have been reported in Joseph (2009); Joseph et al. (2010a; 20010b; 2009); Schlangen and Joseph (2009); and, Joseph et al. (2007). This chapter presents the results for sets four and six, details of the specimen preparation, the experimental procedure and analysis of the test results. This chapter will also outline the preliminary investigation study that was carried out in order to establish the type of encapsulation method and to find the most effective healing agent.

## **3.2 Preliminary Investigations**

The preliminary investigation considered several aspects of the autonomic healing system that included encapsulation method, healing agent, the percentage of reinforcement and the cementitious mix design.

### **3.2 1 Encapsulation methods**

Hollow borosilicate glass tubes were sourced and the measured dimensions of the tubes used are given in Table 3.1.

Table 3.1 Properties of capillary tubes used in preliminary investigation

<b>Tube diameter (mm)</b>	<b>0.8</b>	<b>1.5</b>	<b>3.0</b>
<b>Wall thickness (mm)</b>	-	-	0.5
<b>Length (mm)</b>	75	75	100
<b>Internal volume of single tube, excluding end plugs (<math>\mu</math>l)</b>	34	118	650



The glass tubes were filled with adhesive by positioning them horizontally, almost parallel to the adhesive surface, with one end slightly submerged in the adhesive. As a result, the capillary attractive force drew the adhesive into the tube. This method minimised the amount of air that could potentially become trapped inside the tubes. Both ends were then sealed with a wax compound.

The tubes were then placed in mortar specimens during the casting process, with two configurations explored, similar to that studied by Li et al. (1998a). These were: (a) a single layer of 5No. tubes (SL-5), and; (b) a double layer of 5No. tubes (DL-5), as illustrated in Figure 3.2. The observations are discussed in Section 3.2.5.

### **3.2.2 Healing agents**

Three types of healing agent were initially proposed, chosen with the potential to satisfy the criteria of being readily available and having suitable bonding properties and viscosity. In order to develop an effective self-healing response, the healing agent eventually adopted would need to provide a bond strength between two crack surfaces greater than the strength of the cementitious matrix. It was also noted that the bond strength would be irrelevant if the healing agent did not penetrate the micro-cracks as a result of having too higher viscosity. Consequently, for the potential use in construction applications, a low cost, low viscosity, off the shelf healing agent was needed to provide an attractive solution in a cost sensitive industry. The issue of moisture resistance and further long term effects of the healing agent were not investigated in the current experimental programme.

The healing agents examined were: SICOMET 9000, a methoxyethyl based cyanoacrylate (Henkel Sichel-Werke, 1997); Rite Lok EC-5, an ethyl based cyanoacrylate (Appendix A); and, Tecroc products injection grout TG07, an epoxy resin (Tecroc, 2004).

Preliminary investigations concluded that both cyanoacrylates offered great potential as healing agents for the autonomic healing concept. Investigations showed that storage of both cyanoacrylates in a sealed environment showed no degradation of the

adhesive viscosity over a 60 day post-encapsulation period. Both cyanoacrylates offered quick curing times, low viscosity and a mechanical bond strength greater than that of the cementitious matrix. The cyanoacrylates were also single agents that did not require the mixing of two parts. The chosen healing agent was Rite Lok EC-5 cyanoacrylate, as it offered the lowest viscosity of between 1 – 10 centipose, compared to 15 – 25 centipose for SICOMET 9000. It was considered that Rite Lok EC-5 therefore had the greatest self-healing potential to infiltrate micro-cracks. The data sheet is included in Appendix A.

As discussed by Mihashi et al. (2000), the mixing of a two part epoxy resin system requires both encapsulated agents to be released simultaneously. The study found that insufficient mixing occurred, due to the inefficient release of the two part system, and that this led to poor mechanical performance when specimens were reloaded after a period of healing. It was for this reason that the epoxy resin was not examined during the preliminary investigations. Furthermore, the epoxy injection grout had a viscosity of 200 centipose and was not considered suitable for filling micro-cracks.

### **3.2.3 Reinforcement**

The study included the use of reinforced specimens since it was envisaged that the autonomic healing concept would be incorporated into reinforced concrete structures. The reinforcement in this case was also used to control the rate of crack opening during three-point bend tests. The level of reinforcement used complied with the minimum reinforcement requirements of Eurocode 2 (BS EN1992, 2004). For reinforced concrete beams  $0.13\% bd$  was calculated, where  $b$  is the beam breadth and  $d$  is the depth to the centre of the reinforcement. This equates to a 3 mm diameter bar. As illustrated in Figure 3.2, to satisfy this minimum level of reinforcement, a smooth 3.15 mm diameter high yield steel reinforcing bar was used.

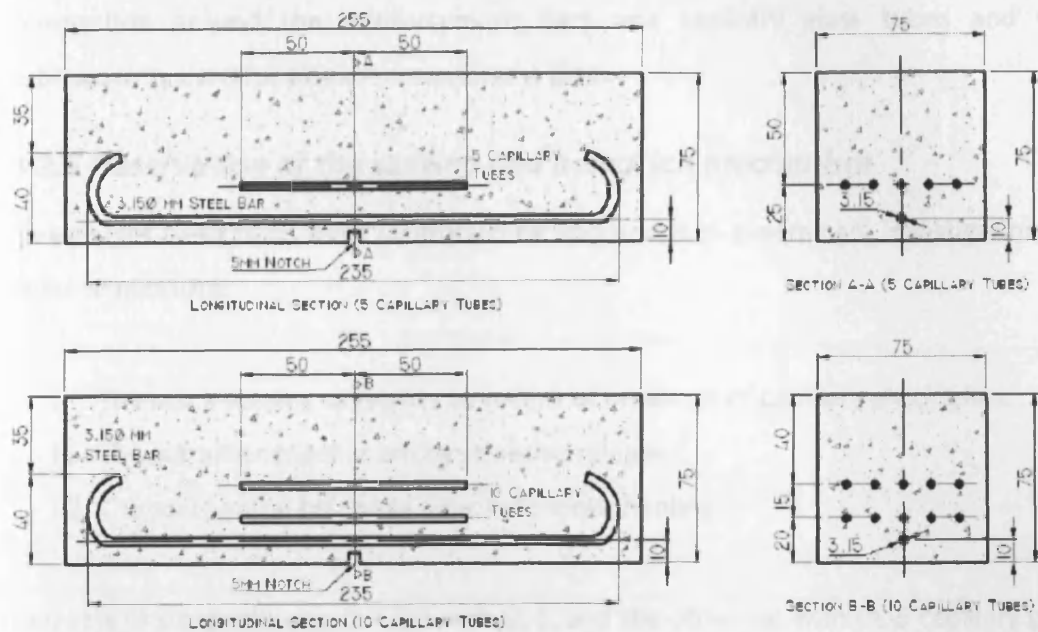


Figure 3.2 Schematic illustration of the specimen configuration for the two preliminary test sets using 3 mm diameter, 100 mm glass capillary tubes with (a) a single layer (SL-5), and (b) a double layer (DL-5) (Joseph et al., 2010a)

A further level of reinforcement was also tested in both the preliminary tests and the experimental programme described in Section 3.4.3. The higher level of reinforcement comprised 6.7 mm diameter smooth high yield steel bars. Both bars were subject to tensile tests in compliance with BS4449:2005 + A2:2009 with the results shown in Table 3.2.

Table 3.2 Mechanical properties for bar diameters 3.15 mm and 6.7 mm

Diameter (mm)	Profile	Elastic modulus (GPa)	0.2 % Proof stress (MPa)	Ultimate strength (MPa)	Elongation at failure (%)
3.15	Smooth	205.2 (0.9%)	563.1 (0.7%)	597.3 (2.1%)	12.0 (9.4%)
6.70	Smooth	192.3 (1.7%)	526.1 (1.2%)	576.3 (0.6%)	12.7 (8.1%)

### 3.2.4 Cementitious mix design

The autonomic self-healing system was studied using small scale prismatic mortar specimens of dimensions 75 x 75 x 255 mm with a mix ratio of 0.6: 1: 3.5 (water: PC: sand (sieved to 2 mm)) by weight. This mix provided suitable workability in terms of

compaction around the reinforcement bars and capillary glass tubes and was subsequently used for all experimental test sets.

### ***3.2.5 Observation of the sensing and actuation mechanism***

Three-point bend tests were conducted on specimens in preliminary investigations in order to measure:

- i). The crack sensing capability by means of breakage of capillary glass tubes.
- ii). The actuation mechanism by adhesive release.
- iii). The mechanical response after autonomic healing.

Two sets of six specimens, one set with SL-5, and the other set with DL-5 capillary glass tubes were tested. Within each set, two control (Ctrl) beams (filled with ink) and four self-healing (SH) beams filled with adhesive were tested. Specimens were subject to an initial loading stage to a predetermined crack width, then allowed to heal for a time period and then loaded to failure in a second loading cycle.

From inspection, a clean break of the glass tubes was visually confirmed and it was concluded that the mechanism of fracture was caused by tensile failure as previously observed by Li et al. (1998a). There was also evidence of a small amount of healing in one of the four SH beams for the DL-5 test sets. Under three-point bend tests a small recovery of the peak load during the second loading cycle was exhibited. Visual confirmation of adhesive release was also reported but this was not sufficient to produce a significant degree of self-healing. It was found that a considerable amount of adhesive remained inside the capillary tubes even after they were broken. This was also evident from the ink release in the control specimens.

It is believed that high negative pressures created by the wax plugs at either end of the capillary tubes resulted in poor dispersion of the adhesive. As illustrated in Figure 3.3, the capillary resistive forces within the tube were greater than both the capillary attractive force caused by the opening crack and the gravitational force. Therefore, only a limited amount of adhesive was released into the crack zone.

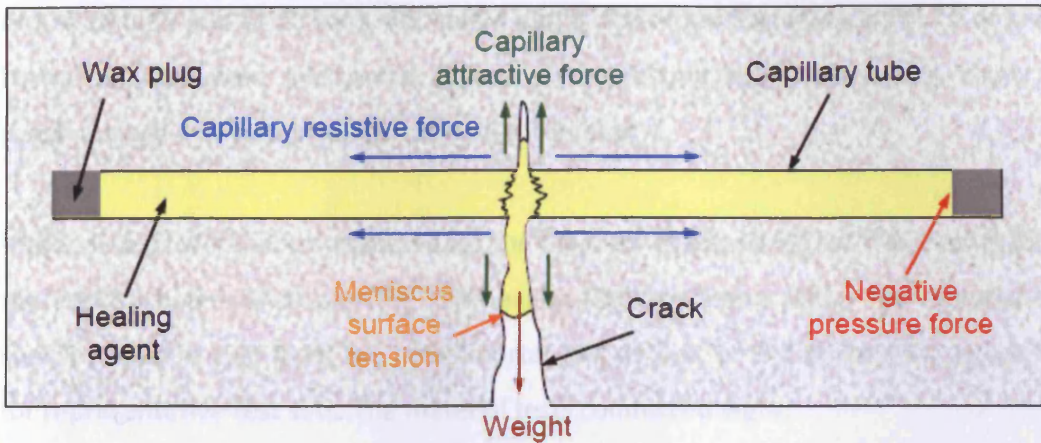


Figure 3.3 Schematic illustration of capillary forces within the glass capillary tubes (Joseph et al., 2010a)

In order to overcome this issue, longer capillary tubes were used in the cementitious matrix for the final experimental setup (Section 3.3.2), which had both ends of the tubes extended out of the specimen and open to the atmosphere. This meant that the adhesive release was free from negative pressure forces supplied by the wax ends.

### 3.3 Experimental procedure

The experimental procedure was established as a result of the preliminary investigation work described above.

#### 3.3.1 Parametric study

The experimental programme comprised six sets of tests. For each set, the specimen configuration was changed in order to investigate several parameters, as shown in Table 3.3. The parameters considered were:

1. The reinforcement level in specimens
2. The loading rate for three-point bend tests
3. The effect of notching specimens in order to localise cracking
4. The specimen age

As shown in Table 3.3, for experimental sets 1, 2, 3 and 5, specimens were loaded to a CMOD of 0.30 mm at 28 days. For sets 4 and 6, specimens were tested at 70 days due to the unanticipated mechanical failure of the testing equipment. As a result, the specimen age was also investigated as a parameter.

Material tests were also completed for the majority of experimental sets in addition to the control beam (Ctrl) and the self-healing (SH) specimen tests. The material test specimens were cast from the same mortar mix as that of the SH and Ctrl specimens for representative test sets. The material tests conducted were:

- Fracture energy tests,  $G_f$  – calculated from the force-central deflection response of the beams in accordance with the RILEM committee FMC-50 (1985). Specimens (255 x 75 x 75 mm) with a central notch of 10 mm were subject to three-point bend tests with a span of 200 mm
- Cube strength tests,  $f_{cu}$  – calculated from 100 mm cubes tested in accordance with BS EN12390-3:2009
- Cylinder splitting tests,  $f_{split}$  – calculated from 100 mm diameter, 200 mm long mortar cylinders tested in accordance with BS EN12390-6:2009

Table 3.3 Specimen configurations for sets one to six of the experimental programme (Joseph et al., 2010a). NOTE: Specimens loaded to a CMOD of 0.30 mm.

	Set 1. Notched, lightly reinforced	Set 2. Notched, lightly reinforced	Set 3. Notched, moderately reinforced	Set 4. Notched, heavily reinforced	Set 5. Un- notched, lightly reinforced	Set 6. Notched, lightly reinforced, variable loading rate
No. of Beams	2 Ctrl & 4 SH	2 Ctrl & 4 SH	2 Ctrl & 4 SH	2 Ctrl & 4 SH	2 Ctrl & 4 SH	1 Ctrl & 3 SH at each loading rate
Age at first test	28 days	28 days	28 days	70 days	28 days	70 days
Mix ratio by weight (water: P.C.s and)	0.55:1:3.5	0.6:1:3.5	0.6:1:3.5	0.6:1:3.5	0.6:1:3.5	0.6:1:3.5
Cube strength, $f_{cu}$ (MPa)	-	27.9 (After 28 days)	24.1 (After 28 days)	35.7 (After 70 days)	24.2 (After 28 days)	33.0 (After 70 days)
Specific fracture energy, $G_f$ (N/mm)	-	-	0.068 (After 28 days)	0.096 (After 70 days)	-	0.077 (After 70 days)
Cylinder's splitting strength, $f_{sp}$ (MPa)	-	2.4 (After 28 days)	2.0 (After 28 days)	3.6 (After 70 days)	2.2 (After 28 days)	3.5 (After 70 days)
Reinforcement	1No. 3.15 mm $\phi$ high yield steel bar	1No. 3.15 mm $\phi$ high yield steel bar	2No. 3.15 mm $\phi$ high yield steel bar	3No. 6.7 mm $\phi$ high yield steel bar	1No. 3.15 mm $\phi$ high yield steel bar	1No. 3.15 mm $\phi$ high yield steel bar
Adhesive supply system	4No. 3 mm ID capillary tubes, open at one end	4No. 3 mm ID capillary tubes, open at both ends	4No. 3 mm ID capillary tubes, open at both ends	4No. 3 mm ID capillary tubes, open at both ends	4No. 3 mm ID capillary tubes, open at both ends	4No. 3 mm ID capillary tubes, open at both ends
5 mm deep notch	Yes	Yes	Yes	Yes	No	Yes
Stroke loading rate (mm/s)	0.003	0.008	0.003	0.008	0.003	0.00075, 0.003 and 0.012

### 3.3.2 Specimen preparation

As shown in Figure 3.4, double specimen moulds were used for casting. Within each specimen mould a 10 mm spacer brick with a 2 mm notch was centrally placed 25 mm from either end of the mould. The reinforcement bars were cut to a length of 480 mm and manually bent in order to provide shear anchorage as a result of the bars smooth profile. The reinforcement bars were then placed into the notch of the small bricks and secured with plastic padding to avoid movement of the reinforcement. The glass tubes were carefully fed through pre-drilled holes of the prismatic moulds with both ends of the glass tubes subsequently filled with wax to prevent any material entering during casting. The wax was removed prior to filling the tubes with healing agent.

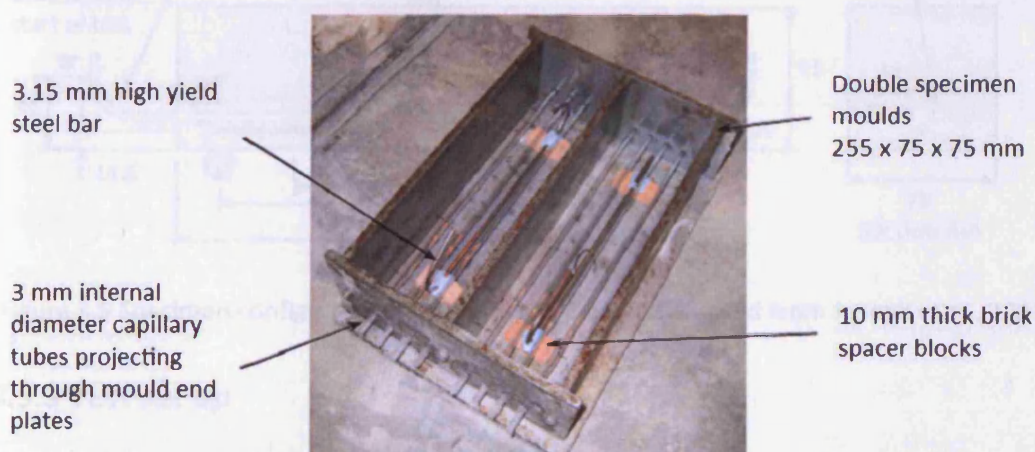


Figure 3.4 Capillary glass tubes and reinforcement preparation for specimens (Joseph et al., 2010a)

The mortar mix was poured into the moulds in 3 layers and subject to vibration in order to expel the majority of the air in the mix. The specimens were then covered with wet hessian and cured for 24 hours before being de-moulded. After de-moulding specimens were notched at the centre span to a depth of 5 mm. Notching was excluded for test set 5.

Plastic curved supply tubes were manufactured that were placed onto the protruding glass tubes in the specimens. After de-moulding, the glass tubes were cleaned out to avoid contamination of the healing agent that was subsequently injected. The supply



tubes were then attached to both ends as illustrated in Figure 3.5, and marked at a height of 45 mm above the bottom of the beam to designate the glue level. For each glass tube, the healing agent was injected with a syringe (to minimise air voids in the tubes) in one end of a supply tube until it reached the marked levels of both supply tubes. For control specimens, the healing agent was replaced with approximately 10 ml of low viscosity ink tracing die.

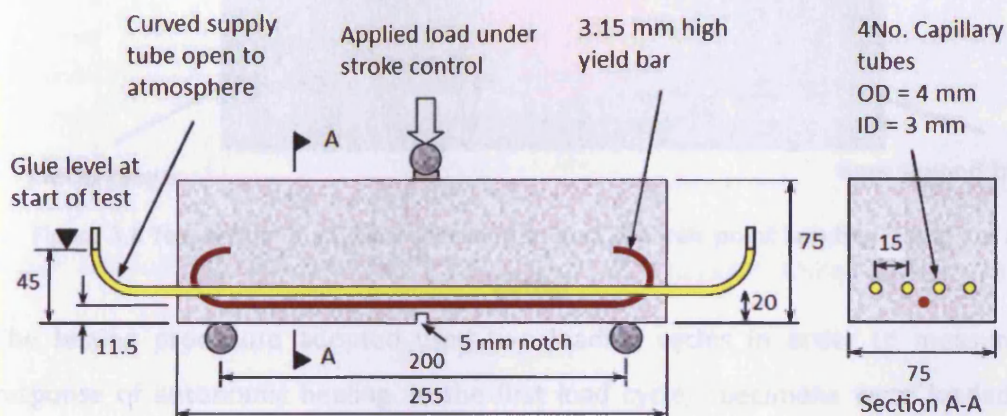


Figure 3.5 Specimen configuration for sets 2, 3, 4, 5 and 6 (adapted from Joseph et al., 2010a)

### 3.3.3 Test set up

The specimens were subject to three-point bend tests using an Avery Denison 7152 universal servo hydraulic testing machine as shown in Figure 3.6. Specimens were loaded in stroke control at the rates outlined in Table 3.3. Central deflection of the specimens was measured with an LVDT (Linear Variable Differential Transducer) gauge in order to avoid bedding in effects. The LVDT gauge was held in place by a custom made aluminium arm that was connected to one side of the specimen as shown in Figure 3.6. A CMOD (Crack Mouth Opening Displacement) gauge was placed in between two knife edges that were attached either side of a notch.

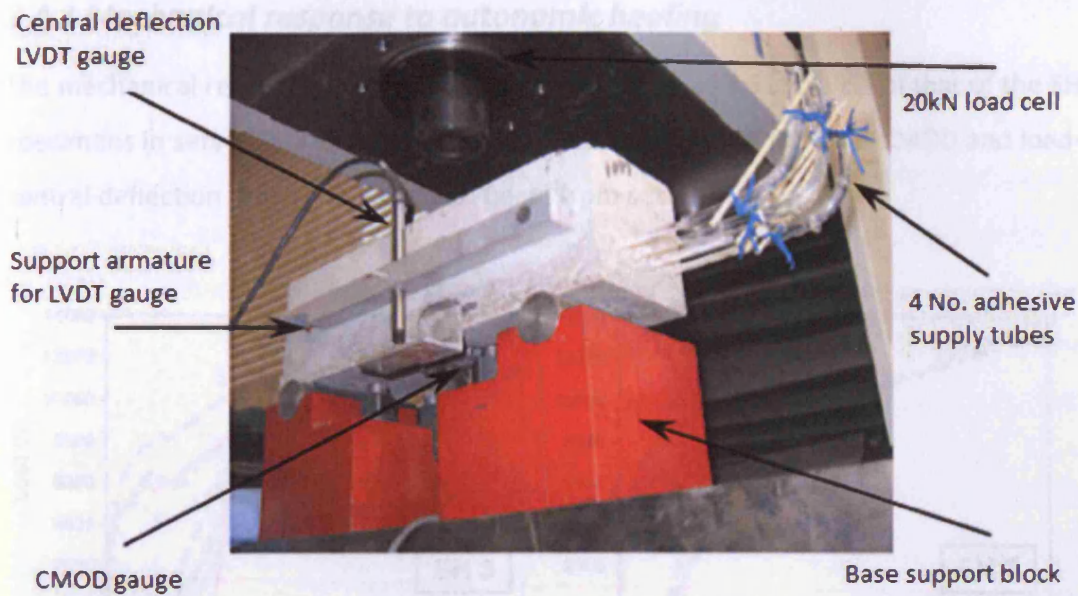


Figure 3.6 Test set up of a typical specimen subject to three-point bending (Joseph et al., 2010a)

The testing procedure adopted used two loading cycles in order to measure the response of autonomic healing. In the first load cycle, specimens were loaded to a crack width of 0.30 mm, and then unloaded. SH specimens were then stored in the laboratory for 24 hours in order to allow full curing of the healing agent. For the second loading cycle, all specimens were tested at the same loading rate as the first cycle until failure of the specimens was exhibited or until a central deflection of at least 3 mm was reached. In the case of control specimens, the second loading cycle took place immediately after the first.

### 3.4 Results and discussion

As mentioned, experimental sets 1, 2, 3, and 5 have been previously reported and discussed in Joseph (2009). For comparison with the results of sets 4 and 6, the results of all sets 1 to 6 are presented in Appendix B.

### 3.4.1 Mechanical response to autonomic healing

The mechanical response of the SH specimens in sets 4 and 6 is typical of that of the SH specimens in sets 1, 2, 3 and 5. Figure 3.7 presents curves of the load-CMOD and load-central deflection data for a typical SH beam from set 4.

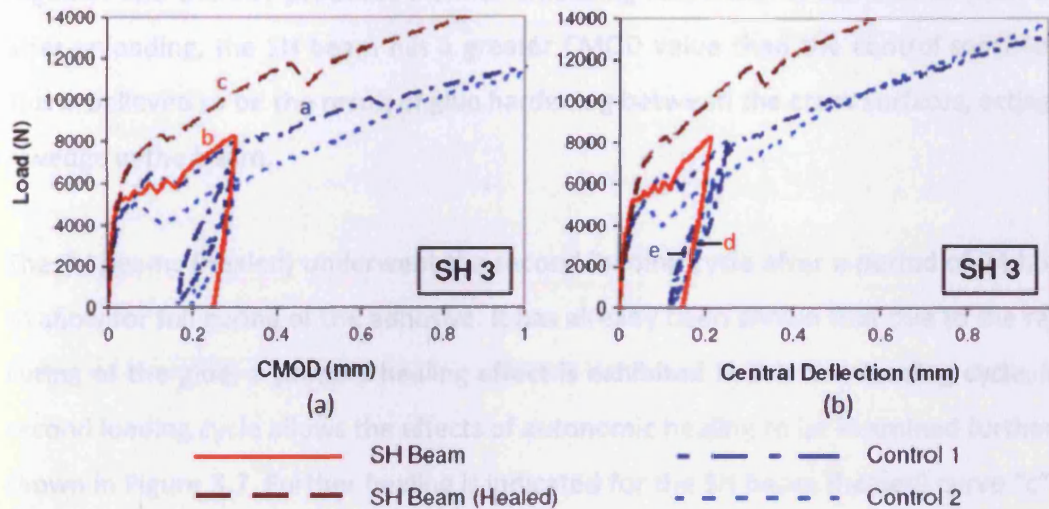


Figure 3.7 SH beam 3 and control 1 from set 4 (a) Load-CMOD and (b) Load-central deflection (adapted from Joseph, 2009)

Figure 3.7 shows that the response is non-linear prior to the peak load, for the first loading cycle of the SH beam and the two control beams, which is assumed to be the result of micro-cracking. The saw-tooth like loading curve is believed to be the result of fracture of all four glass capillary tubes (which can be heard) as represented by four small peaks. Subsequently, the load capacity continues to increase because of the presence of the steel reinforcement.

As shown in Figure 3.7(a) the stiffness of the beams can be represented by the gradients a, b and c for control beam 1, SH beam 3 and SH beam 3 (healed) respectively. It can be seen that gradient "b" is steeper than gradient "a" which is attributed to a primary healing effect as a result of glue release from glass tube fracture. Furthermore, the primary healing effect is believed to be enhanced as a result of accelerated curing of the acidic glue solution in the alkaline cementitious environment as described in the healing agent data sheet (Appendix A).

This primary healing effect can also be shown in the unloading curve for the SH beam. As shown in Figure 3.7(b), the unloading curve for the SH beam “d” is steeper in comparison to the unloading curve for the control beams “e”. Again, it is proposed that the rapid curing of the glue entering the crack zone bonds the crack surfaces together and thereby produces a stiffer unloading response. It can also be seen that after unloading, the SH beam has a greater CMOD value than the control specimens. This is believed to be the result of glue hardening between the crack surfaces, acting as a wedge in the beam.

The SH beams (healed) underwent the second loading cycle after a period of 24 hours to allow for full curing of the adhesive. It has already been shown that due to the rapid curing of the glue, a primary healing effect is exhibited in the first loading cycle. The second loading cycle allows the effects of autonomic healing to be examined further as shown in Figure 3.7. Further healing is indicated for the SH beam (healed) curve “c” by a steeper gradient in comparison to both gradients “a” and “b”. The peak load for the SH beam (healed) is also approximately 20 % greater than the initial peak load, and the response after the peak suggests a more ductile behaviour. It is also shown that the loading curve for the SH beam (healed) in the second loading cycle has the same gradient as the unloading curve for the SH beam in the first loading cycle. This also suggests healing as illustrated by the recovery of the stiffness of the specimens.

For SH beams, the stiffness recovery and increase in peak load during the second loading cycle confirms that autonomic healing has been achieved. This is further emphasised by comparing the stiffness response of these specimens with that of the control specimens during unloading and reloading. The healing effect is believed to be the result of the successful development of the autonomic healing system providing suitable sensing, actuation and response mechanisms. Fracture of the glass capillary tubes is exhibited in response to the cracking of the beam under loading. The healing agent is subsequently released, and is able to penetrate the crack zone due to its low viscosity and form a bond between the two crack surfaces that increases the strength and recovers the stiffness of the beam.

### 3.4.2 Effect of loading rate

In experimental set 6, the effect of three loading rates, 0.00075 mm/s, 0.003 mm/s and 0.012 mm/s was examined on lightly reinforced mortar beams. In Figure 3.8, the load-CMOD response for three typical SH beams tested at the different loading rates is shown.

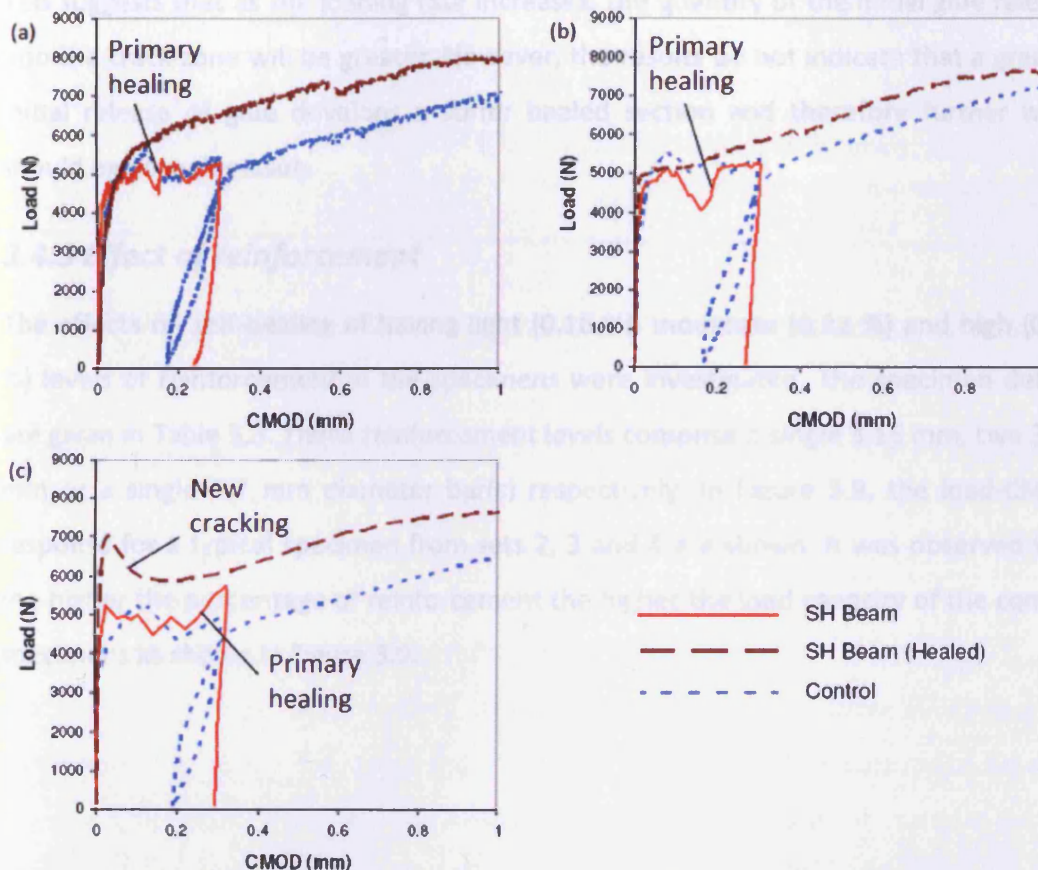


Figure 3.8 Load-CMOD response for loading rates (a) 0.00075 mm/s, SH beam 1 from set 6 (b) 0.003 mm/s, SH beam 4 from set 6, and (c) 0.012 mm/s, SH beam 7 from set 6 (Joseph et al., 2010a)

From Figure 3.8, it can be seen that the main effect of loading rate is on the primary healing response of the SH beams. As the loading rate is increased, the stiffness of the primary healing response decreases. The slower loading rate results in a slower rate of crack opening that in turn slows the migration of the glue into the crack zone. This provides a longer time for bonding between the crack surfaces and is believed to be the reason for a stiffer response in the primary healing phase.

In Figure 3.8(c), new crack formation in the SH beam (healed) is indicated by a peak load followed by a sharp drop. The peak load and stiffness gradient of the SH beam (healed) is increased in comparison with both the SH beam during the first load cycle and the control specimen. It may also be seen that as the loading rate was increased, the cracking of the individual glass capillary tubes occurred over a smaller time period. This suggests that as the loading rate increases, the quantity of the initial glue release into the crack zone will be greater. However, the results do not indicate that a greater initial release of glue develops a stiffer healed section and therefore further work should explore this issue.

### ***3.4.3 Effect of reinforcement***

The effects on self-healing of having light (0.16 %), moderate (0.32 %) and high (0.72 %) levels of reinforcement in the specimens were investigated. The specimen details are given in Table 3.3. These reinforcement levels comprise a single 3.15 mm, two 3.15 mm or a single 6.7 mm diameter bar(s) respectively. In Figure 3.9, the load-CMOD response for a typical specimen from sets 2, 3 and 4 are shown. It was observed that the higher the percentage of reinforcement the higher the load capacity of the control specimens as shown in Figure 3.9.

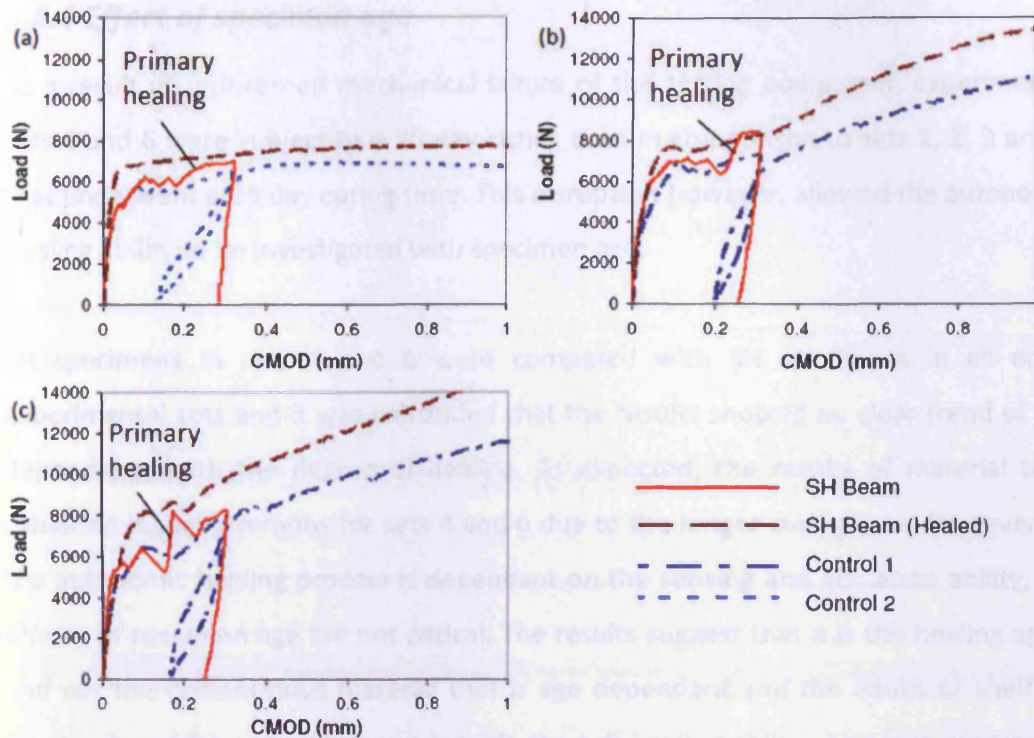


Figure 3.9 Load-CMOD response of (a) Single 3.15 mm reinforcement, SH beam 1 from set 2 (b) Double 3.15 mm reinforcement, SH beam 3 from set 1, and (c) Single 6.7 mm reinforcement, SH beam 4 from set 4 (Joseph et al., 2010a)

As shown in Figure 3.9 the effect of varying the reinforcement percentage is also evident in the primary healing effect. It is believed that the greater the reinforcement percentage, the slower the rate of crack opening. As a result, the migration of the glue into the crack zone is slower. This allows a longer bonding time for the glue on the crack surfaces, which in turn leads to an increase in stiffness. Although the glue migrates more slowly into smaller cracks under capillary flow, this flow is still fast relative to the loading rate. However, the key question here is how the relative and absolute increases in stiffness (between the SH and control specimens) vary with reinforcement percentage. As shown in Figure 3.9(c), single 6.7 mm reinforced specimens developed the greatest secondary healing stiffness response. It is believed that in this case internal cracking is greater due to the larger diameter reinforcement and therefore there is a greater migration of glue which in turn leads to a stiffer response to loading.

### **3.4.4 Effect of specimen age**

As a result of unforeseen mechanical failure of the testing equipment, experimental sets 4 and 6 were subject to a 70 day curing time in comparison to sets 1, 2, 3 and 5 that underwent a 28 day curing time. This disruption however, allowed the autonomic healing ability to be investigated with specimen age.

SH specimens in sets 4 and 6 were compared with SH specimens in all other experimental sets and it was concluded that the results showed no clear trend of age dependency with the degree of healing. As expected, the results of material tests exhibited higher strengths for sets 4 and 6 due to the longer curing time. However, as the autonomic healing process is dependant on the sensing and actuation ability, the effects of specimen age are not critical. The results suggest that it is the healing agent and not the cementitious material that is age dependant and the issues of shelf life need to be addressed in order to provide the self-healing ability. This is in contrast to the effects of autogenous healing, where it has been observed that the healing ability is greater in early age specimens as discussed in Section 2.3.1(Edvardsen, 1999).

### **3.4.5 Qualitative results**

Further to the results of the mechanical testing, qualitative observations of crack formation and glue release were observed during the self-healing tests.

#### **3.4.5.1 New crack formation**

As shown in Figure 3.10, SH specimens exhibited new crack formation during second cycle loading as a result of the autonomic healing of the cracks induced in the first loading cycles.



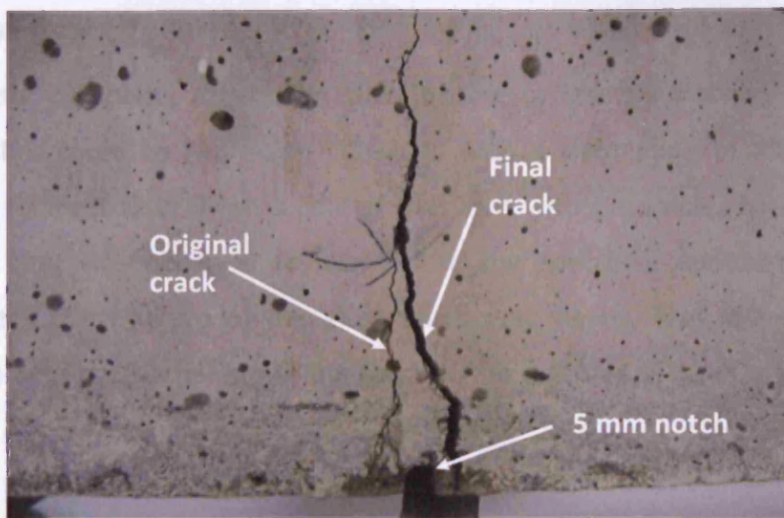


Figure 3.10 New crack formation as a result of autonomic healing of the original crack for SH beam 1 from set 6

New crack formation was not exhibited in control specimens and remained exclusive to SH specimens. This shows that the autonomic healing process was effective in healing pre-formed cracks and the use of Rite-lok EC5 cyanoacrylate provided sufficient bond between the crack surfaces. Further evidence of the effectiveness of the healing agent is provided by the occurrence of glue stringing and glue bridging which may be seen in Figure 3.11.

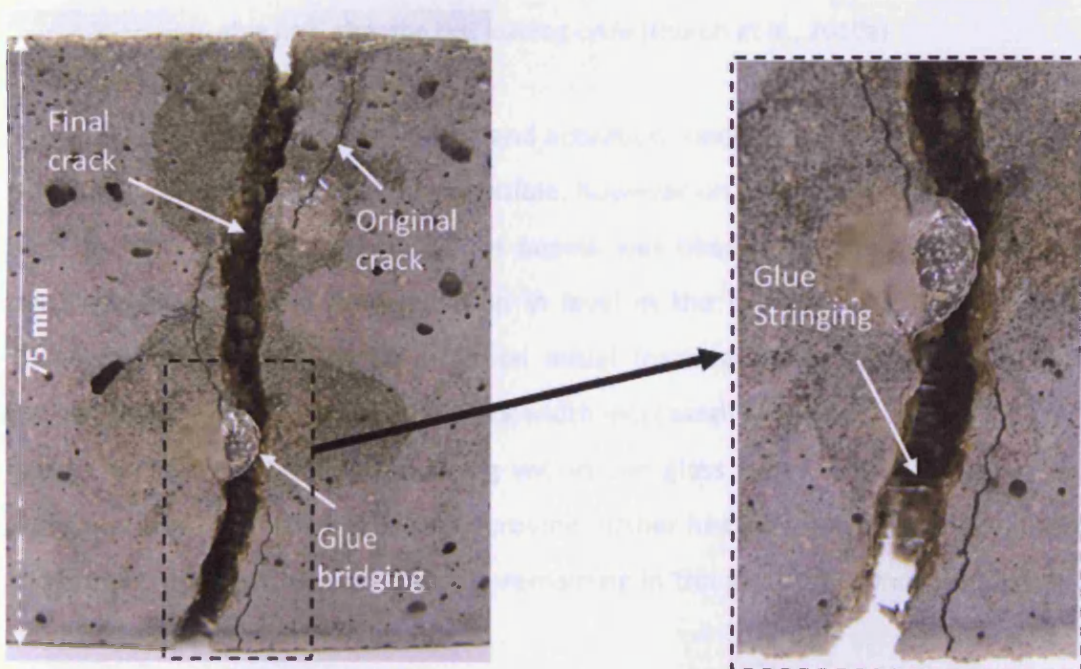


Figure 3.11 Typical examples of glue stringing and bonding exhibited in specimens

### 3.4.5.2 Glue flow

As previously described, during the first loading cycles the fracture of the glass capillary tubes could be heard and coincided with a sharp drop in the strength of specimens. Figure 3.12(a) shows a control specimen with glass tubes filled with an ink tracing dye that was observed to leak out of the specimen approximately 20–30 seconds after the fracture of the glass tubes was heard. This indicated that an appropriate sensing mechanism in the form of the fracture of glass tubes had been identified.

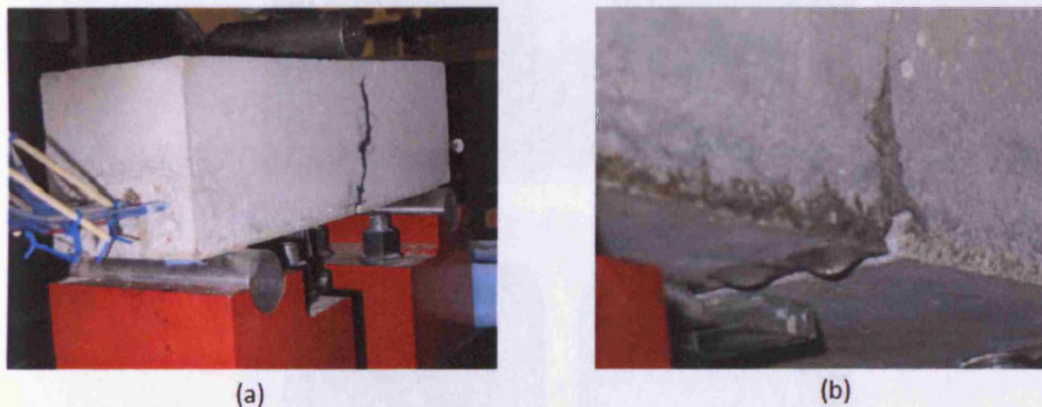


Figure 3.12 (a) control specimen exhibiting ink migration during testing (b) SH beam exhibiting glue flow after the first loading cycle (Joseph et al., 2010a)

Figure 3.12(b) also shows the sensing and actuation mechanisms in the SH beams. As the glue is colourless, it is not clearly visible, however on close inspection, the release of glue into the crack zone of the SH beams was observed. The quantity of glue released was measured from the drop in level in the supply tubes. The measured quantities varied from 0.1 to 0.3 ml upon initial fracture of the glass tubes with a further drop being observed as the crack width increased. It was noted that after crack healing there was still glue remaining within the glass tubes. The presence of the remaining glue in the glass tubes may provide further healing from crack re-opening or additional cracking. However, the glue remaining in the glass tubes must not set as a result of being exposed to open air.

For a given crack opening it may be expected that there is a correlation between the amount of glue released and the area of crack that is healed. As shown for SH beam 1 in Figure 3.13(a), an approximate capillary rise of 10 mm corresponded to a minimal healing response. In contrast, SH beam 4 in Figure 3.13(b) exhibited a 30mm rise and a mechanical response in which there was an increase in peak load and stiffness during the second loading cycle.

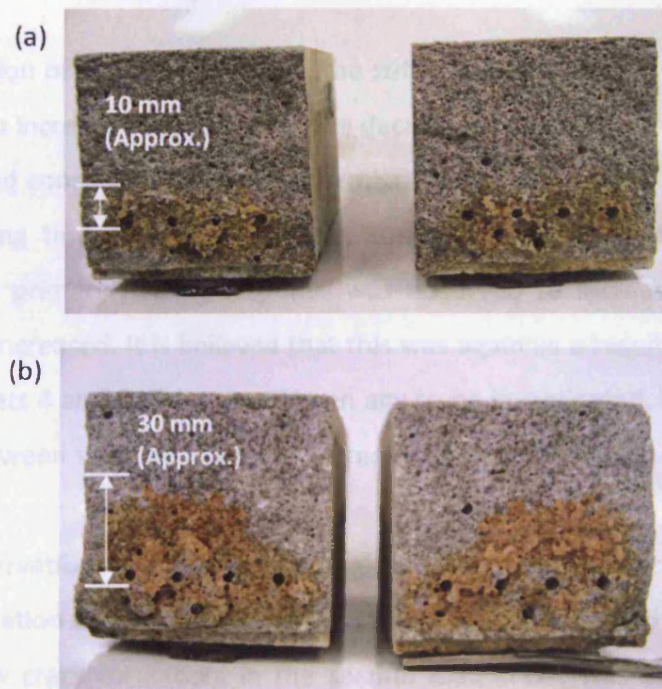


Figure 3.13 Capillary rise of glue in crack zone (a) SH beam 1 (b) SH beam 4, for set 1 specimens

Furthermore, when the surfaces were separated at the end of the experiment, discolouration of the mortar was observed. This enabled a direct measurement of the extent of glue migration to be made. Although, Rite-Lok EC5 is a colourless adhesive, the staining of the mortar is believed to be the result of the glue release.

### 3.5 Conclusions

This chapter has described the experimental results from 1 preliminary and 6 subsequent (main) series of tests on autonomic healing of cementitious materials. Prismatic mortar specimens with varying reinforcement levels and adhesive filled embedded glass tubes have been subject to three-point bending. Experimental sets 4

and 6 have been reported in detail in this chapter. Sets 1, 2, 3 and 5 had previously been described in Joseph (2009). The mechanical response of specimens with the autonomic healing system included has been contrasted with that from control tests with no such system. Qualitative observations of healing mechanisms have also been discussed. It is concluded that two healing mechanisms exist; primary healing, which is an almost immediate response following glass tube fracture and a secondary healing response which was observed in the second load cycle.

From investigation of experimental set 6, the stiffness of the primary healing response was observed to increase as the loading rate decreased. This was due to a slower crack opening rate and consequently slower glue migration into the crack zone, allowing for a longer bonding time between the crack surfaces. From experimental set 4, the stiffness of the primary healing response was observed to increase as the level of reinforcement increased. It is believed that this was again as a result of a slower crack opening rate. Sets 4 and 6 allowed specimen age to be investigated, however, no clear relationship between specimen age and degree of healing was observed.

Qualitative observations also identified that glass tube fracture (which could be heard) resulted in migration of both the healing agent in the SH beams and ink in the control specimens. New crack formation, in the second load cycle, was also observed as a result of the autonomic healing of the initial crack during the first load cycle.

The healing of cracks serves to improve the durability of cementitious materials. The use of a low viscosity cyanoacrylate to heal cracks and enhance the strength of the cementitious matrix has been shown. The ability of specimens to sense and respond to damage in a passive manner also makes the autonomic healing concept attractive for commercial use. However, the concept is still very much laboratory based and the integration of autonomic healing systems into commercial structures will require further work. In addition, autonomic healing requires the use of a healing agent that is not generic in the make up of cementitious materials. Autogenous healing is however, the natural ability of cementitious materials to self-heal as described in Section 2.3 and is addressed in the following chapters.

## Chapter 4

### Autogenous healing (proof of concept)

#### 4.1 Introduction

This chapter describes an experimental investigation into the development of a new material system for crack closure of cementitious materials using shrinkable polymer tendons. It includes discussion of the concept, initial polymer screening tests including the experimental investigation of the chosen polymer, specimen preparation and the experimental procedure adopted for the testing of the cementitious material system. In addition, the results of a proof of concept study are presented and discussed.

The polymer testing programme described in this chapter is shown in Table 4.1 and further details of a full parametric investigation are reported by Dunn (2010).

Table 4.1 Polymer investigation

<b>Test</b>	<b>Section</b>	<b>Conducted by</b>
Screening tests	4.4.1	Netcomposites
Preliminary tests - first phase	4.4.2	Cardiff University
Preliminary tests – second phase	4.4.3	Cardiff University
• Constant displacement tests	4.4.3.1	
• Constant load tests	4.4.3.2	
PET Shrink-tite experimental investigation	4.5	Cardiff University

## 4.2 The concept

The basic concept of the material system investigated in the current study is summarised below and illustrated in Figure 4.1.

- Cracking of cementitious materials occurs due to thermal effects, early age shrinkage and/or mechanical loading
- Polymer shrinkage is activated by heating in order to produce a prestress which closes cracks and applies a compressive stress across the closed crack faces
- Autogenous healing is enhanced by compression across the closed crack faces

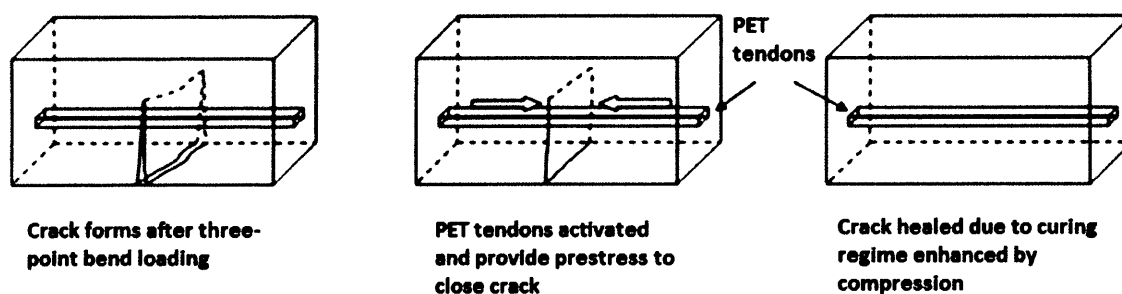


Figure 4.1 Schematic illustration of concept for the material system LatConX (Isaacs et al., 2010)

The resulting material system, which has been christened LatConX, is the subject of a patent application (Patent application PCT/GB2008/002651) which is described in Jefferson et al. (2010); Lark et al. (2009); Isaacs et al. (2009); and Dunn et al. (2009).

It is envisaged that the durability of cementitious materials could be greatly enhanced as a result of the crack closure provided by the shrinkable polymer tendons. This method of crack closure to enhance autogenous healing is one of four classes that are being investigated. As shown in Table 4.2, each class is characterised by the polymer shrinkage stress that can be generated. The shrinkage stress for class I and II is defined as the stress required by the polymer tendon to provide effective crack closure of specimens. Class III refers to 1D prestressing (i.e. conventional prestressing), whereas class IV is envisaged to be full triaxial confinement. The stresses shown were derived

assuming that the polymer tendon was 2 % of the area of the cementitious specimen under consideration and were based on a nominal tensile strength of the cementitious matrix of approximately 2 MPa.

Table 4.2 Material system classes

<b>Class</b>	<b>Definition</b>	<b>Minimum tendon shrinkage stress (MPa)</b>	<b>Minimum tendon tensile strength (MPa)</b>
<b>Class I</b>	Crack closure/ Enhanced autogenous healing	15	100
<b>Class II</b>	Crack prevention	30	100
<b>Class III</b>	Partial confinement	100	2000
<b>Class IV</b>	Full triaxial confinement	1000	2000

At present, only Class I has been investigated and trial tests for polymers with higher shrinkage stresses suitable for classes II, III and IV are ongoing.

### 4.3 Polymer criteria

Several criteria were identified in order to establish a suitable polymer for the proposed system. These are described in the following sub-sections.

#### 4.3.1 Activation temperature

The activation temperature is required to be at least 60 °C and less than 100 °C. A minimum temperature of 60 °C is required to avoid activation by heat from climatic conditions and also from heat as a result of hydration. Activation has to be below 100 °C in order to sustain suitable conditions for autogenous healing to occur. Subjecting cementitious materials to temperatures greater than 100 °C can cause damage to the matrix and evaporate water in the matrix which could influence the degree of hydration and autogenous healing.

#### 4.3.2 Minimum shrinkage stress

The minimum shrinkage stress generated by the polymer is to be 20 MPa. As discussed in Section 2.3.2, ter Heide et al. (2005) showed that a minimum compressive stress of

0.5 MPa enhances autogenous healing. This criterion was calculated on the basis that a minimum shrinkage stress of 20 MPa is required to provide crack closure and put a crack into a compression of at least 1 MPa (Jefferson et al., 2010), for an eccentric tendon of 2% of the gross concrete area.

### **4.3.3 Young Modulus**

The polymer should have a Young's Modulus of less than 6 GPa in order to limit creep and shrinkage losses in the concrete. This is an arbitrary value but the lower the E-value of the polymer, the lower the loss of stress in the polymer; for any given contraction of the cementitious matrix.

### **4.3.4 Resistant to an alkaline environment**

Due to the alkaline environment of the cementitious matrix, it is necessary for the polymer to be resistant to an alkalinity of up to pH 12.

### **4.3.5 Relaxation**

In order to maintain the prestress over time, the relaxation losses in the polymer should be no more than 30 % over 50 years. This has been based on trying to ensure a service life of concrete structures of at least 50 years. The loss in relaxation is less relevant for class I in comparison to classes II, III and IV. In the case of class I, the polymer is activated at an early age in order to provide crack closure to enhance autogenous healing.

## **4.4 Polymer investigation**

### **4.4.1 Screening tests**

The screening tests were conducted in collaboration with the technology company NetComposites. The semi-crystalline polymers polyethylene (PE), polyethylene terephthalate (PET) and polypropylene (PP) were tested because they were identified as having the potential to develop suitable shrinkage stresses (20 – 80 MPa) for the LatConX system (Long and Ward, 1991; Gupta et al., 1994). These initial candidate polymers are presented in Table 4.3.



Table 4.3 Candidate materials studied in collaboration with NetComposites

Name	Polymer	Description	Form	Area <sup>a</sup> (mm <sup>2</sup> )	Supplier
PP Pure	PP	Orientated PP tape coextruded with PP-PE copolymer	Tape	0.126	Lankhorst
PP Armordon	PP	Orientated PP tape coextruded with PP-PE copolymer	Tape	0.224	Don & Low
PP Lotrak	PP	Orientated PP tape	Tape	0.10	Don & Low
PE Certran	PE	Melt spun PE continuous filament yarn	Yarn	0.061	University of Leeds
PP Multiprof	PP	Orientated PP tape coextruded with heat sealing layer, fibrillated	Fibrillated tape	0.24	Lankhorst
PET Shrink-tite	PET	Orientated PET tape	Tape	0.10	Aerovac

**(Appendix D)**

<sup>a</sup>Area = original cross-sectional area of specimen.

These polymers were subjected to an initial programme of testing in order to identify those which met the criteria outlined in Section 4.3. Specimens of length 280 mm were subject to heating from ambient (25 °C) at a rate of 1 °C per minute until failure in a tensile loading rig built into a thermal chamber. The results concluded that only one of the candidate materials satisfied the criterion of developing a shrinkage stress greater than 20 MPa. As shown in Figure 4.2, PET Shrink-tite developed a peak stress of 31.5 MPa. This candidate polymer also had the advantage of being an off the shelf product that could be provided in the form of 32 mm wide x 0.046 mm thick tape.

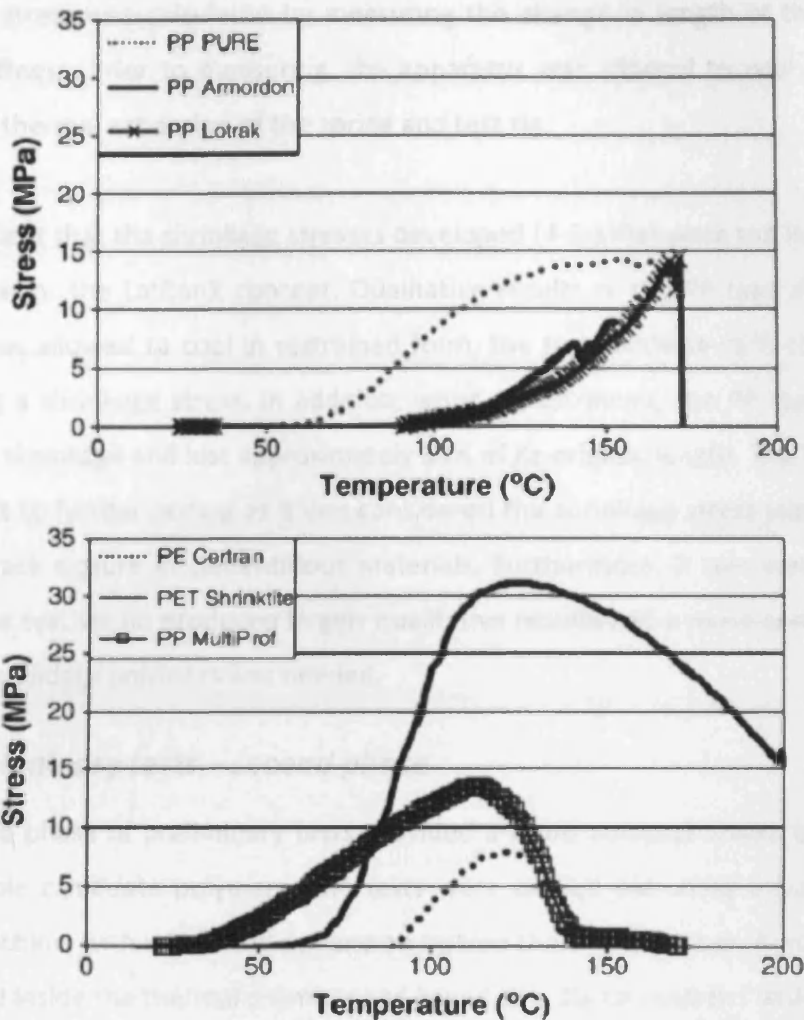


Figure 4.2 Results from candidate material tests (Jefferson et al., 2010)

#### 4.4.2 Preliminary tests – first phase

In addition to the limited screening tests undertaken by NetComposites, a preliminary series of tests (first and second phase) to confirm their findings and to obtain more statistically reliable data were undertaken. For this purpose, a polypropylene tape (PP tape) was used. The PP tape was prepared into individual strips measuring 0.06 x 2 x 250 mm and a tendon specimen was formed by placing 10 strips on top of one another.

In the first phase of preliminary tests the tendons were attached between a spring of known stiffness and a fixed support and subject to heating at 120°C for 2 hours. The

shrinkage stress was calculated by measuring the change in length of the spring of known stiffness. Prior to measuring, the apparatus was allowed to cool in order to overcome thermal expansion of the spring and test rig.

It was evident that the shrinkage stresses developed (4-5 MPa) were too low to satisfy the criteria for the LatConX concept. Qualitative results of the PP tape showed that when it was allowed to cool in restrained form, the tape became stiff, consequently generating a shrinkage stress. In addition, when unrestrained, the PP tape exhibited significant shrinkage and lost approximately 90% of its original length. The PP tape was not subject to further testing as it was considered the shrinkage stress was too low to provide crack closure in cementitious materials. Furthermore, it was concluded that the current test set up produced largely qualitative results and a more comprehensive study of candidate polymers was needed.

#### ***4.4.3 Preliminary tests – second phase***

The second phase of preliminary tests provided a more comprehensive investigation into suitable candidate polymers. The tests were carried out using a Dartec tensile testing machine, with a 5kN load cell and an Instron thermal chamber. A thermocouple was placed inside the thermal chamber and linked to a digital recorder which was used to measure the real-time temperature. The polymers investigated in this study were:

- Glass fibre reinforced polypropylene strips (GFRPP strips)
- Woven polypropylene strips (WPP strips)
- Polyethylene Terephthalate Shrink-tite tapes (PET tape)

Two types of test were carried out on these candidate polymers. Constant displacement tests were undertaken that enabled the shrinkage stress to be measured and constant load tests that enabled the displacement to be measured as a result of thermally activating the polymers.

#### **4.4.3.1 Constant displacement tests**

The candidate specimens were placed inside the thermal chamber and gripped at both ends by the tensile machine grips. The grip distance remained constant and a prestress of 30 MPa was applied. The stress developed in the polymers, the temperature of the thermal chamber and the displacement between the grips were continuously measured. Specimens were heated to designated temperatures until a stress plateau was observed on the graph data. Heating was subsequently stopped and the temperature inside the thermal chamber was allowed to return to ambient. For all specimens, several temperatures and soak times were investigated in order to find the maximum shrinkage stresses. As a result, the test procedure was modified.

From the results of all polymers tested, a stress increase was associated with an increase in temperature and subsequent cooling. The results of GFRPP strip specimens are shown in Figure 4.3. A stress of 1 Mpa was generated during heating at 140 °C. After the heat was removed, the specimens exhibited a significant stress increase. As shown in Figure 4.3a, a maximum stress of approximately 9 MPa was observed after exposure to a temperature of 140 °C for 2 hours. It is believed that thermal contraction of the glass fibres in the polypropylene (GFRPP) specimens provided an increase in tensile strength as a result of the cooling temperature. The results also showed a significant loss of stress due to relaxation in the polymer specimens, which was approximately 25 % over a period of 70 hours.

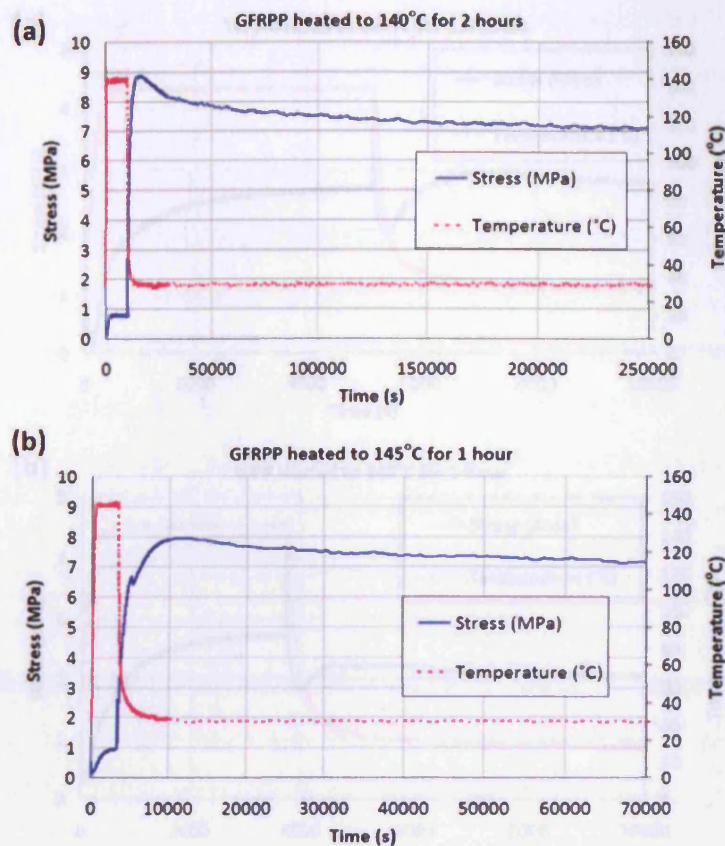


Figure 4.3 Restraint heating tests for GFRPP strips for: (a) 140 °C for 2 hours, and (b) 145 °C for 1 hour

The results for typical WPP strip specimens exposed to a temperature of 140 °C for 1.5 hours or 145 °C for 1 hour are shown in Figure 4.4. The WPP strip specimens did not satisfy the 20MPa shrinkage stress criterion. At the highest tested temperature of 155 °C it was observed that the maximum stress reached was only 3.5 MPa. Qualitative observations showed delamination and bulging of the WPP strips as a result of heating and confirmed that the polymer was unsatisfactory for the LatConX concept.

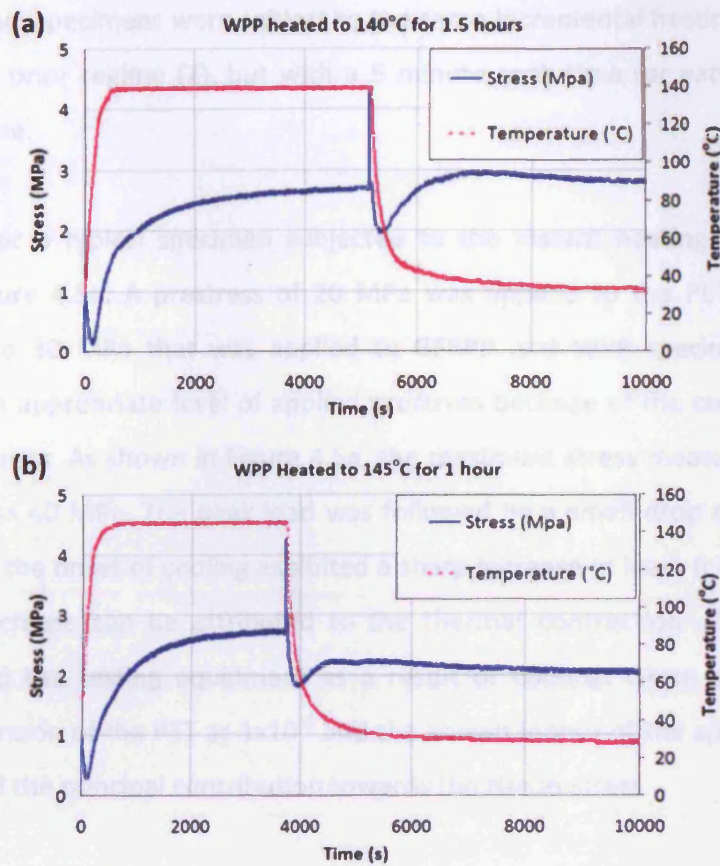


Figure 4.4 Restrainted heating tests for WPP strips for: (a) 140 °C for 1.5 hours, and (b) 145 °C for 1 hour

PET tape specimens were subject to a more comprehensive heating regime as they were considered the primary candidate polymer from screening tests. The three heating rates investigated were:

1. Instant heating: specimens were subject to heating at 90 °C for 3 hours after which time the temperature was allowed to return to ambient conditions
2. Incremental heating: specimens were subject to heating at 10 °C increments from 30 °C to 120 °C. As soon as the designated temperature was reached, the thermal chamber temperature was increased to the next increment.

3. Soaking: specimens were subject to the same incremental heating as described in the prior regime (2), but with a 5 minute soak time for each temperature increase.

The results for a typical specimen subjected to the instant heating regime (1) are shown in Figure 4.5a. A prestress of 20 MPa was applied to the PET specimens in comparison to 30 MPa that was applied to GFRPP and WPP specimens. This was considered an appropriate level of applied prestress because of the cross section size of PET specimens. As shown in Figure 4.5a, the maximum stress measured as a result of heating was 40 MPa. The peak load was followed by a small drop during the soak period but at the onset of cooling exhibited a sharp increase in load. It is believed that this sharp increase can be attributed to the thermal contraction of both the PET specimen and the testing equipment as a result of cooling. Given a coefficient of thermal expansion of the PET as  $1 \times 10^{-4}$  and the known length of the specimens, it can be considered the principal contribution towards the rise in stress.

The results of a typical specimen subject to the incremental heating and soaking regimes are shown in Figures 4.5b and 4.5c respectively. In both Figures 4.5b and c, a maximum stress of approximately 33 MPa at a temperature of 120 °C is shown. By comparison of the incremental heating regime (2) and the soaking regime (3), the specimens tested in both these cases showed comparable shrinkage stresses for the same temperatures. This is indicated by the plateau for each temperature increment as shown in Figure 4.5c.

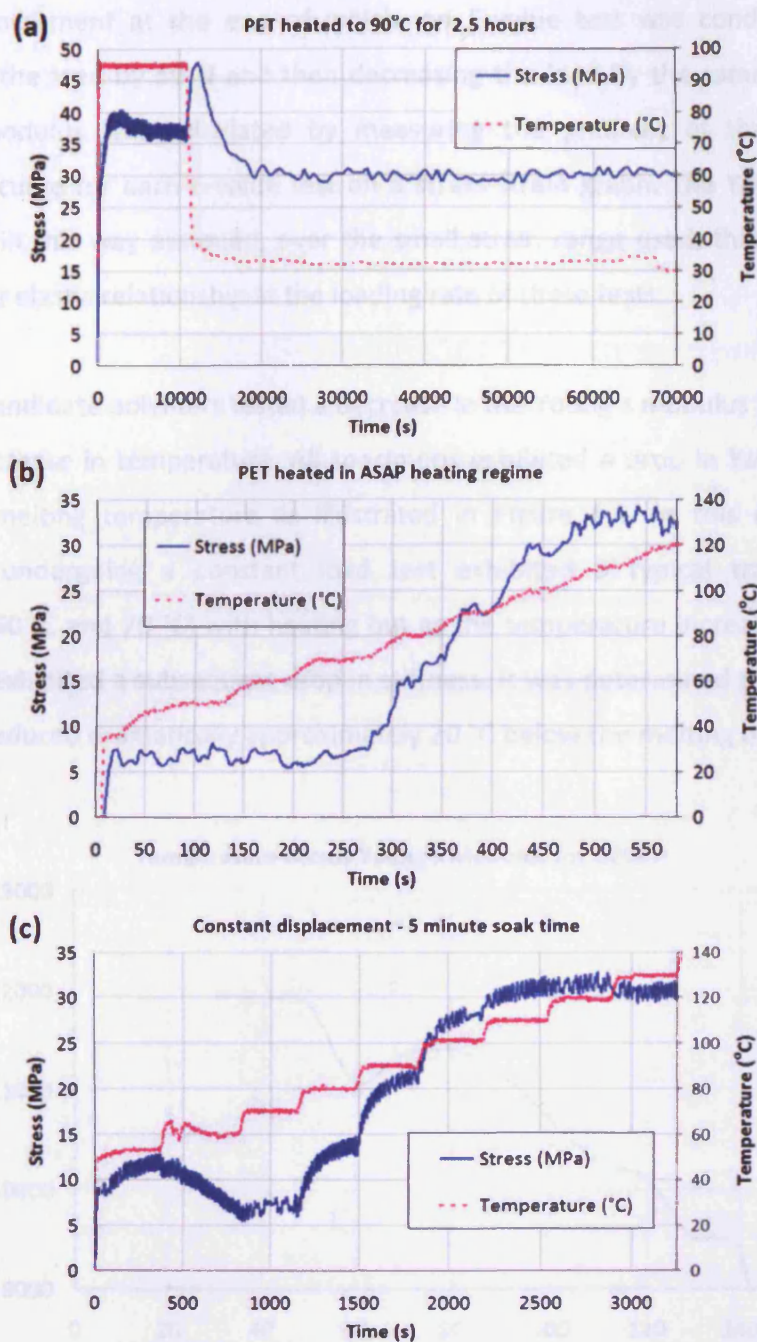


Figure 4.5 Restrained heating tests for PET tape with heating rates: (a) Instant heating, (b) Incremental heating, and (c) Soaking

#### 4.4.3.2 Constant load tests

The purpose of the constant load tests was to find out how the Young's modulus varied with temperature. Specimens were subject to a prestress of 80 MPa and heated from 30 °C to 160 °C in increments of 10 °C. A soak time of 5 minutes was employed



for each increment at the end of which, an E-value test was conducted by first increasing the load by 50 N and then decreasing the load by the same amount. The Young's modulus was calculated by measuring the gradient of the loading and unloading curve for each E-value test on a stress-strain graph. The Young's modulus calculated in this way assumed, over the small strain range used, that the polymers had a linear elastic relationship at the loading rate of these tests.

In all the candidate polymers tested a decrease in the Young's modulus was associated with an increase in temperature. All specimens exhibited a drop in Young's modulus near the melting temperature as illustrated in Figure 4.6. In this case, a GFRPP specimen undergoing a constant load test exhibited a typical transition phase (between 50 °C and 70 °C) with heating but as the temperature increased further the specimen exhibited a subsequent drop in stiffness. It was determined that the Young's Modulus reduced dramatically approximately 20 °C below the melting temperature for specimens.

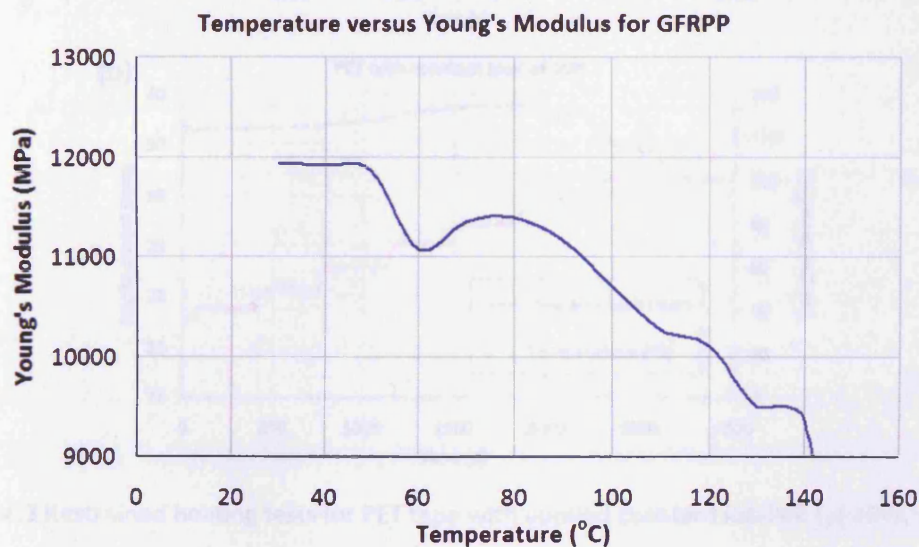


Figure 4.6 Young's modulus-temperature for GFRPP

In addition to the standard constant load tests, a prestress of 20 MPa and 30 MPa was applied to PET specimens as shown in Figures 4.7a and 4.7b respectively. In Figure 4.7a, the results for a typical PET specimen exhibit the effects of shrinkage at approximately 80 °C with this continuing until ambient temperature. In Figure 4.7b, at

a temperature of 110 °C the specimen indicates failure has occurred and it is believed that an excessive preload is the main cause for this failure. It was concluded that for further PET testing, a prestress of 20 MPa would be suitable. Additionally, in the early stages of temperature increase, the PET specimens expanded as indicated by displacement measurements between 50 °C and 80 °C as shown in Figure 4.7a. This can be attributed to the thermal expansion of both the testing equipment and the PET specimen. It is noted that the latter were checked in another series of tests which are discussed in Section 4.5.4 of this chapter.

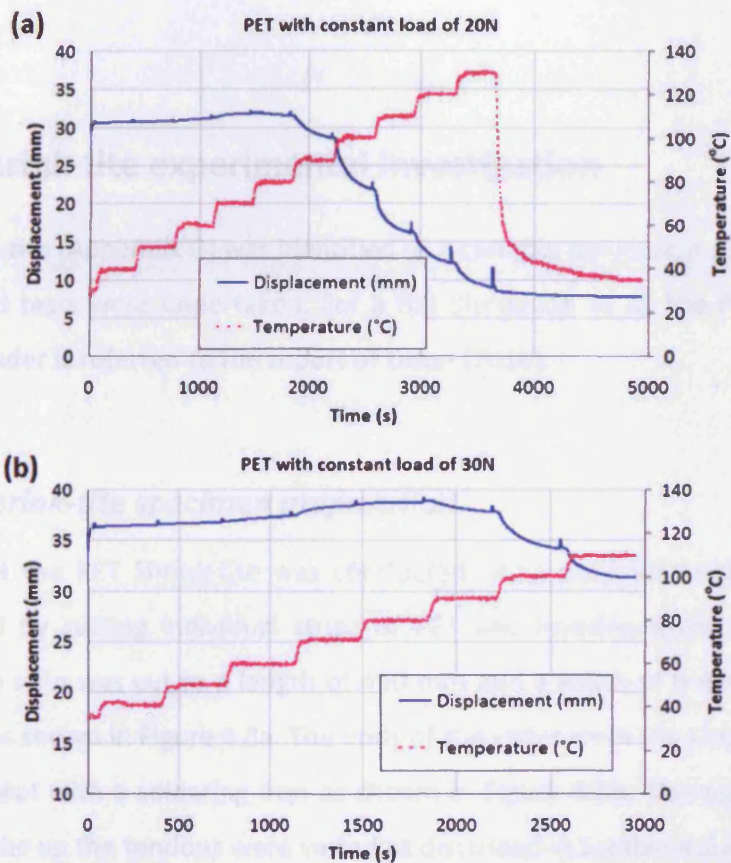


Figure 4.7 Restrained heating tests for PET tape with applied constant load of: (a) 20 N, and (b) 30 N

#### 4.4.4 Conclusion of preliminary tests

From the results of the screening tests conducted by NetComposites and the preliminary tests carried out at Cardiff University, it was concluded that PET Shrink-tite was suitable for the LatConX system. A maximum shrinkage stress of 33 MPa was measured at a temperature of 90 °C which satisfied the 20 MPa shrinkage stress

criterion and met the specified temperature range of 60 °C to 100 °C. In terms of identifying a candidate polymer for the LatConX concept, the tests undertaken were considered satisfactory for the measurements of shrinkage stresses, displacement and temperature. However, for further testing of the PET Shrink-tite it was determined that the technique for gripping specimens in tensile tests needed improvement. As a result, steel plates were attached to the ends of PET tendons which could be gripped in the tensile test machine. This is explained further in Section 4.5.1 and this also matched the method of anchorage used in the cementitious beam tests discussed in Section 4.6.2.

## **4.5 PET Shrink-tite experimental investigation**

As PET Shrink-tite (Appendix D) was identified as a suitable polymer, a series of further, more detailed tests were undertaken. For a full discussion of all the PET parameters tested the reader is referred to the report of Dunn (2010).

### ***4.5.1 PET Shrink-tite specimen preparation***

The testing of the PET Shrink-tite was conducted using polymer tendons that were manufactured by cutting individual strips of PET and layering them on top of one another. Each strip was cut to a length of 450 mm and a width of 6 mm in a specially prepared jig as shown in Figure 4.8a. The ends of the strips were then bonded together by applying heat with a soldering iron as shown in Figure 4.8b. The quantities of PET strips that make up the tendons were varied as discussed in Section 4.5.4.

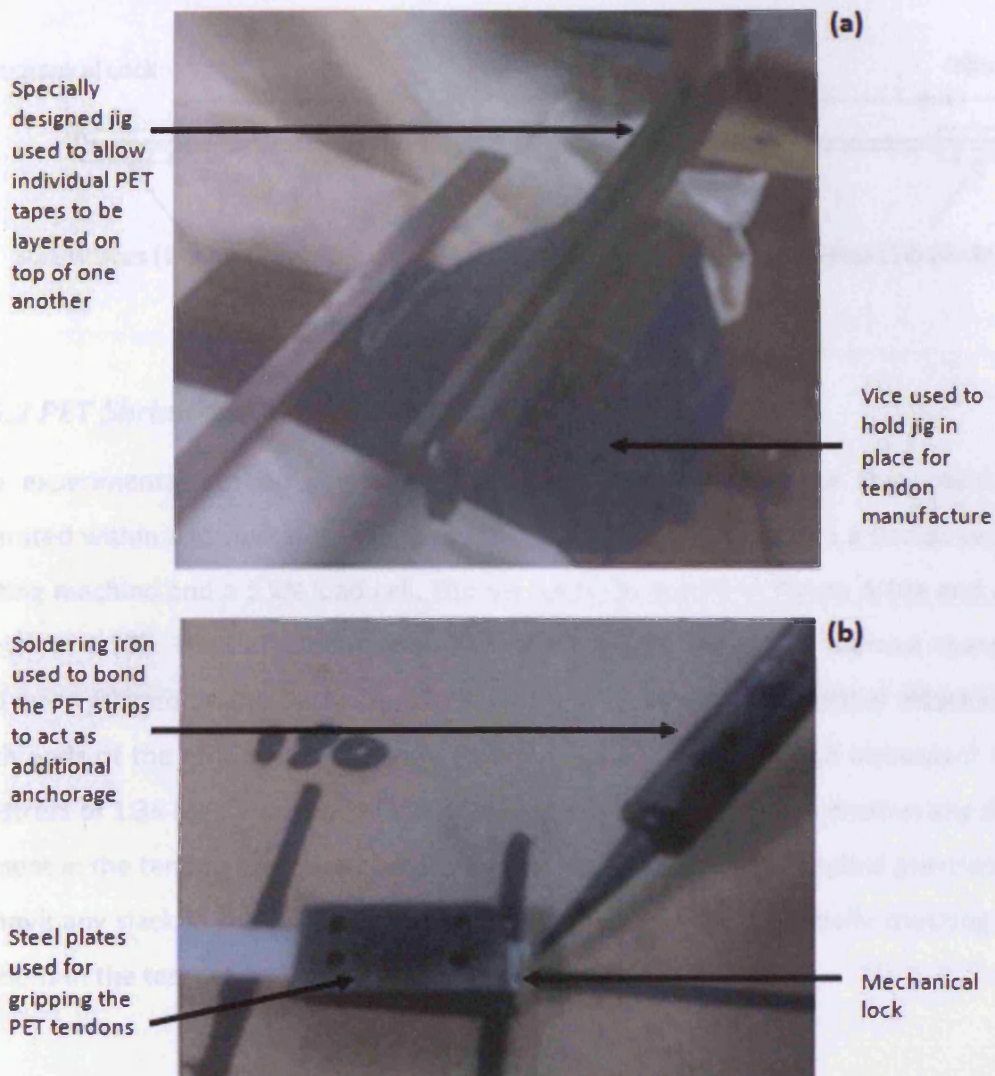


Figure 4.8 Specimen preparations: (a) Specially designed jig for specimen manufacture, and (b) Bonding of strips (Dunn et al., 2010)

As illustrated in Figure 4.9, two steel plates (10 x 20 x 3 mm) were attached to both ends of the PET tendon with a distance of 360 mm between them. The remaining ends of the PET strips were melted to form mechanical anchor plugs to minimise slippage between the steel plates. The steel plates were also used for gripping the PET tendons for tensile tests. Initial tests conducted on slippage of the anchor system concluded that there was no local slippage between the steel plates. Furthermore, there was no evidence to suggest that the heating used to form the mechanical anchor plugs for the PET tendons influenced the behaviour of the PET.

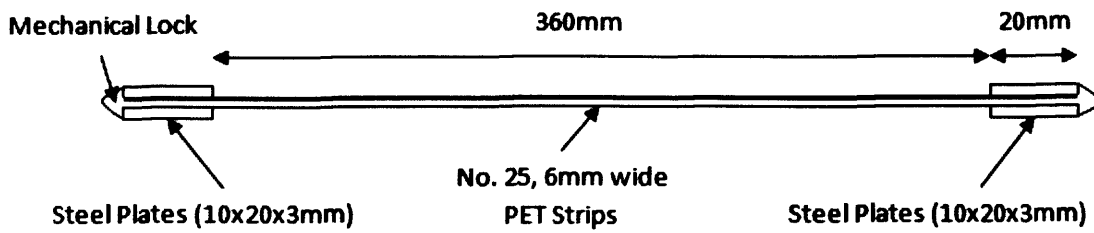


Figure 4.9 Tendon specimen set up (Dunn et al., 2010)

#### **4.5.2 PET Shrink-tite experimental set up**

The experimental set up comprised an Instron thermal chamber that could be operated within a temperature range of -50 °C to +250 °C attached to a Dartec tensile testing machine and a 5 kN load cell. The set up is illustrated in Figure 4.10a and also shown in 4.10b. The PET tendon specimens were placed inside the thermal chamber and were gripped by the Dartec tensile machine grips via the steel plates attached to both ends of the tendons as shown in Figure 4.10c. A small pre-load equivalent to a prestress of 1.36 MPa was applied by the tensile machine in order to remove any slack present in the tendon specimens before testing. In addition to the applied prestress to remove any slack in the tendons, this was further confirmed by visually checking the tendons in the test set up.

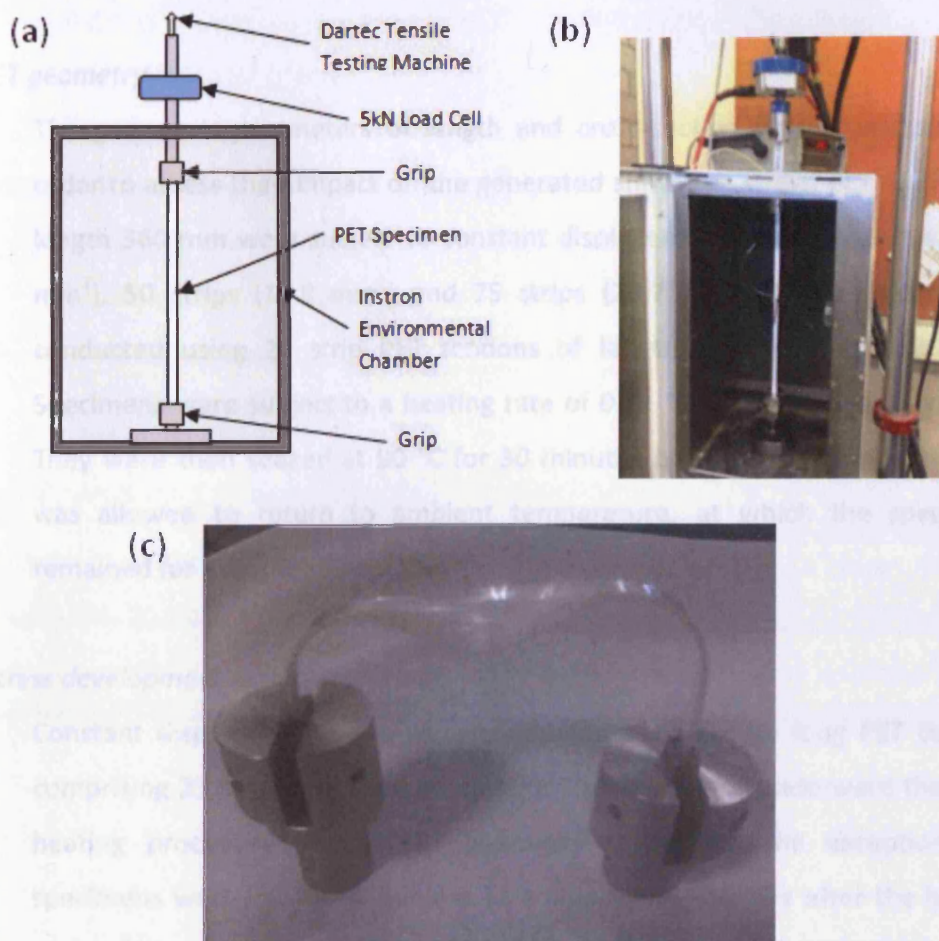


Figure 4.10 Experimental set up: (a) Schematic illustration of test arrangement, (b) Specimen inside thermal chamber, and (c) Tensile machine grips (Dunn et al., 2010)

#### 4.5.3 PET Shrink-tite parametric investigation

A parametric investigation of the PET was undertaken to study the effects of the PET geometry, stress development with temperature and soak time, Young's modulus with temperature and the free shrinkage development with temperature. In this study, the term "soak" refers to specimens being subject to heating for a period of time. In all tests, heating was conducted in a dry thermal chamber. For each test, the displacement at the grips, temperature inside the thermal chamber and the load were continuously measured using a data logger that could measure a maximum of 100 readings per second. The maximum reading rate was utilised when temperature or loading rate were at a maximum. The parameters investigated were:

*(I) PET geometry*

The geometric parameters of length and cross-section were investigated in order to assess their impact on the generated shrinkage stress. PET tendons of length 360 mm were subject to constant displacement tests for 25 strips (6.9 mm<sup>2</sup>), 50 strips (13.8 mm<sup>2</sup>) and 75 strips (20.7 mm<sup>2</sup>). Further tests were conducted using 25 strip PET tendons of lengths 360 mm and 180 mm. Specimens were subject to a heating rate of 0.41 °C/s from ambient to 90 °C. They were then soaked at 90 °C for 30 minutes before the thermal chamber was allowed to return to ambient temperature, at which the specimens remained for a further 10 minutes.

*(II) Stress development with temperature*

Constant displacement tests were conducted on 360 mm long PET tendons comprising 25 strips (standard specimen). The specimens underwent the same heating procedure as the PET geometry tests with the exception that specimens were left for 60 minutes at ambient temperature after the heating phase. This was carried out in order to monitor the stress development of the PET during cooling.

*(III) Stress development with soak time*

Standard specimens were subject to heating between 30 °C and 170 °C in increments of 10 °C. The rate of heating between increments was 0.13 °C/s and three soak times were investigated. These were a 1 minute soak time, a 5 minute soak and a 1 hour soak.

*(IV) Young's Modulus with soak time*

Young's modulus tests were conducted during constant load tests in the same method described in Section 4.4.3.2. Standard specimens were subject to the same incremental heating regime as described for the soak time tests. In this case, specimens were only subjected to a 5 minute soak and then E-value tests were subsequently carried out that applied an additional 10 N loading and

unloading cycle at a designated rate. The rates applied in the E-value tests were 0.1 N/s, 1 N/s and 10 N/s.

*(V) Free shrinkage development with temperature*

For Young's modulus tests the stress remains constant, but the strain changes as indicated by the results that the Young's Modulus changes. Therefore, the displacement of specimens was recorded that allowed a temperature-shrinkage relationship to be identified.

**4.5.4. Results and discussion**

The results of the PET geometry tests have shown that an average shrinkage stress of approximately 29 MPa was generated at a temperature of 90 °C with a 30 minute soak time as shown in Figure 4.11a. The results confirmed PET Shrink-tite's suitability as a polymer for the LatConX concept. The shrinkage stress curves shown in Figure 4.11a exhibit a very similar relationship and the difference in peak load between specimens was minimal (maximum of 4 %). However, the results in Figure 4.11a indicate a greater shrinkage stress in the 180 mm specimens during cooling. As previously addressed in Section 4.4.3.1, the rise in shrinkage stress upon cooling can be attributed to the thermal contraction of both the testing equipment and the PET specimens. In the case of 180 mm specimens, the 2 MPa rise can be attributed primarily to the thermal contraction of an aluminium extension arm that was placed inside the thermal chamber for use in testing the shorter 180 mm specimens. The 2 MPa rise can be calculated from the contraction of the extension arm as a result of the change in temperature after heating at 90 °C and the measured Young's Modulus of the PET.



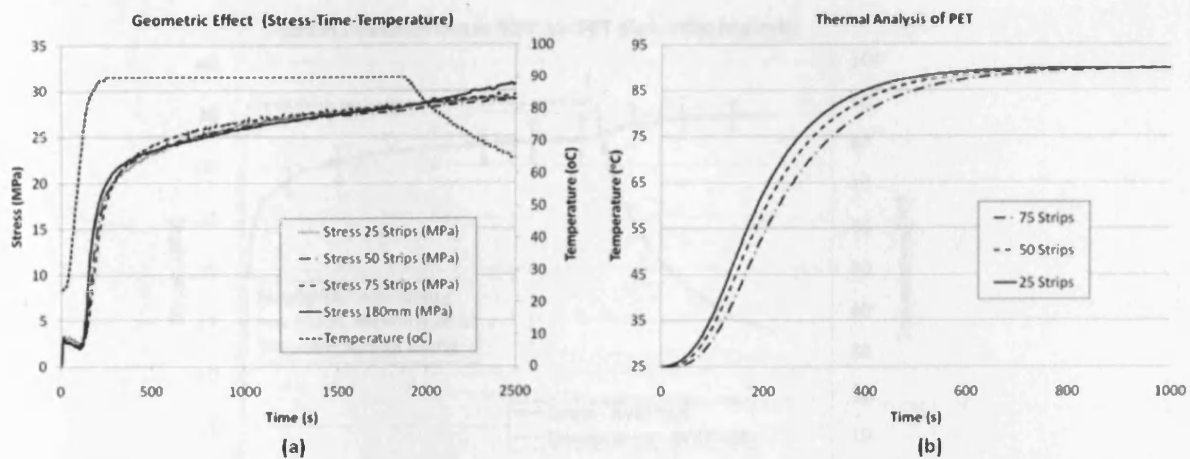


Figure 4.11 (a) Restrained heating tests for PET tendons of various strips, and (b) Thermal analysis of PET (Dunn et al., 2010)

The results in Figure 4.11a indicate a slight variation in the stress paths for the various geometries of the PET tendons tested. A thermal analysis was conducted by Dunn et al. (2010) in order to evaluate the significance of the number of strips and the temperature variation of the specimens tested. Using this analysis, as shown in Figure 4.11b, a decrease in the number of strips is associated with a faster increase in the specimen temperature. Therefore, a smaller cross-section is associated with faster heating between the outer surface and the centre. It was calculated that full temperature saturation in all three cross-sections was achieved in 930 seconds (15.5 minutes).

The test results investigating stress development with temperature and time show a plateau of approximately 32.5 MPa following a 3 hour soak time at a temperature of 90 °C as shown in Figure 4.12. These stress values were found to be consistent with the shrinkage stress values reported by Pakula and Trznadel (1985) and the stress plateau is consistent with the findings of Gupta et al. (1994). Furthermore, the stress rise at the end of the test can be attributed to thermal contraction of the polymer upon cooling.

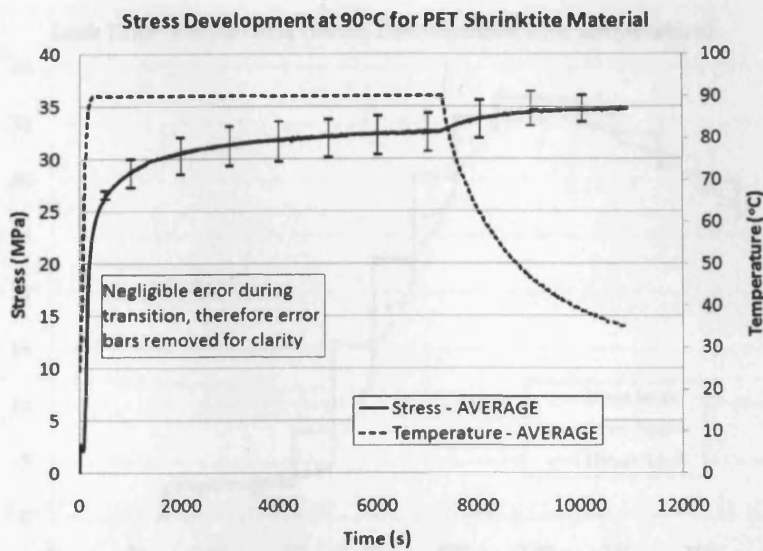


Figure 4.12 Stress development with temperature (Dunn et al., 2010)

The results investigating the average stress development for the three chosen soak times (1 minute, 5 minutes and 1 hour) are shown in Figure 4.13. A clear trend exhibited in all three soak times is the increase in stress at a temperature of approximately 70 °C. This increase can be attributed to the onset of shrinkage that is associated with the glass transition ( $T_g \approx 70$  °C) for PET. In addition, the peak stresses observed in the specimens tested for all three soak times show very consistent results between 35.5 and 37 MPa. In the  $T_g$  region, the average stress increases by approximately 7.5 MPa per 10 °C, until a peak is reached at a temperature of 120 °C beyond which the stress decreases.

For the temperature range between 60 and 120 °C, the specimens subject to the 1 and 5 minute soak times exhibit a consistently increasing stress value. By comparison, the specimens for the 1 hour soak time exhibit stress relaxation between heat increments. Dunn (2010) identifies that two competing mechanisms are occurring at different rates, namely shrinkage and stress relaxation. Shrinkage is a relatively fast mechanism which stabilises in approximately 5 minutes, whilst the stress relaxation mechanism is slower and is apparent in the 1 hour soak tests (Dunn et al., 2010).

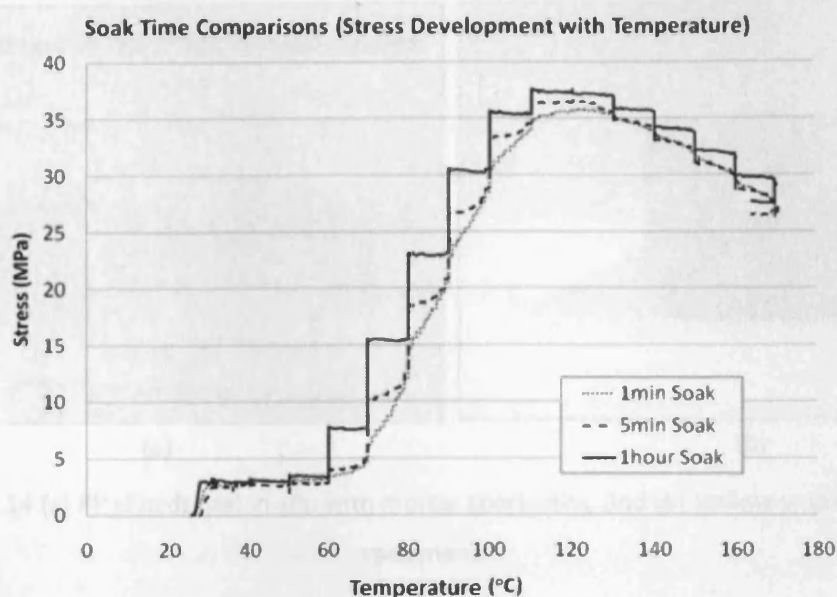


Figure 4.13 Stress development with soak time (Dunn et al., 2010)

The results of these tests have shown that the PET can consistently generate a shrinkage stress when subject to heating. In addition, the parametric investigation has shown that provided an appropriate soak time of approximately 16 minutes is used, PET specimens are independent of cross-section and length.

## 4.6 Cementitious material investigation

### 4.6.1 Specimen preparation

Several trial material systems were investigated prior to establishing the final specimen configuration. An initial series of trials investigated the use of PP chords and composite E glass/PP chords that were cast in mortar prisms as shown in Figure 4.14a. Five 3 x 10 x 250 mm chords were placed in 75 x 75 x 255 mm mortar prisms using the same method as that used for the placement of reinforcement in the autonomic healing specimens described in Section 3.3.2. Demec pips were attached to the top and bottom surfaces of the specimens in order to measure strain. The mortar specimens were covered in wet hessian and wrapped in cling film in order to retain moisture and were subsequently cured for 1 week.

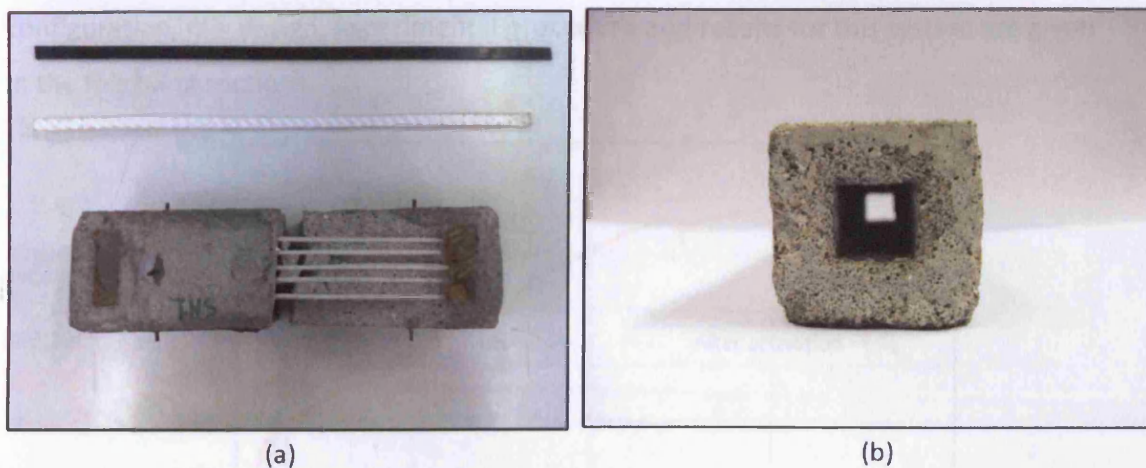


Figure 4.14 (a) PP chords cast in-situ with mortar specimens, and (b) Hollow void in mortar specimens

After the curing phase, the specimens were heated in a dry oven for 12 hours at 150 °C in order to activate the PP chords to generate a shrinkage stress. The results from the strain measurements suggested that the generated shrinkage stress in the chords was too low to develop a prestress in the specimens. This suggested that because the chords had been cast into mortar specimens, the shrinkage stresses generated in them were too low to overcome the restraining force provided by the mortar. Specimens were consequently manufactured as hollow beams to ensure that the polymer tendons did not bond with the cementitious matrix as shown in Figure 4.14b. The hollow void through the specimens was produced by inserting polystyrene rectangular formers prior to casting. These were then removed on day 3 after casting. In addition, it was concluded that the low shrinkage stresses associated with the PP chords was insufficient to actively close cracks in specimens.

As discussed in Section 4.5, the PET tendons generated the highest shrinkage stresses and were therefore chosen for the crack closure mechanism. Initial tests with hollow prismatic mortar specimens post-tensioned with the PET tendons demonstrated the concept of crack closure. In Figure 4.15 the results for a typical specimen show a load recovery of approximately 75 % in the second load cycle. This demonstrated that the activated PET tendons provided a shrinkage stress that enabled crack closure and effectively applied axial compression across the crack faces. This specimen

configuration, mix design, experimental procedure and results for this system are given in the following sections.

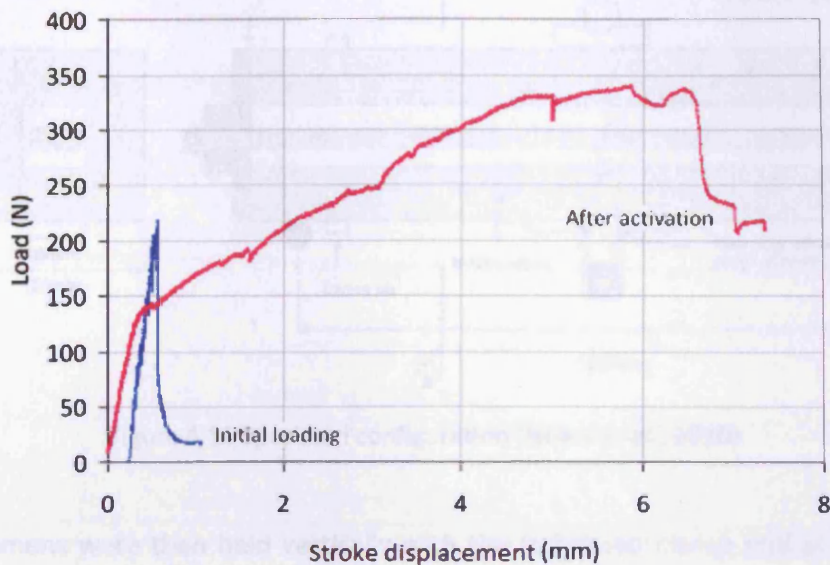


Figure 4.15 Load displacement responses in initial tests

#### 4.6.2 Specimen configuration

Figure 4.16 illustrates the specimen configuration. A central 3 mm notch was cut, as shown in Figure 4.16, so as to predetermine the location of the crack. The shrinkable polymer tendons comprised 75 individual Polyethylene terephthalate (PET) strips, each measuring 6 mm x 0.046 mm. The tendons had a cross-sectional area of approximately 4% of the un-notched specimen. The ends of the tendons were bonded together using a soldering iron and were inserted into the hollow voids of the specimens. An end plate and clamp system were securely attached to one end of the tendon to act as anchorage. This system was thoroughly tested in trials on isolated tendons prior to the inclusion in mortar specimen tests.

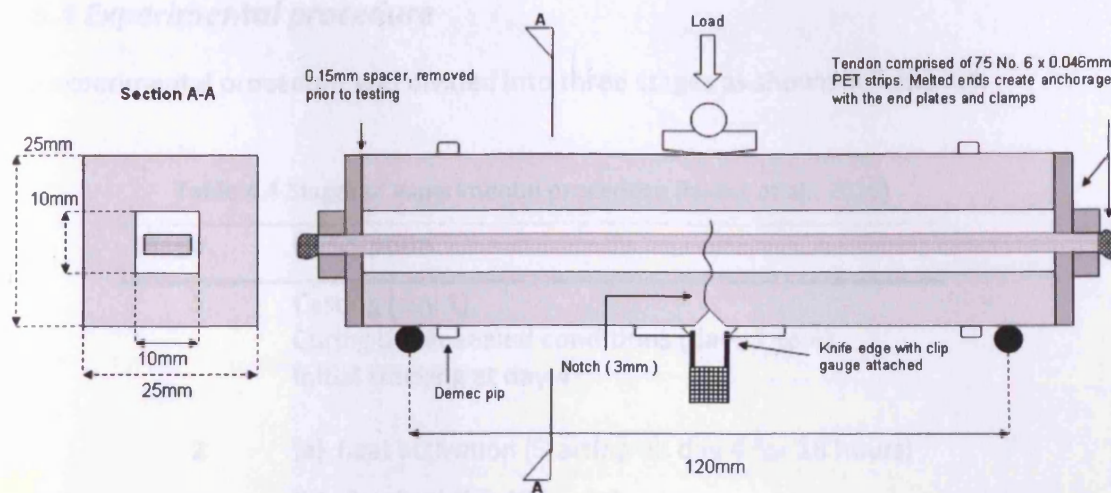


Figure 4.16 Specimen configuration (Isaacs et al., 2010)

The specimens were then held vertically with the tightened clamp end at the top so that a 1 kg weight could be hung from the clamp to be attached at the bottom end of the tendon and a 0.15 mm spacer inserted between the beam and the end plate. With the spacer in place, the lower clamping system was securely tightened. The spacers were removed prior to testing, their thickness having been calculated so that the tendons would not provide any prestress to the specimens prior to heat activation. This ensured that the tendons remained completely loose within the specimens during stage 1 testing.

#### 4.6.3 Cementitious mix design

All mortar specimens were cast using a water:cement:sand mix ratio of 306 kg/m<sup>3</sup>: 510 kg/m<sup>3</sup> : 1530 kg/m<sup>3</sup> respectively, (or 0.6 : 1 : 3 by weight). The cement used was Portland-fly ash cement, designation CEM II/V-V32.5 R, supplied by Lafarge, Aberthaw. The sand was 0/4 mm, EN12610 compliant sea dredged sand. Prior to mixing, the sand particles were passed through a 1 mm sieve to give a maximum aggregate size of 1 mm because of the small scale nature of the specimens. The mixer used was a CreteAngle<sup>®</sup> Model "S" pan type mixer.

#### **4.6.4 Experimental procedure**

The experimental procedure was divided into three stages as shown in Table 4.4.

Table 4.4 Stages of experimental procedure (Isaacs et al., 2010)

<b>Stage</b>	<b>Description</b>
<b>1</b>	Casting (day 1) Curing under sealed conditions (days 1 to 4) Initial cracking at day 4
<b>2</b>	(a) heat activation (Starting on day 4 for 18 hours) (b) 'healing' (for 48 hours)
<b>3</b>	Loading to failure at day 8

It is noted that henceforth the curing regime during the 'healing' phase will be referred to as the healing regime.

The testing described here was carried out over the relatively short time period of 8 days because previous investigations have shown that cracks are most likely to autogenously heal under early age conditions (ter Heide et al., 2005; Edvardsen, 1999). Furthermore, it has also been shown that strength recovery decreases as the time of first cracking increases (ter Heide et al., 2005).

The experimental procedure adopted in the proof of concept tests comprised small scale hollow prismatic mortar beams that were tested in a series of three-point bend experiments. In stage 1, specimens were loaded under three-point bending at a rate 0.001 mm/s to a crack mouth opening displacement (CMOD) of 0.30 mm and then unloaded. This CMOD was measured by a light crack mouth opening displacement gauge (CMOD<sub>CG</sub>), which was inserted between two knife edges that were glued either side of the notch on the underside of the specimens. Load was controlled via feedback from an LVDT which measured the displacement of the loading platen, as shown in Figure 4.17.

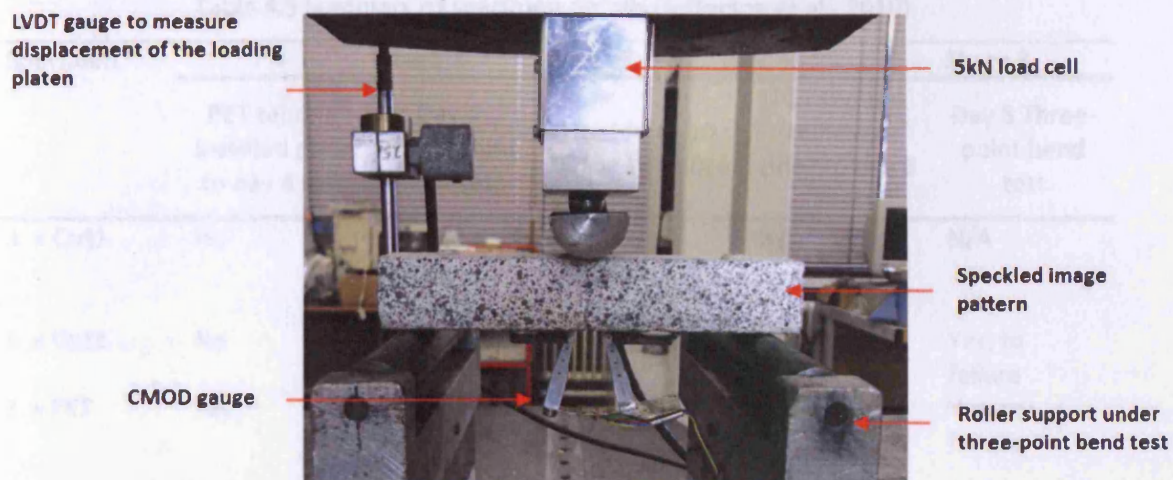


Figure 4.17 Three-point bend test set up (Isaacs et al., 2010)

In stage 2a, the specimens were subjected to heat treatment at 90 °C for 18 hours in order to activate the polymer tendons. This generated a prestress in the specimens which it was believed would result in closure of the crack formed in stage 1. Then, in stage 2b, the specimens were subject to healing for a further 48 hours. At the end of the healing stage (2b), the specimens were then tested to failure in stage 3 in order to identify whether the tendons had effectively closed the pre-formed crack and whether any autogenous healing had taken place.

Twelve 145 mm x 25 mm x 25 mm specimens were cast for each of the procedures. For each procedure, the twelve specimens were divided into four groups of three beams. Three of the beams had the polymer tendon left inside the beam for all stages (PET\_a to PET\_c); three of the beams had the tendon left in place for stages 1 and 2, but removed before stage 3, (PETr\_a to PETr\_c) and six control beams were tested to failure with no tendons, three of which were tested at stage 1 (Ctrl1\_a to Ctrl1\_c) and three tested at stage 3 (Ctrl2\_a to Ctrl2\_c). A summary of the testing stages and parameters for each group are shown in Table 4.5.



Table 4.5 Summary of specimen details (Jefferson et al., 2010)

Specimen	Stage 1		Stage 2		Stage 3
	PET tendon inserted prior to day 4 test	Day 4 Three-point bend test	Heated at 90 °C for 18 hours	PET tendon removed prior to day 8 test	Day 8 Three-point bend test
3 x Ctrl1	No	Yes, to failure	N/A	N/A	N/A
3 x Ctrl2	No	No	Yes	N/A	Yes, to failure
3 x PET	Yes	Yes, to 0.3 mm CMOD <sub>CG</sub> <sup>a</sup>	Yes	No	Yes, to failure
3 x PETr	Yes	Yes, to 0.3 mm CMOD <sub>CG</sub> <sup>a</sup>	Yes	Yes	Yes, to failure

<sup>a</sup>CMOD<sub>CG</sub> = Crack Mouth Opening Displacement by clip gauge.

Tests on the PETr specimens, in which the PET tendon was removed prior to stage 3, were conducted in order to assess the degree of autogenous healing after crack closure. Ctrl1 specimens were used to ensure that the response of specimens with no tendons was the same as specimens with loose tendons. Ctrl2 specimens were subject to the same healing regime as the specimens with tendons and were used to assess the effect of additional curing and heating on the strength of specimens.

#### 4.6.5 Results and discussion

The proof of concept test series was conducted to assess the ability of activated PET tendons to close cracks in mortar specimens and provide axial compression across the crack faces. Table 4.6 presents the results for all specimens. The load recovery was used to measure the effectiveness of crack closure and potential autogenous healing in specimens. Load recovery (LR) is defined as the ratio between the mean peak load values at stage 3 and 1 respectively i.e  $LR = (\text{stage 3 load}) / (\text{stage 1 load}) \times 100 \%$ . It would have been possible to include the relative strength gain in control specimens tested at stage 3 but it was considered more appropriate to present the load recovery relative to the peak time of first damage i.e stage 1.

Table 4.6 Mean load, coefficient of variance and load recovery percentages

Specimen	Stage 1		Stage 3		Load recovery (%)
	Mean peak load (N)	Coefficient of Variance (Range)	Mean peak load (N)	Coefficient of Variance (Range)	
6 control specimens	207	7 (193-223)	296	10 (262-316)	-( <sup>b</sup> )
3 PET specimens	204	9 (183-214)	222	12 (203-254)	109
3 PETr specimens	194	5 (183-201)	9	13 (8-10)	5

<sup>b</sup>No load recovery as a result of control specimens being tested to failure at stages 1 and 3.

Material tests were also carried out to determine the fracture energy, tensile strength, Young's modulus and compressive strength of the mortar mix as shown in Table 4.7.

Table 4.7 Measured material properties (Jefferson et al., 2010)

	E	E <sub>p</sub>	f <sub>cu</sub>	f <sub>t (stage1)</sub>	f <sub>t (stage 3)</sub>	G <sub>f</sub>
	kN/mm <sup>2</sup>	kN/mm <sup>2</sup>	N/mm <sup>2</sup>	N/mm <sup>2</sup>	N/mm <sup>2</sup>	N/mm
Mean	24.8	6.0	23	2.0	0.09	0.025
CoV %	1.6	2.5	8.3	7.3	10.6	11.7

In Figures 4.16 to 4.18, the results of load-CMOD for typical specimens are given. It is worth noting that in these Figures the CMOD values are presented by CMOD<sub>DIC</sub> measurements. The CMOD was measured independently using two methods (a) CMOD<sub>CG</sub> and, (b) CMOD<sub>DIC</sub>. Further details of CMOD<sub>DIC</sub> are given in Section 5.3 which explains the Digital Image Correlation (DIC) system that was used for capturing full 2D displacement and strain information. The CMOD<sub>CG</sub> readings were consistent with the CMOD<sub>DIC</sub> measurements and hence, CMOD<sub>DIC</sub> was chosen for presentation of the results in Figures 4.18 to 4.20.

In Figure 4.18, the results from the PET and Ctrl specimens showed good consistency with a range of peak loads between 193 to 223N. The tendons in the PET specimens were loose during stage 1 loading as a result of spacers fitted between the anchorage

mechanisms. The specimens were unloaded at a  $CMOD_{CG}$  of 0.3 mm which equates to 0.22 mm for the  $CMOD_{DIC}$  measurement as highlighted. Comparison of the PET and Ctrl specimens results shows that the tendons had an insignificant effect upon the response of the PET specimens during stage 1 tests.

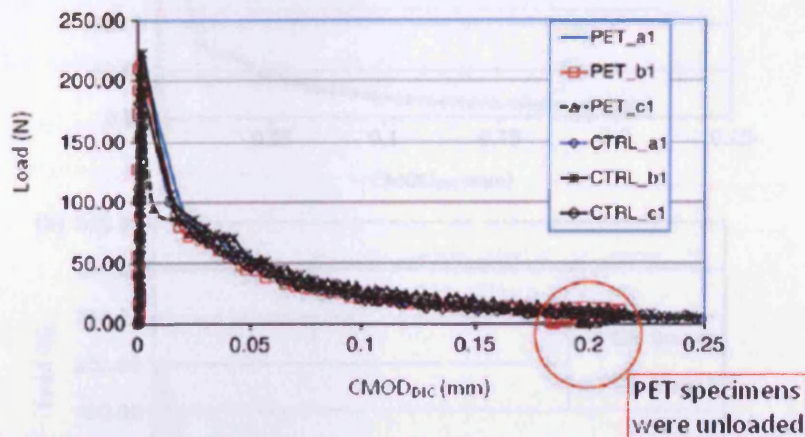


Figure 4.18 Load-CMOD results for specimens loaded in stage 1 (Jefferson et al., 2010)

The effects of post-tensioning as a result of PET tendon activation are shown in Figure 4.19. The response for a typical specimen with the PET tendon remaining during stage 3 is shown in Figure 4.19a. The response for a typical specimen with the PET tendon removed prior to stage 3 loading is shown in Figure 4.19b.

Figure 4.19a shows a load of 120 N, the  $CMOD_{DIC}$  value indicates a fully closed crack state. This suggests the activated tendons provided a post-tensioning effect to assist crack closure. At a load of 200 N, the  $CMOD_{DIC}$  also indicates a predominantly closed crack condition with a value of less than 0.005 mm. The stage 3 curve subsequently decreases as a result of the activated tendon providing post-tensioning and a peak load of approximately 210 N was obtained.

The response for a typical PET specimen is shown in Figure 4.19b. The stage 3 loading curve suggests minimal autogenous healing and no opening. PET specimens showed a 5% load recovery in stage 3 compared to Table 4.6. As discussed in Section 2.3.3, the enhancement of autogenous healing requires the presence of moisture. In this case, a dry heat activation and dry healing regime between stages 1 and 3 activated the tendons, but was detrimental to the effect of autogenous healing. A parasitic

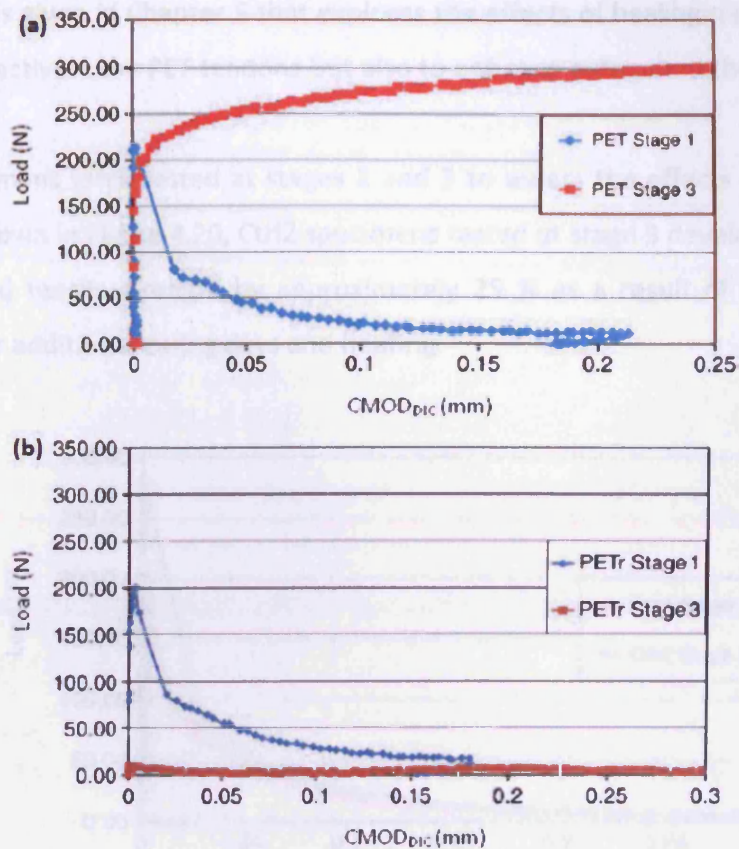


Figure 4.19 Load-CMOD results for stages 1 and 3 for: (a) PET specimens and, (b) PETr specimens (Jefferson et al., 2010)

In Figure 4.19a, up to a load of 150 N, the CMOD<sub>DIC</sub> value indicates a fully closed crack state. This suggests the activated tendons provided a post-tensioning effect to enable crack closure. At a load of 200 N, the CMOD<sub>DIC</sub> also indicates a predominantly closed crack condition with a value of less than 0.005 mm. The stage 3 curve subsequently plateaus as a result of the activated tendon providing post-tensioning and a peak load of approximately 300 N was obtained.

The response for a typical PETr specimen is shown in Figure 4.19b. The stage 3 loading curve suggests minimal autogenous healing and on average, PETr specimens showed a 5 % load recovery in stage 3 as shown in Table 4.6. As discussed in Section 2.3.3, the enhancement of autogenous healing requires the presence of moisture. In this case, a dry heat activation and dry healing regime between stages 1 and 3 activated the tendons, but was detrimental to the effect of autogenous healing. A parametric

investigation is given in Chapter 5 that explores the effects of healing regimes that not only serve to activate the PET tendons but also to enhance autogenous healing.

Control specimens were tested at stages 1 and 3 to assess the effects of the healing regime. As shown in Figure 4.20, Ctrl2 specimens tested at stage 3 developed a greater peak load and tensile strength by approximately 25 % as a result of the combined effects of four additional curing days and heating.

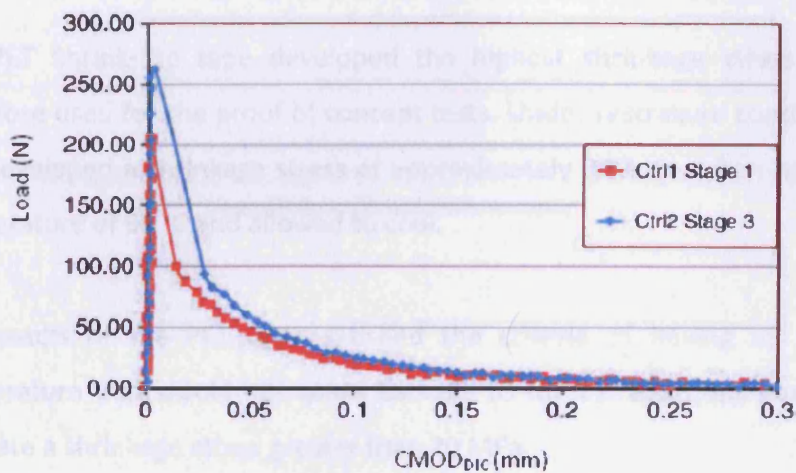


Figure 4.20 Control specimens (Jefferson et al., 2010)

After stage 1 loading, specimens were cracked to a  $CMOD_{CG}$  of 0.3 mm, as shown in Figure 4.21a. Following tendon activation in stage 2, it may be seen that the crack is no longer visible as shown in Figure 4.21b.

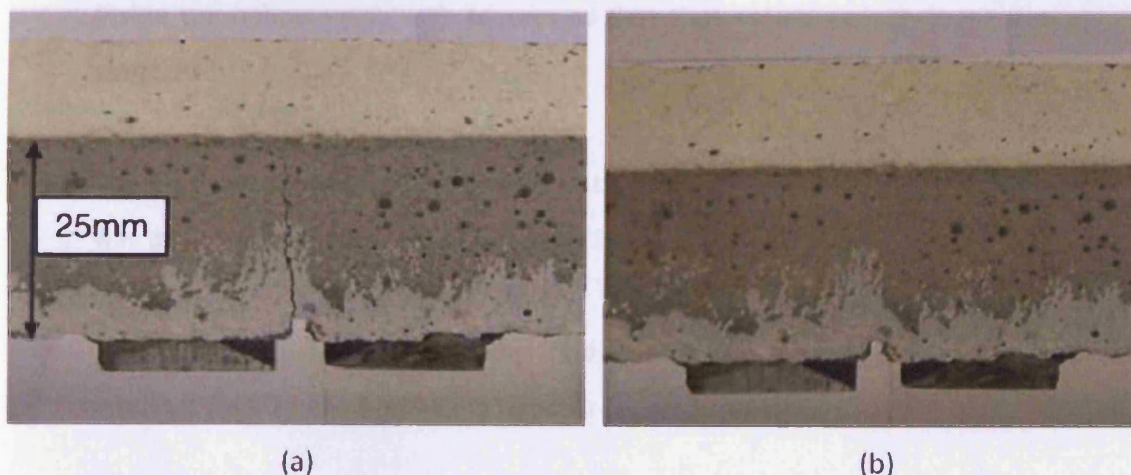


Figure 4.21 PET specimen: (a) cracked after stage 1 loading and, (b) with crack closed as a result of tendon activation (stage 3) (Jefferson et al., 2010)

## 4.7 Conclusion

The experimental results presented in this chapter show that the concept of post-tensioning mortar beams with shape memory polymers is viable for a crack closure system.

The results of the polymer investigation established that:

- The PET Shrink-tite tape developed the highest shrinkage stress and was therefore used for the proof of concept tests. Under restrained conditions, the PET developed a shrinkage stress of approximately 34 MPa when heated to a temperature of 90 °C and allowed to cool.
- The results of the PET tests satisfied the criteria of having an activation temperature that would not cause damage to the cementitious material and generate a shrinkage stress greater than 20 MPa.

The results of the proof of concept experimental procedure showed that:

- The presence of the PET tendons in all specimens tested at stage 1 had no influence on the fracture softening response. The tendons were initially placed inside the hollow voids with spacers so that they would remain loose during stage 1 tests.
- The studies confirmed that upon activation of the PET tendons, crack closure was provided by a prestress of between 1.5 – 2 MPa.
- The study confirms from previous finding that the presence of moisture is required for autogenous healing to occur (Edvardsen, 1999).

- The results of specimens with the PET tendons removed prior to stage 3 testing showed no significant crack healing as a result of a dry heating and dry curing regime between stages 2 and 3.
- The results from control specimens also confirmed that the mortar specimens increased in strength by approximately 25 % between days 4 and 8 as a result of the additional curing time and heating.

## Chapter 5

### Autogenous healing (parametric investigation)

#### 5.1 Introduction

The load recovery response of the proof of concept test specimens observed in Chapter 4 can be attributed to the thermally activated polymer tendons providing a post-tensioning effect. The generated shrinkage stresses enabled crack closure to be achieved and a load recovery of approximately 109 % was observed for the specimens in which the PET tendons remained throughout the second loading stage. The mechanical response of the specimens from which the PET tendons had been removed in order to measure autogenous healing was however, observed to be minimal. It was also recognised that the dry heating and dry curing regime that had been adopted between test stages 1 and 3 actually hindered the ongoing hydration that is needed for autogenous healing.

Studies of the autogenous healing of cementitious materials have been discussed in Chapter 2 and from these studies it has been identified that the degree of crack healing is a function of crack opening, with there being little likelihood of healing in cracks wider than 0.1 mm (Reinhardt and Jooss, 2003). Furthermore, it was noted that ter Heide et al., (2005) had demonstrated that autogenous healing is significantly enhanced if a crack is subject to compression. The effects of temperature and permeability on self-healing have also been investigated (Reinhardt and Jooss, 2003) and other studies have confirmed that the younger the concrete the greater the potential for autogenous healing (Edvardsen, 1999; ter Heide et al., 2005).

In addition, Edvardsen (1999) observed that the presence of moisture is required for autogenous healing. In the proof of concept tests, the dry heat (to activate PET tendons) and dry curing in the healing stage only served to minimise moisture in the



cementitious material. In this chapter, the results of a parametric investigation aimed at investigating how autogenous healing can be enhanced are given. The testing programme described investigates the use of various heat activation methods and curing regimes for optimising tendon activation and the enhancement of autogenous healing respectively. In addition, the use of innovative technology known as Digital Image Correlation (DIC) is described. This non-destructive testing technique was used to capture the displacement of specimens in order to calculate the CMOD.

## **5.2 Testing programme**

The intended functions of the material system (for Class I) are that of crack closure and autogenous healing. For crack closure to be achieved, the PET tendons require heat activation in order to generate a shrinkage stress. In the specimens used for this study it was not possible to exclusively heat the tendons and as a result, both the cementitious material and the tendons were subject to the same heating regime. However, alternative activation methods to exclusively activate the tendons by such techniques as passing an electric current through them are to be investigated in future work.

In order to complete the functions of crack closure and autogenous healing the specimens require exposure to heat to activate the tendons and, following crack closure, exposure to moisture to enhance autogenous healing. The scheduled testing programme was developed to investigate these conditions. As shown in Table 5.1, three Activation-Healing (AH) regimes for stages 2a and 2b were undertaken. These AH regimes were investigated in order to optimise the functions of both crack closure and autogenous healing. The specimen configuration, cementitious mix design and experimental procedure remained the same as the proof of concept tests described in Sections 4.6.2, 4.6.3 and 4.6.4 respectively.

Table 5.1 Heat activation methods and healing regimes (Isaacs et al., 2010)

AH regime	Heat activation method			Healing regime	
	Description	Temp. (°C)	Time (Hrs)	Description	Time (Hrs)
1	Dry heat activation	90	18	Cured in water at ambient temperature	48
2	Steam heat activation	90 <sup>a</sup>	18	Specimens left in the steam chamber with the steam production turned off and the chamber allowed to return to ambient conditions	48
3	Water heat activation	90	18	Specimens left in the water tank with the temperature allowed to return to ambient conditions	48

Note: <sup>a</sup>the atmospheric temperature was measured at 90 °C and the water in the tank was heated to 100 °C in order to produce steam conditions.

A summary of the specimen details has previously been given in Table 4.5, Chapter 4. Twelve 145 mm x 25 mm x 25 mm specimens were cast for each of the procedures. For each procedure, the twelve specimens were divided into four groups of three beams. Three of the beams had the polymer tendon left inside the beam for all stages (PET specimens); three of the beams had the tendon left in place for stages 1 and 2, but removed before stage 3 (PETr specimens); and six control beams were tested to failure with no tendons, three of which were tested at stage 1 (Ctrl1 specimens) and three tested at stage 3 (Ctrl2 specimens). Material tests were also carried out using six small scale 25 mm x 25 mm x 25 mm cubes to determine the compressive strength and six 160 mm x 40 mm x 40 mm prismatic mortar beams, three of which were used for fracture energy tests and three for elastic modulus tests.

### 5.3 Digital Image Correlation

A non-destructive technique known as DIC was used to determine the CMOD values of specimens. One side face of each specimen was sprayed with a black and white speckled pattern for use with the DIC system in order to capture full 2D displacement and strain information (Guo et al., 2008; Bornert et al., 2009; Sutton et al., 2009). The LIMESS DIC system and Correlated Solutions Vic Snap 3D software was used to analyse the data obtained. The system has an accuracy of 1  $\mu\text{m}$  for displacements for the chosen grid size of 120 x 25 mm ([www.limess.com](http://www.limess.com)). The DIC set up is shown in Figure 5.1.



Figure 5.1 Test set up of a typical specimen subject to three-point bending with DIC measurement

Two cameras were set up that tracked the speckled pattern side of the beam every 5 seconds throughout the test. The tracking of the speckled pattern between captured images enabled displacements and strains to be determined. The selection of two points either side of the notch allowed the CMOD to be determined. This provided a second measurement of the CMOD which is denoted  $\text{CMOD}_{\text{DIC}}$ . The two points adopted were 1.75 mm above the lower surface of the specimens, a height that was chosen in order to maintain a constant tracking height for determining the  $\text{CMOD}_{\text{DIC}}$ , as shown in Figure 5.2. The two points were placed on the very first image that corresponds to the minimum load i.e. at the start of the test. This was classed as the reference image for estimating the  $\text{CMOD}_{\text{DIC}}$ . The selected points in the reference image (i) were then located in the next image (i+1) by performing image correlation.

This allowed new reference coordinates to be calculated with the corresponding load values. Processing the displacement coordinates between images allows the CMOD to be determined as a function of load.

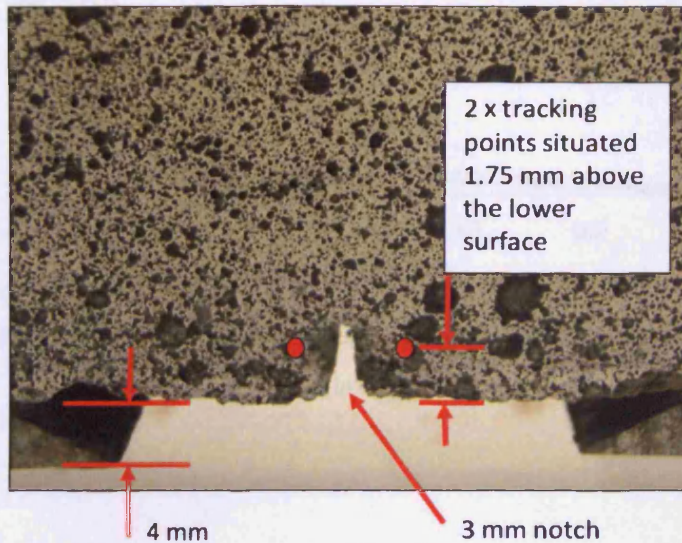


Figure 5.2 Speckled image pattern for correlation

The CMOD of specimens was therefore measured independently using two methods. The first method used the clip gauge ( $CMOD_{CG}$ ) as a real-time measurement for stage 1 tests in order to detect the unloading point. The second method used DIC that obtained  $CMOD_{DIC}$  values by post-processing images in the method described above. The  $CMOD_{CG}$  readings were measured between two knife edges situated on the underside of the beam, approximately 4 mm below the bottom of the surface as shown in Figure 5.2. As a result, the  $CMOD_{CG}$  readings are slightly higher in comparison to the  $CMOD_{DIC}$  readings and this can be attributed to the lower level at which the  $CMOD_{CG}$  readings were measured. As shown for a typical specimen in Figure 5.3, good consistency was achieved between the two methods.

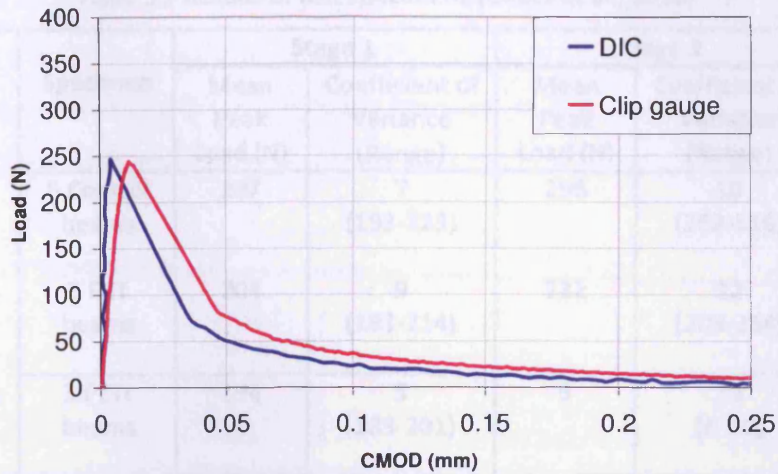


Figure 5.3 Comparisons between DIC and clip gauge CMOD values for Ctrl2b specimen in AH regime 2

## 5.4 Results

The results of all the specimens for the three AH regimes studied in this chapter are presented in Appendix C.

### 5.4.1 Recovery of mechanical properties

Table 5.2 presents mean results of all specimens for the three AH regimes employed as well as results from the initial proof of concept tests given in Chapter 4. Load recovery (LR) is defined as the ratio between the mean peak load values at stages 3 and 1 respectively i.e.  $LR = (\text{stage 3 load}) / (\text{stage 1 load}) \times 100\%$ . It would have been possible to include the relative strength gain in control specimens tested at stage 3 but it was considered more appropriate to present the load recovery relative to the peak at the time of first damage i.e. Stage 1.

Table 5.2 Results of test specimens (Isaacs et al., 2010)

Treatment regime	Specimen	Stage 1		Stage 3		Load Recovery (%)
		Mean Peak Load (N)	Coefficient of Variance (Range)	Mean Peak Load (N)	Coefficient of Variance (Range)	
Dry heat at 90°C and dry healing (Proof of concept, Chapter 4)	6 Control beams	207	7 (193-223)	296	10 (262-316)	-( <sup>b</sup> )
	3 PET beams	204	9 (183-214)	222	12 (203-254)	109
	3 PETr beams	194	5 (183-201)	9	13 (8-10)	5
AH1 Dry heat at 90°C and water healing	6 Control beams	235	2 (232-237)	230	9 (207-245)	-
	3 PET beams	236	13 (206-266)	299	16 (246-334)	127
	3 PETr beams	225	7 (215-241)	176	10 (162-197)	79
AH2 Steam heat and healing	6 Control beams	170	15 (145-197)	254	3 (246-261)	-
	3 PET beams	151	10 (138-167)	294	8 (267-313)	194
	3 PETr beams	159	19 (128-189)	125	10 (114-139)	79
AH3 Water heat at 90°C and water healing	6 Control beams	254	3 (245-260)	311	6 (290-326)	-
	3 PET beams	233	7 (219-250)	216 <sup>(c)</sup>	4 (277-295)	93
	3 PETr beams	255	16 (214-286)	42	16 (35-47)	17

Note: <sup>b</sup>No load recovery because these were control specimens tested to failure at stages 1 and 3.

<sup>c</sup>In most cases this was a first peak load and was associated with cracking of the mortar. However, where no first peak existed, this load was taken as the point at which the stiffness first changed significantly.

The gradient of the pre-peak loading curves was measured at both stages 1 and 3 to give an indication of stiffness recovery. The mean gradient at stage 1 of all tests was 78 N/m. The percentage change in the mean gradient of specimens for each regime at stage 3, relative to the stage 1 value, is shown in Table 5.3.

Table 5.3 Mean gradient recovery for loading curves of typical specimen's pre-peak at stage 3 testing (Isaacs et al., 2010)

	AH1 (%)	AH2 (%)	AH3 (%)
PET specimens	125	104	102
PETr specimens	95	72	35

The same material tests as that for the proof of concept tests in Section 4.6.4 were undertaken in associated AH regimes. Table 5.4 presents the measured material properties.

Table 5.4 Measured material properties (Isaacs et al., 2010)

Regime		E kN/mm <sup>2</sup>	f <sub>cu</sub> N/mm <sup>2</sup>	G <sub>f</sub> N/mm
AH1	Mean	20.80	23.00	0.017
	CoV %	3.20	8.31	8.32
AH2	Mean	20.72	25.64	0.025
	CoV %	4.59	8.60	1.22
AH3	Mean	24.28	34.83	0.025
	CoV %	2.11	6.62	4.11

E = Young's modulus of mortar, f<sub>cu</sub> = cube strength of mortar, G<sub>f</sub> = fracture energy

The graphs presented in Figures 5.4 to 5.7 use data that was captured by the DIC system. Figures 5.4a to 5.6b present typical stage 1 and stage 3 results for each of the three AH regimes for both the PETr and PET cases. The former (PETr) cases show directly the amount of autogenous healing or recovery ratio. Figures 5.7a and 5.7b show results of control specimens at stages 1 and 3 for each AH regime. These show the effect of curing between stages 1 and 3 on the strength of the specimens.

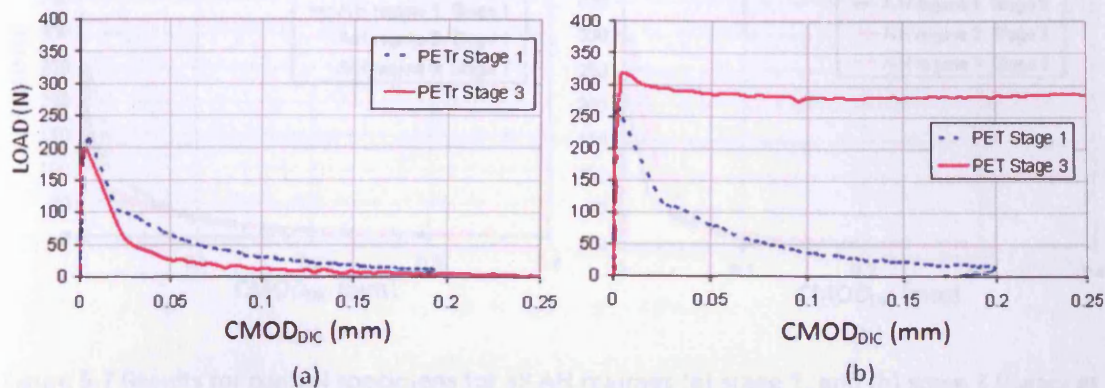


Figure 5.4 Results for typical specimens in AH1: (a) PETr, and (b) PET (Isaacs et al., 2010)

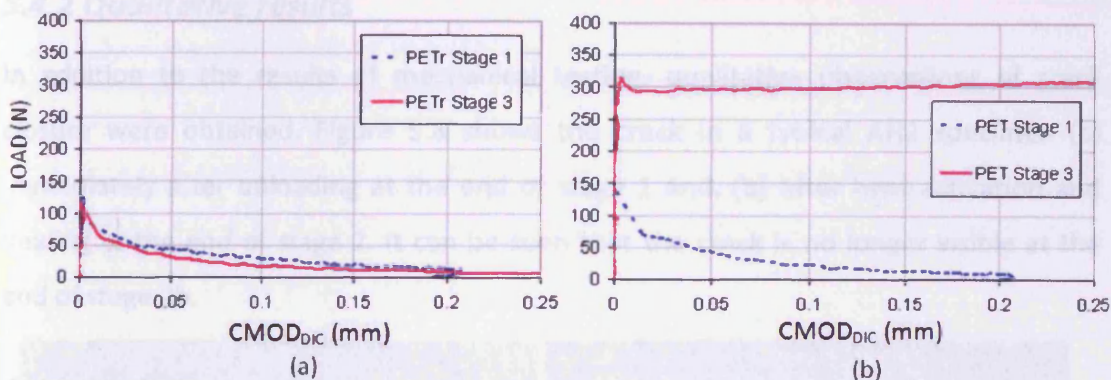


Figure 5.5 Results for typical specimens in AH2: (a) PETr, and (b) PET (Isaacs et al., 2010)

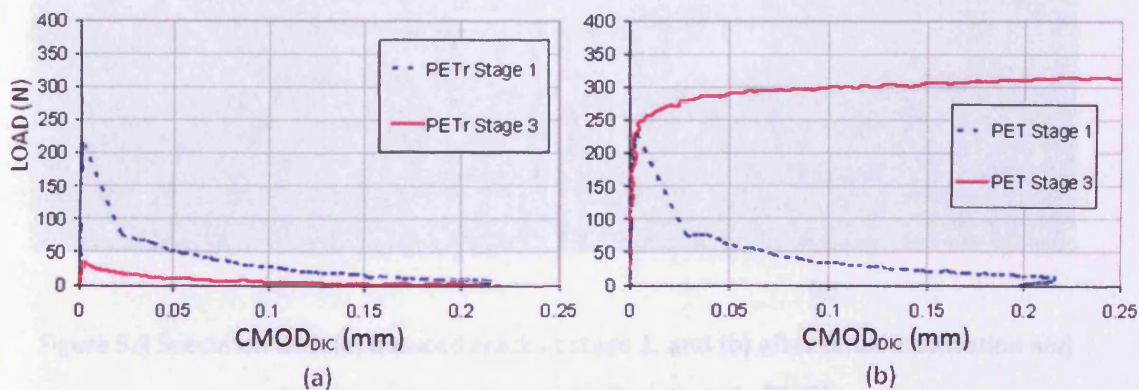


Figure 5.6 Results for typical specimens in AH3: (a) PETr, and (b) PET (Isaacs et al., 2010)

An attempt to identify the formation of new crack paths was made. However, in stage 3 tests it was difficult to distinguish whether a new crack path had formed or the opening of an existing crack had occurred. This aspect of crack identification could be enhanced by the use of EBM or equivalent that has been used in previous studies in



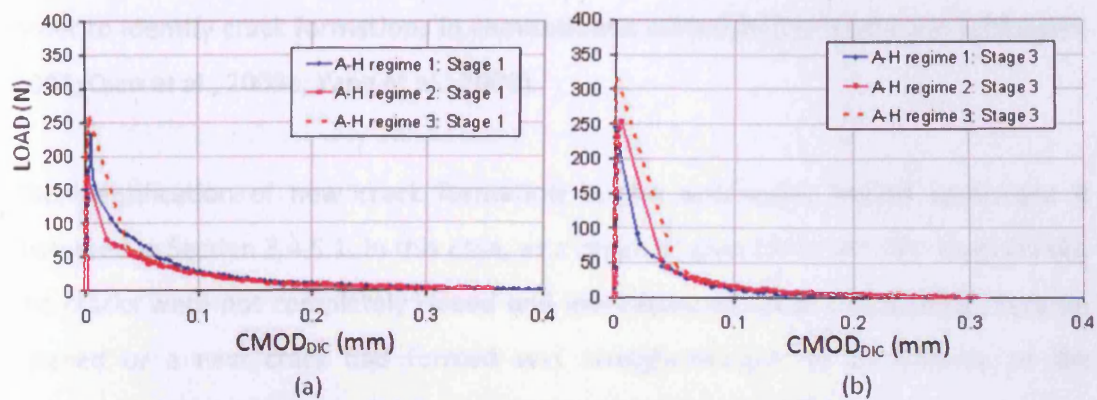


Figure 5.7 Results for control specimens for all AH regimes (a) stage 1, and (b) stage 3 (Isaacs et al., 2010)

### 5.4.2 Qualitative results

In addition to the results of mechanical testing, qualitative observations of crack closure were obtained. Figure 5.8 shows the crack in a typical AH2 specimen (a) immediately after unloading at the end of stage 1 and, (b) after heat activation and healing at the end of stage 2. It can be seen that the crack is no longer visible at the end of stage 2b.

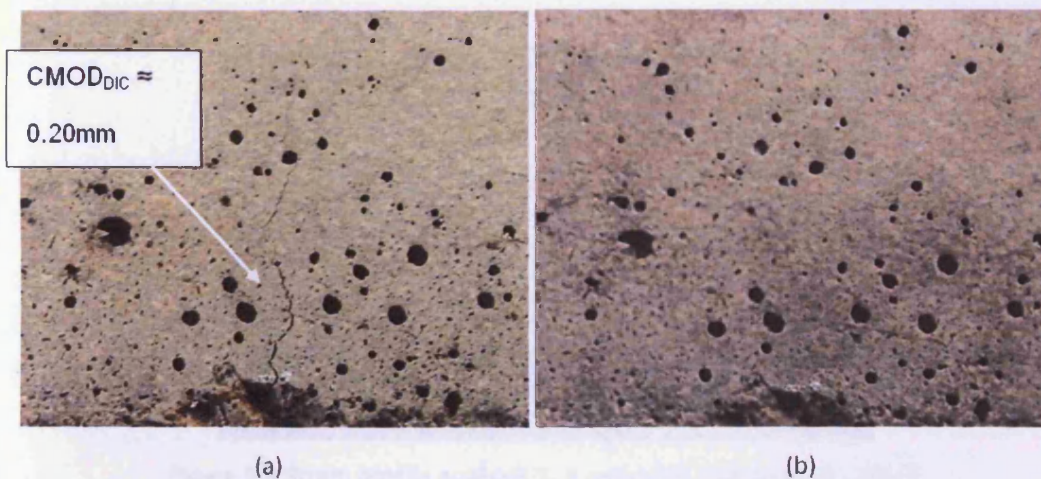


Figure 5.8 Specimen with (a) induced crack at stage 1, and (b) after tendon activation and healing at stages 2a and 2b (Isaacs et al., 2010)

An attempt to identify the formation of new crack paths was made. However, in stage 3 tests it was difficult to distinguish whether a new crack path had formed or the opening of an existing crack had occurred. This aspect of crack identification could be enhanced by the use of ESEM or equivalent that has been used in previous studies in

order to identify crack formations in cementitious materials (ter Heide and Schlangen, 2007; Qian et al., 2009a; Yang et al., 2009).

The identification of new crack formation in the autonomic healed specimens is discussed in Section 3.4.5.1. In this case, as a result of glue filling the first stage cracks, the cracks were not completely closed and identifying whether the existing crack re-opened or a new crack had formed was straightforward. In comparison to the specimens discussed in this chapter, when the autogenous healing effect is a result of crack closure provided by the activated tendons, identifying new crack formation was more difficult.

### **5.4.3 Autogenous healing measured using DIC**

The autogenous healing of specimens was also investigated using DIC. A further measurement of crack closure/healing was made by processing strain profiles across the notched region of the specimens. As shown in Figure 5.9, four strain profiles, each consisting of 100 data points, were processed.

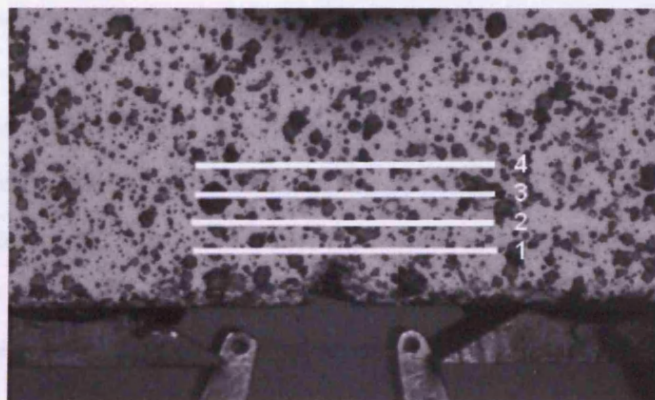


Figure 5.9 Strain profile analysis 1- 4 using DIC (Isaacs et al., 2010)

The strain profiles were analysed at three CMOD values, as shown in Figure 5.10. The values of which in this case are shown for a typical PETr specimen subject to an AH2 regime. The first profile (denoted CMOD I) was measured at a load just before the peak load in stage 1. The second profile (CMOD II) was taken immediately prior to unloading in stage 1, which was at a  $CMOD_{DIC}$  of approximately 0.2 mm. The third strain profile (CMOD III) was measured at a load just before the peak load in stage 3. Comparison between the strain profiles at CMOD I and CMOD III enabled further assessment of the degree of autogenous healing to be made.

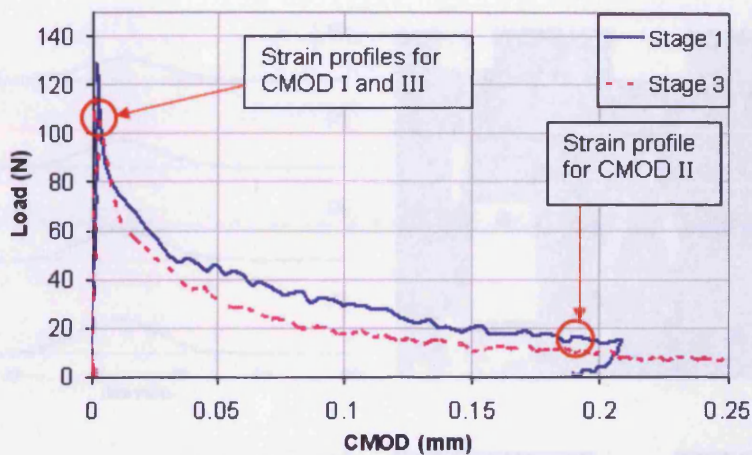


Figure 5.10 Strain profile CMOD points (Isaacs et al., 2010)

The results of the strain values at each CMOD point for a typical specimen are shown in Figure 5.11. The results for PET and PETr specimens subject to an AH2 regime are presented in Appendix E. It may be seen that no strain localisation is present in the plots for CMOD I or III cases, the latter indicating that complete healing was achieved. As would be expected, strain localisation is clear in the cracked case (CMOD II).

## 5.5 Discussion

The aim of this study was to explore the arrangement of autogenous healing as a consequence of the thermal action on repaired high-strength steel fibres in the proposed material system. As such, the AH regime adopted offers the opportunity

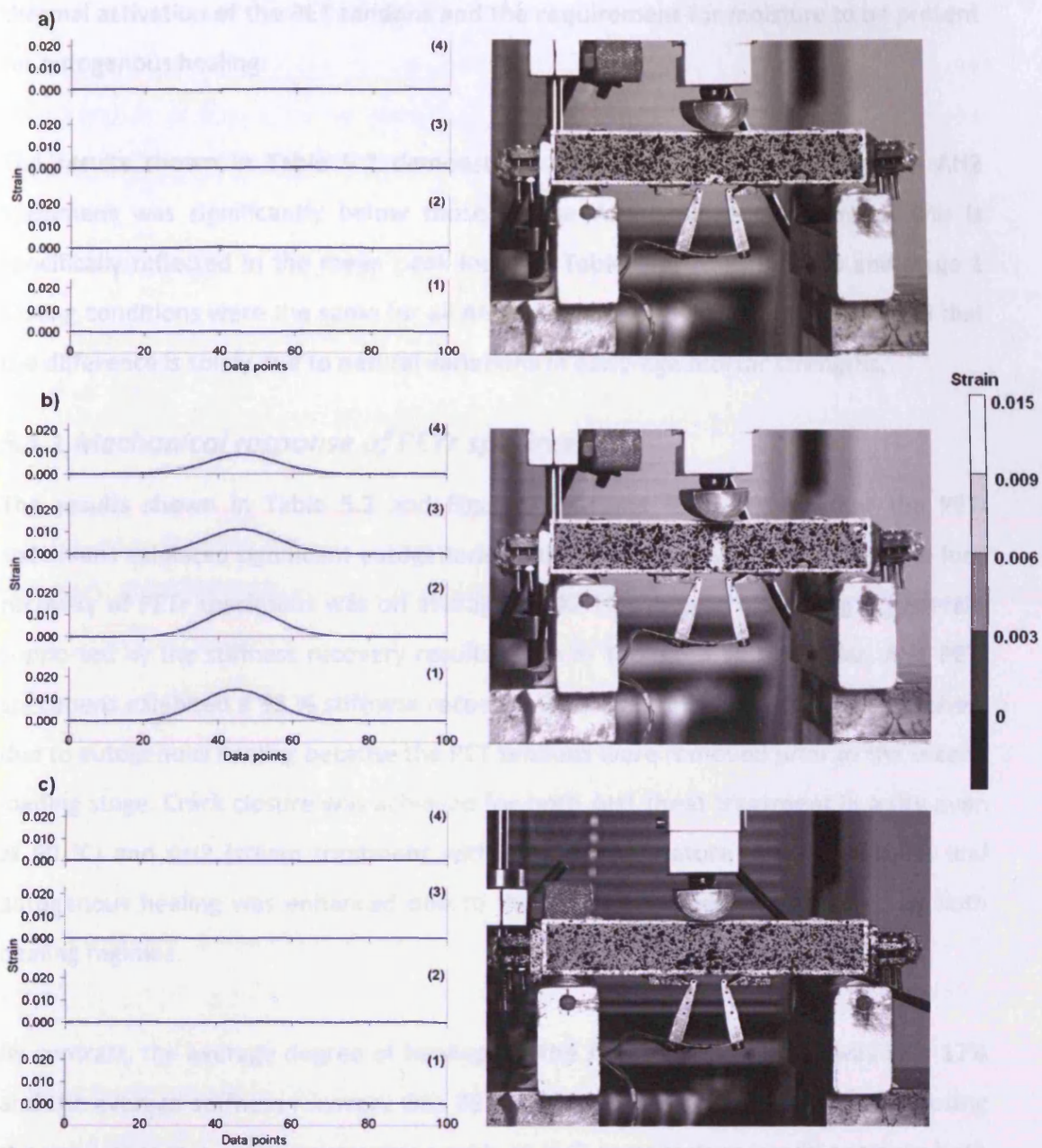


Figure 5.11 Strain profiles for a healed specimen using DIC: (a) CMOD I, (b) CMOD II, and (c) CMOD III (Isaacs et al., 2010)

## 5.5 Discussion

The aim of this study was to explore the enhancement of autogenous healing as a consequence of the thermal activation required to generate crack closure in the proposed material system. As such, the AH regimes adopted reflect the need for

thermal activation of the PET tendons and the requirement for moisture to be present for autogenous healing.

The results shown in Table 5.2 demonstrate that the 4-day strength of the AH2 specimens was significantly below those of the AH1 and AH3 specimens. This is specifically reflected in the mean peak loads in Table 5.2. The mix ratio and stage 1 testing conditions were the same for all AH regimes and thus it must be assumed that the difference is solely due to natural variations in early-age mortar strengths.

### ***5.5.1 Mechanical response of PETr specimens***

The results shown in Table 5.2 and Figures 5.4a and 5.5a suggest that the PETr specimens exhibited significant autogenous healing. In regimes AH1 and AH2, the load recovery of PETr specimens was on average 80 %. This degree of healing is generally supported by the stiffness recovery results given in Table 5.3. In particular, AH1 PETr specimens exhibited a 95 % stiffness recovery. This load recovery must be exclusively due to autogenous healing because the PET tendons were removed prior to the second loading stage. Crack closure was achieved for both AH1 (heat treatment in a dry oven at 90 °C) and AH2 (steam treatment with an air temperature of 90 °) regimes and autogenous healing was enhanced due to the moisture conditions provided by both healing regimes.

By contrast, the average degree of healing for the AH3 PETr specimens was only 17% and the average stiffness recovery was 35 %. It was originally expected that exposing the specimens to a continuous water supply at high temperature would promote both tendon activation and an enhancement in autogenous healing. However, this was found not to be the case and when a first set of tests showed little healing, a second set was undertaken. This gave a very similar set of results thereby confirming that very little self-healing was achieved.

In order to obtain a better understanding of the effects of temperature and curing regime on autogenous healing, a further set of tests was undertaken to measure the strength of the cementitious material under AH regimes 1, 2 and 3. This set of tests

comprised six small scale (25 mm x 25 mm x 25 mm) mortar cubes for each investigated regime. The aim of this additional series was to isolate the effect of the curing regime on the hydration process. The results from this supporting investigation are given in Table 5.5 whereby the investigated AH regimes are called AH1/B, AH2/B and AH3/B.

Table 5.5 Compressive strength of small scale mortar cubes (Isaacs et al., 2010)

	AH1/B	AH2/B	AH3/B
<b>Av. strength of cubes (N/mm<sup>2</sup>)</b>	16.5	31.0	26.0

The results of the cube tests confirm that a higher curing temperature generally causes high early strength as a result of rapid hydration, which is consistent with the findings of previous investigators (Lura et al., 2001, Lothenbach et al., 2007). AH2/B and AH3/B cubes developed approximately twice the strength of AH1/B cubes which is attributed to moisture exposure in addition to the high temperature during curing promoting more rapid hydration. However, the AH3/B results shown in Table 5.5 do not explain why the mechanical response of AH3 PETr specimens exhibited such low loads and poor stiffness recovery. It has been proposed that this might be due to the formation of air bubbles in the hot water, which disrupt the formation of a continuous layer of material between the crack surfaces. Furthermore, it is considered that the high water temperature may cause leaching out of the Portland materials. However, there is no specific evidence in both cases and further work is required to verify this and identify if there are ways of overcoming it.

### ***5.5.2 Mechanical response of PET specimens***

The PET specimens developed higher peak loads in comparison to the associated PETr specimens subject to the same AH regimes as shown in Table 5.2. This is attributed to the tendons remaining in the PET specimens that act as reinforcement during the second loading stage. This is further confirmed by a stiffer loading response of the PET specimens during the second loading stage in comparison to the PETr specimens as shown in Table 5.3.

In all AH regimes, the PET specimens developed a significant load recovery as shown in Table 5.2. In regimes AH1 and AH2, the PET specimens developed a load recovery of 127 % and 194 % as shown in Figures 5.4b and 5.5b respectively. In both cases, evidence of autogenous healing in the PET specimens is shown by a peak load followed by a stress drop. This is assumed to be associated with the formation of new cracking. This characteristic was not notable for associated PETr specimens, although a significant load recovery (80 %) was still exhibited. In the case of the PET specimens, not only was a full load recovery observed, but an increase in strength and stiffness was measured. The increase in load and stiffness recovery in the PET specimens for AH1 and AH2 during the second loading stage can be attributed to both the prestress provided by the tendon and autogenous healing.

Although the AH3 PET specimens did not exhibit a full load recovery, on average a 93 % recovery was measured as shown in Table 5.2 and Figure 5.6b. In this case it is considered that the PET specimens did not exhibit autogenous healing, which is confirmed by the associated PETr specimens. However, the addition of prestress provided by the activated tendons enabled the specimens to exhibit a load recovery of almost 100 %.

## 5.6 Conclusions

The experimental data presented in this chapter have demonstrated that crack closure and autogenous healing can be achieved on small scale hollow prismatic mortar beams post-tensioned with shrinkable polymer tendons. Crack closure was achieved as a result of the shrinkage stress developed by the activated PET tendons. Two of the AH regimes adopted for activating and healing the specimens also demonstrated effective autogenous healing, namely:

- Dry heat activation and water based healing (AH1)
- Steam activation and healing (AH2)

In the former case, the initial mechanical stiffness was recovered and strength recoveries of approximately 80 % (PETr) and 125 % (PET) were achieved and, in the latter case, the initial mechanical stiffness was again recovered and load recoveries of approximately 80 % (PETr) and 200 % (PET) were achieved. It is concluded that both dry heat activation followed by water curing, and steam activation and curing are both effective heating/healing regimes, with the latter providing the highest prestress force.

Only 17% of the initial strength was recovered in specimens activated and healed in water at 90 °C although the regime did activate the tendons and produce sufficient prestress to achieve crack closure. It is believed that that the reason for the reduced level of self-healing in this case was related to the formation of bubbles in the crack impeding the healing process.



## Chapter 6

### Theoretical analysis

#### 6.1 Introduction

The mechanical response of the small scale mortar specimens described in Chapter 5 results from a combination of post-tensioning, provided by the activated PET tendons, and autogenous healing, enhanced by crack closure. In this chapter an analytical and a numerical model, which simulate this response, are discussed. The analytical solution was envisaged to be part of a design procedure for the system, whilst a numerical solution was developed to aid understanding of the behaviour. The two methods essentially solve the same equations, which relate to a prismatic beam with a central crack. In both cases, a moment-curvature relationship has been considered for the fracture process zone.

#### 6.2 Analysis

The development of the LatConX material system will require the issues of safety, serviceability and functionality to be addressed. Current codes of practice do not cover every aspect of design relevant to this new material system, but a proven design procedure will be required if the material system is to be used commercially. At this early stage of development, the verification of the mechanical response of the system is considered to be the most important issue.

In order to consider the mechanical response of the LatConX specimens in an objective manner, a parameter independent of size was required. As highlighted by Bažant and Planas (1998), a flexural strength measure would not be objective because specimens formed from cementitious composites exhibit a strong size effect which is mainly due to the existence of a micro-cracking zone around the ahead of a macro-crack. In the case of the small scale specimens investigated in this study the effects of micro-cracks

lead to apparent flexural strengths that are significantly higher than the first damage stress.

The use of an existing size-effect model was considered (Bažant and Planas, 1998) to resolve the issue of micro-cracks in small scale specimens. However, the specimen configuration adopted for this study did not make this possible due to the central voids in specimens. In addition, the cases of both prestressed and non-prestressed specimens needed to be addressed. As a result, the theoretical approach accounts for crack softening by consideration of a moment-curvature relationship for the fracture process zone. A linear softening curve is considered that accounts for the transfer of stresses across the micro-cracking region as shown in Figure 6.1.

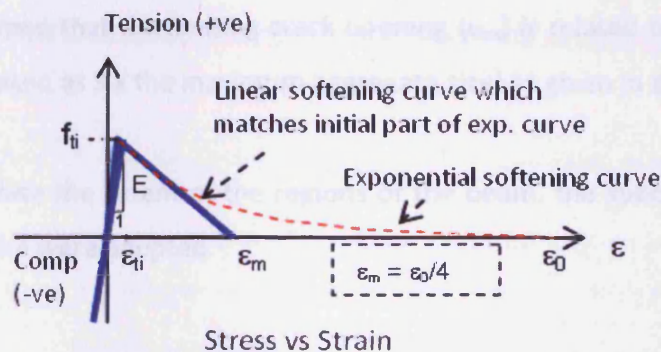


Figure 6.1 Crack softening relationship (Isaacs et al., 2010)

In order to measure the stress transfer across the micro-cracking region and identify the failure location, the beam section was divided into four regions as illustrated in Figure 6.2.

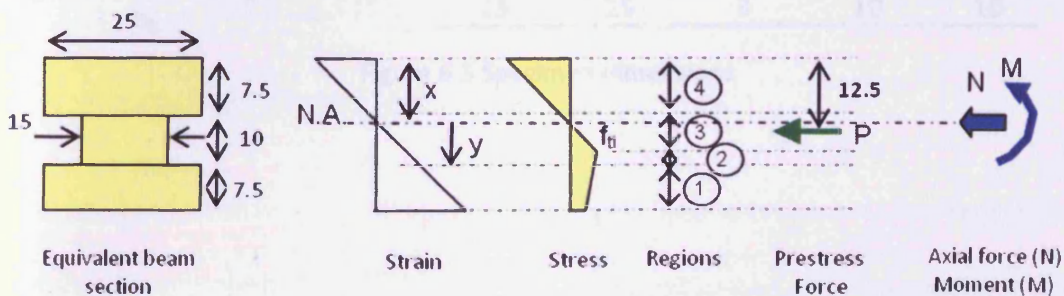


Figure 6.2 Beam model (Isaacs et al., 2010)

The basic constitutive model adopted may be summarised as follows;

$$\begin{aligned} \sigma &= E\varepsilon && \text{if } \varepsilon \leq \varepsilon_{ti} \\ \sigma &= f_{ti} \frac{\varepsilon_m - \varepsilon}{\varepsilon_m - \varepsilon_{ti}} && \text{if } \varepsilon_m \geq \varepsilon > \varepsilon_{ti} \\ \sigma &= 0 && \text{if } \varepsilon > \varepsilon_m \end{aligned} \quad (1)$$

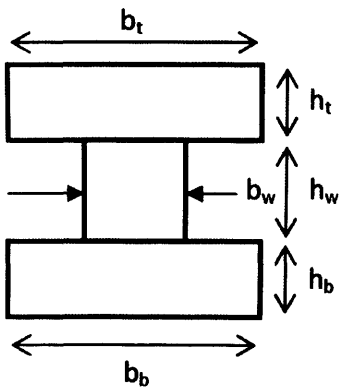
In which  $\sigma$  is the beam fibre stress,  $\varepsilon$  the strain and subscripts  $m$  and  $ti$  denote a limiting value and first damage respectively.

The strain at a given level  $y$  depends upon the curvature ( $\psi$ ) and is given by

$$\varepsilon = y(x) \cdot \psi \quad (2)$$

It is further assumed that the limiting crack opening ( $u_m$ ) is related to  $\varepsilon_m$  by the crack band width  $w_c$  (taken as 3 x the maximum aggregate size) as given in equation 2.

In order to calculate the extent of the regions of the beam, the specimen dimensions shown in Figure 6.3 were adopted.



The properties include,  $b$ , the width of specimen,  $h$ , the height of specimen,  $dn$ , the notch depth,  $b_w$ , the base of the central void, and  $h_w$ , the height of the central void.

Table 6.1 shows the dimensions.

$b$ (mm)	$h$ (mm)	$dn$ (mm)	$b_w$ (mm)	$h_w$ (mm)
25	25	3	10	10

Figure 6.3 Specimen dimensions

The height and width of the bottom flange, web and top flange were calculated using the expressions summarised below:

$$\begin{aligned}
 b_b &= b & h_w &= h_w & b_t &= b & h_s &= h_b + h_w + h_t \\
 b_w &= b - b_w & h_t &= \frac{h - h_w}{2} & h_b &= \frac{h - h_w}{2} - d_n & A &= h_s \cdot b - h_w \cdot b_w \quad (3)
 \end{aligned}$$

For the analytical model it was necessary to consider two cases relating to the level of the top of the micro-cracking zone (at which  $\sigma=f_{ti}$ ), i.e. (i)  $\sigma=f_{ti}$  occurs in the web (case 1) and (ii) in the top flange (case 2).

*Case 1: Top of micro-cracking zone occurs in the web*

The depth to the interface between each region is given by the condition  $(x + \frac{\epsilon_t}{\psi} - h_t) \geq 0$ ; in which  $\epsilon$  is the strain,  $\psi$  is the curvature and the subscript  $t$  denotes first damage. In addition, the level  $y$  is considered positive down, as shown in Figure 6.2. The depths are defined by the functions shown in 4a and b, where  $y$  corresponds to the depth and  $b$  corresponds to the width.

$$y_f(x, \psi) = [(h_s - x)(h_s - h_b - x) \left(\frac{\epsilon_t}{\psi}\right) (h_t - x)(-x)] \quad 4(a)$$

$$b_z(x, \psi) = [(b_b)(b_w)(b_w)(b_t)] \quad 4(b)$$

*Case 2: Top of micro-cracking zone occurs in the top flange*

In this case, the condition to define the depth to the top of the micro-cracking zone in the top flange is given when  $(x + \frac{\epsilon_t}{\psi} - h_t) < 0$ . The depths are defined in equations 5a and b.

$$y_f(x, \psi) = [(h_s - x)(h_s - h_b - x)(h_t - x)\left(\frac{\epsilon_t}{\psi}\right)(-x)] \quad 5(a)$$

$$b_z(x, \psi) = [(b_b)(b_w)(b_t)(b_t)] \quad 5(b)$$

The equations of axial and moment equilibrium comprise summations over the regions as shown in Figure 6.2, with these being modified if first damage occurs in the web or the top flange, as highlighted for the idealised section.

$$N = \sum_{i=1}^{n_{regions}} b_i \Delta y_i \cdot \left( \frac{\sigma_{i+1} + \sigma_i}{2} \right) + P = 0 \quad (6)$$

$$M = \sum_{i=1}^{n_{regions}} b_i \Delta y_i \cdot \left( \frac{\sigma_i}{6} \cdot (2y_i + y_{i+1}) + \frac{\sigma_{i+1}}{6} \cdot (y_i + 2y_{i+1}) \right) + P \cdot \left( \frac{h}{2} - x \right) \quad (7)$$

In which  $b_i$  = width of region  $i$ ,  $h$  = depth of un-notched beam (i.e. 25mm) and  $\Delta y = (y_i - y_{i+1})$ .

It may be seen that the linear softening curve has been chosen such that the initial slope approximately matches that of an exponential softening curve of the form  $\sigma = f_{ti} \exp(-5 \cdot ((\epsilon - \epsilon_{ti}) / (\epsilon - \epsilon_m)))$ . The reason for this is that the peak load is generally associated with the early stages of micro-cracking.  $\epsilon_0$  is computed from the fracture energy and therefore the implied fracture energy of the proposed model would not be correct if it were applied over the full range of opening. The moment-curvature relationship is considered for an analytical and numerical solution.

### 6.3 Analytical solution

The analytical approach addresses axial equilibrium and determination of the maximum moment as shown in equations 6 and 7. Equation 8 shows the axial equilibrium expression for the top of micro-cracking in the web conditions.

$$\begin{aligned}
 N(x) = & \left[ x \left[ \psi \left( \frac{f_t}{\epsilon_{mt}} \right) \left[ b \left( \frac{h-h_v}{2} - dn \right) \right] \right] \right] + \left[ b \left( \frac{h-h_v}{2} - dn \right) \left[ \frac{f_t}{2 \epsilon_{mt}} \left[ 2 \epsilon_m - \left( \frac{h-h_v}{2} - dn \right) \psi - 2 h_v \psi - 2 \left( \frac{h-h_v}{2} \right) \psi \right] \right] \right] \\
 & + \left[ -x^2 \left[ (b-b_v) \left[ \frac{f_t \left( \frac{\psi}{\epsilon_{mt}} \right)}{2} \right] \right] - x \left[ (b-b_v) \left[ \frac{f_t \left[ \frac{\epsilon_m - \left( \frac{h+h_v}{2} \right) \psi}{\epsilon_{mt}} \right] + E \left( \frac{\epsilon_t}{\psi} \right) \psi}{2} \right] \right] + x \left[ \left( \frac{f_t \psi}{2 \epsilon_{mt}} \right) (b-b_v) \left( \frac{h+h_v}{2} - \frac{\epsilon_t}{\psi} \right) \right] \right] \\
 & + \left[ (b-b_v) \left( \frac{h+h_v}{2} - \frac{\epsilon_t}{\psi} \right) \left[ \frac{f_t \left[ \frac{\epsilon_m - \left( \frac{h+h_v}{2} \right) \psi}{\epsilon_{mt}} \right] + E \left( \frac{\epsilon_t}{\psi} \right) \psi}{2} \right] \right] + \left[ -x^2 \left[ (b-b_v) \left( \frac{E \psi}{2} \right) \right] + x \left[ (b-b_v) \left[ \frac{E \epsilon_t}{\psi} \psi + \left[ E \left( \frac{h-h_v}{2} \right) \psi \right] \right] \right] \right] \\
 & + \left[ x \left[ \left( \frac{E \psi}{2} \right) (b-b_v) \left( \frac{\epsilon_t}{\psi} - \frac{h-h_v}{2} \right) \right] + \left[ (b-b_v) \left( \frac{\epsilon_t}{\psi} - \frac{h-h_v}{2} \right) \left[ \frac{E \epsilon_t}{\psi} \psi + \left[ E \left( \frac{h-h_v}{2} \right) \psi \right] \right] \right] \right] \\
 & - x (E \psi) \left[ b \left( \frac{h-h_v}{2} \right) \right] + \left[ b \left( \frac{h-h_v}{2} \right) \left[ \frac{E \left( \frac{h-h_v}{2} \right) \psi}{2} \right] \right] \tag{8}
 \end{aligned}$$

The expression for axial equilibrium shown in equation 8 is rearranged in terms of  $x$  and solved for a given  $\psi$  in the quadratic form  $ax^2 + bx + c$  to find the depth to the neutral axis. It was envisaged that prior to a solution for  $x$  being obtained using the quadratic equation of the form,  $x = \frac{-b \pm \sqrt{b^2 - 4.a.c}}{2a}$  an expression for  $x$  could be substituted into the moment equation which is given in equation 9. An attempt was made to develop a closed form solution in this case; however after several iterations the moment expressions became intractable. Therefore, the resulting semi-analytical solution is directly equivalent to the numerical solution discussed in Section 6.4. The moment for the top of micro-cracking in the web condition is shown in equation 9.

$$\begin{aligned}
 M(x) = & \left[ b_b \left[ h_s - x - (h_s - h_b - x) \right] \left[ \frac{\sigma_1}{6} \left[ 2(h_s - x) + (h_s - h_b - x) \right] + \frac{\sigma_2}{6} \left[ h_s - x + 2(h_s - h_b - x) \right] \right] \right] \\
 & + b_w \left( h_s - h_b - x - \frac{\epsilon_t}{\psi} \right) \left[ \frac{\sigma_2}{6} \left[ 2(h_s - h_b - x) + \frac{\epsilon_t}{\psi} \right] + \frac{\sigma_3}{6} \left[ h_s - h_b - x + 2 \frac{\epsilon_t}{\psi} \right] \right] \\
 & + \left[ b_w \left[ \frac{\epsilon_t}{\psi} - (h_t - x) \right] \left[ \frac{\sigma_3}{6} \left[ 2 \frac{\epsilon_t}{\psi} + (h_t - x) \right] + \frac{\sigma_4}{6} \left[ \frac{\epsilon_t}{\psi} + 2(h_t - x) \right] \right] \right] \\
 & + b_t \left[ h_t - x - (-x) \right] \left[ \frac{\sigma_4}{6} \left[ 2(h_t - x) + (-x) \right] + \frac{\sigma_5}{6} \left[ h_t - x + 2(-x) \right] \right] \tag{9}
 \end{aligned}$$

## 6.4 Numerical solution

The numerical solution has been developed in a Mathcad sheet in which  $x$  (the neutral axis depth) is found by using equation 6 and then the maximum moment (or moment at first cracking) is found from equation 7. The functions of axial equilibrium and the moment are shown in equations 10 and 11 respectively.

$$N(x, \psi) := \begin{cases} y \leftarrow yf(x, \psi) \\ bb \leftarrow bz(x, \psi) \\ \varepsilon \leftarrow y \cdot \psi \\ \text{for } i \in 1..nz + 1 \\ \quad \sigma_i \leftarrow \sigma f(\varepsilon_i) \\ \sum_{i=1}^{nz} \left[ bb_i \cdot (y_i - y_{i+1}) \cdot \frac{(\sigma_{i+1} + \sigma_i)}{2} \right] + P_p \end{cases} \quad (10)$$

$$M(x, \psi) := \begin{cases} y \leftarrow yf(x, \psi) \\ bb \leftarrow bz(x, \psi) \\ \varepsilon \leftarrow y \cdot \psi \\ \text{for } i \in 1..nz + 1 \\ \quad \sigma_i \leftarrow \sigma f(\varepsilon_i) \\ \sum_{i=1}^{nz} \left[ bb_i \cdot (y_i - y_{i+1}) \cdot \left[ \frac{\sigma_i}{6} \cdot (2 \cdot y_i + y_{i+1}) + \frac{\sigma_{i+1}}{6} \cdot (y_i + 2 \cdot y_{i+1}) \right] \right] + P_p \cdot \left( \frac{h}{2} - x \right) \end{cases} \quad (11)$$

A crack opening may be extracted from the product of the strain at the notch level and the fracture process zone width i.e.  $(\psi_{y_{\text{notch}}}) \cdot w_c$ , as illustrated in Figure 6.4. The load (F) associated with the moment  $M$  is calculated from statics.

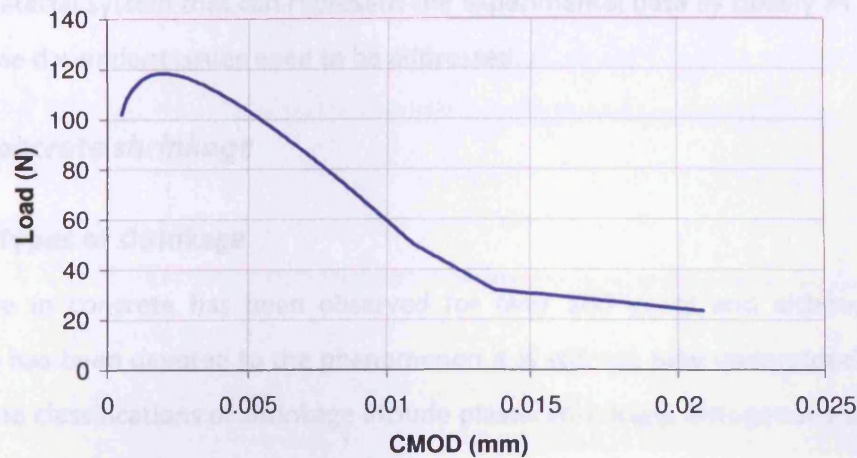


Figure 6.4 Numerical response

## 6.5 Concrete behaviour

As highlighted in the introduction of this chapter, the material systems active components are the PET tendons which provide post-tensioning and bring about crack closure. Autogenous healing is then enhanced by the use of the combined activation/healing regimes described in Chapter 5. The theoretical analysis therefore has to account for the behaviour of the material system after post-tensioning and crack closure.

In this case, the resulting crack closure is followed by a healing time in order to enhance the degree of autogenous healing prior to a second loading stage. This time dependency has already been discussed in Section 2.3.1 where it was observed that autogenous healing was greater in early age specimens (Edvardsen, 1999).

Time dependent behaviour is an important issue when the durability of cementitious materials is considered. The time dependent effects most notably include changes in elastic properties, shrinkage and creep. In these cases, the stress-strain relationships include the conditions of sustained loading that exhibit creep as the strain increases with time and cementitious materials undergo shrinkage as a result of the material contracting on drying, whether subject to a load or not (Neville, 1999). Since the PET tendons apply prestress to the cementitious matrix, creep deformations, associated with this stress, will also occur. Therefore, in developing an analysis for the behaviour



of the material system that can represent the experimental data as closely as possible, these time dependent issues need to be addressed.

### **6.5.1 Concrete shrinkage**

#### **6.5.1.1 Types of shrinkage**

Shrinkage in concrete has been observed for over 100 years and although much research has been devoted to the phenomenon it is still not fully understood (Bažant, 2001). The classifications of shrinkage include plastic shrinkage, autogenous shrinkage, carbonation shrinkage and drying shrinkage.

Plastic shrinkage is exhibited in early volume changes when the concrete is in its plastic state. This is typically exhibited by the shrinkage of the cement paste that is in a plastic state, and is associated with the loss of water from surface evaporation and the loss of water by suction of the underlying material (Neville, 1999). Autogenous shrinkage relates to a volume change in moisture sealed conditions in the process of self-desiccation, whereby the unhydrated cement consumes water from the capillary pores. This type of shrinkage is most prominent in low water/cement ratios and in general it is not considered exclusively unless large structures with low water/cement ratios are used (Acker and Ulm, 2001; Neville, 1999). Carbonation shrinkage is the reaction of the cement hydration products and  $\text{CO}_2$  to form carbonates ( $\text{CaCO}_3$ ). This type of shrinkage occurs on the same time scale as drying shrinkage but the formation of  $\text{CaCO}_3$  can enhance the strength and reduce permeability in cementitious materials.

For the investigated material system, the specimens undergo a heating stage in order to activate the PET tendons and this tends to produce rapid drying shrinkage, which is considered highly influential. Drying shrinkage can be defined as the withdrawal of water from concrete stored in unsaturated air (Neville, 1999). In this type of shrinkage, the magnitude of moisture loss can be influenced by the surrounding environment by such parameters as temperature, ambient relative humidity and wind velocity. The drying shrinkage can also depend on the thickness of the structural element, the porosity (free evaporable water) of the concrete, the volume of the paste and the

fineness of the binder (Acker and Ulm, 2001). The loss of evaporable water is considered one of the main causes of moisture loss (Bisschop, 2002) and the shrinkage can also be influenced by the water/cement ratio and the degree of hydration.

As a result of drying shrinkage, Acker and Ulm (2001) describe two modes of cracking that can occur. The first mode of cracking, that occurs in the very early stages (hours) of curing, corresponds to cracks that are limited to the upper surface of the concrete. The second mode of cracking corresponds to the long term drying that is an extremely slow process (years) and increases with the thickness of the structure. This is confirmed by the fact that moisture loss is larger nearer the surface (Neville, 1999). At a more fundamental level, the drying shrinkage can be explained by the mechanisms of capillary tension, solid surface tension, movement of interlayer water and disjoining (Bažant, 2001), although these nanoscale mechanisms of drying shrinkage have not yet been fully established (Bisschop, 2002).

#### **6.5.1.2 Actions of shrinkage**

Acker and Ulm (2001) discuss three actions of shrinkage; mechanical, thermal and hygral. In the former, it is considered that displacements prescribed as boundary conditions and/or external forces that act on the surface or in the volume (dead weight) can influence concrete deformation. These actions can be addressed in the design stage of concrete structures.

It is however the thermal and hygral actions that often cause large mechanical effects, especially at an early age. The thermal actions can result in significant temperature gradients within a structure. These thermal actions can be of natural origin (climatic conditions), industrial origin (thermal treatment) or be caused by the heat of hydration, which is more significant in larger structures. The hygral actions are the consequence of concrete being a porous material. As capillary pores are emptied they are subject to tensile forces that can induce compression in the concrete skeleton.

In summary, the severity of shrinkage is dependent on the moisture loss in cementitious materials and can be influenced by various factors that include mix

design, specimen size, temperature, ambient relative humidity, and wind velocity. For the investigated material system, it is considered that the shrinkage is influenced most by the loss of moisture during the heating stage that is undertaken to activate the PET tendons. However, in the parametric investigation, in order to enhance autogenous healing the specimens were thermally activated in the presence of moisture. This provided a saturated environment in which drying shrinkage could be potentially minimised. In addition, it is envisaged that further investigation of the specimen mix design could serve to enhance autogenous healing and minimise the effects of shrinkage.

### **6.5.2 Concrete creep**

As discussed by Bažant (2001), mechanisms causing, or influencing, creep have been identified and studied. Creep can be described as the time-dependent strain that occurs in concrete as a result of an applied constant stress. The dual phenomena to creep is relaxation, whereby for a constant strain, a reduction in the stress occurs over a period of time. Creep is a function of the volumetric content of cement paste. In cementitious materials it is the cement paste that generally undergoes creep and in concrete, the aggregate acts primarily as a restraint to creep (Neville, 1999).

Acker and Ulm (2001) discussed the critical role of water content on the behaviour of creep. In conditions where there is no exchange of water with ambient temperature, the lower the evaporable water, the lower the creep. This is contradictory to dry atmospheric conditions where the greater the drying, the greater the creep. In cementitious materials where there is no evaporable water, creep will not be exhibited (Neville, 1999).

Creep can be identified by two superposed strains:

1. Basic creep, which is exhibited under conditions of no moisture movement. The time dependent strain development occurs at a constant load for a constant relative humidity, and;

2. Drying creep, which is the deformation in excess of basic creep strain under constant load and when the material is exposed to drying conditions. In this case there is moisture movement.

Two mechanisms have been discussed that identify the different stages of basic creep (Acker and Ulm, 2001). In regard to the mobility of water, a short term mechanism (days) defines the stress-induced movement of water towards the largest diameter pores which can generate strains and stresses that induce micro-cracking and short term creep. The second mechanism, also referred to as long term creep, corresponds to the movement of interlayer water that becomes increasingly inhibited over time.

Furthermore, Bažant et al. (2004) describe that the modelling of creep and shrinkage in concrete has been driven by the three complex phenomena that is the aging of concrete, the drying creep, and the transitional thermal creep. There have been many studies on creep behaviour in cementitious materials and a number of numerical models for simulating this behaviour have been proposed (Bažant, 2001; Bažant et al., 2004).

The modelling of creep and shrinkage for the LatConX material system is beyond the scope of this thesis and the simplified numerical approach described in the previous sections addresses (directly) only the mechanical behaviour of the specimens at the time of testing. However, the issues of creep and shrinkage in the investigated LatConX material system are being addressed from a numerical approach by Dunn (2010) which presents a proposed numerical model accounting for creep and shrinkage. Dunn's model also accounts for the effects of relaxation in the PET tendons that were determined from the experimental investigation discussed in Chapter 4 of this thesis.

## 6.6 Results and discussion

The results in terms of the peak loads ( $F$ ), and cracking stress ( $f_{ti}$ ), which equals  $f_{healed}$  in stage 3, fracture energy  $G_f$  (relating to the exponential curve) and the polymer prestress after losses ( $\sigma_p$ ) are given in Table 6.2. It is noted that separate fracture

energy tests were conducted at day 9, as given in Table 5.4 in Chapter 5 but the fracture energy will be less at day 4 and slightly less at day 8. Therefore the fracture energies were also computed from the control specimens for all AH regimes.

Table 6.2 Numerical solution data

Regime / Stage	Predicted peak load <sup>a</sup> F(N)	Peak load Exp. range	$G_f$ (N/mm)	$f_{ti}$ Or $f_{healed}$ (N/mm <sup>2</sup> )	$\sigma_p$ (N/mm <sup>2</sup> )	% Healing
AH1 Stage 1 (PET)	236	206 – 266	0.025	2.2	-	
Stage 3 PETr	163	162 – 197	0.013	1.5	-	68
Stage 3 PET	335	246 - 334	0.013	1.5	27.5	
AH2 Stage 1 (PET)	154	138 – 167	0.020	1.3	-	
Stage 3 PETr	118	114 – 139	0.013	1.05	-	81
Stage 3 PET	316	267 - 313	0.013	1.05	29.5	
AH3 Stage 1 (PET)	236	219 – 250	0.025	2.2	-	
Stage 3 PETr	46	35 – 47	0.006	0.35	-	16
Stage 3 PET	261 <sup>b</sup>	209 - 222	0.006	0.35	29.5	

Note: <sup>a</sup>In most cases this was a first peak load and was associated with cracking of the mortar however, where no first peak existed; <sup>b</sup>this load was taken as the point at which the stiffness first changed significantly.

In Table 6.2 the peak load data obtained from the numerical solution is within the range of the associated AH regime experimental peak load data. For respective AH regimes,  $f_{healed}$  at stage 3 is nominally the same for PETr and PET specimens because in both cases the prestress is provided by the tendon during activation and healing.

In the numerical solution of the PET specimens, it was assumed that the healed stress ( $f_{healed}$ ) was the same as that calculated from the associated PETr data. Furthermore, it was assumed that the prestress could be determined from the temperature and time of heating, taking into account shrinkage, thermal contraction and relaxation losses using the data obtained on isolated tendons as discussed in Section 4.5, Dunn (2010) and Dunn et al. (2010) which are illustrated in Figures 6.5 and 6.6.

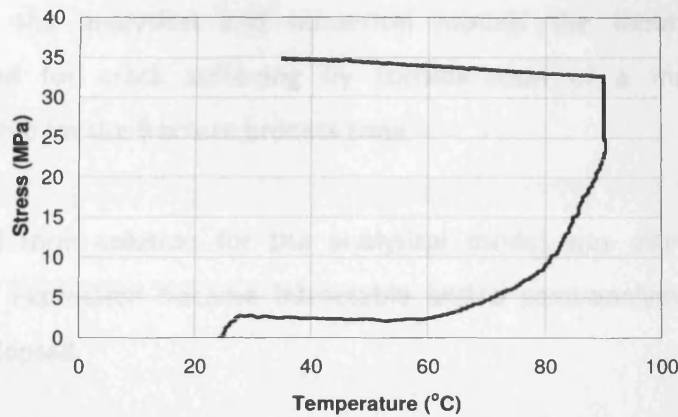


Figure 6.5 Stress development of PET (Dunn et al., 2010)

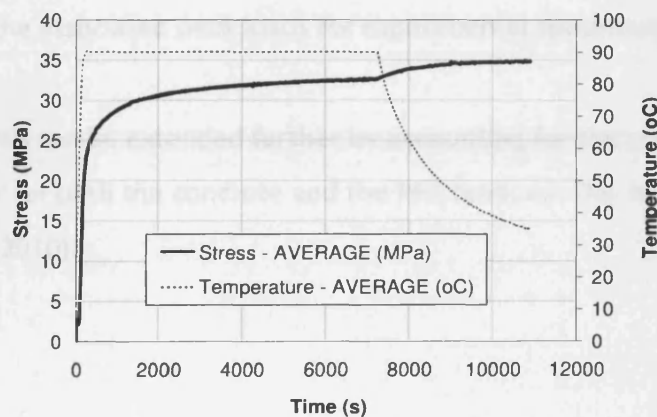


Figure 6.6 Stress development of PET at 90 °C (Dunn et al., 2010)

These data suggest that a higher degree of axial compression will be provided by the tendons in AH2 and AH3, than in AH1, due to the longer exposure time to elevated temperatures. Using the above assumptions it was found that the predicted peak loads for all AH regimes, shown in Table 6.2, were within the range of those obtained experimentally, which gave confidence in the analysis method and parameters extracted using the procedures described.

## 6.7 Conclusions

- An analytical and a numerical model have been presented to simulate the mechanical response for crack closure and autogenous healing for LatConX specimens.

- In both the analytical and numerical models the theoretical approach accounted for crack softening by consideration of a moment-curvature relationship for the fracture process zone.
- A closed form solution for the analytical model was attempted, but the moment expression became intractable and a semi-analytical solution was finally adopted.
- The numerical model peak loads for all AH regime specimens were within the range of the associated peak loads for experimental specimens.
- The analysis can be extended further by accounting for the creep and shrinkage behaviour for both the concrete and the PET tendons. This has been addressed by Dunn (2010).

## **Chapter 7**

# **Conclusions and recommendations for further work**

This chapter reviews the general conclusions that have been made as a result of the investigations that are presented in this thesis. In addition, recommendations for further research are given.

### **7.1 Conclusions**

As highlighted in Chapter 1, the scope and objectives of the research were to:

- I. Investigate the self-healing mechanisms associated with both autonomic and autogenous healing of cementitious materials
- II. Develop a novel self-healing composite material system with the use of shrinkable polymers to provide crack closure
- III. Investigate techniques and parameters that can provide crack closure and enhance the self-healing capability
- IV. Develop a simplified numerical model to measure the response of crack closure

In satisfying these objectives, research was undertaken which has led to the following conclusions:

- I. Using a cyanoacrylate adhesive encapsulation in glass capillary tubes to provide a mechanism for autonomic healing:
  - A primary healing response was exhibited during the first loading stage. Specimens were loaded under three-point bending to a pre-defined crack width and a primary healing response was shown to improve with a decreasing loading rate and an increasing level of reinforcement;



- A secondary healing response was exhibited during the second loading stage. Specimens were reloaded 24 hours after the first loading stage in order to provide full curing for the cyanoacrylate adhesive prior to a second loading stage. The specimens exhibited a secondary healing response that resulted in an increase in the peak load and a full recovery of stiffness;
  - New cracks were formed during the second loading cycle as a result of glue release into cracks formed during the first loading cycle.
- II. A new cementitious material system in which autogenous healing is advanced by shrinkable polymers was a feasible concept. This was confirmed by the selection of a suitable polymer and the results for a range of proof of concept tests. The main findings were that:
- PET Shrink-tite developed the highest shrinkage stress as a result of thermal activation. This was approximately 34 MPa when thermally activated to a temperature of 90 °C and allowed to cool. This satisfied the requirement for a minimum shrinkage stress criteria of 20 MPa and a suitable activation temperature that had been identified previously;
  - The results of a parametric study on PET showed that the effects of the cross section (number of strips) were negligible for specimens subject to a temperature of 90 °C for 30 minutes;
  - The presence of the PET tendons in all specimens tested at stage 1 for the developed cementitious material had no influence on the unloading response;
  - The development of a tendon which comprised 75 individual strips of PET tape layered on top of one another was capable of providing crack closure;

- For the specimens from which the PET tendons were removed prior to stage 3 testing, no significant crack healing was exhibited as a result of the dry heating and dry healing regime.

III. By careful control of both the activation and healing stages of the proposed material system, crack healing facilitated by the crack closure generated by thermally activating shrinkable polymers could be enhanced. The main conclusions of this particular study were that:

- Crack closure was achieved as a result of the shrinkage stress developed by thermal activation of the polymer tendons;
- Two of the regimes adopted for activating and healing the specimens demonstrated effective autogenous healing, namely:
  - a) Dry heat activation and water based healing (AH1)
  - b) Steam activation and healing (AH2)
- For the AH1 specimens, the initial mechanical stiffness was recovered and load recoveries of approximately 80 % (PETr) and 125 % (PET) were achieved;
- For the AH2 specimens, the initial mechanical stiffness was recovered and load recoveries of approximately 80 % (PETr) and 200 % (PET) were achieved;
- It was concluded that both dry heat activation followed by healing under water, and steam activation and healing were both effective activation-healing regimes, with the latter providing the highest prestress force;

- For the water activation and healing (AH3) regime, the PETr specimens exhibited only 16% strength recovery and the PET specimens exhibited approximately 100% strength recovery.

IV. The self-healing response measured during experimental tests has been modelled by a simplified numerical analysis. A moment-curvature relationship for the fracture process zone was used to account for the transfer of stresses across the micro-cracking region. The main conclusions were that:

- The assumed healed stresses ( $f_{\text{healed}}$ ) in the PET specimens was the same as those calculated from the associated PETr data;
- The predicted peak loads for all AH regimes were within the range of all associated peak loads obtained experimentally, and;
- The model could be improved by quantifying the behaviour of the cementitious material (shrinkage and creep) and relaxation of the polymer tendon. This has been addressed by Dunn (2010).

## 7.2 Recommendations for further work

It is not difficult to imagine the application of self-healing materials commercially, but the current research is still largely in its infancy. Interestingly, Ghosh (2009) describes that in order for self-healing materials to be accepted commercially, several milestones will need to be overcome. These milestones include the initial idea (preliminary level), laboratory implementation (product level), scaling (process level) and finally, the application for use in industry (marketing).

The research undertaken on the self-healing of cementitious materials reported in this thesis is at the preliminary and product level. Nevertheless this work gives confidence that a self-healing concrete has great potential for use in all aspects of everyday construction.

The problems associated with concrete durability have been presented in Chapter 1 and the concept of self-healing to enhance this durability has been the key focus of this thesis. This section presents recommendations for the further work that needs to be undertaken for both the autonomic and autogenous healing concepts presented in this thesis to move them first to a process and subsequently, a marketing level.

### **7.2.1 Autonomic healing**

The autonomic healing system investigated in this thesis has shown that the release of an encapsulated healing agent can provide a self-healing ability. It is clear however, that there are several practicality issues that confine the autonomic healing system to laboratory based study. One of the main challenges that remain is the development of full scale systems that could be used commercially. The next steps required in order to meet this challenge therefore relies heavily on developing appropriate delivery networks. These will need to be flexible enough to withstand casting whilst still retaining the autonomic detection of cracks and the ability to release a healing agent into cracks.

In the current autonomic healing system presented in Chapter 3, when a glass tube cracks there is the potential for a healing agent to dry and plug the area of fracture. Therefore, the specimen is limited to a single fracture before the self-healing function is removed. It is proposed that this could be overcome by providing a multi-network system and a continuous supply that will allow for the multiple healing of cracks. A dual-layer supply tube could be used in which a flexible, perforated (porous) rubber tube is used inside the brittle glass tube as illustrated in Figure 7.1. The flexible rubber tube could be supplied with a continuous flow of adhesive and it would only be the glass tube that could become blocked at the point of fracture.

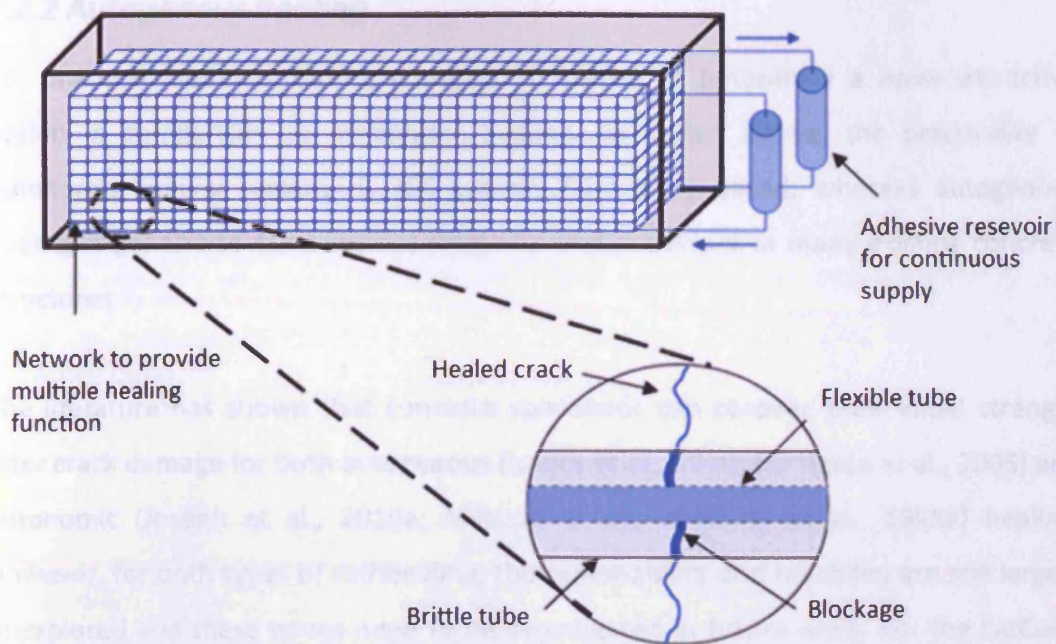


Figure 7.1 Autonomic healing system with continuous supply network and a dual-layer supply tube set up that prevents blockages

As part of the future recommendations for an experimental programme to further investigate the practicality of autonomic healing, the effect of loading rate needs to be addressed in order to understand more fully the primary healing that is present during first stage load cycles. This aspect of the research also needs to investigate the levels of reinforcement and their influence on the primary healing. The proposed experimental programme will conduct a series of experiments to examine the effects of loading rate on the primary healing for:

- Notched specimens with moderate levels of reinforcement (0.32 %);
- Notched specimens with high levels of reinforcement (0.72 %), and;
- The effective stiffness gain during primary healing after the fracture of the glass tubes.

In addition, methods of establishing glue uptake for various crack widths and the mechanics of the migration of the glue into the crack zone have largely been qualitative to date and it is recommended that an exploration by environmental scanning electron microscope (ESEM) may provide more information.

### **7.2.2 Autogenous healing**

For practical implementation, autogenous healing is potentially a more attractive option in comparison to autonomic healing. As stated above, the practicality of autonomic healing systems is still entirely laboratory based, whereas autogenous healing is generic to cementitious materials and is evident in many existing concrete structures.

The literature has shown that concrete specimens can recover their initial strength after crack damage for both autogenous (Isaacs et al., 2010; ter Heide et al., 2005) and autonomic (Joseph et al., 2010a; Mihashi et al., 2000; Li et al., 1998a) healing. However, for both types of self-healing, the repeatability and reliability are still largely unexplored and these issues need to be investigated in future work. For the LatConX healing system discussed in this thesis, it is suggested that the next programme of work should investigate the repeatability of the current technique. The proposed recommendations will conduct a series of experiments to examine the heat activation methods and the healing regimes for:

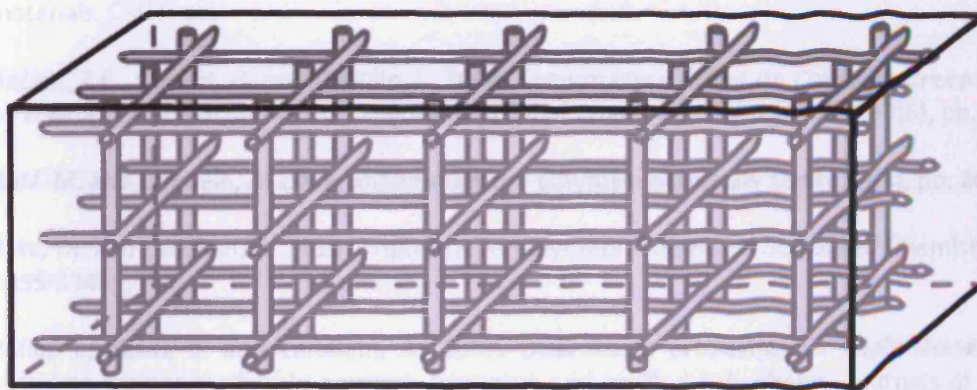
- Notched specimens subject to water activation and healing, and;
- Notched specimens subject to steam activation and healing.

In addition, further recommendations include:

- The development of larger scale specimens that will require the use of shrinkable polymers that develop higher shrinkage stresses;
- A study of how autogenous healing can be optimised by mix design, and;
- The use of cement replacement materials in the mix design, which has been largely unexplored for studies on autogenous healing.

Furthermore, crack width dependency is an important factor for autogenous healing. As discussed in Chapter 2, several studies report conflicting maximum allowable crack widths. In the field it is difficult to foresee the development of consistent crack widths and it is envisaged that further studies are needed to investigate the significance of cracks of various width.

Finally, it must be emphasised that in order for the LatConX system to be used in practical applications the system has to be activated when and where it is required, has longevity, be capable of repairing multiple cracks and ensure full recovery of the original material strength. As illustrated in Figure 7.2, it is envisaged that an encased polymer network grid could provide full triaxial confinement. This would have the benefit of not only enhancing the durability of the composite but also its strength and ductility thereby creating a truly robust cementitious composite.



- Polymer tendons placed as a 3D grid
- Potential to activate tendons at selective points
- Enhancement of autogenous healing by mix design
- Potential to minimise levels of steel reinforcement

Alternative tendon activation methods include electricity, UV light and magnetism



Figure 7.2 Triaxial confinement for the shrinkable polymer cementitious material system

## References

- Acker, P. and Ulm, F.-J. 2001. Creep and shrinkage of concrete: physical origins and practical measurements. *Nuclear Engineering and Design* 203, pp. 143-158.
- Ahn, T.H. and Kishi, T. 2009. Crack Healing Behaviour of Cementitious Composite Materials incorporating Geo-Materials. *Proceedings of the Second International Conference on Self-Healing Materials*, Chicago, IL USA.
- Bažant, Z.P. 2001. Prediction of concrete creep and shrinkage: past, present and future. *Nuclear Engineering and Design* 203, pp. 27-38.
- Bažant, Z.P. and Planas. J. 1998. *Fracture and Size effect in concrete and other quasibrittle materials*. CRC Press.
- Bažant, Z.P., Cusatis, G. and Cedolin, L. 2004. Temperature Effect on Concrete Creep Modelled by Microprestressing-Solidification Theory. *Journal of Engineering Mechanics* 130(6), pp. 691-699.
- Behl, M. and Lendlein, A. 2007. Shape-memory polymer. *Materials Today* 10(4), pp. 20-28.
- Behl, M. and Lendlein, A. 2010. Triple-shape polymers. *The Royal Society of Chemistry* 20, pp. 3335-3345.
- Bellin, I., Kelch, S. and Lendlein, A. 2007. Dual-shape properties of triple-shape polymer networks with crystallisable network segments and grafted side chains. *Journals of Materials Chemistry* 17(28), pp. 2885-2891.
- Bellin, I., Kelch, S., Langer, R. and Lendlein, A. 2006. Polymeric triple-shape materials. *Proceedings of the National Academy of Science of the United States of America* 103(48), pp. 18043-18047.
- Bhushan, B. 2009. Biomimetics: lessons from nature - an overview. *Philosophical Transactions of The Royal Society A*, 367 (1893), pp. 1445-1486.
- Biercuk, M.J., Llaguno, M.C., Radosavljevic, M., Hyun, J.K. and Johnson, A.T. 2002. Carbon nanotube composites for thermal management. *Applied Physics Letters* 80(15), pp. 2767-2769.
- Bisschop, J. 2002. *Drying shrinkage microcracking in cement-based materials*. DUP Science.
- Blaiszik, B.J., Sottos, N.R. and White, S.R. 2008. Nanocapsules for self-healing materials. *Composites Science and Technology* 68(3-4), pp. 978-986.
- Bornert, M., Brémand, F., Doumalin, P., Dupré, J.C., Fazzini, M., Grédiac, M., Hild, F., Mistou, S., Molimard, J., Orteu, J.J., Robert, L., Surrel, Y., Vacher, P. and Wattrisse, B. 2009. Assessment of Digital Image Correlation Measurement Errors: Methodology and Results. *Exp Mech* 49, pp.353-370.
- BS EN12390-3:2009. Testing hardened concrete. Compressive strength of test specimens.
- BS EN12390-6:2009. Testing hardened concrete. Tensile splitting strength of test specimens.



## References

---

BS4449:2005 + A2:2009. Steel for the reinforcement of concrete. Weldable reinforcing steel. Bar, coil and decoiled product. Specification.

BS EN1992. 2004. Eurocode 2: Design of concrete structures - Part 1-1: General rules and rules for buildings.

Buehler, W.H., Gilfrich, J.V. and Wiley, R.C. 1963. Effect of low temperature phase changes on the mechanical properties of alloys near composition TiNi. *Journal of Applied Physics* 34, pp. 1475-1477.

Chang, L.C. and Read, T.A. 1951. Plastic deformation and diffusionless phase changes in metals - the Gold-Cadmium beta phase. *The American Institute of Mining, Metallurgical, and Petroleum Engineers* 191, pp. 47-52.

Chong, K.P. and Garboczi, E.J. 2002. Smart and designer structural material systems. *Progress in Structural Engineering and Materials* 4(4), pp. 417-430.

Clear, C.A. 1985. Effects of autogenous healing upon the leakage of water through cracks in concrete. Technical Report - Cement and Concrete Association 31p.

Czaderski, C., Hahnebach, B. and Motavalli, M. 2006. RC beam with variable stiffness and strength. *Construction and Building Materials* 20(9), pp. 824-833.

Dry, C. and Corsaw, M. 2003. A comparison of bending strength between adhesive and steel reinforced concrete with steel only reinforced concrete. *Cement and Concrete Research* 33(11), pp. 1723-1727.

Dry, C. and Unzicker, J. 1998. Preserving performance of concrete members under seismic loading conditions. In proceedings of Smart Structures and Materials 1998: Smart Systems for Bridges, Structures, and Highways. The International Society for Optical Engineering, San Diego, CA, United States, Mar 1998, 3325, pp. 74-80.

Dry, C.M. 1994. Matrix cracking repair and filling using active and passive modes for smart timed release of chemicals from fibres into cement matrices. *Smart Materials and Structures* 3(2), pp. 118-123.

Dry, C.M. 1996. Procedures developed for self-repair of polymeric matrix composite materials. *Composite Structures* 35, pp. 263-269.

Dry, C.M. 2000. Three designs for the internal release of sealants, adhesives, and waterproofing chemicals into concrete to reduce permeability. *Cement and Concrete Research* 30(12), pp. 1969-1977.

Dunn, S.C. 2010. A Novel Self-Healing Shape Memory Polymer-Cementitious System. PhD Thesis, Cardiff University.

Dunn, S.C., Jefferson, A.D., Lark, R.J., Isaacs, B. and Joseph, C. 2009. A Numerical Model for the Shrinkage of Polymer Elements in Active Self-Healing. Proceedings of the Second International Conference on Self-Healing Materials, Chicago, IL USA. ICSHM2009.

## References

---

Dunn, S.C., Jefferson, A.D., Lark, R.J. & Isaacs, B. 2010. Investigation into the shrinkage behaviour of Polyethylene Terephthalate (PET) for a new cementitious-shrinkable polymer material system. *Journal of Applied Polymer Science*, 120(5), pp.2516-2526.

Edvardsen, C. 1999. Water Permeability and Autogenous Healing of Cracks in Concrete. *American Concrete Institute: Materials Journal* 96(4), pp.448-454.

El-Tawil, S. & Ortega-Rosales, J. 2004. Prestressing Concrete Using Shape Memory Alloy Tendons. *ACI Structural Journal* 101 (6), pp. 846-851.

Evans, J. 2006. Magnetic appeal of shape-change polymer. *Chemistry World* [Online]. Available at: <http://www.rsc.org/chemistryworld/News/2006/February/28020601.asp> [Accessed: 12 December 2007].

Gall, K., Dunn, M.L., Liu, Y., Finch, D., Lake, M. and Munshi, N.A. 2002. Shape memory polymer nanocomposites. *Acta Materialia* 50, pp. 5115-5126.

Gall, K., Kreiner, P., Turner, D. and Hulse, M. 2004. Shape-Memory Polymers for Microelectromechanical Systems. *Journal of Microelectromechanical Systems*, 13(3) pp. 472-483.

Ghosh, S.K. 2009. *Self-healing Materials: Fundamentals, Design Strategies, and Applications*. Wiley-VCH.

Granger, S., Loukili, A., Pijaudier-Cabot, G. and Chanvillard, G. 2007. Experimental characterization of the self-healing of cracks in an ultra high performance cementitious material: Mechanical tests and acoustic emission analysis. *Cement and Concrete Research* 37, pp. 519-527.

Guo, L-P., Sun, W., He, X-Y. and Xu, Z-B. 2008. Application of DSCM in prediction of potential fatigue crack path on concrete surface. *Engineering Fracture Mechanics* 75, pp. 643-651.

Gupta, V.B., Radhakrishnana, J. and Sett, S.K. 1994. Effect of processing history on shrinkage stress in axially oriented poly(ethylene terephthalate) fibres and films. *Polymer*, 35(12), pp. 2560-2567.

Hayashi, S., Tasaka, Y., Hayashi, N. and Akita, Y. 2004. Development of Smart Polymer Materials and its Various Applications. Mitsubishi Heavy Industries, Ltd. Technical Review [Online] 41(1). Available at: <https://www.mhi.co.jp/technology/review/pdf/e411/e411062.pdf> [Accessed: 28 September 2007].

Hearn, N. 1998. Self-sealing, autogenous healing and continued hydration: What is the difference? *Materials and Structures* 31, pp. 563-567.

Helmer, M. 2001. Plastic, heal thyself: Fatigued materials have a new self-help cure. *Nature science update*. 15 February 2001.

Henkel Sichel-Werke. 1997. Technical data sheet for SICOMET 9000. Henkel Sichel-Werke Ltd. [www.henkel.com](http://www.henkel.com) [Accessed: 8 August 2010].

## References

---

- Homma, D., Mihashi, H. and Nishiwaki, T. 2009. Self-Healing Capability of Fibre Reinforced Cementitious Composites. *Journal of Advanced Concrete Technology* 7(2), pp. 217-228.
- Huang, W.M., Lee, C.W. and Teo, H.P. 2006. Thermomechanical behaviour of a polyurethane shape memory polymer foam. *Journal of Intelligent Material Systems and Structures* 17(8-9), pp. 753-760.
- Isaacs, B., Joseph, C., Jefferson, A.D., Lark, R.J. and Dunn, S.C. 2009. Enhancement of Self-Healing in Cementitious Materials, Post-Tensioned with Shrinkable Polymers. *Proceedings of the Second International Conference on Self-Healing Materials, Chicago, IL USA. ICSHM2009.*
- Isaacs, B., Lark, R.J., Jefferson, A.D., Dunn, S.C. & Joseph, C. 2010. Crack healing using a shrinkable polymer cementitious material system. *Cement and Concrete Composites*. Submitted September 2010.
- Jacobsen, S. and Sellevold, E.J. 1996. Self-healing of high strength concrete after deterioration by freeze/thaw. *Cement and Concrete Research* 26(1), pp. 55-62.
- Jacobsen, S., Marchand, J. and Boisvert, L. 1996. Effect of cracking and healing on chloride transport in OPC concrete. *Cement and Concrete Research* 26(6), pp. 869-881.
- Janke, L., Czaderski, C., Motavalli, M. and Ruth, J. 2005. Applications of shape memory alloys in civil engineering structures - Overview, limits and new ideas. *Materials and Structures* 38, pp. 578-592.
- Jefferson, A.D., Joseph, C., Lark, R.J., Dunn, S.C., Isaacs, B. and Weager, B. 2010. A new system for crack closure of cementitious materials using shrinkable polymers. *Cement and Concrete Research*, 40(5), pp.795-801.
- Jeong, H.M., Ahn, B.K. and Kim, B.K. 2000. Temperature sensitive water vapour permeability and shape memory effect of polyurethane with crystalline reversible phase and hydrophilic segments. *Polymer International* 49(12), pp. 1714-1721.
- Jonkers, H.M. and Schlangen, E. 2009. Towards a sustainable bacterially-mediated self-healing concrete. *Proceedings of the Second International Conference on Self-Healing Materials, Chicago, IL USA.*
- Jonkers, H.M., Thijssen, A., Muyzer, G., Copuroglu, O., and Schlangen, E. 2010. Application of bacteria as self-healing agent for the development of sustainable concrete. *Ecological Engineering* 36, pp. 230-235.
- Joseph, C. 2009. Experimental and numerical study of the fracture and self-healing of cementitious materials. PhD Thesis, Cardiff University.
- Joseph, C., Gardner, D., Jefferson, A.D., Isaacs, B. & Lark, R.J. 2010b. Self-Healing Cementitious Materials: A review of recent work. *Proceedings of the ICE: Construction Materials*, 164(CM1), pp.29-41.
- Joseph, C., Jefferson, A.D. and Cantoni, M. 2007. Issues relating to the autonomic healing of cementitious materials. 1st international conference on self-healing materials. Noordwijk, Holland, April 2007.

## References

---

- Joseph, C., Jefferson, A.D., Isaacs, B., Lark, R.J. and Gardner, D. 2009. Adhesive Based Self-Healing of Cementitious Materials. Proceedings of the Second International Conference on Self-Healing Materials, Chicago, IL USA. ICSHM2009.
- Joseph, C., Jefferson, A.D., Isaacs, B., Lark, R.J. & Gardner, D. 2010a. Experimental investigation of adhesive-based self-healing of cementitious materials. Magazine of Concrete Research, 62(11), pp.831-843.
- Kessler, M.R., Sottos, N.R. and White, S.R. 2003. Self-healing structural composite materials. Composites Part A: Applied Science and Manufacturing 34(8), pp. 743-753.
- Kishi, T., Ahn, T-H., Hosoda, A., Suzuki, S. and Takaoka, H. 2007. Self-healing behaviour by cementitious recrystallisation of cracked concrete incorporating expansive agent. Proceedings of the First International Conference on Self-Healing Materials, Noordwijk aan Zee, The Netherlands.
- Kuosa, H. 2000. Smart concretes and concrete structures. Technical Research Centre of Finland. Research Notes (Finland) 2048, pp. 44.
- Lark, R.J., Jefferson, A.D., Joseph, C., Dunn, S.C. & Isaacs, B. 2009. Active Confinement of Cementitious Composites with Shape Memory Plastics. Proceedings of the Second International Conference on Self-Healing Materials, Chicago, IL USA. ICSHM2009.
- Lees, J. 2001. Fibre-reinforced polymers in reinforced and prestressed concrete applications: moving forward. In: Erki, M-A, et al. eds. Progress in Structural Engineering and Materials 3(2). John Wiley & Sons, Ltd, pp. 122-131.
- Lendlein, A. 2002. Shape Memory Polymers - Biodegradable Sutures. Materials World 10(7), pp. 29-30.
- Lendlein, A. and Kelch, S. 2002. Shape-Memory Polymers. Angewandte Chemie International Edition 41, pp. 2034-2057.
- Lendlein, A. and Langer, R. 2002. Biodegradable, Elastic Shape-Memory Polymers for Potential Biomedical Applications. Science 296, pp. 1673-1676.
- Lendlein, A., Jiang, H., Junger, O. and Langer, R. 2005. Light-induced shape-memory polymers. Nature 434, pp. 879-882.
- Li, F., Chen, Y., Zhang, X. and Xu, M. 1998b. Shape memory effect of polyethylene/nylon 6 graft copolymers. Polymer 39(26), pp. 6929-6934.
- Li, F., Zhu, W., Zhang, X., Zhao, C. and Xu, M. 1999. Shape Memory Effect of Ethylene-Vinyl Acetate Copolymers. Journal of Applied Polymer Science 71(7), pp. 1063-1070.
- Li, V.C. and Kanda, T. 1998. Engineered Cementitious Composites for Structural Applications. Journal of Materials in Civil Engineering 10(2), pp. 66-69.
- Li, V.C., Lim, Y.M. and Chan, Y-W. 1998a. Feasibility study of a passive smart self-healing cementitious composite. Composites Part B 29B, pp. 819-827.

## References

---

- Limess. 2009. Available at: <http://www.limess.com/>. [Accessed March 2009].
- Liu, C., Qin, H. and Mather, P.T. 2007. Review of progress in shape-memory polymers. *The Royal Society of Chemistry* 17, pp. 1543-1558.
- Liu, Y., Gall, K., Dunn, M.L. and McCluskey, P. 2004. Thermomechanics of shape memory polymer nanocomposites. *Mechanics of Materials* 36(10), pp. 929-940.
- Liu, Y., Gall, K., Dunn, M.L., Greenberg, A.R. and Diani, J. 2006. Thermomechanics of shape memory polymers: Uniaxial experiments and constitutive modeling. *International Journal of Plasticity* 22, pp. 279-313.
- Long, S.D. and Ward, I.M. 1991. Shrinkage force studies of orientated polyethylene terephthalate. *Journal of applied polymer science*, 42(7), pp. 1921-1929.
- Lothenbach B, Winnefeld F, Alder C, Wieland E, Lunk P. 2007. Effect of temperature on the pore solution, microstructure and hydration products of Portland cement pastes. *Cement and Concrete Research* 37, pp. 483-491.
- Lura P, van Breugel K, Maruyama I. 2001. Effect of curing temperature and type of cement on early-age shrinkage of high-performance concrete. *Cement and Concrete Research* 31, pp.1867-1872.
- Maitland, D.J., Metzger, M.F., Schumann, D., Lee, A. and Wilson, T.S. 2002. Photothermal Properties of Shape Memory Polymer Micro-Actuators for Treating Stroke. *Lasers in Surgery and Medicine* 30, pp. 1-11.
- Meyer, C. 2009. The greening of the concrete industry. *Cement and Concrete Composites* 31, pp. 601-605.
- Mihashi, H., Kaneko, Y., Nishiwaki, T. and Otsuka, K. 2000. Fundamental study on development of intelligent concrete characterised by self-healing capability for strength. *Transactions of the Japan Concrete Institute* 22, pp. 441-450.
- Mohr, R., Kratz, K., Weigel, T., Lucka-Gabor, M., Moneke, M. and Lendlein, A. 2006. Initiation of shape-memory effect by inductive heating of magnetic nanoparticles in thermoplastic polymers. *Proceedings of the National Academy of Sciences of the United States of America* 103(10), pp. 3540-3545.
- Mookhoek, S.D., Fischer, H.R. and van der Zwaag, S. 2009. Enhancing Liquid Based Self-Healing Materials by Applying Compartmented Polymer Fibres. *Proceedings of the Second International Conference on Self-Healing Materials*, Chicago, IL USA.
- Neville, A.M. 1999. *Properties of Concrete*. Fourth and Final Edition. John Wiley & Sons, Inc.
- Ni, Q-Q., Zhang, C-S., Fu, Y., Dai, G. and Kimura, T. 2007. Shape memory effect and mechanical properties of carbon nanotube/shape memory polymer nanocomposites. *Composite Structures* 81, pp. 176-184.

## References

---

Nishiwaki, T., Mihashi, H., Gunji, Y. and Okuhara, Y. 2007. Development of smart concrete with self-healing system using selective heating device. Proceedings of the First International Conference on Concrete Under Severe Conditions: Environment and Loading.

Nishiwaki, T., Mihashi, H., Okuhara, Y. and Terashima, H. 2009. Development of self-repairing concrete system using selective heating devices. Proceedings of the Second International Conference on Self-Healing Materials, Chicago, IL USA.

Ohki, T., Ni, Q-Q., Ohsako, N. and Iwamoto, M. 2004. Mechanical and shape memory behaviour of composites with shape memory polymer. Composites Part A: applied science and manufacturing 35, pp. 1065-1073.

ONS. 2008. Construction statistics: Sources and outputs. Office for National Statistics.

Otsuka, K. and Ren, X. 1999. Recent developments in the research of shape memory alloys. Intermetallics 7. pp. 511-528.

Pakula, T. and Trznadel, M., 1985. Thermally stimulated shrinkage forces in oriented polymers. I: Temperature dependence. *Polymer*, 26(7), pp.1011-18.

Patent application PCT/GB2008/002651 "Prestressing or confinement of materials using polymers". Filed 1st August 2008, Priority date 3rd August 2007.

Polymer Age. 2006. SMP Orthodontics Technology Update. Polymer Age. Available at: [http://www.polymer-age.co.uk/back\\_issues/June06/Tech%20Update.pdf](http://www.polymer-age.co.uk/back_issues/June06/Tech%20Update.pdf) [Accessed: 12 December 2007].

Qian, S., Zhou, J., De Rooij, M.R., Schlangen, E., Ye, G. and van Breugel, K. 2009a. Self-healing behaviour of strain hardening cementitious composites incorporating local waste materials. Cement and Concrete Composites 31, pp. 613-621.

Qian, S., Zhou, J., Liu, H., De Rooij, M.R., Schlangen, E., Gard, W., and van de Kuillen, J.W. 2009b. Self-Healing Cementitious Composites under Bending Loads. Proceedings of the Second International Conference on Self-Healing Materials, Chicago, IL USA.

Ratna, D. and Karger-Kocsis, J. 2008. Recent advances in shape memory polymers and composites: a review. Journal of Materials Science 43, pp. 254-269.

Reinhardt, H-W. and Jooss, M. 2003. Permeability and self-healing of cracked concrete as a function of temperature and crack width. Cement and Concrete Research 33, pp. 981-985.

Richardson, M.G. 2002. Fundamentals of Durable Reinforced Concrete. Taylor and Francis.

RILEM Committee FMC-50. 1985. Determination of the fracture energy of mortar and concrete by means of three-point bending tests on notched beams. Material and Structures, 18(106), pp. 285-290.

RILEM STAR report. 2011. Self-healing phenomena in cement based materials (to be published 2011).

## References

---

- Rosen, S.L. 1993. *Fundamental Principles of Polymeric Materials*. Second Edition. John Wiley and Sons Inc.
- Rousseau, I.A. 2008. Challenges of Shape Memory Polymers: A review of the Progress Toward Overcoming SMP's Limitations. *Polymer Engineering and Science* 48(11), pp. 2075-2089.
- Schlangen, E. and Joseph, C. 2009. Self-healing Processes in Concrete. In: Ghosh, S.K. *Self-healing Materials: Fundamentals, Design Strategies, and Applications*. Wiley-VCH, pp. 141-182.
- Scmets, A.J.M. 2003. Self-healing: an emerging property for new materials. *Leonardo Times*. Available at: <http://www.tudelft.nl/live/binaries/1cb5c99a-1a97-4ef6-b6e7-563a391bd413/doc/Self%20Healing%20Materials%20article.pdf> [Accessed: 20 July 2010].
- Sharp, S.R. and Clemena, G.G. 2004. State-of-the-art survey of advanced materials and their potential application in highway infrastructure. Charlottesville: Virginia Transportation Research Council, pp. 1-41.
- Small IV, W., Singhal, P., Wilson, S.T. and Maitland, D.J. 2010. Biomedical applications of thermally activated shape memory polymers. *Journal of Materials Chemistry* 20(17), pp. 3356-3366.
- Song, G., Ma, N. and Li, H-N. 2006. Applications of shape memory alloys in civil structures. *Engineering Structures* 28, pp. 1266-1274.
- Sottos, N.R. 2009. Recent Advances in Microcapsule and Microvascular Based Self-Healing Polymers. *Proceedings of the Second International Conference on Self-Healing Materials*, Chicago, IL USA.
- Stinson, S. 2001. Plastic mends its own cracks: Microcapsules in composite release healing agent when stressed. *Chemical & Engineering News*, 79(8), p. 13.
- Sutton, M.A., Orteu, J-J. and Schreier, H.W. 2009. *Image correlation for shape, motion and deformation measurements: basic concepts, theory and applications*. Springer.
- Takagi, T. 1996. Recent Research on Intelligent Materials. *Journal of intelligent Material Systems and Structures* 7(3), pp. 346-352.
- Tecroc (2004). Technical data sheet for epoxy injection grouts TG6, TG7, and TG10. Tecroc Products Ltd. Available at: [http://www.tecroc.com/Technical\\_Data\\_Sheets/15\\_EPOXY\\_INJECTION\\_GROUT.pdf](http://www.tecroc.com/Technical_Data_Sheets/15_EPOXY_INJECTION_GROUT.pdf) [Accessed: 8 August 2008].
- ter Heide, N. and Schlangen, E. 2007. Self-healing of early age cracks in concrete. *Proceedings of the First International Conference on Self-Healing Materials*, Noordwijk aan Zee, The Netherlands.
- ter Heide, N. Schlangen, E. and van Breugel, K. 2005. Experimental Study of Crack Healing of Early Age Cracks. In *proceedings Knud Hojgaard conference on Advanced Cement-Based Materials*, Technical University of Denmark.

## References

---

- Tobushi, H., Hara, H., Yamada, E. and Hayashi, S. 1996. Thermomechanical properties in a thin film of shape memory polymer of polyurethane series. *Smart Materials and Structures* 5(4), pp. 483-491.
- Tobushi, H., Okumura, K., Hayashi, S. and Ito, N. 2001. Thermomechanical constitutive model of shape memory polymer. *Mechanics of Materials* 33, pp. 545-554.
- Toensmeier, P.A. 2005. Shape Memory Polymers Reshape Product Design. *Plastics Engineering* [Online]. Available at: [http://goliath.ecnext.com/coms2/gi\\_0199-3768005/Shape-memory-polymers-reshape-product.html](http://goliath.ecnext.com/coms2/gi_0199-3768005/Shape-memory-polymers-reshape-product.html) [Accessed: 4 November 2007].
- van der Zwaag, S. 2007. *Self-Healing Materials: An alternative Approach to 20 Centuries of Materials Science*. Springer.
- van Humbeeck, J. 2001. Shape Memory Alloys: A material and a Technology. *Advanced Engineering Materials*, 3(11) pp. 837-850.
- van Krevelan, D.W. 1997. *Properties of Polymers: Third completely revised edition*. Elsevier.
- van Oss, H.G. 2005. Background Facts and Issues Concerning Cement and Cement Data. Open-File report 2005-1152, U.S Department of the interior and U.S Geological Survey.
- van Tittelboom, K. and De Belie, N. 2009a. Autogenous healing of cracks in cementitious materials with varying mix compositions. *Proceedings of the Second International Conference on Self-Healing Materials*, Chicago, IL USA.
- van Tittelboom, K. and De Belie, N. 2009b. Self-healing concrete by the internal release of adhesive from hollow glass tubes embedded in the matrix. *Proceedings of the Second International Conference on Self-Healing Materials*, Chicago, IL USA.
- Vincent, J.F.V., Bogatyreva, O.A., Bogatyrev, N.R., Bowyer, A. & Pahl, A-K. 2006. Biomimetics: its practise and theory. *Journal of The Royal Society Interface*, 3, pp. 471-482.
- Wache, H.M., Tartakowska, D.J., Hentrich, A. and Wagner, M.H. 2003. Development of a polymer stent with shape memory effects as a drug delivery system. *Journal of Materials Science* 14, pp. 109-112.
- Wang, W., Ping, P., Chen, X. and Jing, X. 2006. Polyactide-based polyurethane and its shape-memory behaviour. *European Polymer Journal* 42, pp. 1240-1249.
- Ward, I.M. 1979. *Mechanical Properties of Solid Polymers*. Second Edition. John Wiley and Sons Inc.
- Ward, I.M. and Sweeney, J. 2004. *An Introduction to the Mechanical Properties of Solid Polymers*. John Wiley and Sons Inc.
- Wayman, C.M. 1964. *Introduction to the Crystallography of Martensitic transformations*. The Macmillan Company, New York.
- Wayman, C.M. and Duerig, T.W. 1990. An Introduction to Martensite and Shape Memory. In: *Engineering Aspects of Shape Memory Alloys*. London: Butterworth-Heinemann, pp. 3-20.



## References

---

- Wei, Z.G., Sandstrom, R. and Miyazaki, S. 1998. Shape-memory materials and hybrid composites for smart systems. *Journal of Materials Science* 33, pp. 3743-3762.
- White, S.R., Sottos, N.R., Geubelle, P.H., Moore, J.S., Kessler, M.R., Sriram, S.R., Brown, E.N. and Viswanathan, S. 2001. Autonomic healing of polymer composites. *Nature* 409, pp. 794-797.
- Yang, B., Hunag, W.M., Li, C. and Li, L. 2006. Effects of moisture on the thermomechanical properties of a polyurethane shape memory polymer. *Polymer* 47, pp. 1348-1356.
- Yang, Y., Lepech, M.D., Yang, E-H. and Li, V.C. 2009. Autogenous healing of engineered cementitious composites under wet-dry cycles. *Cement and Concrete Research* 39, pp. 382-390.
- Zhang, C-S. and Ni, Q-Q. 2007. Bending behaviour of shape memory polymer based laminates. *Composite Structures* 78(2), pp. 153-161.
- Zheng, X., Zhou, S., Li, X. and Weng, J. 2006. Shape memory properties of poly(D,L-lactide)/hydroxyapatite composites. *Biomaterials* 27, pp. 4288-4295.
- Zhong, W. and Yao, W. 2008. Influence of damage degree on self-healing of concrete. *Construction and Building Materials* 22, pp. 1137-1142.

## Appendix A

Rite-Lok cyanoacrylate adhesive EC5 data sheet. This adhesive has been used exclusively as the healing agent in the final self-healing experimental programme presented in Section 3.3.



# RITE-LOK™ Cyanoacrylate Adhesive EC5

### Product Data Sheet

Updated : February 2007  
Supersedes : New

**Product Description** RITE-LOK EC5 is a low viscosity (5 cPs) Ethyl Cyanoacrylate based adhesive. EC5 is suitable for bonding a wide range of materials where very fast cure speed is required.

**Key Features** EC5 is specially formulated for high strength, general purpose bonding of most plastics, rubbers, metals and other common substrates. Recommended for use on assemblies with very close fitting parts and smooth, even surfaces. Can be used as a post-assembly adhesive to wick into parts.

Physical Properties	Base	Ethyl
	Soluble In	Acetone, MEK
	Viscosity (cps)	Range 1-10 Typical Value 5
	Specific Gravity	1.06
	Colour	Clear

Performance Characteristics	Maximum Gap Fill (best results are obtained with very thin bond lines)	0.05mm
	Fixture Time	5-15secs
	Tensile Strength (ISO 6922)	20 N/mm <sup>2</sup>
	Full Cure	24hrs
	Speed of Cure	The speed of cure of cyanoacrylates varies according to the substrate to be bonded. Acidic surfaces such as paper and leather will have longer cure times than most plastics and rubbers.
	Moisture Resistance	Low resistance to high levels of moisture and humidity over time.
	Service Temperature Range	-50 to +80°C

## Appendix A – Rite-Lok cyanoacrylate adhesive EC5 data sheet

---

Date: February 2007  
RITE-LOK  
Cyanoacrylate Adhesive EC5

---

<b>Additional Product Information</b>	RITE-LOK Activators AC11 and AC12 may be used in conjunction with RITE-LOK cyanoacrylates where cure speed needs to be accelerated. Cure speeds of less than 2 seconds can be obtained with most RITE-LOK cyanoacrylates. The use of an activator can reduce the final bond strength by up to 30%.
<b>Application Techniques</b>	Bond speed is very fast so ensure that parts are properly aligned before bonding. RITE-LOK Activators may be required if there are gaps or porous surfaces. Some plastics may require application of RITE-LOK AC77 Primer. Ensure parts are clean, dry and free from oil and grease. Product is normally hand applied from the bottle. Apply sparingly to one surface and press parts firmly together until handling strength is achieved. As a general rule, as little cyanoacrylate as possible should be used – over application will result in slow cure speed and lower bond strength.
<b>Storage Conditions</b>	Once opened, keep the adhesive in a cool, dry place away from direct sunlight. Under such conditions shelf life at room temperature will be 12 months.  Refrigeration to 5°C gives optimum storage stability.
<b>Shelf Life</b>	12 months from date of despatch by 3M when stored in the original carton at 21°C
<b>Precautionary Information</b>	Refer to product label and material Safety Data Sheet for health and safety information before using the product. For information please contact your local 3M Office. <a href="http://www.3M.com">www.3M.com</a>
<b>For Additional Information</b>	To request additional information or to arrange for sales assistance, call 0870 6080050 Address correspondence to: 3M United Kingdom PLC, 3M House, 28 Great Jackson Street, Manchester, M15 4PA
<b>Product Use</b>	All statements, technical information and recommendations contained in this document are based upon tests or experience that 3M believes are reliable. However, many factors beyond 3M's control can affect the use and performance of a 3M product in a particular application, including the conditions under which the product is used and the time and environmental conditions in which the product is expected to perform. Since these factors are uniquely within the user's knowledge and control, it is essential that the user evaluate the 3M product to determine whether it is fit for a particular purpose and suitable the user's method or application.
<b>Note</b>	Values presented have been determined by standard test methods and are average values not to be used for specification purposes. Our recommendations on the use of our products are based on tests believed to be reliable but we would ask that you conduct your own tests to determine their suitability for your applications. This is because 3M cannot accept any responsibility or liability direct or consequential for loss or damage caused as a result of our recommendation

---

3M and RITE-LOK are trademarks of the 3M Company.

Industrial Adhesives & Tapes Division

© 3M United Kingdom PLC 2000

3M United Kingdom PLC  
3M House,  
28 Great Jackson Street,  
Manchester,  
M15 4PA

Product Information :  
Tel 0870 60 800 50  
Fax 0870 60 700 99

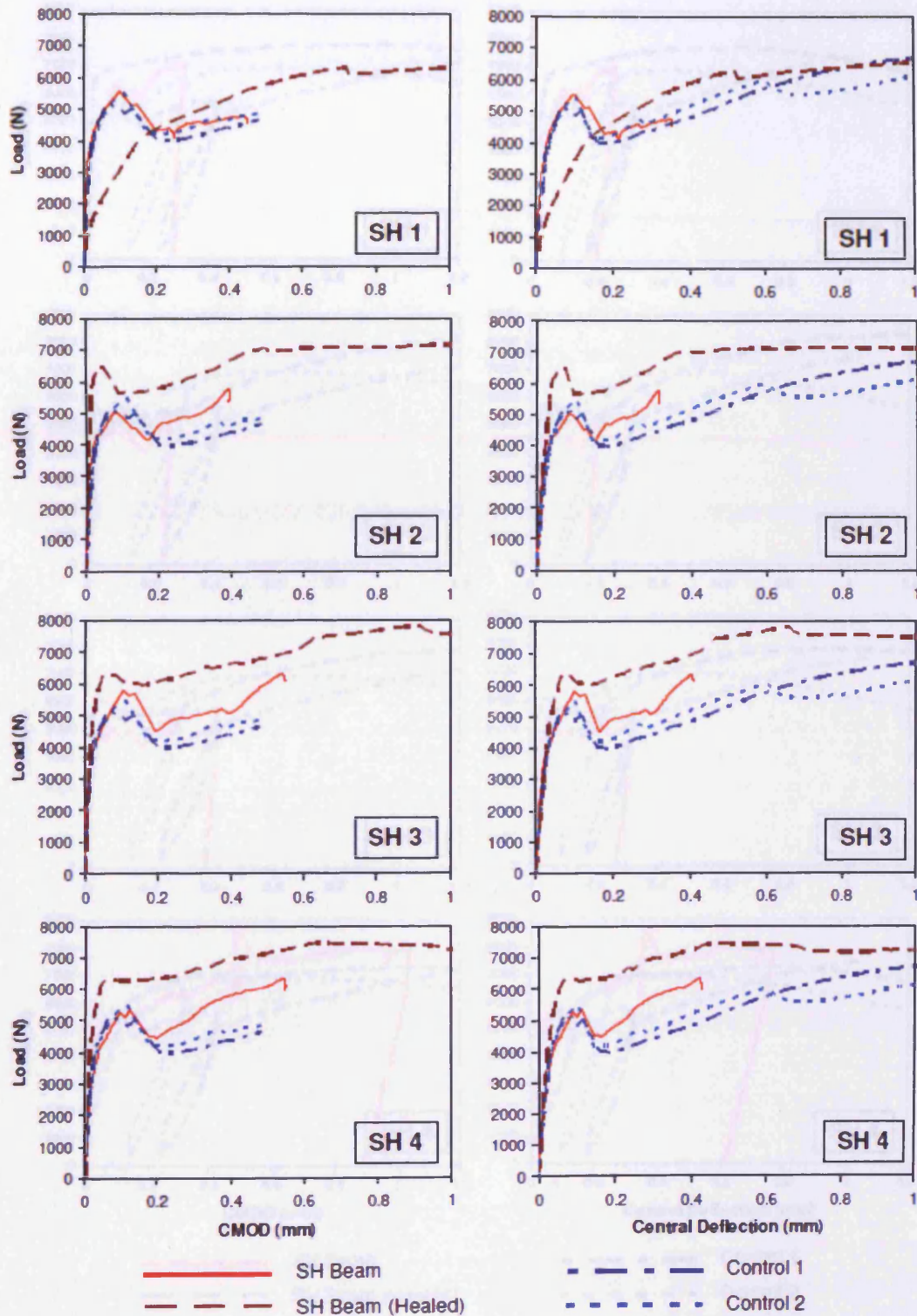
3M Ireland  
3M House, Adelphi Centre,  
Upper Georges Street,  
Dun Laoghaire, Co. Dublin, Ireland

Customer Service :  
Tel (01) 280 3555  
Fax (01) 280 3509

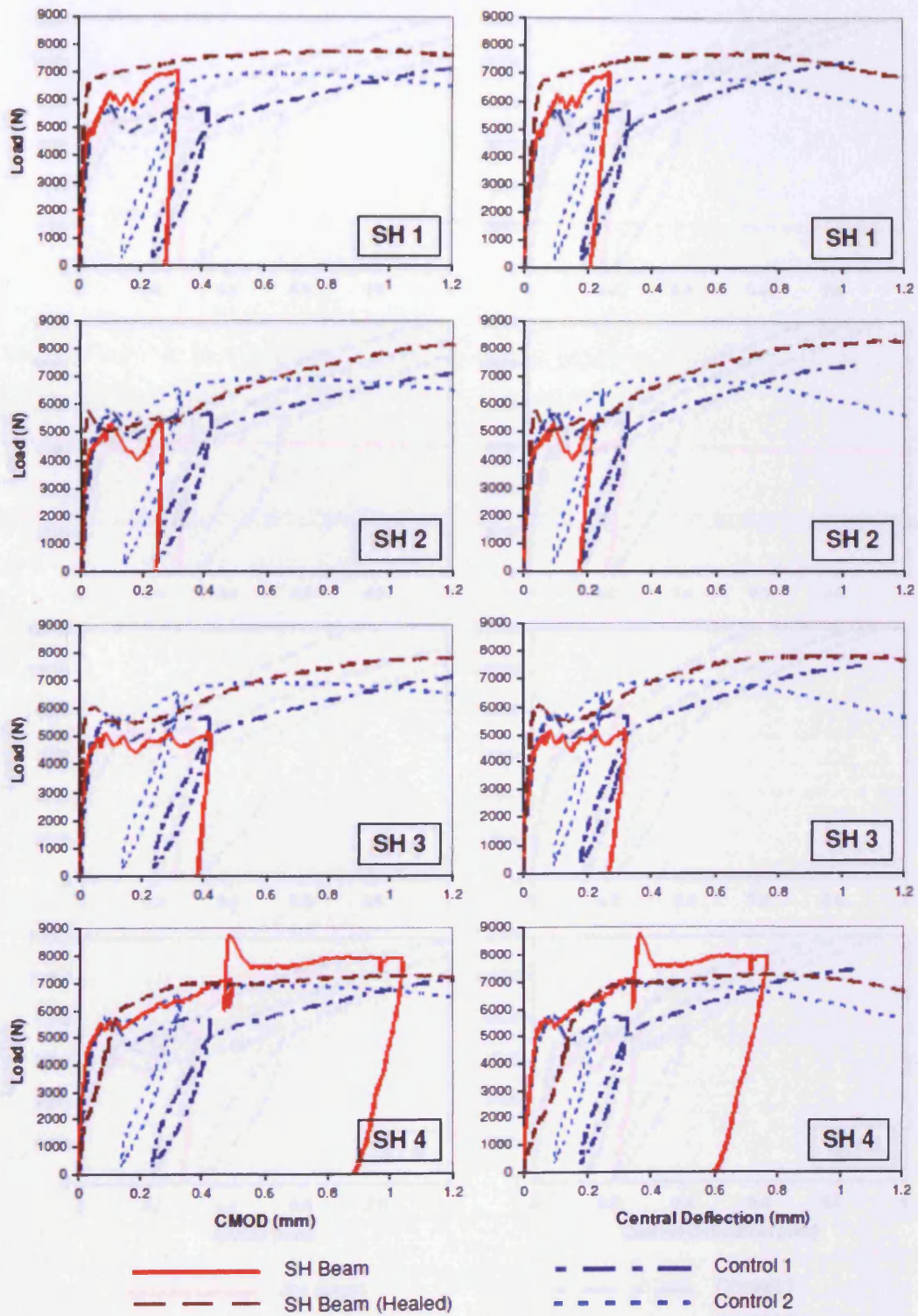
## **Appendix B**

This appendix contains all the results of the autonomic healing experimental tests for sets 1 to 6. Graphs of force-CMOD and force-central displacement results for all six sets are given. The specimen configurations for all sets have been given in Section 3.3.1, Table 3.3.

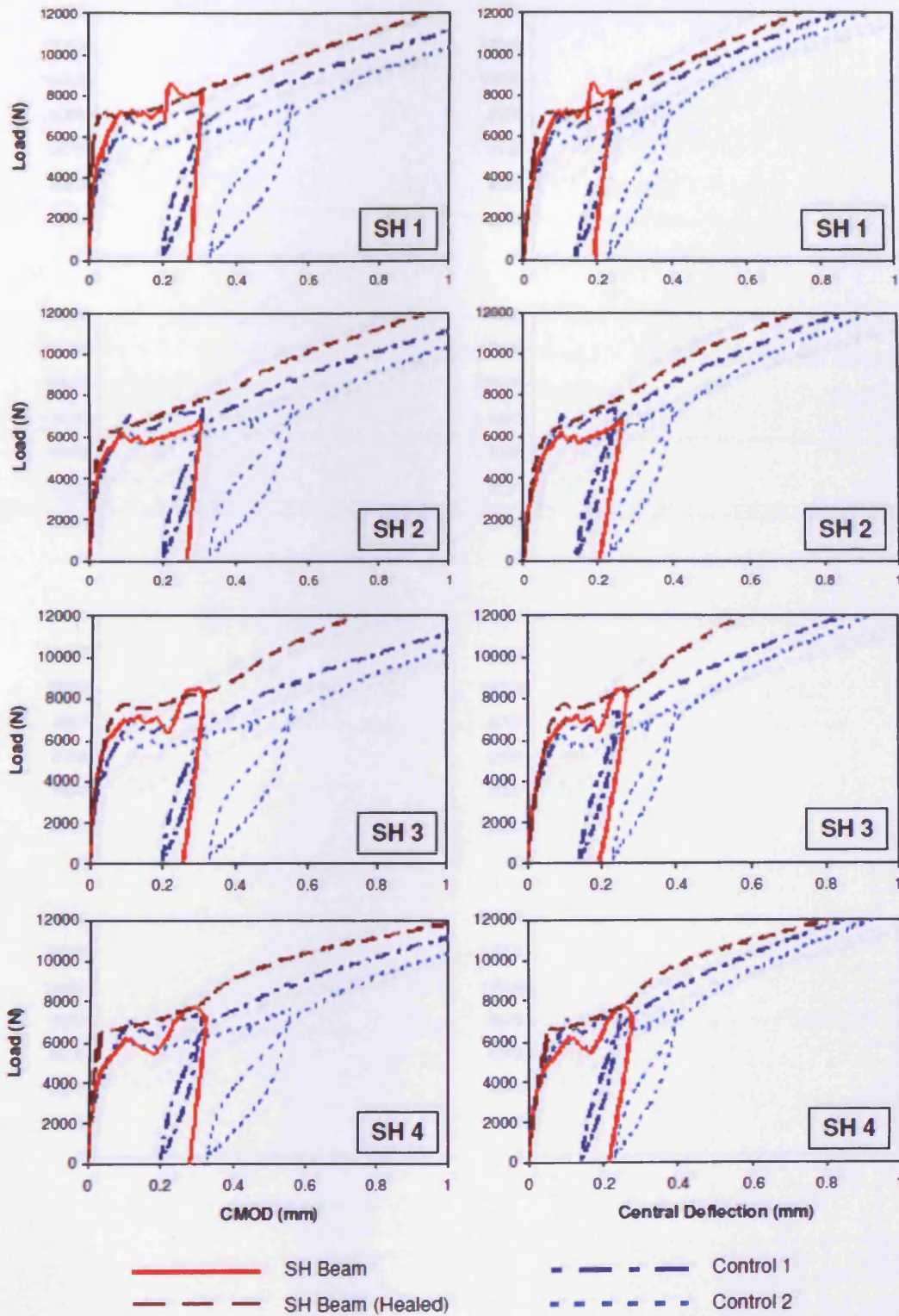
Set 1. Lightly reinforced, notched beams



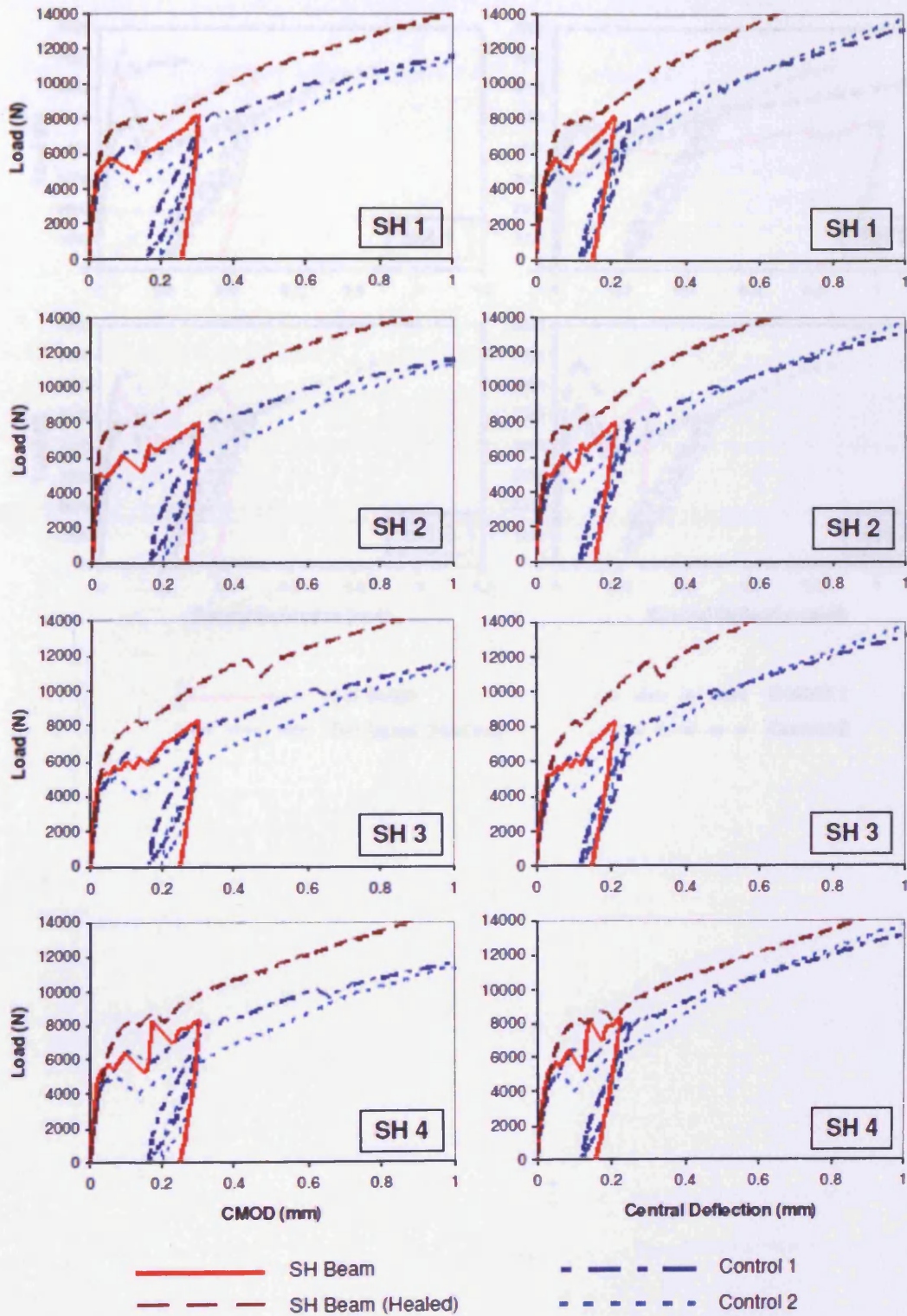
**Set 2. Lightly reinforced, notched beams**



**Set 3. Moderately reinforced, notched beams**

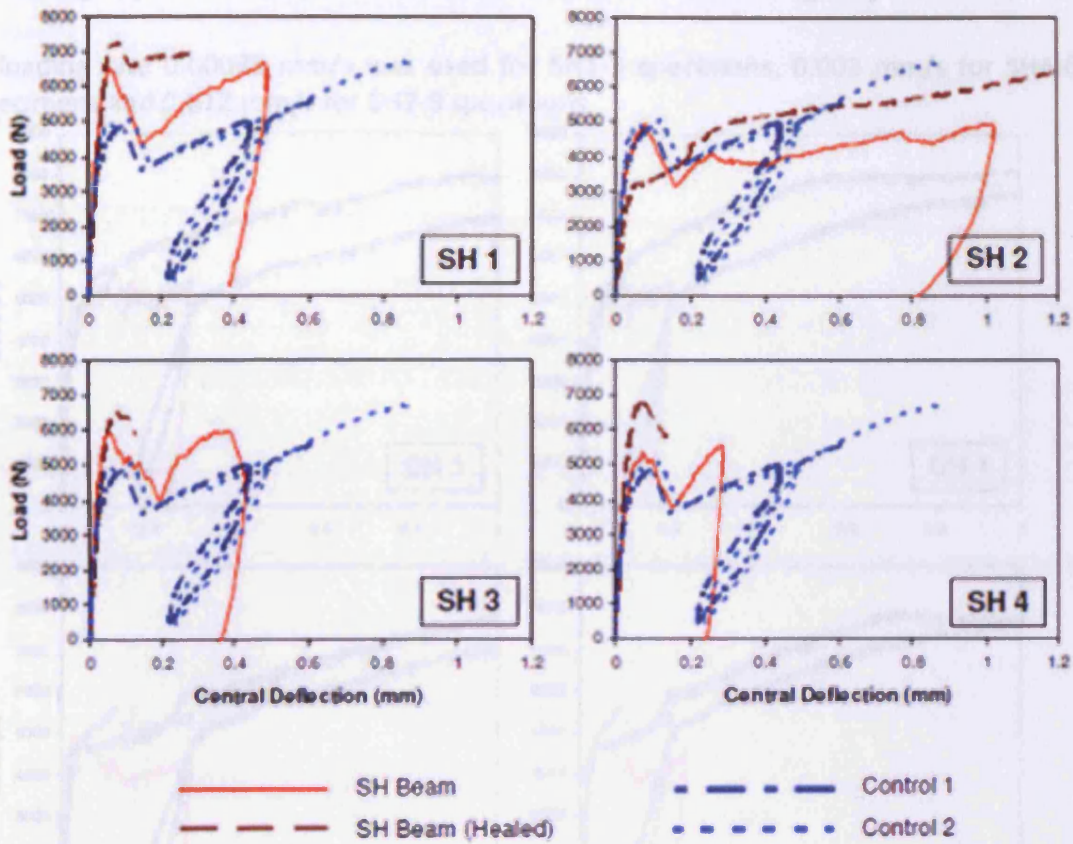


**Set 4. Heavily reinforced, notched beams**



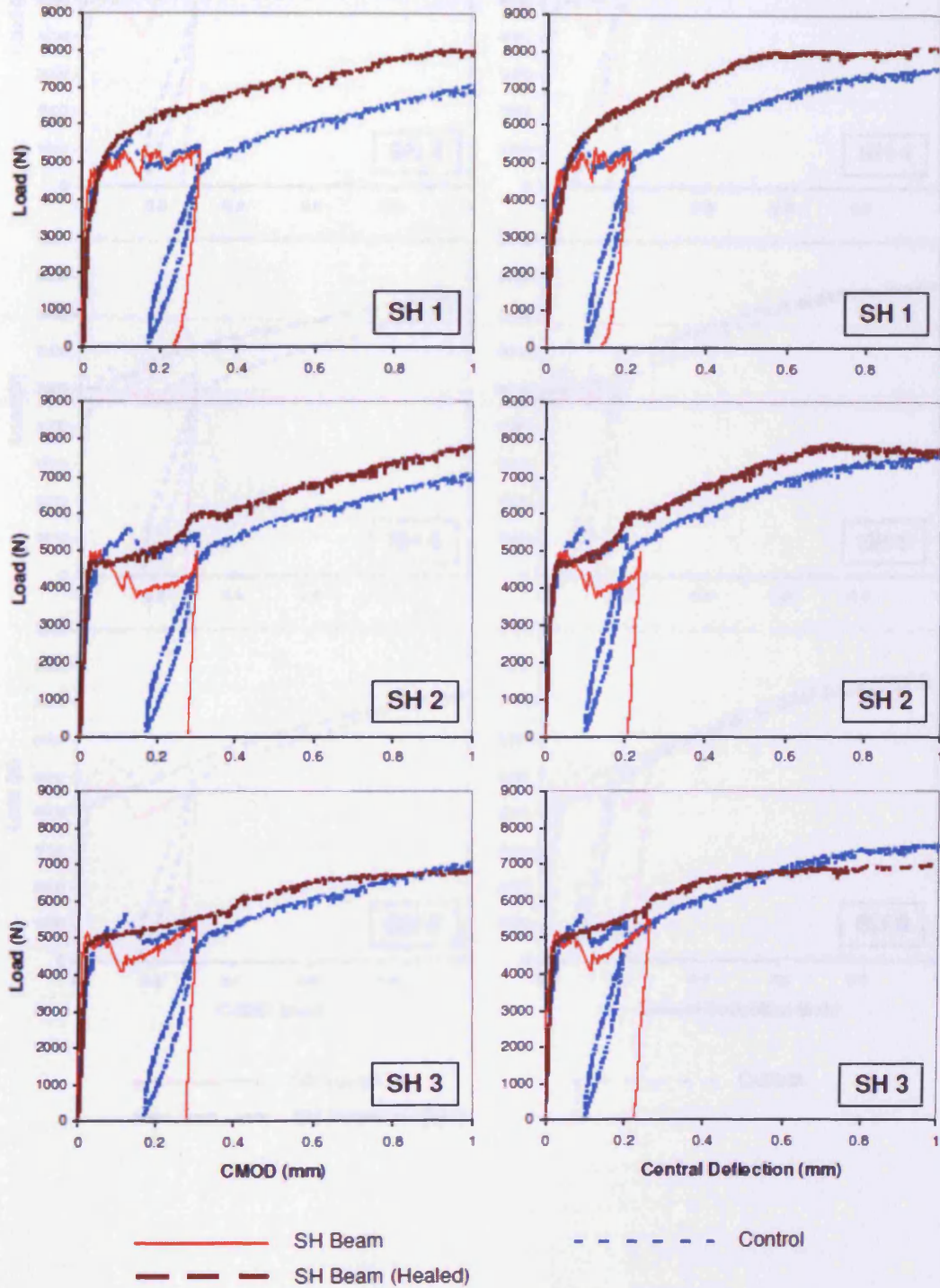


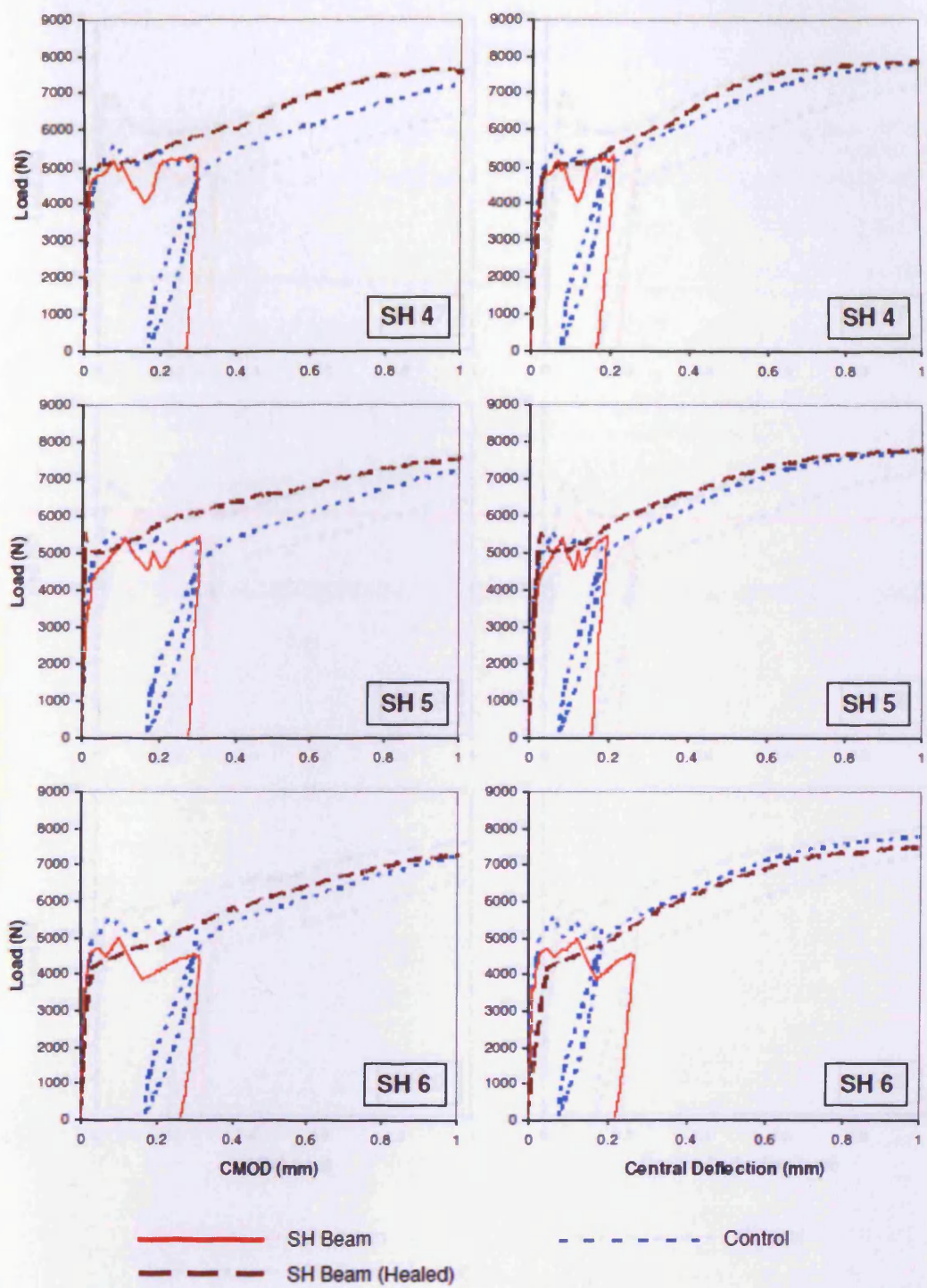
Set 5. Lightly reinforced, un-notched beams

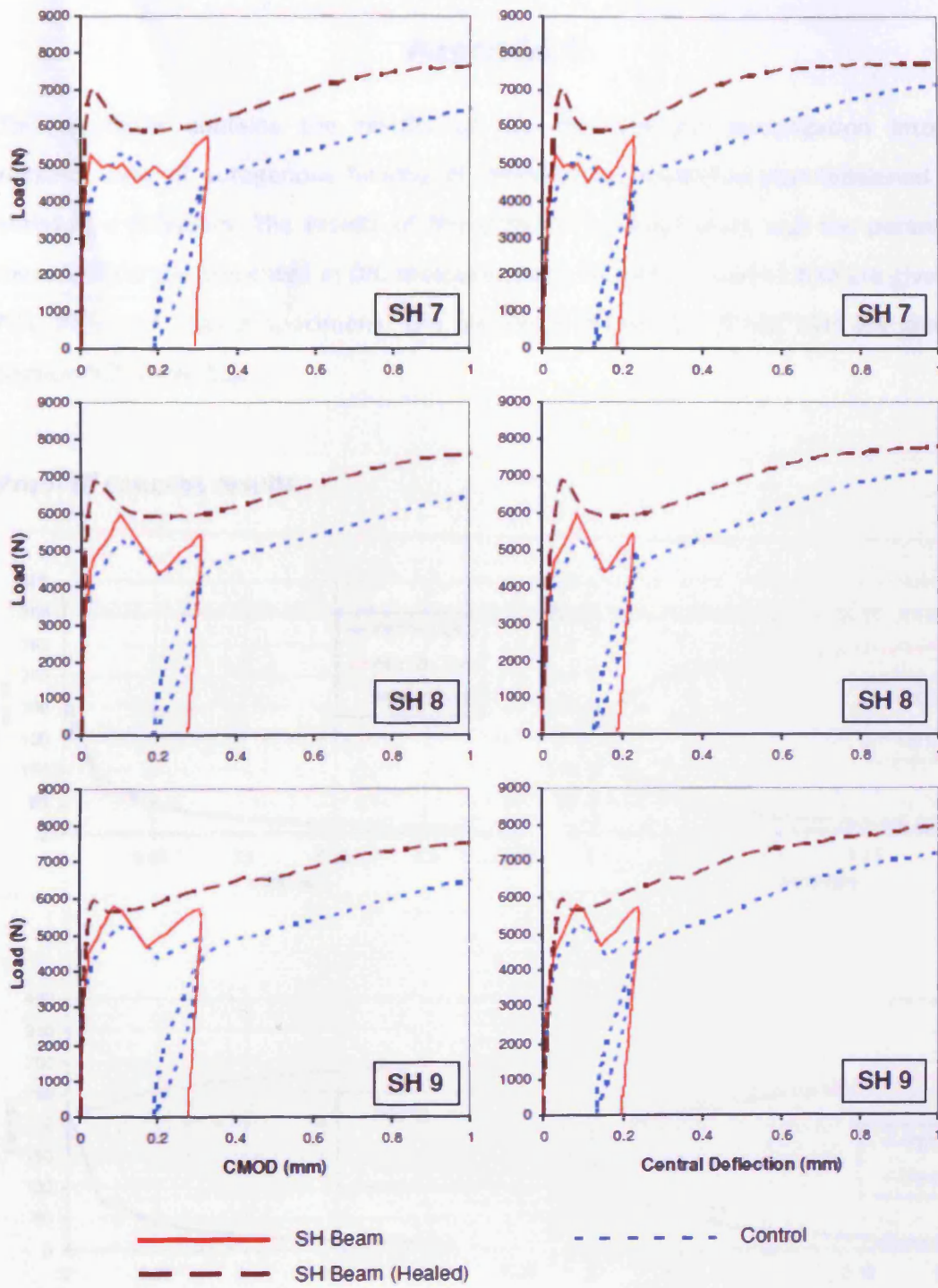


### Set 6. Lightly reinforced, notched beams with varied loading rate

A loading rate 0.00075 mm/s was used for SH1-3 specimens, 0.003 mm/s for SH4-6 specimens and 0.012 mm/s for SH7-9 specimens.



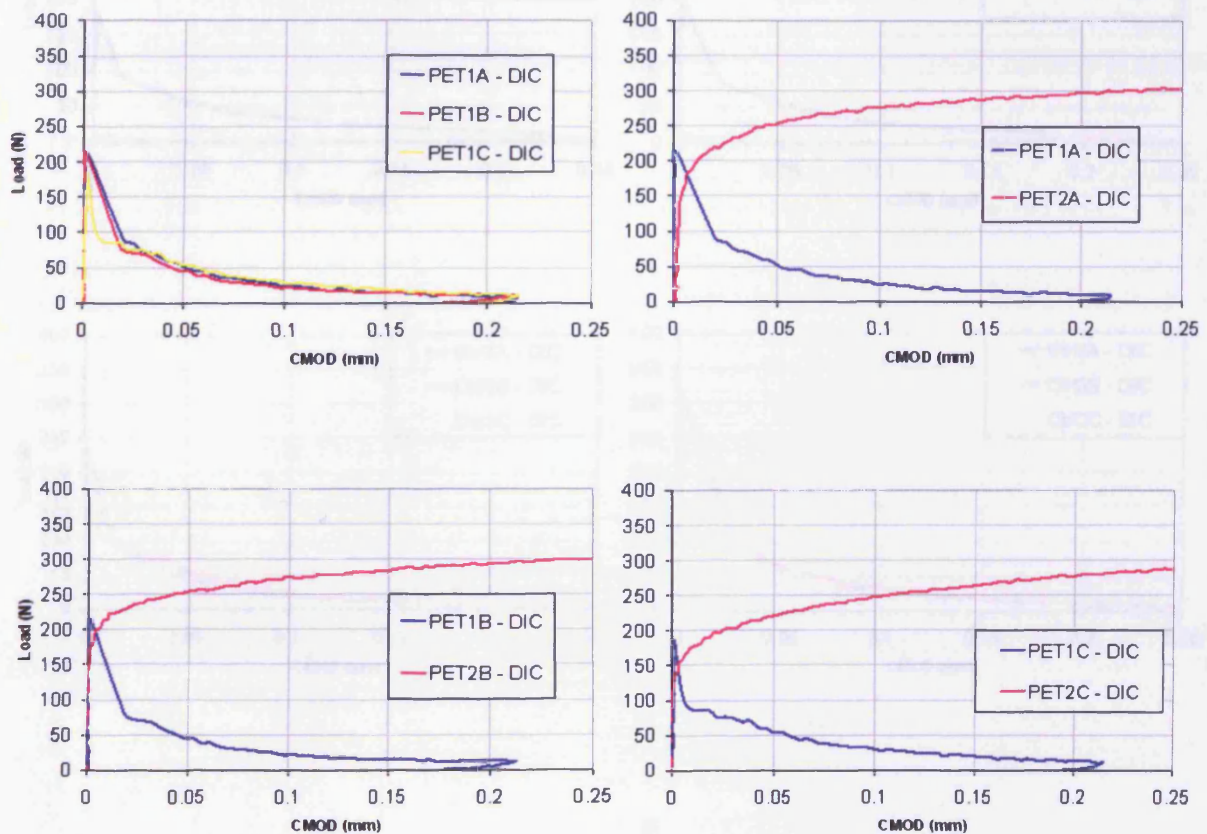




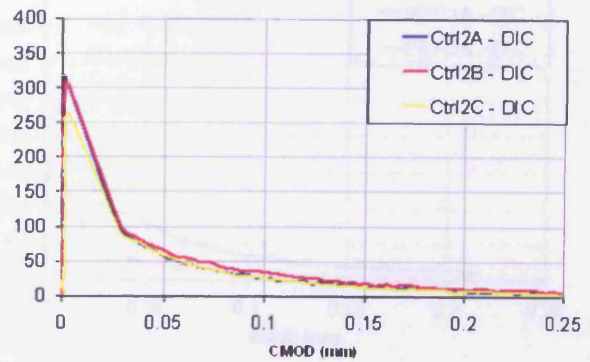
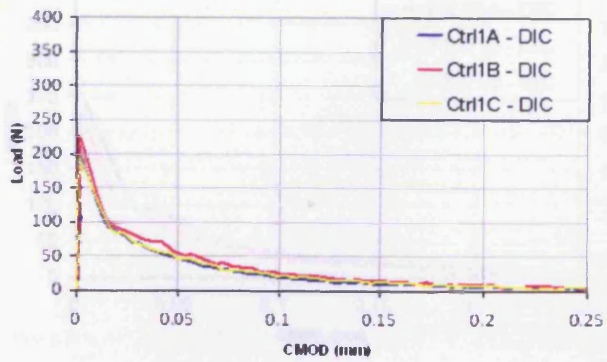
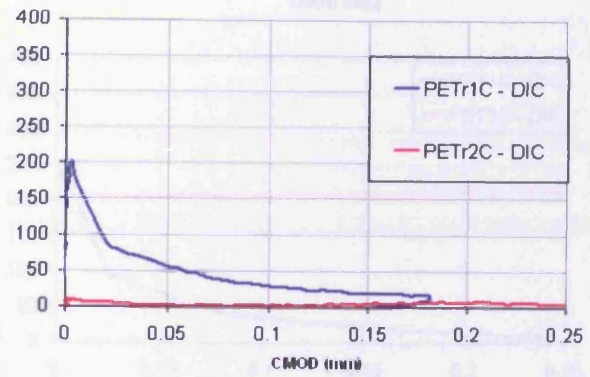
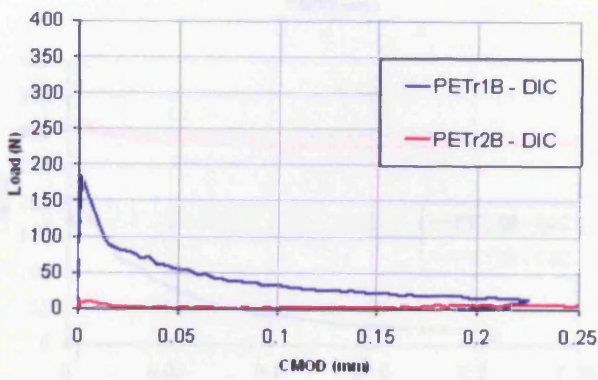
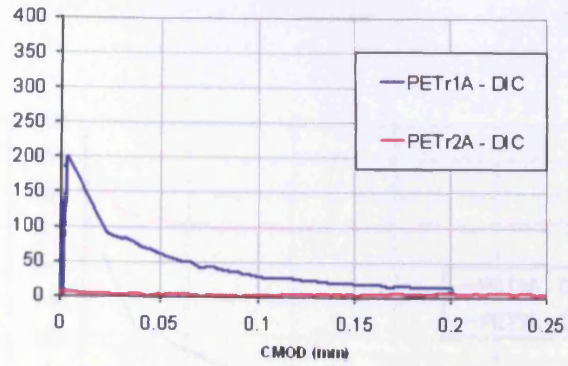
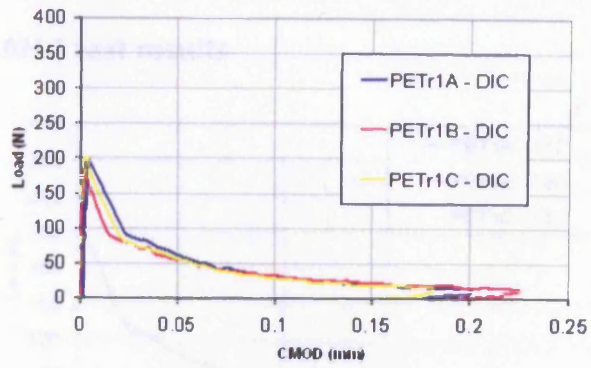
## Appendix C

This appendix contains the results of the experimental investigation into the enhancement of autogenous healing of cementitious materials post-tensioned with shrinkable polymers. The results of the proof of concept tests and the parametric investigation are presented in DIC measurements. Graphs of load-CMOD are given for PET, PETr and control specimens. The specimen details for all test sets are given in Section 5.2, Table 5.1.

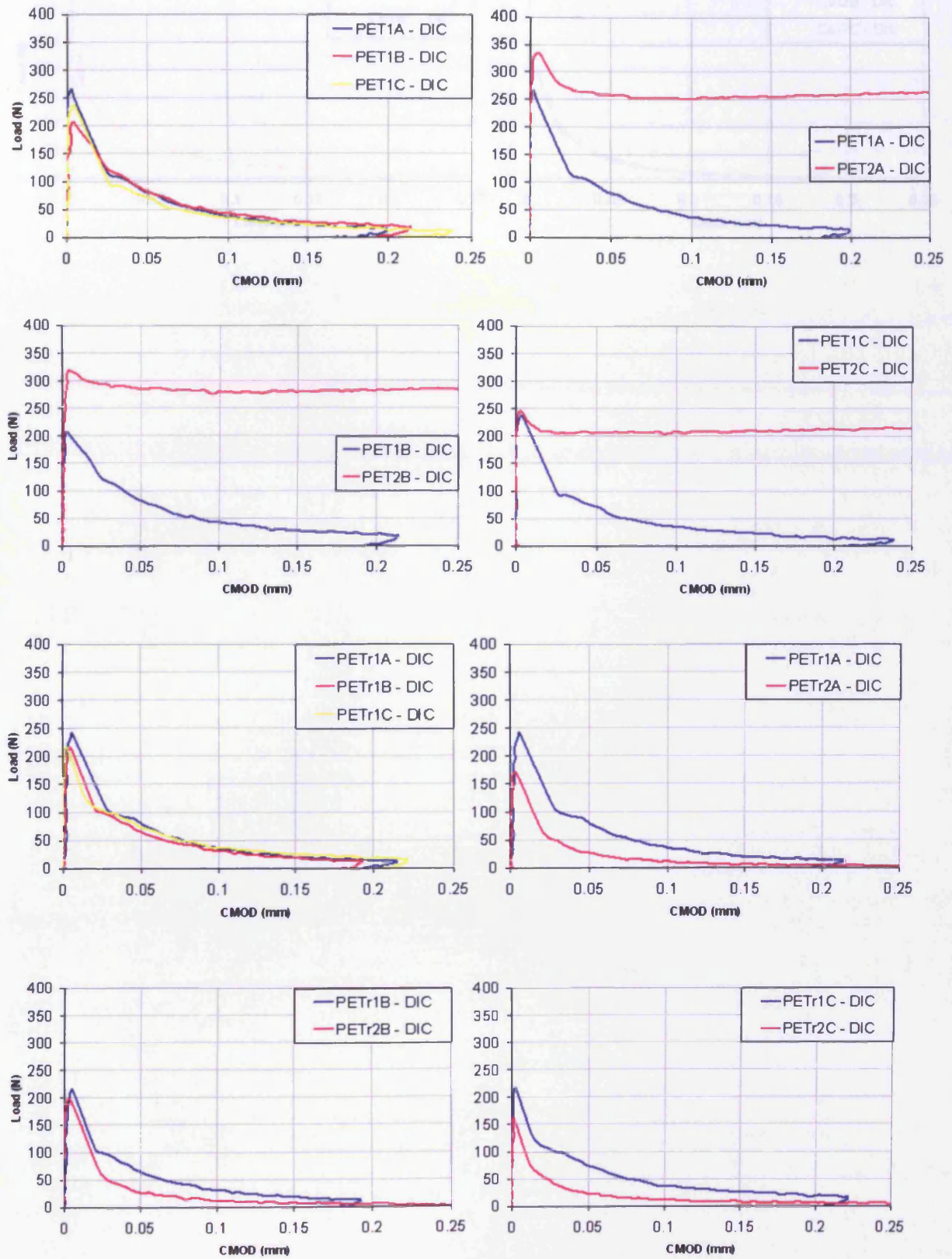
### Proof of concept results



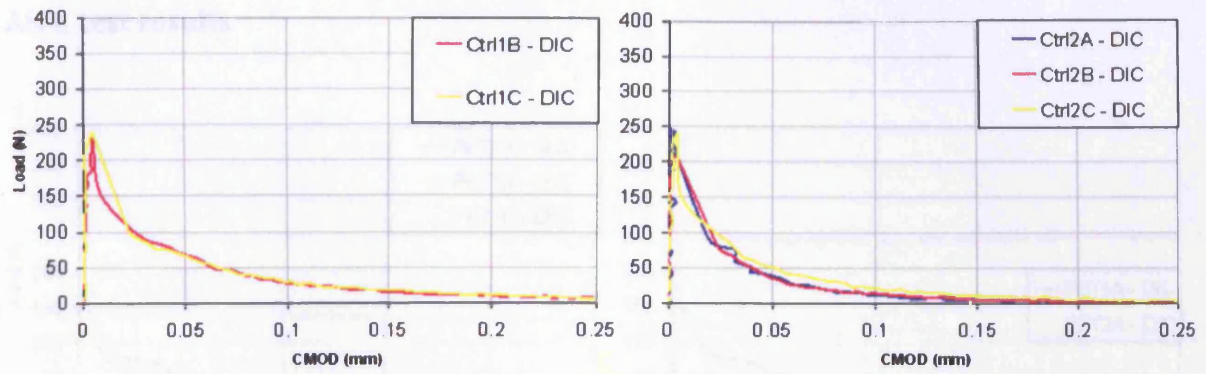
Appendix C – Experimental results for shrinkable polymer cementitious material system



### AH 1 test results

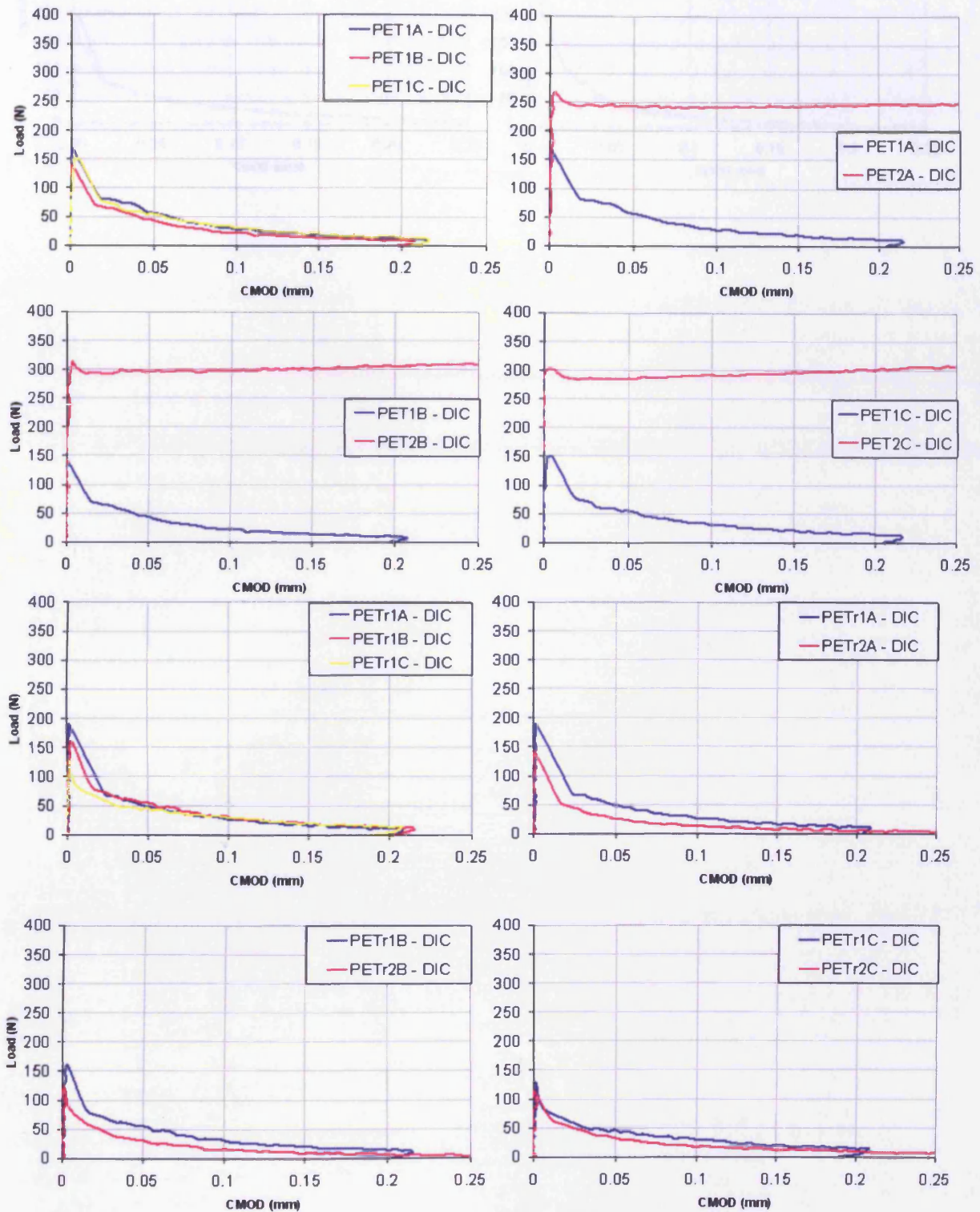


Appendix C – Experimental results for shrinkable polymer cementitious material system

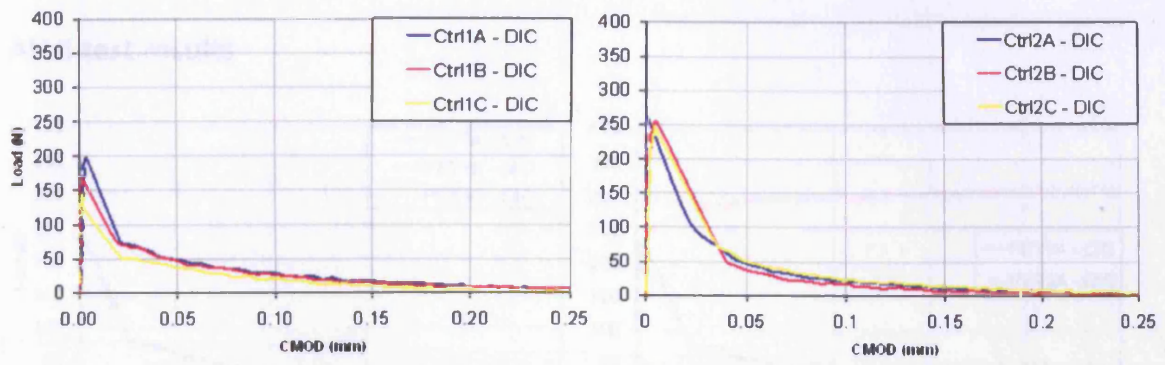




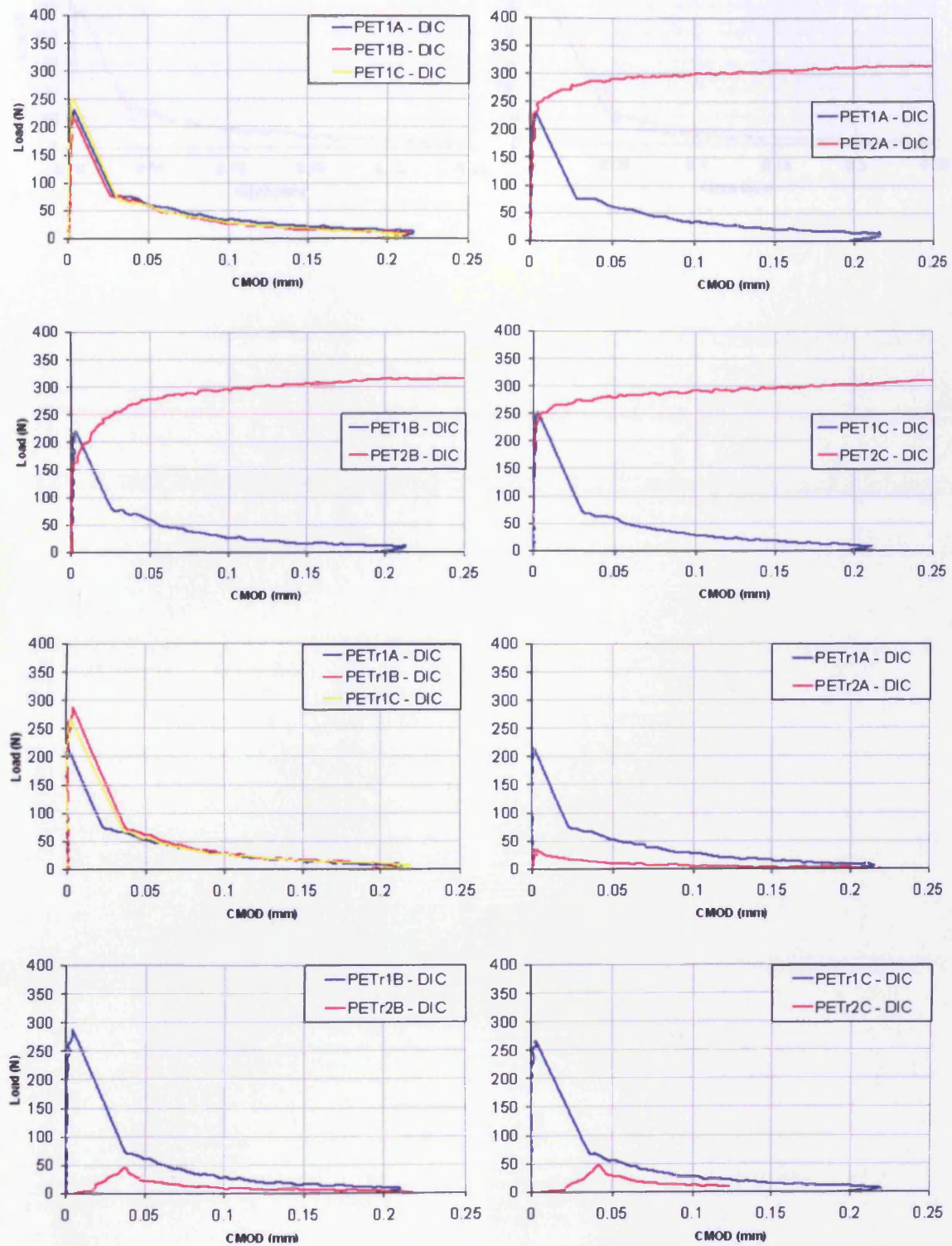
### AH 2 test results



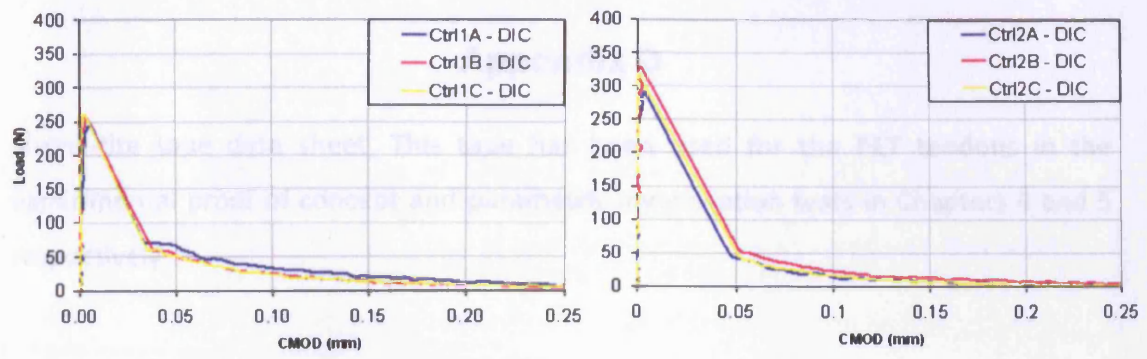
Appendix C – Experimental results for shrinkable polymer cementitious material system



AH 3 test results



Appendix C – Experimental results for shrinkable polymer cementitious material system



## **Appendix D**

Shrink-tite tape data sheet. This tape has been used for the PET tendons in the experimental proof of concept and parametric investigation tests in Chapters 4 and 5 respectively.

## Shrink Tite Tape

- Shrink-tite tape is a post modified polyester, which when heated undergoes shrinkage in the length wise direction only
- This characteristic is used to consolidate mandrel wound composite preforms and uncured rubbers, to form high quality low voidage components
- The shrink-tite tape is fastened off with suitably rated adhesive flashtape, and spiral wound along the component
- A single layer exerts a maximum loading of up to  $\text{cm}^2/\text{Kg}$  on a small diameter mandrel. (Reducing as the diameter increases). The pressure exerted increases proportionally to the number of layers used
- Shrinkage starts at  $80^\circ\text{C}$  and gives highest pressure at  $148^\circ\text{C}$ . Over  $148^\circ\text{C}$  the pressure reduces. If multilayer wrapping is used, shrinking each layer with a heat gun will prevent wrinkling in the underlying layers
- The tapes natural release properties are limited and to ensure clean release after cure, a suitable release film or peel ply should be applied to the mandrel before the shrink-tite tape
- Also available, self releasing on upper surface

### SPECIFICATION

• Optimum use temperature	148°C
• Initial shrinkage occurs	80°C
• Maximum Use Temperature	200°C
• Melt temperature	245°C
• Nominal shrinkage length	20%
• Width shrinkage	zero
• Maximum length shrink force	175 $\text{cm}^2/\text{Kg}$
• Time to reach maximum shrinkage	10 minutes
• Chemical resistance	to oils, moisture, resins, varnishes and most solvents
• Flammability	auto ignition over $480^\circ\text{C}$
• Tensile strength	over 1757 $\text{cm}^2/\text{Kg}$

### AVAILABILITY & PACKAGING

• Thickness	0.05 mm (standard)
• Widths	32mm & 64mm
• Length of roll	91.44m

### STORAGE & HANDLING

- Store away from heat

Cont.

### Aerovac Systems Ltd.

Tel 01274 550500 Fax 01274 550501 e-mail: sales@aerovac.com website: www.aerovac.com

All statements, technical information and recommendations contained in this publication are based on tests believed to be reliable, but their accuracy and/or completeness are not guaranteed. The user shall determine the suitability for this particular purpose and shall assume all risk and liability in connection herewith.

APPENDIX E

Calculation to determine the approx. psi compression force exerted by Shrink Tite Tape over a cylindrical object

**Compression force (psi)** =  $2 \times 2500 \times \text{Thickness} \times \text{laps} \div \text{Diameter}$

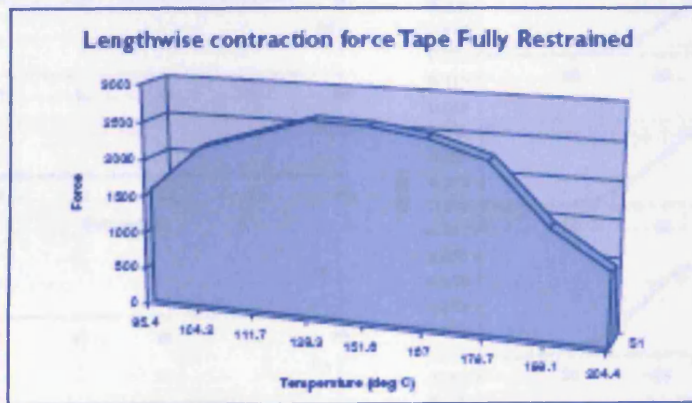
Where: **2500** = psi Shrink force of the tape @ 148.9°C (longitudinal force)

**Thickness** = Thickness of the Shrink Tite Tape (0.002" or 0.005")

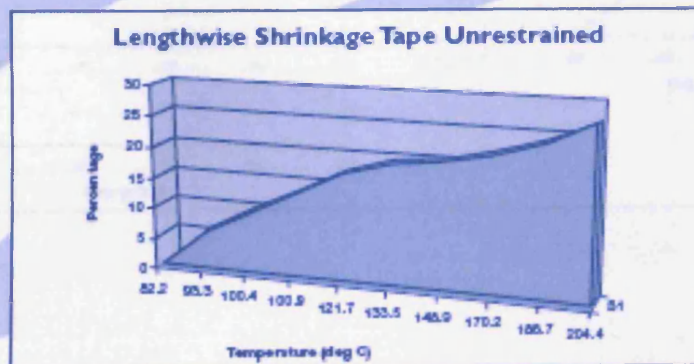
**Laps** = Number of layers of the Shrink Tite Tape

**Diameter** = Outside diameter of the cylinder (inches)

- Graph 1) This graph represents the lengthwise contraction force tape fully restrained



- Graph 2) This graph represents lengthwise shrinkage tape unrestrained



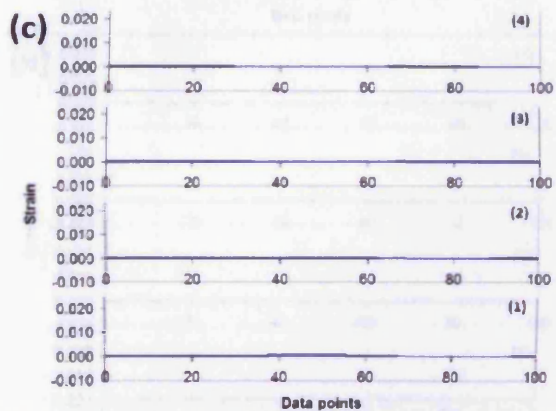
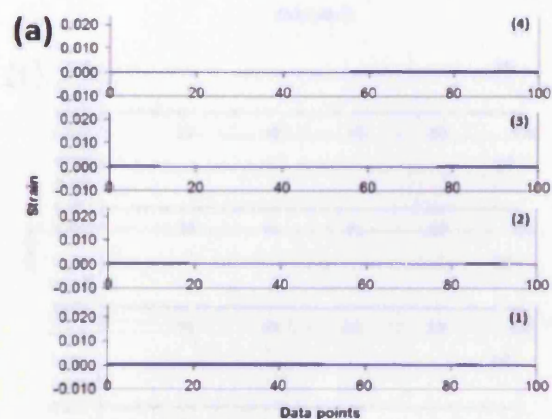
**Aerovac Systems Ltd.**

Tel 01274 550500 Fax 01274 550501 e-mail: sales@aerovac.com website: www.aerovac.com

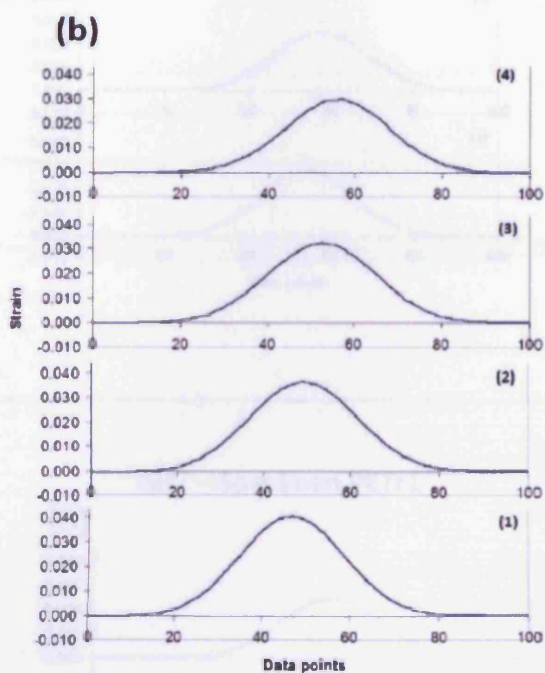
All statements, technical information and recommendations contained in this publication are based on tests believed to be reliable, but their accuracy and/or completeness are not guaranteed. The user shall determine the suitability for this particular purpose and shall assume all risk and liability in connection herewith.

## Appendix E

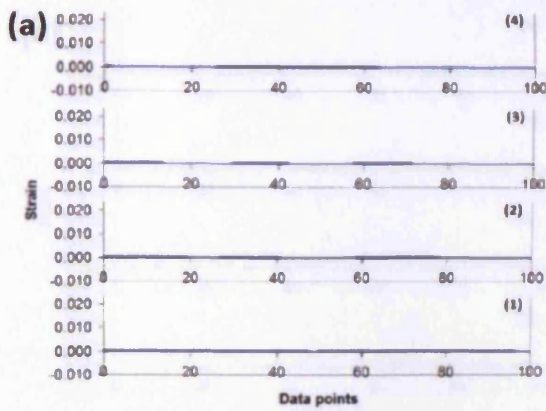
This appendix contains data for PET and PETr specimens that were subject to regime AH2 (Steam heat and healing). DIC was used to measure the strain profiles at four levels across the notched region of specimens as described in Section 5.4.3. Data for AH2 specimen PET 2 is given in Figure 5.11 in Section 5.4.3



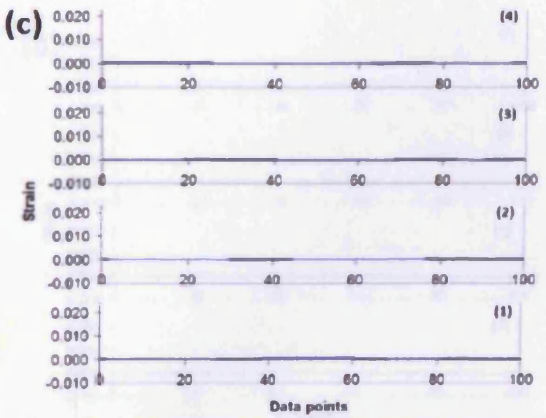
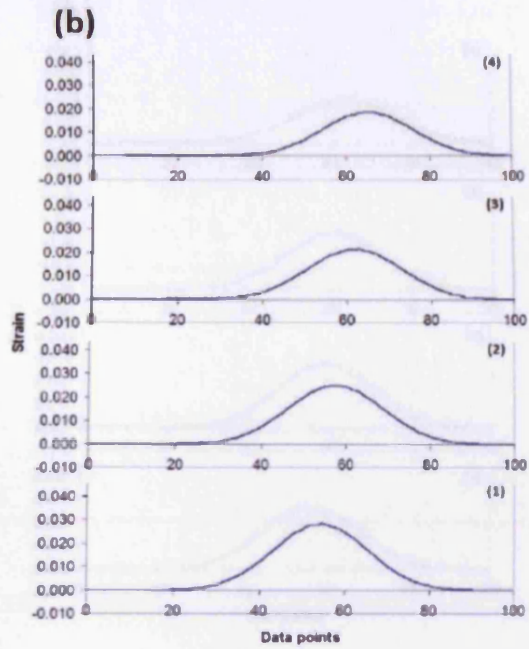
AH2: Specimen PET 1



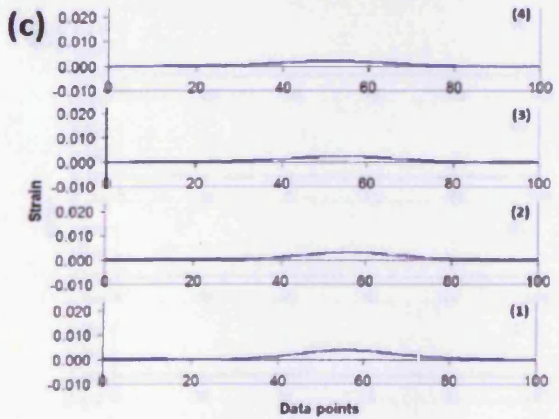
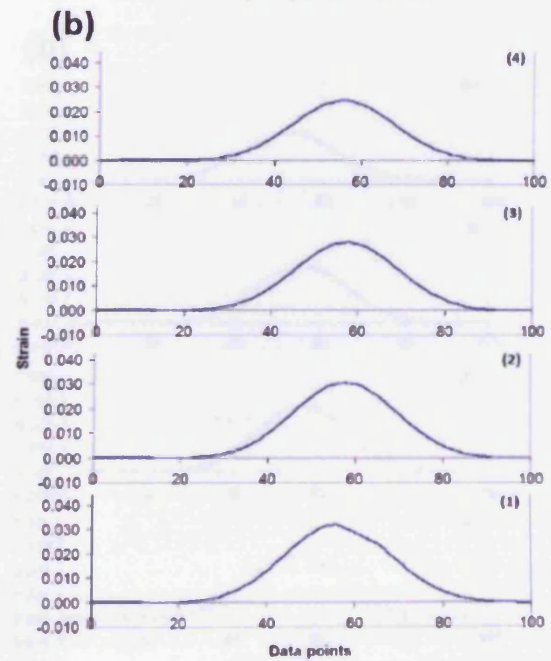
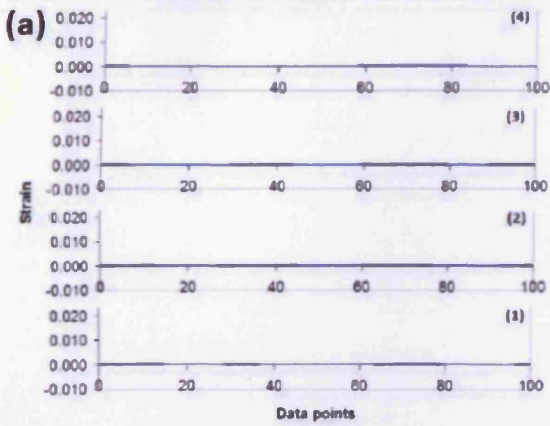


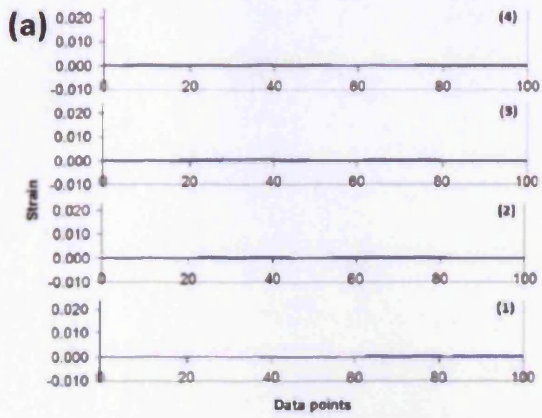


AH2 – Specimen PET 3

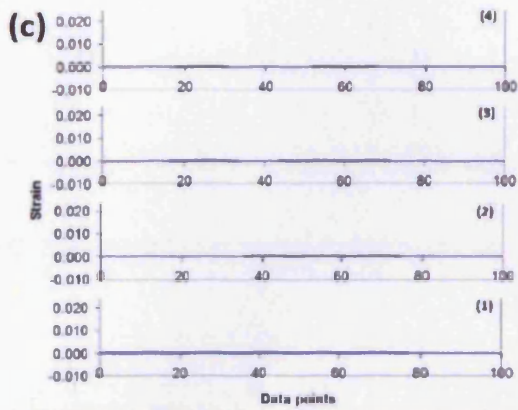
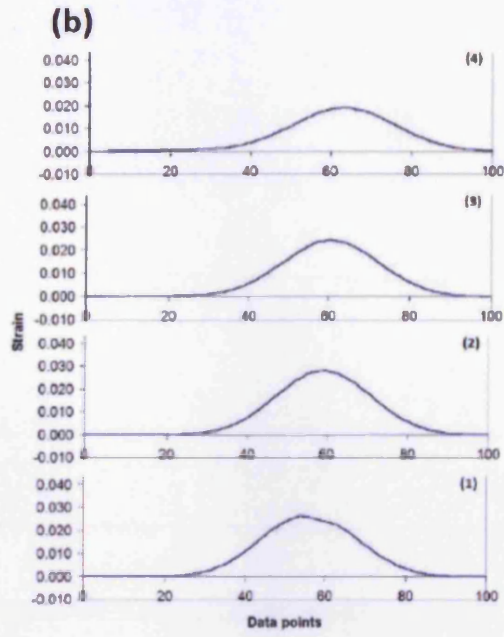


AH2 – Specimen PETr1





AH2 – Specimen PETr2



AH2 – Specimen PETr3

